A GEOMORPHOLOGICAL ASSESSMENT OF ARMORED DEPOSITS ALONG THE SOUTHERN FLANKS OF GRAND MESA, CO, USA

A Thesis

by

TIMOTHY JAMES BRUNK

Submitted to the Office of Graduate Studies of
Texas A&M University
in partial fulfillment of the requirements for the degree of

MASTER OF SCIENCE

May 2010

Major Subject: Geology

A GEOMORPHOLOGICAL ASSESSMENT OF ARMORED DEPOSITS ALONG THE SOUTHERN FLANKS OF GRAND MESA, CO, USA

A Thesis

by

TIMOTHY JAMES BRUNK

Submitted to the Office of Graduate Studies of
Texas A&M University
in partial fulfillment of the requirements for the degree of

MASTER OF SCIENCE

Approved by:

Chair of Committee,	John R. Giardino
Committee Members,	John D. Vitek
	Michael C. Pope
Head of Department,	Andreas Kronenberg

May 2010

Major Subject: Geology

ABSTRACT

A Geomorphological Assessment of Armored Deposits Along

the Southern Flanks of Grand Mesa, Co, USA.

Timothy James Brunk, B.A., Texas A&M University

Chair of Advisory Committee: Dr. John R. Giardino

A series of deposits, located along the southern flanks of Grand Mesa, Colorado, and extending to the south, are problematic, and the processes related to emplacement are not understood. The overall area is dominated by two landform systems, Grand Mesa, which supported a Pleistocene ice cap, and the North Fork Gunnison River drainage. Thus, one has to ask: Are these deposits the result of the melting of the ice cap or are they fluvial terraces associated with the evolution of the ancestral Gunnison River? The goal of this research was to map the areal extent of the deposits and to interpret the formation and climatic significance in understanding the evolution of the Pleistocene landscape in the region.

An extensive exposure, parallel to State Highway 65 near Cory Grade, was used for detailed description and sampling. Three additional exposures, ~10 to 20 km (~6 to 12 mi) were used to extend the areal extent of sampling. The study area was mapped using aerial photography and traditional field mapping aided by GPS. From the field work, a detailed stratigraphic column, including lithology and erodability, was constructed. Vertical exposures of the deposits were described, mapped, and recorded in

the field and using detailed photo mosaics. Samples were collected from each stratum of the deposits for grain-size, shape, and sorting analyses. Five distinct depositional facies were identified.

Sieve analysis on collected samples shows that four distinct grain-sizes occur in the outcrops; coarse sand, very-coarse sand, granule, and pebble and boulder. Mean grain-sizes range from 0.0722 to 0.9617 Φ, -0.0948 to -0.9456 Φ, -1.0566 to -1.9053 Φ, and -2.0050 to -3.4643 Φ, respectively.

Glacio-fluvial depositional environments were identified and supported with observations of sedimentary structures and clast composition. Two major environments of deposition are recorded in the deposits; fluvial deposits from glacial outburst floods, and debris flow deposits. Imbrication of clasts in the strata suggests the flow came from the direction of Grand Mesa to the north. Facies and subsequent sequences were constructed to portray evidence that supports the glacio-fluvial mode of deposition.

DEDICATION

To my family and friends who have been there for me, and helped me struggle through the graduate school experience.

ACKNOWLEDGEMENTS

First and foremost, I would like to thank my parents for putting up with this geological "nonsense" through seven long years of college. For without them, I would not have been able to achieve such high goals.

I must acknowledge and sincerely thank my colleagues, Adam Lee, Bree McClenning, and Daynna Rodosovich, for their assistance with field work and sample collection. I also want to additionally thank Adam Lee and Bree McClenning for their help, opinions, and insight that went into the interpretation portion of this thesis. Appreciation and thanks go to Jonathan Strand for his creative and artistic ideas that went into the design of my interpretive graphics. I would also like to thank Netra Regmi for his insight and help with software packages, statistical interpretations, and many other miscellaneous anecdotes during my time in graduate school.

I would like to thank my committee members, Jack Vitek and Mike Pope, for their help, support, and encouragement. I would also like to acknowledge and sincerely thank the chair of my committee, Rick Giardino, for his help, guidance, and most of all friendship through this thesis project. For it is he, along with his charisma, that saved me from a sizeable "geographical" error.

TABLE OF CONTENTS

Page

LIST OF FIGURES

Page

Page

LIST OF TABLES

1. INTRODUCTION AND PROBLEM STATEMENT

A series of deposits located along the southern slopes of Grand Mesa, CO, are problematic (Fig. 1). This area is dominated by two landform systems: Grand Mesa, which was covered with a Pleistocene ice cap, and the drainage associated with the North Fork Gunnison River. These series of deposits extend from the upper slopes of Grand Mesa to the floodplain of the modern Gunnison River. Cole and others (1981) suggest they might be associated with the ancestral Gunnison and Colorado rivers, but unfortunately, their data do not explicitly show this. Therefore, the origin of these deposits is unexplained and leads one to ask: Are these glacio-fluvial deposits associated with the melting of the ice cap or are they fluvial terraces associated with the evolution of the ancestral Gunnison River? I hypothesize that the deposits are glacio-fluvial formed during melting of the ice cap from late Pleistocene climatic warming.

The goal of this research is to map the areal extent of the deposits and to interpret the formation and climatic significance as steps to understanding the development of the Pleistocene/Holocene landscape in the region. This thesis will document and interpret the geomorphic development of the area.

To achieve the goal of this research, cumulative frequency diagrams were created to visually analyze grain-size data. Sedimentary structures, clast composition, and photographs and diagrams from the literature were analyzed to better understand the

---

This thesis follows the style of *Geomorphology*.

sites in question for this thesis. Facies were determined, and a depositional sequence was identified to better understand the geomorphic history of the region.

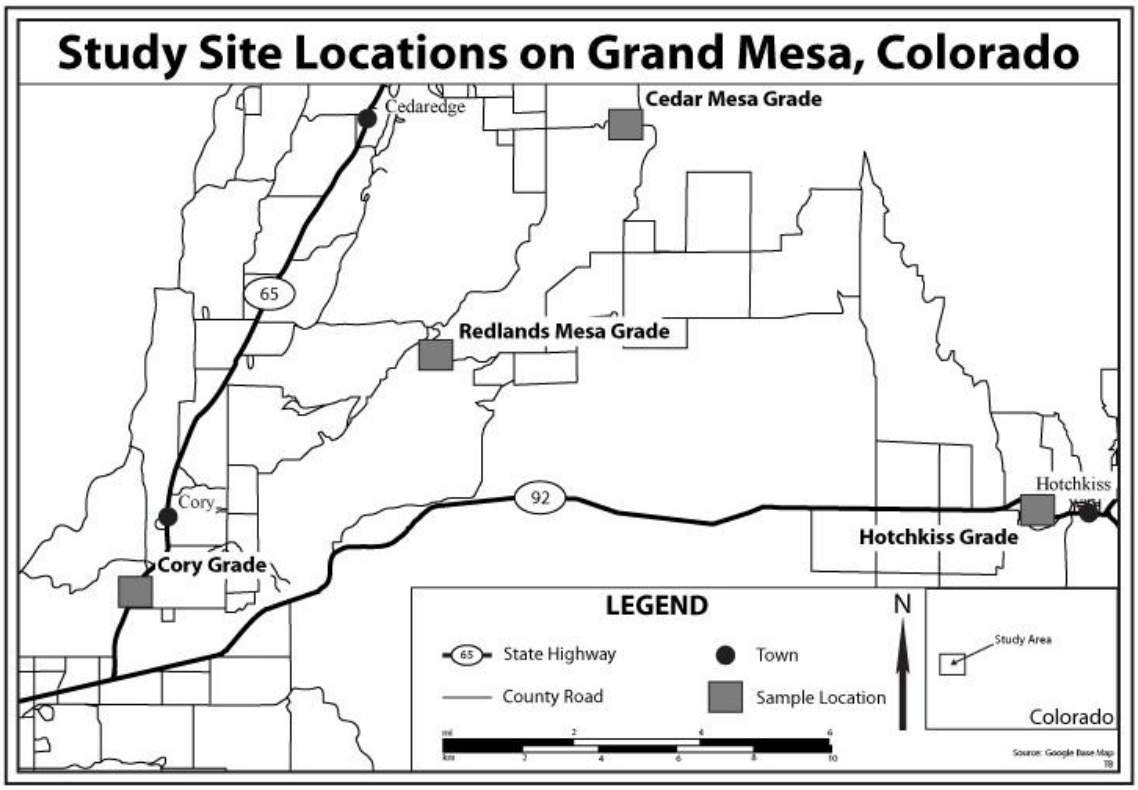

Fig. 1. Study site locations on the southern flanks of Grand Mesa.

1.1 Objectives

To accomplish the goal for this thesis, the following objectives were established:

1) Map the aerial extent of the deposits to identify sediment sources,
2) Determine the depositional environments associated with the strata in the deposits, and
3) Determine the depositional sequence of events recorded in the deposits and correlate over space.

1.2 Hypothesis

The research for this thesis is driven by the hypothesis:

H_1: The deposits are glacio-fluvial and associated with melting of the ice cap from Pleistocene climatic warming.

The null hypothesis is:

H_0: The deposits are not glacio-fluvial and are associated with the ancestral Gunnison River drainage.

1.3 Study Area

The largest mesa in the world, Grand Mesa (Fig. 1), is a basalt-capped plateau at an elevation of ~3,050 m (~10,000 ft.) in the Southern Piceance Creek Basin of southwestern Colorado (Cole and Sexton, 1981). Grand Mesa is bordered by the Gunnison and North Fork rivers to the south and the Colorado River to the north. Erosion of the basalt-capped mesa has resulted in the creation of moraines, pediments, alluvial fans, glacial outwash deposits, landslides, and colluvial deposits that flank

Grand Mesa (Cole and Sexton, 1981). Two dominant landscapes exist in the study area, mesas and foothills, and encompass ~600 km^2 (~230 mi^2).

Rock units in the area range from Jurassic to Quaternary; however, the study area is primarily Cretaceous shale (Mancos) and unconsolidated Quaternary deposits. Miocene basalts cap the mesa and are the dominant clasts in Quaternary deposits.

The oldest rocks in the area are Jurassic sandstones and shales (Morrison Formation), overlain by Cretaceous sandstones, shales, and coal (Dakota Sandstone, Mancos Shale, and Mesaverde Formation). Above the Cretaceous rocks are Tertiary sandstones and shales (Wasatch Formation, Green River Formation, Uinta Formation, and North Park Formation). Grand Mesa is capped by a series of Miocene basalt flows. (Cole and Sexton, 1981; Baker, 2002).

The youngest deposits in the area are Quaternary in age (Retzer, 1954; Cole and Sexton, 1981). Three successive glaciations occurred on Grand Mesa: Pre-Bull Lake (oxygen isotope stage 8, 12, 14, and 16); Bull Lake (oxygen isotope stage 6 and 8); and Pinedale (oxygen isotope stage 2) (Retzer, 1954; Richmond, 1965; Robinson and Dea, 1981; Richmond, 1986; Armour et al., 2002). Sinnock (1978) suggests four periods of late Pleistocene glaciation occurred; two Bull Lake and two Pinedale in age.

The climate of the area varies from semi-arid conditions at low elevations (~1520 m; ~5,000 ft.) near the base of the mesa and transitions to sub-humid/sub-alpine conditions on the upper slopes and top of the mesa (~2440 to 3050 m; ~8,000 to 10,000 ft.) (Yeend, 1965). According to the High Plains Regional Climate Center (2000), the maximum average temperature in Cedaredge, Colorado, from 1971-2000 was 17.5^{o} C

(63.5° F), with an average low of 1.6° C (34.8° F), and an average annual precipitation of 34.01 cm (13.39 in.). The highest average temperatures occur between June to August with a maximum of 31.3° C (88.3° F) in July. The lowest average temperatures occur between December to February with a minimum of -9.5° C (14.8° F) in January. Maximum precipitation occurs between September to November with a maximum of 3.9 cm (1.55 in.) in October.

This study was conducted on the slopes of Grand Mesa, where the vegetation types of the mesas and foothills merge (Ramaley, 1927). The sagebrush shrublands on the slopes of Grand Mesa below ~2,440 m (~8,000 ft.) are blanketed with ~0.6 to 2.1 m (~2 to 7 ft.) tall greenish-gray sage bushes (Mutel and Emerick, 1992). The upper slopes of Grand Mesa from ~2,440 to 3,050 m (~8,000 to 10,000 ft.) below the high mountain forests are dominated by the Piñon Pine – Juniper woodlands vegetation zone (Mutel and Emerick, 1992). This zone has barren, rocky ground with Juniper trees transitioning to Piñon Pines at higher elevations (Mutel and Emerick, 1992).

Access to the study area is provided by State Highways 65 and 92, with additional access provided by Cedar Mesa Road and North Road (Fig. 1). An exposure of the deposits is located northeast of Delta, CO, north of the Gunnison River and east of State Highway 65 (Fig. 1). This outcrop (Cory Grade) is the primary study site for field work. Secondary outcrops that were studied include Hotchkiss Grade ~1 km (~0.6 mi) west of the town of Hotchkiss and south of State Highway 92, Redlands Mesa Grade ~4 km (~2.5 mi.) east of State Highway 65 and ~4 km (~2.5 mi.) north of State Highway 92

on North Road, and Cedar Mesa Grade ~6 km (~3.7 mi.) east of the town of Cedaredge adjacent to Cedar Mesa Road.

2. LITERATURE REVIEW

The geology and geomorphology of Grand Mesa has been extensively studied over the past one hundred years. Most research has focused on the erosional history and surrounding deposits of the mesa (Henderson, 1923; Retzer, 1954; Yeend, 1965; Sinnock, 1981; Cole and Sexton, 1981; Cole, 2001; Aslan et al., 2005; Rider et al., 2006; Darling et al., 2007a), rates of incision of the surrounding rivers and streams (Baker et al., 2002; Baker, 2002; Sandoval, 2007; Darling et al., 2007b; Darling et al., 2009), and methods of dating the numerous surficial deposits (Baker, 2002; Darling et al., 2007b; Darling et al., 2009).

The occurrence of glaciation on Grand Mesa was first recognized by Henderson (1923), who traversed the mesa on horseback and described and documented the various glacial deposits and landforms on the mesa. A later study by Retzer (1954) further discussed the glacial deposits and presented evidence for three glacial stages and the soil development on the mesa. Formation and preservation processes of glacio-fluvial deposits are briefly discussed by Sinnock (1981) whereas outwash terrace location, sedimentology, and basic depositional interpretation were discussed by Cole and Sexton (1981). These studies qualitatively describe the glacial deposits on Grand Mesa; however, no quantitative measurements were reported.

Rates of incision of the adjacent Gunnison and Colorado rivers were studied by Baker and others (2002), Darling and others (2007b), Sandoval (2007), and Darling and others (2009). Darling and others (2009) calculates rates of incision by using dating

techniques for the Lava Creek B ash beds occurring throughout the study area. Aslan and Cole (2002) found two Lava Creek B ash localities in the Grand Mesa area, with the goal of applying similar dating techniques to the deposits flanking Grand Mesa. Baker (2002) measured weathering rinds on basalt gravels in an attempt to date the deposits and found a relationship between rind thickness and climate; however, no correlation between rind thickness and age of the landform was determined. Dating techniques for Lava Creek B ash have yet to be applied to date the deposits; however, it appears promising for future studies.

The erosional history of Grand Mesa was well documented by Cole (2001), Aslan and others (2005), Rider and others (2006), and Darling and others (2007b); unfortunately, only abstracts of their research have been published. Rider and others (2006) and Darling and others (2007a) mapped and qualitatively characterized the deposits. These published abstracts show only minimal results; complete studies of these topics would be very useful to this research if the methodology, data analysis, and quantitative results were discussed.

Studies of the erosional history and Quaternary deposits of Grand Mesa were completed by Yeend (1965), Cole and Sexton (1981), and Sinnock (1981). Yeend's (1965) study is the most extensive to date and includes mapping, description, and interpretation of the Quaternary deposits. Cole and Sexton (1981) provide a detailed, qualitative description of the Pleistocene deposits in the Grand Mesa area. An overview of the depositional processes, active during the Pleistocene, are brought together for the first time in the literature. The authors compare landform classifications put forth by

previous authors for each of the three glacial stages. Sinnock (1981) discusses Pleistocene glacial landforms in the Grand Valley, including locations, composition, and genesis.

Overall the literature includes extensive work on rates of incision of rivers and streams in the study area, several dating techniques associated with surficial deposits of Grand Mesa, and many qualitative sedimentary studies of deposits. My study involves qualitative interpretation and quantitative analysis of samples. I will be comparing my interpretations to previously published data, but will support my interpretations with quantitative data.

3. METHODS

A total of one hundred and twenty-six (126) samples were collected in the field area for analysis. The majority of the study focuses on the Cory Grade outcrop, with three other satellite outcrops used mainly for visual correlation purposes (Fig. 1). Because of instability and disaggregation of the outcrop, only the lower portions of outcrops that could be safely reached were sampled and analyzed. Because of safety concerns, the entire vertical exposures were not sampled at any of the four outcrops.

3.1 Assess the Aerial Extent of the Deposits

Terrain Navigator® software was used to access aerial photographs and topographic maps at scales of 1:12,000 and 1:24,000, respectively. These were analyzed for possible outcrop locations for use in correlation with the known Cory Grade outcrop. Possible drainage pathways from the mesa were identified and mapped to determine locations of possible outcrops of deposits. Known outcrops were then geomorphically mapped according to principles outlined by Crofts (1981).

GIS software (ArcGis®) was utilized in initial mapping of the deposits. Three-dimensional relief maps and hill shade models were constructed from digital elevation models to help establish drainage pathways from the mesa. Soil maps were overlain on topographic maps to find an association, if any, between known outcrops and other possible outcrops.

Upon arrival in the field, a day of reconnaissance was used to positively identify outcrops located through geomorphic mapping. A total of four outcrops were located;

Cory Grade, Redlands Mesa Grade, Cedar Mesa Grade, and Hotchkiss Grade (Fig. 1). All, but one outcrop, were located along highway right-of-ways, therefore, on public property. Landowner permission was not granted to access Cedar Mesa Grade, and it could not be sampled. Outcrop photos, perpendicular to the deposit, were taken, and photographic analysis was performed for the Cedar Mesa Grade outcrop.

3.2 Determine Depositional Environment Associated with Strata

All outcrops were examined and photographed. Surveying flags were used to visually separate the strata for follow up sample collection. A naming convention was created for each outcrop based on outcrop name and strata letter (i.e., C1NA: Cory Grade outcrop, Section #1, North side of Section #1, strata A).

Each outcrop was photographed in detail using a Canon Powershot SX20 IS. For consistency, photographs were taken from set distances normal to the face of the outcrop (~20 m), and set distances (~3 to 5 m) parallel to the outcrop. Outcrop photographs were then stitched together into a photo mosaic using a photo stitching program (i.e., Canon® software) for photographic analysis.

Cory Grade, Hotchkiss Grade, and Redlands Mesa Grade outcrops were measured and described in detail. Sampling lines were chosen based on portions of the outcrop that showed high variability in morphology. Contacts between different strata were identified and marked with surveying tape. Each strata sampled was thoroughly described, and the thickness of individual stratum was measured using techniques outline by Compton (1985) and Graham (1988).

At lower levels of the outcrop a small shovel was used to collect sediment from strata (Fig. 2). The shovel was inserted into the loose sediment, removed, and the contents were placed into a quart-size plastic bag. For strata that were out of reach of the shovel, a plastic pipe was used to dislodge sediment, catching the sediment as it traveled down the pipe (Fig. 3). The collection pipe has a narrow opening, limiting collection to pebble and smaller grains. Each stratum that was out of arms reach was sampled with the collection pipe. Caution was used so that each sample is representative of only one stratum; however, because of the disaggregation of the outcrops, a small error is associated with cross-contamination of samples.

Each sample was processed using standard sedimentological techniques (Krumbein, 1934; Sahu, 1964; King, 1967; Folk, 1974; McManus, 1988; Dalsgaard et al., 1991; McCave and Syvitski, 1991; Ritter et al., 2002) using a Gilson SS-8R sieve/rotap shaker with U.S.A. Standard Testing Sieve screens with mesh sizes of 38.09 mm, 9.53 mm, 4.76 mm, 2.38 mm, 2.00 mm, 1.19 mm, 0.841 mm, 0.595 mm, 0.420 mm, 0.250 mm, 0.125 mm (1.5 inches, .375 inches, #4, #8, #10, #16, #20, #30, #40, #60, and #120). Samples were processed for ten minutes, and the amount retained on each screen was weighed using an Adam CP-310 portable balance. Cumulative frequency diagrams were created for each sample using a program by Balsillie and others (2002) to graphically display grain-size distributions and calculate basic statistics: mean, median, standard deviation, skewness, and kurtosis.

Stratigraphic columns were created using techniques outlined by Compton (1985) to show weathering profiles and sedimentary structures for each outcrop that was

Fig. 2. Sample collection using shovel and rock hammer (August 2009).

Fig. 3. Sample collection of higher unit using plastic collection pipe (August 2009).

sampled. A combination of grain-size analysis, sedimentary structures, grain composition, bed forms, and photographic comparison with Pettijohn (1975), Miall (1978), Rust (1978), Rust and Koster (1984), Collinson and Thompson (1982), Nemec and Steel (1984), Bradzikowski and van Loon (1991), Collinson (2006), and Miller (2006) were used to evaluate possible depositional environments.

3.3 Determine the Depositional Sequence of Events and Correlate

The stratum was dated using relative dating. At the Cory Grade outcrop, correlations were made for continuous strata throughout the horizontal length of the outcrop with the constructed sediment logs. A depositional sequence of events was determined from facies analysis and sieve data. A sequence was identified based upon previous sequences and stratigraphic columns of similar deposits published by Pettijohn (1975), Miall (1978), Rust (1978), Rust and Koster (1984), Collinson and Thompson (1982), Nemec and Steel (1984), Bradzikowski and van Loon (1991), Collinson (2006), and Miller (2006), as well as repeatable facies patterns in the outcrops.

4. ANALYSIS

Observations and quantitative analysis were used to interpret facies and sequences, and to reconstruct the geomorphic history of the study area. Sieve data for grain-sizes are first presented and supported with observations of clast composition, sedimentary structures, and photographic comparison to published works. Only one sample was collected at Cedar Mesa Grade because of complications with land ownership. Because of limited sampling of Cedar Mesa Grade, data collected on this outcrop was not used in the grain-size analysis of this thesis.

4.1 Analysis of Grain-Size

Three outcrop locations were sampled; Cory Grade, Hotchkiss Grade, and Redlands Mesa Grade. A total of 126 samples were collected between the three locations; 105 at Cory Grade, 12 at Redlands Mesa Grade, and 9 at Hotchkiss Grade. The majority of the study was focused on Cory Grade; secondary study sites (Hotchkiss Grade, Redlands Mesa Grade) were used for correlation purposes.

Cory Grade was sampled over a series of nine vertical successions, and a total of 105 samples were collected. Redlands Mesa Grade was sampled on one vertical succession with 12 samples collected, and 9 samples from Hotchkiss Grade on one vertical succession. Sampling lines were chosen in areas with high, vertical and horizontal, grain-size variability.

A statistical program designed by Balsillie and others (2002) was used to calculate statistical parameters, and construct cumulative-frequency diagrams for the

collected samples. After sieve analysis, the 126 samples were divided into four grain-size categories based on mean grain-size using the Udden-Wentworth grain scale. A total of 35 samples are coarse sand and finer (≥ 0 Φ), 16 are very-coarse sand (-1.0 to 0 Φ), 21 are granule (-2.0 to -1.0 Φ), and 54 are pebble to boulder (≤ -2.0 Φ). Cumulative-frequency diagrams were constructed for each sample to visually interpret the sorting. Outcrops were analyzed separately into the four grain-size categories.

4.1.1 Cory Grade

A total of 32 coarse sand samples (Table 1) were collected at Cory Grade (Fig. 4). Sample means range from 0.9617 Φ to 0.0722 Φ, with medians ranging from 0.2140 Φ to -0.3154 Φ. Standard deviations range from 0.2162 Φ units to 1.5044 Φ units, and skewness ranges from -7.3923 to -0.9742. The population mean is 0.6121 Φ.

A total of 12 very-coarse sand samples were collected (Table 2). Sample means range from -0.0948 Φ to -0.9456 Φ, with medians ranging from 0.2143 Φ to -1.5490 Φ. Standard deviations range from 0.9013 Φ units to 1.8895 Φ units, and skewness ranges from -1.4634 Φ to -0.1431 Φ. The population mean is -0.3297 Φ.

A total of 12 granule samples were collected (Table 3). Sample means range from -1.1714 Φ to -1.9053 Φ, with medians ranging from -1.4110 Φ to -2.7534 Φ. Standard deviations range from 1.6715 Φ units to 2.0653 Φ units, and skewness ranges from -0.0508 to 0.4213. The population mean is -1.5943 Φ.

A total of 49 pebble and larger samples were collected (Table 4). Sample means range from -2.0050 Φ to -3.4643 Φ, with medians ranging from -3.7277 Φ to -2.0581 Φ.

Standard deviations range from 1.9460 Φ units to 1.0155 Φ units, and skewness ranges from 0.5107 to 3.6571. The population mean is -2.6907 Φ.

Fig. 4. Cory Grade (August 2009).

Table 1. Cory Grade sieve data for samples ≥ 0 Φ.

SIEVE DATA Cory Grade: ≥ 0 Φ						
Sample	**Mean (Φ)**	**Median (Φ)**	**Std Dev (Φ units)**	**Skewness**	**Kurtosis**	**Sedimentary Structures**
C4NC	0.9617	0.1301	0.2162	-7.3923	69.8237	Ripples
C2MB	0.9526	0.1318	0.2316	-6.9487	68.2708	
C2NF	0.9491	0.1327	0.2278	-6.0066	51.3318	
C4NF	0.9003	0.1355	0.4216	-5.6022	39.0465	Ripples
C1NH	0.8960	0.1354	0.4503	-5.6675	38.7002	
C2SA	0.8915	0.1351	0.4490	-4.9771	29.7090	
C2MD	0.8828	0.1469	0.2902	-2.5262	10.3701	
C3NH	0.8207	0.1469	0.5340	-4.2359	25.2509	
C3SB	0.8204	0.1561	0.4153	-3.1769	16.9080	Ripples
C3SE	0.8149	0.1443	0.5456	-3.2803	13.4777	Ripples
C3ND	0.8059	0.1402	0.6509	-3.7083	16.3728	Ripples
C4NI	0.7362	0.1525	0.7047	-3.2709	13.9986	
C2SE	0.7012	0.1922	0.4715	-2.3111	12.8254	
C2MI Sand	0.7003	0.1518	0.7982	-3.0107	11.4731	
C1NA	0.6969	0.1719	0.6040	-2.5796	10.7818	Ripples
C2SN	0.6705	0.1542	0.8524	-3.0673	12.4404	Ripples
C1SA	0.6673	0.1438	1.0769	-3.4645	13.6966	Ripples
C3NF Sand	0.6475	0.1927	0.5863	-2.2586	9.7166	Imbricated/RGB
C2MA	0.6429	0.1596	0.7850	-2.2649	7.2832	Ripples
C2MJ	0.6355	0.1508	1.0215	-3.1912	12.5257	
C2NA	0.6211	0.1471	1.1227	-3.1991	12.0712	Ripples
C3NB	0.5905	0.2140	0.6562	-3.0466	16.9235	
C1NC	0.4204	0.2135	0.9896	-2.4460	9.3660	
C2SG	0.4160	-0.0418	0.7152	-1.3815	4.9744	
C1NE	0.4154	0.2468	0.7906	-1.7422	6.2621	
C2NB Sand	0.2939	-0.0710	0.9086	-1.5491	5.2881	Ripples
C3NE	0.2851	-0.1381	0.8064	-0.9742	3.1955	GB
C4SC Sand	0.2440	-0.0645	1.0168	-1.7514	6.1240	Ripples
C2SK	0.1836	-0.3154	0.7862	-1.1802	4.8230	
C4SF	0.1531	0.1796	1.5044	-1.5760	4.0087	
C1NK	0.0991	-0.2194	1.0607	-1.2533	3.9322	Ripples
C3SJ	0.0722	-0.0195	1.3314	-1.5919	4.5518	
MEAN	**0.6121**					

Table terminology: GB – graded bedding; RGB – inversely graded bedding; Imbricated – imbricated bedding.

Table 2. Cory Grade sieve data for samples 0 to -1 Φ.

SIEVE DATA Cory Grade: 0 to -1 Φ						
Sample	**Mean (Φ)**	**Median (Φ)**	**Std Dev (Φ units)**	**Skewness**	**Kurtosis**	**Sedimentary Structures**
C2S(-B)	-0.0948	0.2173	1.7172	-1.3811	3.2577	
C3SD	-0.0980	0.2143	1.6946	-1.3187	3.1270	Imbricated
C1NG	-0.1119	-0.0928	1.4588	-1.2272	3.3236	
C4ND	-0.1121	-0.3601	1.2304	-1.0511	3.3237	
C3SH	-0.1132	-0.5919	0.9013	-0.4286	2.3561	
C1N(-B)	-0.1241	-0.1975	1.5144	-1.4634	3.8780	
C2NC	-0.1414	-0.4042	1.2605	-1.2184	3.9191	Imbricated
C1SE	-0.2018	-0.4494	1.2806	-1.1484	3.6351	
C2NG	-0.3766	-0.5052	1.4517	-0.7807	2.4490	
C4NJ	-0.7777	-0.5723	1.8895	-0.5230	1.6383	Imbricated
C2SO	-0.8592	-1.1968	1.5701	-0.3594	1.8908	
C4SD	-0.9456	-1.5490	1.5036	-0.1431	1.9037	
MEAN	**-0.3297**					

Table terminology: GB – graded bedding; RGB – inversely graded bedding; Imbricated – imbricated bedding.

Table 3. Cory Grade sieve data for samples -1 to -2 Φ.

SIEVE DATA Cory Grade: -1 to -2 Φ						
Sample	**Mean (Φ)**	**Median (Φ)**	**Std Dev (Φ units)**	**Skewness**	**Kurtosis**	**Sedimentary Structures**
C4NG	-1.1714	-1.5638	1.6715	-0.2321	1.7991	
C4SG	-1.1779	-1.4110	1.9192	-0.1678	1.3861	Imbricated
C2MK	-1.2692	-1.6763	1.7591	-0.1104	1.5840	
C3SK	-1.5012	-1.7738	1.6922	-0.0508	1.6755	Imbricated
C3SF	-1.5759	-2.0853	2.0653	0.0879	1.2225	
C4S(-A)	-1.6773	-2.5019	1.9840	0.1893	1.3166	Imbricated
C2SB	-1.7163	-2.4265	1.7499	0.2912	1.6758	
C4NH	-1.7249	-2.4376	1.7129	0.3241	1.7548	Imbricated
C2SC	-1.7659	-2.6403	1.7932	0.3386	1.6148	Imbricated
C2SJ	-1.8105	-2.5964	1.8555	0.2897	1.4959	Imbricated
C4SE	-1.8358	-2.7534	1.8068	0.4096	1.6574	
C2MC	-1.9053	-2.6714	1.7355	0.4213	1.7679	GB
MEAN	**-1.5943**					

Table terminology: GB – graded bedding; RGB – inversely graded bedding; Imbricated – imbricated bedding.

Table 4. Cory Grade sieve data for samples ≤ -2 Φ.

SIEVE DATA Cory Grade: ≤ -2 Φ						
Sample	**Mean (Φ)**	**Median (Φ)**	**Std Dev (Φ units)**	**Skewness**	**Kurtosis**	**Sedimentary Structures**
C1SF	-2.0050	-2.9202	1.7576	0.5168	1.8066	
C4NA	-2.0389	-3.1547	1.8176	0.4993	1.6653	Imbricated
C2SI	-2.0637	-3.0777	1.7969	0.5107	1.7300	
C4NM	-2.0864	-3.7277	1.9460	0.6025	1.6504	
C3SG	-2.1950	-3.2680	1.7083	0.6281	1.9442	Imbricated
C2MF	-2.2264	-3.1917	1.6463	0.5943	1.9697	
C4NE	-2.2481	-3.5403	1.8708	0.7392	1.8583	Imbricated/GB
C4SA	-2.2504	-3.4959	1.8743	0.7526	1.9041	GB
C3NF Cong	-2.2729	-3.6223	1.7919	0.8379	2.1565	
C2ME	-2.3127	-3.5652	1.7817	0.7803	2.0210	Imbricated
C3SI	-2.3187	-3.4384	1.8354	0.8148	2.0111	Imbricated
C2SL	-2.3427	-3.4252	1.6219	0.8547	2.4088	
C2MH	-2.3610	-3.2400	1.5008	0.8961	2.7357	
C2SM	-2.3937	-3.6859	1.7298	0.9519	2.3957	
C3NI	-2.4813	-3.3312	1.7127	0.9599	2.3289	Imbricated
C2NB Cong	-2.5263	-3.2074	1.7109	1.0366	2.5005	RGB
C3NG	-2.5448	-3.4647	1.6110	1.0792	2.7819	Imbricated/RGB
C2NE	-2.5486	-3.4359	1.6451	1.1275	2.8316	
C2SH	-2.6239	-3.0688	1.6701	1.1894	2.8868	
C4SC Cong	-2.6427	-2.9091	1.7121	1.2046	2.8326	
C4NB	-2.6443	-2.7582	1.7866	1.2065	2.7067	Imbricated
C4NK	-2.6557	-3.4045	1.5435	1.2842	3.3616	Imbricated/GB
C4S(-C)	-2.6648	-2.6472	1.8220	1.2270	2.6806	
C1N(-C)	-2.6845	-2.7519	1.7164	1.2076	2.7526	
C2S(-A)	-2.6880	-2.8563	1.7225	1.3235	3.0980	
C2MI Cong	-2.7768	-2.9995	1.5694	1.5048	3.8613	
C2S(-C)	-2.7830	-2.6507	1.6836	1.4046	3.2698	Imbricated
C3SC	-2.7878	-2.8222	1.6079	1.4550	3.5793	Imbricated
C2SD	-2.8101	-2.7981	1.5668	1.4538	3.6442	
C1NF	-2.8268	-3.1248	1.4247	1.5103	4.1249	
C1SC	-2.8431	-3.0704	1.4109	1.4739	3.9380	
C2MG	-2.8787	-2.6697	1.5939	1.6597	4.1859	
C3NC	-2.8815	-2.4969	1.6869	1.6419	3.9301	Imbricated
C4SB	-2.8998	-2.5527	1.5928	1.6073	3.9365	
C3SA	-2.9254	-2.4622	1.6003	1.6348	3.9884	
C4SH	-2.9424	-2.4705	1.5818	1.6794	4.1435	
C3NA	-3.0065	-2.4701	1.4860	1.8062	4.7256	Imbricated
C4S(-B)	-3.0143	-2.4391	1.5009	1.8361	4.7958	Imbricated/GB

Table terminology: GB – graded bedding; RGB – inversely graded bedding; Imbricated – imbricated bedding.

Table 4. continued.

SIEVE DATA Cory Grade: ≤ -2 Φ						
Sample	**Mean (Φ)**	**Median (Φ)**	**Std Dev (Φ units)**	**Skewness**	**Kurtosis**	**Sedimentary Structures**
C1ND	-3.0149	-2.4778	1.4861	1.8632	4.9370	Imbricated
C2N(-A)	-3.0174	-2.5683	1.4194	1.8413	4.9865	Imbricated
C1SD	-3.0320	-2.5220	1.4174	1.8509	4.9878	
C2ND	-3.0425	-2.6220	1.3426	1.8999	5.4479	
C2SF	-3.0431	-2.6337	1.3217	1.8621	5.3388	
C1NJ	-3.0848	-2.4406	1.3893	1.9844	5.5321	
C1N(-A)	-3.1289	-2.3463	1.3870	2.0958	5.8957	Imbricated
C1NB	-3.1351	-2.4883	1.2790	2.1333	6.4378	
C1NI	-3.3097	-2.2723	1.1143	2.7065	9.4899	
C2M(-A)	-3.3725	-2.1471	1.1388	3.1205	11.4780	Imbricated
C1S(-A)	-3.4643	-2.0581	1.0155	3.6571	15.1794	Imbricated
MEAN	**-2.6907**					

Table terminology: GB – graded bedding; RGB – inversely graded bedding; Imbricated – imbricated bedding.

4.1.2 Hotchkiss Grade

A total of three coarse sand samples (Table 5) were collected at Hotchkiss Grade (Fig. 5). Sample means range from 0.9304 Φ to 0.2188 Φ, with medians ranging from 0.1356 Φ to -0.2160 Φ. Standard deviations range from 0.2633 Φ units to 0.8411 Φ units, and skewness ranges from -4.7105 to -0.9330. The population mean is 0.6606 Φ.

Two very-coarse sand samples were collected (Table 6). Sample means range from -0.6149 Φ to -0.7227 Φ, with medians ranging from -1.1755 Φ to -1.1062 Φ. Standard deviations range from 1.2519 Φ units to 1.4998 Φ units, and skewness ranges from -0.0979 Φ to -0.3030 Φ. The population mean is -0.6688 Φ.

One granule samples was collected (Table 7). The sample/population mean is -1.4811 Φ, with a median of -2.1636 Φ. The standard deviation is 1.4212 Φ units, and a skewness of 0.3206 Φ.

Three samples of pebbles and larger fragments were collected (Table 8). Sample means range from -2.4224 Φ to -3.4274 Φ, with medians ranging from -2.1554 Φ to -3.5010 Φ. Standard deviations range from 1.0021 Φ units to 1.6901 Φ units, and skewness ranges from 0.8933 Φ to 3.4794 Φ. The population mean is -2.8615 Φ.

Fig. 5. Hotchkiss Grade (August 2009).

Table 5. Hotchkiss Grade sieve data for samples ≥ 0 Φ.

SIEVE DATA Hotchkiss Grade: ≥ 0 Φ						
Sample	**Mean (Φ)**	**Median (Φ)**	**Std Dev (Φ units)**	**Skewness**	**Kurtosis**	**Sedimentary Structures**
HB	0.9304	0.1356	0.2633	-4.7105	30.7016	Ripples
HE	0.8326	0.1394	0.6782	-5.5168	35.5259	Ripples
HH	0.2188	-0.2160	0.8411	-0.9330	3.2491	
MEAN	**0.6606**					

Table terminology: GB – graded bedding; RGB – inversely graded bedding; Imbricated – imbricated bedding.

Table 6. Hotchkiss Grade sieve data for samples 0 to -1 Φ.

SIEVE DATA Hotchkiss Grade: 0 to -1 Φ						
Sample	**Mean (Φ)**	**Median (Φ)**	**Std Dev (Φ units)**	**Skewness**	**Kurtosis**	**Sedimentary Structures**
HF	-0.6149	-1.1755	1.2519	-0.0979	1.8351	
HC	-0.7227	-1.1062	1.4998	-0.3030	1.7854	
MEAN	**-0.6688**					

Table terminology: GB – graded bedding; RGB – inversely graded bedding; Imbricated – imbricated bedding.

Table 7. Hotchkiss Grade sieve data for samples -1 to -2 Φ.

SIEVE DATA Hotchkiss Grade: -1 to -2 Φ						
Sample	**Mean (Φ)**	**Median (Φ)**	**Std Dev (Φ units)**	**Skewness**	**Kurtosis**	**Sedimentary Structures**
HG	-1.4811	-2.1636	1.4212	0.3206	2.1298	
MEAN	**-1.4811**					

Table terminology: GB – graded bedding; RGB – inversely graded bedding; Imbricated – imbricated bedding.

Table 8. Hotchkiss Grade sieve data for samples ≤ -2 Φ.

SIEVE DATA Hotchkiss Grade: ≤ -2 Φ						
Sample	**Mean (Φ)**	**Median (Φ)**	**Std Dev (Φ units)**	**Skewness**	**Kurtosis**	**Sedimentary Structures**
HI	-2.4224	-3.5010	1.6844	0.8933	2.3493	
HA	-2.7347	-2.7319	1.6901	1.3329	3.1276	Imbricated
HD	-3.4274	-2.1554	1.0021	3.4794	14.4513	Imbricated
MEAN	**-2.8615**					

Table terminology: GB – graded bedding; RGB – inversely graded bedding; Imbricated – imbricated bedding.

4.1.3 Redlands Mesa Grade

No coarse sand samples were found at this outcrop location (Fig. 6). Two very-coarse sand samples were acquired from Redlands Mesa Grade (Table 9). Sample means range from -0.2771 Φ to -0.5524 Φ, with medians ranging from -0.3497 Φ to -0.9384 Φ. Standard deviations range from 1.4921 Φ units to 1.3771 Φ units, and skewness ranges from -1.0570 Φ to -0.4450 Φ. The population mean is -0.4148 Φ.

Eight granule samples were collected (Table 10). Sample means range from -1.0566 Φ to -1.9857 Φ, with medians ranging from -1.6578 Φ to -2.9937 Φ. Standard deviations range from 1.3811 Φ units to 2.0577 Φ units, and skewness ranges from -0.0941 Φ to 0.6177 Φ. The population mean is -1.5648 Φ.

Two samples of pebbles and larger fragments were collected (Table 11). Sample means range from -2.1529 Φ to -2.1810 Φ, with medians ranging from -3.4789 Φ to -3.5545 Φ. Standard deviations range from 1.9866 Φ units to 1.8970 Φ units, and skewness ranges from 0.6774 Φ to 0.6595 Φ. The population mean is -2.1670 Φ.

Fig. 6. Redlands Mesa Grade (August 2009).

Table 9. Redlands Mesa Grade sieve data for samples 0 to -1 Φ.

SIEVE DATA Redlands Mesa Grade: 0 to -1 Φ						
Sample	**Mean (Φ)**	**Median (Φ)**	**Std Dev (Φ units)**	**Skewness**	**Kurtosis**	**Sedimentary Structures**
RMG	-0.2771	-0.3497	1.4921	-1.0570	3.0020	Ripples
RML	-0.5524	-0.9384	1.3771	-0.4450	2.1039	RGB
MEAN	**-0.4148**					

Table terminology: GB – graded bedding; RGB – inversely graded bedding; Imbricated – imbricated bedding.

Table 10. Redlands Mesa Grade sieve data for samples -1 to -2 Φ.

SIEVE DATA Redlands Mesa Grade: -1 to -2 Φ						
Sample	**Mean (Φ)**	**Median (Φ)**	**Std Dev (Φ units)**	**Skewness**	**Kurtosis**	**Sedimentary Structures**
RME	-1.0566	-1.6578	1.5665	-0.0941	1.7990	
RMH	-1.0631	-1.8486	1.3811	0.2282	1.8384	
RMF	-1.4736	-1.8775	1.9758	0.0280	1.3249	Imbricated
RMK	-1.5917	-2.3725	2.0350	0.1526	1.2826	
RMJ	-1.6350	-2.3126	1.7140	0.2541	1.7258	
RMB	-1.8228	-3.2576	2.0577	0.3592	1.3411	
RMC	-1.8896	-2.7063	1.8017	0.4105	1.6727	Imbricated
RMI	-1.9857	-2.9937	1.6846	0.6177	1.9908	
MEAN	**-1.5648**					

Table terminology: GB – graded bedding; RGB – inversely graded bedding; Imbricated – imbricated bedding.

Table 11. Redlands Mesa Grade sieve data for samples ≤ -2 Φ.

SIEVE DATA Redlands Mesa Grade: ≤ -2 Φ						
Sample	**Mean (Φ)**	**Median (Φ)**	**Std Dev (Φ units)**	**Skewness**	**Kurtosis**	**Sedimentary Structures**
RMD	-2.1529	-3.4789	1.9866	0.6774	1.6879	Imbricated
RMA	-2.1810	-3.5545	1.8970	0.6595	1.7544	
MEAN	**-2.1670**					

Table terminology: GB – graded bedding; RGB – inversely graded bedding; Imbricated – imbricated bedding.

4.2 Clast Composition

Clasts that are granule and larger are almost exclusively composed of basalt (~95%). The remaining clasts (~5%) are brightly colored cherts, quartzites, and felsic to intermediate igneous rocks. Cohesive clay clasts ranging in size from very-coarse sand to cobble were found throughout the stata. Vesicular and massive basalt occurs in approximately equal amounts.

Fine-grained units ($\geq 0\ \Phi$) are composed of a mixture of basalt and quartz sand. As sediments decrease in size from very-coarse sand, the fraction of quartz present in the sample increases (~50%). As the sediments increase in size to very-coarse sand, the basalt content increases (~90%). The change in clast composition from quartz to basalt occurs between coarse sand and very-coarse sand.

4.3 Sedimentary Structures

Several sedimentary structures and bed forms were observed in the units of the outcrops. The most common structures were cross-bedding (trough cross-bedding and varying degrees of cross-lamination), laminated bedding (sand, granule, and pebble grain-size), graded bedding, para- and orthoconglomerates, imbricated bedding, low sinuosity channel deposits, and ice rafted clasts.

Orthoconglomerates and paraconglomerates (Fig. 7a, 7b) are two categories of conglomerates based on sorting and whether they are grain- or matrix-supported (Pettijohn, 1975; Collinson and Thompson, 1982). Orthoconglomerates are clast-supported with a bimodal to polymodal grain distribution, and have an open to filled matrix framework (Collinson and Thompson, 1982). Orthoconglomerates are created by

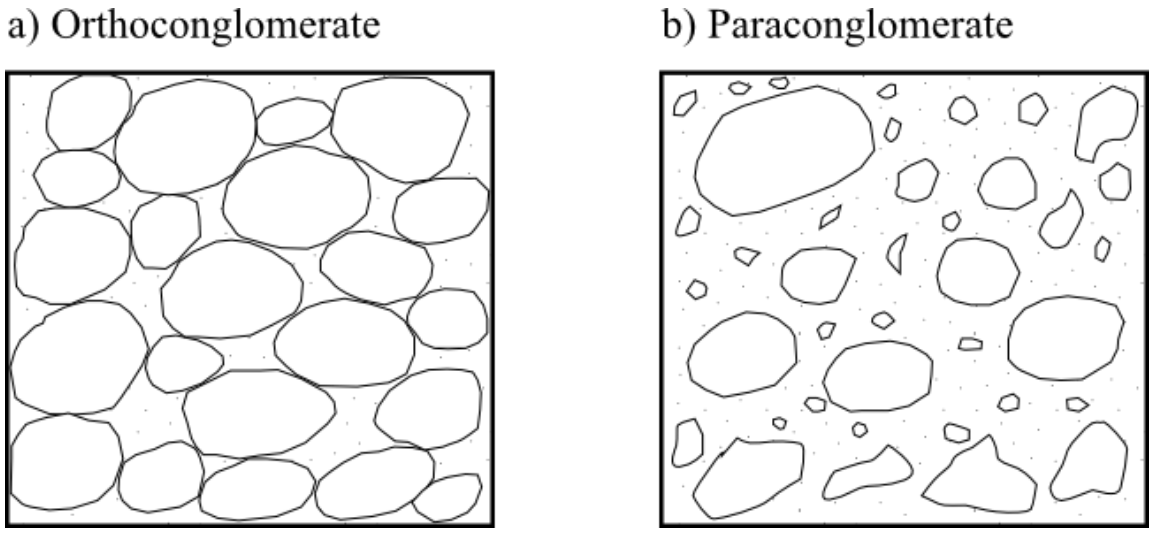

Fig. 7. Diagram adapted from Collinson and Thompson (1982) depicting the difference between clast-supported and matrix-supported conglomerates. (a) Orthoconglomerate; (b) Paraconglomerate

high-velocity stream deposition, and can be further divided into two groups: orthoquartzitic conglomerates, composed primarily of quartz and chert; and metastable rock fragment conglomerates composed of rock fragments (Pettijohn, 1975).

Ripples and cross-bedding occur predominantly in coarse-grained sand, with only one example in very-coarse sand. Trough cross-bedding occurs at Cory Grade, Redlands Mesa Grade, and Hotchkiss Grade in coarse to very-coarse sand beds.

Laminated granule lag beds occur within strata with sand-grain sizes. Laminated granule beds occur above finer-grained units containing trough cross-bedding, and below grain-supported conglomerates. Sand laminations were found in some strata, but no pebbles were present.

Graded bedding in coarse-grained units occurs at Cory Grade, Hotchkiss Grade, and Redlands Mesa Grade. Many grain-supported conglomerate deposits are graded whereas matrix-supported conglomerate deposits are not. Three beds, exhibiting

inversely graded bedding, were observed in the outcrops; most likely an indication of sediments being reworked by the ancestral Gunnison River.

Two forms of conglomerates occur in the study area; orthoconglomerates and paraconglomerates. Orthoconglomerates are grain-supported with grain-sizes ranging from granule to boulder. Paraconglomerates are matrix-supported with 10 to 20% clasts. Clasts vary in size from very-coarse sand to boulder.

Imbricated bedding occurs in orthoconglomerate deposits with grain-sizes ranging from granule to boulder. Five examples of imbrication were identified in coarse to very-coarse sand units. Orientation of imbrication in beds ranging from granule to boulder indicates fluid flow directed from the mesa. No imbrication occurs in any of the paraconglomerate deposits.

Channelized deposits occur at Cory Grade, Hotchkiss Grade, and Redlands Mesa Grade as sand and gravel lenses of varying thicknesses. Channelized deposits appear to be oriented with a flow direction approximately perpendicular to the orientation of the outcrops.

Ice-rafted clasts are found at Cory Grade, Redlands Mesa Grade, and Hotchkiss Grade. Clasts are massive and/or vesicular basalt, and are found in finer-grained units randomly throughout each outcrop. Ice-rafted deposits are found within beds ranging from fine sand to cobble grain-size.

4.4 Photographic Comparison

Published photographs of sedimentary structures were located in the literature (Reineck and Singh, 1973; Eyles and Miall, 1984; Nemec and Steel, 1984; Brodzikowski

and van Loon, 1991; Collinson, 2006; Miller, 2006) for comparative analysis to accurately identify structures in the thesis area. Examples include trough cross-bedding, imbricated bedding, orthoconglomerates, paraconglomerates, and channel deposits.

5. DISCUSSION

The following series of questions were posed to form interpretations of the geomorphic evolution of the area: (1) do common characteristics exist in units that can be used to correlate strata; (2) does the unifying characteristic tie the samples to a specific depositional environment; (3) what are the majority of the grains within the deposits composed of; (4) do sedimentary structures within the beds indicate paleocurrent directions; (5) do previously published and described photographs match outcrop photographs from this study? To answer the questions of this study, assumptions were made based on field observations and photographs.

5.1 Analysis of Grain-Size

A program from Balsillie and others (2002) was used to calculate simple statistics (mean, median, standard deviation, skewness, and kurtosis) for each sample. Samples were divided into four categories based on mean grain-size; ≥ 0 Φ, 0 to -1 Φ, -1 to -2 Φ, and $\leq$ -2 Φ. Based on Hjulstrom's Diagram, it is assumed that the two finest grain-size categories in the study area are a result of low to medium flow regimes, deposited during calm conditions experiencing little to no glacial outburst flooding. The two coarser grain-size categories are a result of medium to high flow regimes, deposited during suggested glacial outburst floods. Using grain-size analysis and sedimentary-structure analysis, a series of five facies were deposited in the study area. A detailed discussion of facies in the study area will follow (see section 5.5 Facies Analysis).

5.2 Clast Composition

A large fraction (~95%) of clasts within the granule or larger deposits are composed of a mix of vesicular and massive basalt. Note, the only source for basalt in the area is from the Tertiary basalt cap covering Grand Mesa. As the ice cap that once covered Grand Mesa began to recede, melt-water transported basalt clasts down the southern flanks of the mesa to the present locations.

The sand-size deposits contain two major components; basalt and quartz. The finer the sand, the richer it is in quartz; whereas the coarser it is, the richer it is in basalt. The change in clast composition from quartz to basalt occurs between coarse and very-coarse sand. The deposits that have a mixture of quartz and basalt are more than likely a product of outwash from the mesa because of the source of the basalt. If sand was composed of pure quartz, it was likely a deposit that was either deposited or reworked by the ancestral Gunnison River and was not likely a result of glacial outwash.

A large abundance of cohesive clay clasts are likely the result of the underlying Mancos Shale being ripped up and transported during times of glacial outwash. Multiple sizes of clasts were found ranging from very-coarse sand to cobble. The finer clasts occur in the very-coarse sand units whereas the granule and larger clasts are found in the coarse-grained conglomerate units. Also, it could be argued that the fine-grained material was deposited after flooding and then subsequently re-worked by the next flooding event. Additional study needs to be undertaken to determine the source of the sediment that forms these cohesive clay clasts.

Other exotic clasts occur in sparse amounts randomly distributed throughout all the units. Exotic clasts range from brightly colored granule to pebble-size chert, quartzite, and felsic to intermediate extrusive igneous rocks. The igneous clasts occur in the same conglomerate deposits that were dominated by basalt (Fig. 8); therefore, it is hypothesized that the source area is the top of the mesa. Unfortunately, the source of the chert is unknown.

Fig. 8. Exotic clasts (felsic igneous rocks and chert) surrounded by basalt clasts at Cory Grade (August 2009).

5.3 Sedimentary Structures

Structures include cross-bedding, laminations, graded and inversely graded bedding, imbricated bedding, and channel deposits. The sedimentary structures in this study provide further evidence that the dominant environment of deposition was glacio-fluvial outwash from the Grand Mesa ice cap. Cross-bedding and laminated bedding structures indicate high rates of flow, as well as imbrications indicating flow from Grand Mesa. The dominant depositional environment is presumed to have been very similar to a present-day braided fluvial/braidplain environment (Miller, 2006).

5.3.1 Cross Bedding

Several forms of cross-bedding occur in these units. Trough cross-bedding (Fig. 9) is the most commonly identified form of cross-bedding, and occurs only in coarse to very-coarse sand deposits at Gory Grade, Redlands Mesa Grade, and Hotchkiss Grade. Ripples indicate bimodal flow and are associated with a medium- to high-energy fluvial environment.

Complex cross-bedding with larger wave heights than other outcrops occur at Redlands Mesa Grade (Fig. 10). These structures formed under conditions with high sediment input and rapid sedimentation to preserve the structures. Note, a glacio-fluvial outwash is the likely environment of deposition.

Fig. 9. Trough cross-bedding at Cory Grade (August 2009).

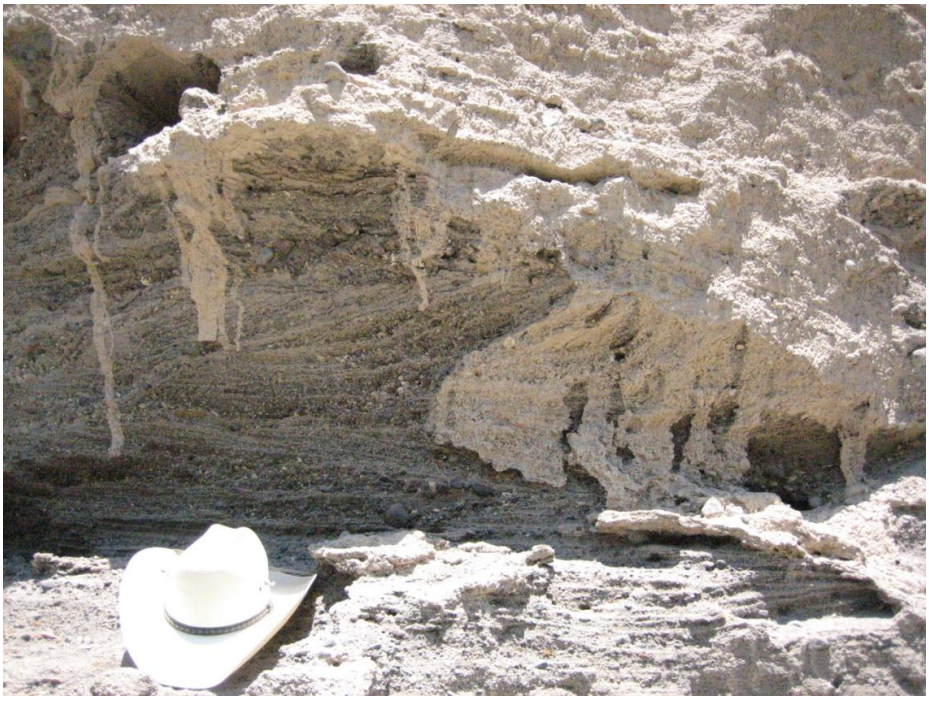

Fig. 10. Complex cross-bedding at Redlands Mesa Grade (August 2009).

5.3.2 Laminations

Laminations occur at Cory Grade, Redlands Mesa Grade and Hotchkiss Grade. Sand laminations (Fig. 11) and pebble laminations (Fig. 12) were identified at all outcrop locations. It is assumed that pebble laminae (Fig. 12) formed during times of over bank flooding. Laminae were deposited on top of trough cross-beds (Fig. 13). A horizontal contact (Fig. 13) forms the boundary between these two structures, and it is assumed to indicate a change in flow from normal to flood stage. The horizontal contact between the two structures indicates an increase in flow velocity, which is assumed to have eroded the trough cross-beds to a flat contact. It is assumed that if no change in flow regime occurred, the contact would follow the top of the underlying ripple structures rather than erode it to near horizontal.

Laminations also were formed in several of the sand beds (Fig. 11). Many sand laminae were visible because of iron oxide staining (Fig. 8, 11). Sand laminations occur in grain-sizes $\geq 0\ \Phi$, and are assumed to be the result of high rates of flow.

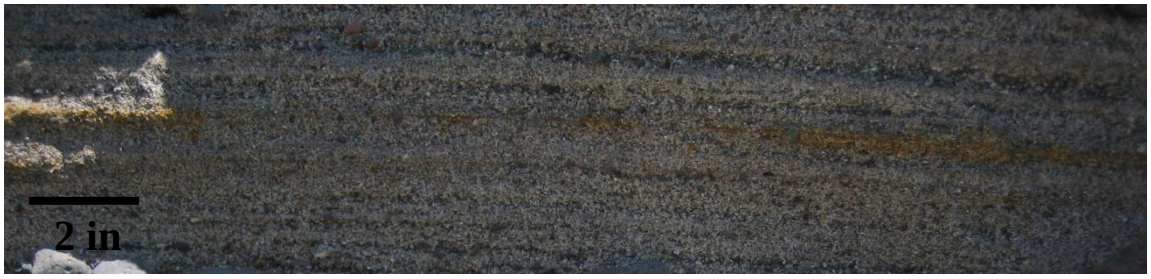

Fig. 11. Sand laminations at Cory Grade (August 2009).

Fig. 12. Pebble laminations at Cory Grade (August 2009).

Fig.13. Near horizontal contact between lower trough cross-beds and upper laminated bedding (August 2009).

5.3.3 Graded/Inversely Graded Bedding

Graded bedding occurs in many of the pebble and larger grain-size beds. Graded bedding occurs in braided fluvial environments if the deposit has not been reworked by another system (Reineck and Singh, 1973; Miller, 2006). Four inversely graded beds were identified at Cory Grade and Redlands Mesa Grade. These units were likely reworked by the ancestral Gunnison River, removing fine-grained material, creating voids between clasts resulting in collapse of the conglomerate structure and the formation of inverse grain arrangements.

5.3.4 Conglomerates

A majority of the conglomerate units within the study area are orthoconglomerates (Fig. 7a). Orthoconglomerates had a polymodal grain distribution with a poorly-sorted matrix framework composed of silt to sand. Crude stratification is apparent in most units. It is assumed that a high-velocity braided fluvial/braidplain system fed by the glacial melt was responsible for the deposition of these deposits. It should be noted that unimodal orthoconglomerates were found, however, not in a high percentage. It is assumed that orthoconglomerates were initially deposited with no fine-grained matrix because flow velocities were too high to allow deposition of fines. After deposition of the coarse-grained clasts, flow velocities subsided, and fine-grained (mud to sand) matrix material was deposited. All conglomerates in the study area had a filled matrix.

Paraconglomerates (Fig. 7b) are matrix-supported, and very poorly sorted, with a highly variable grain-size distribution. In most instances, paraconglomerates are composed of 80 to 90% mud matrix and 10 to 20% clasts (Pettijohn, 1975). The literature describes several forms of paraconglomerates; glacial till, tillite, laminated pebbly mudstone, and muddy-silty high viscosity flows (Pettijohn, 1975; Collinson and Thompson, 1982).

Paraconglomerates in the study area are muddy-silty, high-viscosity flows, or debris flows (Fig. 7b). It is suggested that the debris flows in the area are the result of outburst floods that supersaturated the southern flanks of the mesa and led to the failure

of large slump blocks. This activity resulted in muddy-silty slurries of entrained grains that ranged from sand up to boulder sizes flowing down the flanks of Grand Mesa.

5.3.5 Grain Imbrication

Grain imbrication occurs at Cory Grade, Hotchkiss Grade, and Redlands Mesa Grade (Fig. 14). Imbrications formed in grain-sizes ranging from very-coarse sand to boulders. Most coarse-grained (pebble and larger) units had crude imbrication throughout the entire extent of the units. Excellent examples of imbrications were seen in small amounts, usually with 5 to 10 clasts imbricated within a finer-grained matrix (Fig. 14). Study of the imbricated clasts at the study sites showed a preferred orientation direction from north-northeast to north-northwest. The imbrication suggests flows (paleocurrents) (Fig. 15) from Grand Mesa towards the present day Gunnison River (Cory Grade: S25W; Redlands Mesa Grade: S25W; Hotchkiss Grade: S40E). Figure 15 shows rose diagrams that correspond to three outcrops where grain imbrications were located (29 at Cory Grade, 3 at Redlands Mesa Grade, and 2 at Hotchkiss Grade).

Further study of these deposits revealed no imbrications with paleocurrent direction parallel to the paleoflow direction of the ancestral Gunnison River. Thus, one can conclude if these deposits were the product of Gunnison River deposition, the imbrications would indicate a flow direction from east to west, and not north-northeast, in the direction from Grand Mesa.

Fig. 14. Grain imbrication in a granule to pebble bed at Cory Grade (August 2009).

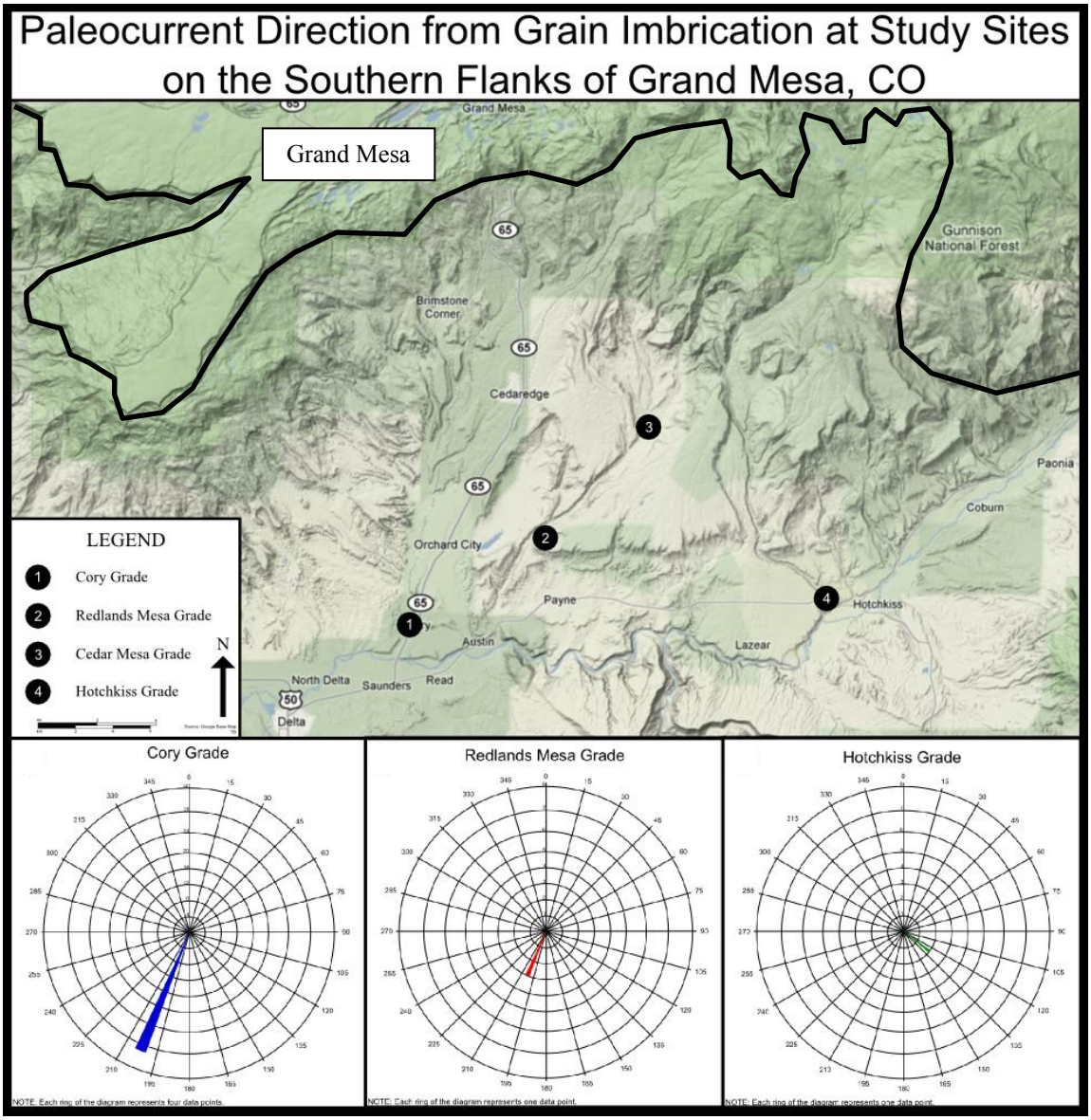

Figure 15. Study site map with rose diagrams indicating paleocurrent flow direction from grain imbrication.

5.3.6 Channel Deposits

Channel deposits were located at Cory Grade, Hotchkiss Grade, and Redlands Mesa Grade (Fig. 16). Mapping of these deposits show the channels to be approximately normal to the face of the outcrops. These deposits, composed of sand to cobble sized clasts, are almost entirely basalt. Water flow coming off of Grand Mesa during times of melting is assumed to have looked similar to a highly braided fluvial system, or braidplain environment. Because of the nature of this type of environment, channels were temporary, and changed course frequently. Thus, it can be assumed that these channel deposits are a result of the fluvial system that carried the outwash material from Grand Mesa.

Fig. 16. Cross-section through a channel deposit at Cory Grade (August 2009).

5.3.7 Ice-Rafted Clasts

Ice-rafted clasts (Fig. 17) are located at Cory Grade, Redlands Mesa Grade, and Hotchkiss Grade. The grain-size of these clasts ranges from cobble to boulder, and are composed of massive and vesicular basalt. As one can see in figure 17, these clasts were randomly deposited in the outcrop. Ice-rafted clasts were deposited by clast-carrying ice, which cleaved off of the ice cap, was carried down the mesa by outwash streams and deposited en masse, or carried in high velocity flows, and then deposited within fine-grained material. After deposition of the ice, melting occurred, releasing any sediment that it carried (Miller, 2006). Figure 17 shows three examples of ice-rafted clasts ranging from ~0.3 to 1 m (~1 to 3.3 ft) in diameter deposited within units of much finer-grained (coarse sand to pebble) material.

Fig. 17. Ice-rafted clasts at Cory Grade (August 2009).

5.4 Photographic Comparison

Sedimentary structures were photographed and documented in the field. A literature search was performed to locate other similarly identified structures in fluvial and glacio-fluvial environments. Examples of trough cross-bedding, imbrication, channel deposits, orthoconglomerates and paraconglomerates were positively identified with published diagrams and photographs from various authors (Reineck and Singh, 1973; Nemec and Steel, 1984; Brodzikowski and van Loon, 1991; Collinson, 2006; Miller, 2006).

5.5 Analysis of Facies

Glacio-fluvial deposits can be divided into three zones (i.e., proximal, intermediate, distal) based primarily on the distance from the source area, which in turn affects the grain-size and sedimentary structures in the deposits. Proximal and intermediate zone facies were identified in the study area, whereas distal facies were not in the study area. In this model, water is confined to a few channels in the proximal zone. Deposits in the proximal zone are generally gravels to boulders and may contain crude horizontal bedding, and have little to no fine-grained deposits (Miller, 2006). Mapping in the field showed gravels, and associated sedimentary structures such as crude horizontal bedding and imbrications, all pointing to a proximal glacio-fluvial facies.

Miller (2006) suggests that the proximal zone can merge into the intermediate zone. The intermediate zone is characterized by distinctly braided, complex networks of wide, shallow channels that frequently shift their boundaries. This zone is composed of

finer-grained (sand) deposits, with trough cross-beds, horizontal laminations, cross-laminations, and ripple-drift structures (Miller, 2006). Mapping in the field showed coarse to very-coarse sand units, and associated sedimentary structures such as trough cross-bedding and laminations, all pointing to an intermediate glacio-fluvial facies.

The distal zone is characterized by shallow flow in well defined channels and can merge into sheet flow during times of flooding. Grain-size in the distal zone is primarily silt to sand and contains a large portion of cross-bedding and laminated structures. Clast size and gradient decreases downstream as the zone transitions from proximal to distal (Miller, 2006).

Analysis of glacio-fluvial deposits was used to suggest five distinct glacio-fluvial facies in the study area. These facies will be discussed in greater detail in sections 5.5.1 through 5.5.5. It is suggested that slow melting of the ice cap created the melt-water, which subsequently created the outwash flows, leading to the deposition of fine-grained fluvial deposits with interspersed slack water or lacustrine facies. During climatic warming, rapid melting of the ice and high rates of discharge created deposits that are comparable to coarse-grained braided fluvial/braidplain facies (Miller, 2006). Interspersed, massively bedded, matrix-supported debris flow deposits also were identified (Fig. 18). Debris flow deposits do not fit into a predictive depositional sequence because of the highly irregular nature of deposition. Lithofacies are described using definitions by Miall (1977, 1978).

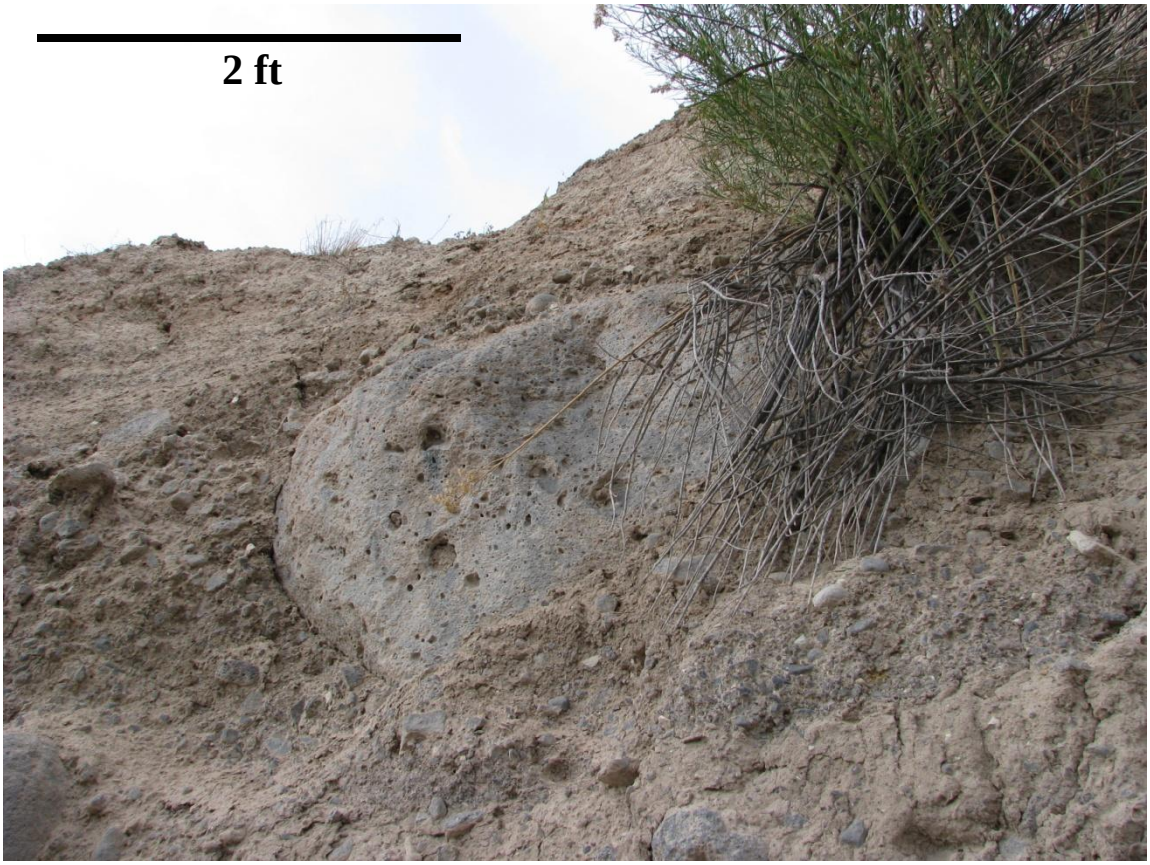

Fig. 18. Massively bedded, matrix-supported debris flow deposit at Hotchkiss Grade (August 2009).

After identification of the five facies, a depositional sequence was constructed based on grain-size analysis data, and photographic analysis. Careful examination of the deposits suggest that because erosional surfaces (Fig. 19) bound the upper and lower contacts of most strata in the study area, original depositional thicknesses may not be present in the outcrops. It is assumed that because of high-energy, coarse-grained, glacio-fluvial outwash, many underlying fine-grained deposits were scoured away during deposition of overlying coarse-grained alluvium, creating erosional surfaces (Miller, 2006). Evidence of scour can be seen in figure 19, where each unit is bounded by highly irregular erosional surfaces. Erosional surfaces border both the top and

bottom, indicating missing section. For the purpose of a complete stratigraphic sequence, an unknown number of fine-grained, over-bank deposits are assumed to have been scoured away by the overriding coarse-grained material. The validity of this assumption is strengthened by the removal of the underlying fine-grained material (silt to sand) by high velocity, coarse-grained material (pebble to boulder) during times of glacial outburst flooding.

Fig. 19. Erosional surfaces bounding both the top and bottom of units at Cory Grade (August 2009).

5.5.1 Facies Fl: Laminated Sand, Silt, Mud

Facies Fl encompasses all fine-grained deposits that are formed in an overbank flood environment as overbank or waning flood deposits (Miall, 1977). Fine laminations and ripples may be present. In the study area, this facies is assumed to be deposited during times of low-energy water flows, which allowed fine-grained material to be deposited in low-energy environments, similar to a lacustrine setting or overbank sheet flow/floodplain. This facies was likely deposited following outburst floods, when flow regimes were significantly reduced, allowing fine-grained material to settle out on the floodplain of the initial channels.

The best examples of Fl are found at Cory Grade and Hotchkiss Grade. No Fl deposits were observed at Redlands Mesa Grade, likely a result of scour during the deposition of overlying coarse-grained deposits, and channelized flow restricting sinuosity and increasing rates of flow; therefore, increasing erosion. No complete examples of Fl were identified because of scouring; thus, accurate stratigraphic thickness of this facies is unknown. Measured outcrop thicknesses of Fl range from ~2 to 30 cm (~1 to 12 in.). The top and bottom of Fl are bounded by erosional surfaces; therefore, measured outcrop thicknesses are not representative of original depositional thicknesses. Grain-sizes range from coarse silt to fine sand, with bedding varying from massive to finely laminated, with some laminations containing ripples.

5.5.2 Facies Str: Trough Cross-Bedded/Ripple Cross-Laminated Sand

For the purpose of this study, facies St and Sr are grouped together and renamed as Str. Facies Str lies unconformably above Fl (Fig. 13). Str has grain-sizes ranging

from very-fine to very-coarse sand with the common presence of granules. According to Miall (1977), sedimentary structures in this facies include trough cross-bedding, planar cross-bedding and climbing ripples. It is assumed that deposits were formed in a braided river environment, with low rates of flow transitioning to high rates of flow, influenced by climatic warming and significant melting of the Grand Mesa ice cap.

Examples of Str are found at Cory Grade, Hotchkiss Grade, and Redlands Mesa Grade. Grain-sizes range from very-fine to very-coarse sand, with the presence of some granules. Str at Redlands Mesa Grade was noticeably coarser-grained than Cory Grade and Hotchkiss Grade, possibly because of its closer location to the source. Trough cross-bedding (Fig. 20) and planar cross-bedding (Fig. 21) are prevalent at all three outcrops. According to Miall (1977), climbing ripples may be present in Str; however, none were observed in the field.

The base of this unit is bounded by a highly irregular erosional contact (Fig. 13), whereas the top of the unit is marked by a near horizontal erosional contact (Fig. 13). The highly irregular erosional contact with underlying Fl is probably a result of scour from increased grain-sizes and rates of flow associated with the deposition of Str. Unit thicknesses range from ~10 to 150 cm (~4 to 60 in). Field observations showed that units that contain sets of trough cross-bedding tended to be thicker within the facies than those without.

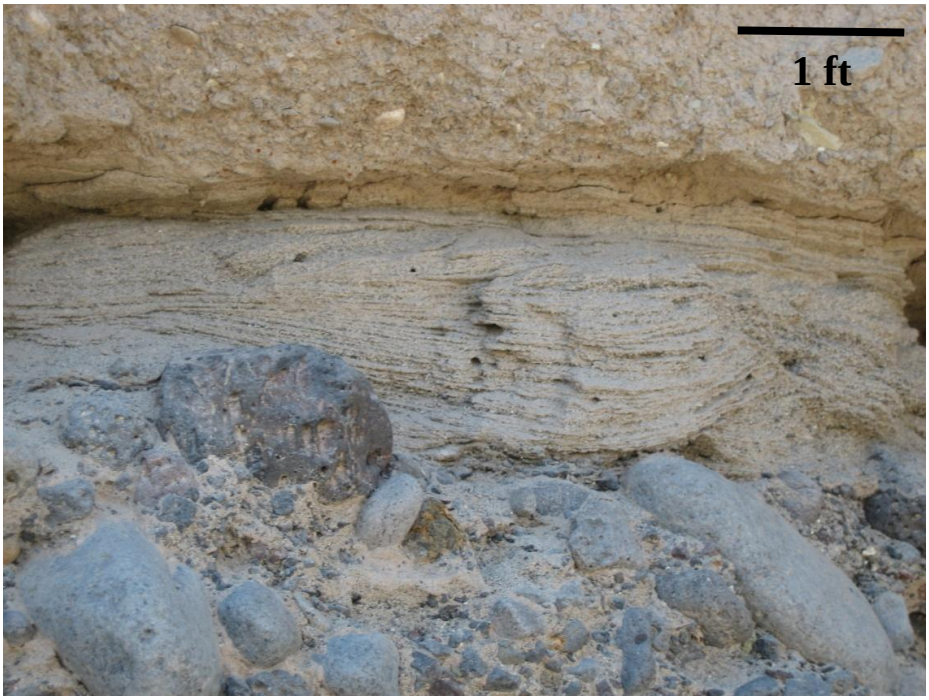

Fig. 20. Trough cross-bedding of Str at Hotchkiss Grade (August 2009).

Fig. 21. Planar cross-bedding of Str at Redlands Mesa Grade (August 2009).

5.5.3 Facies Sh: Horizontally Bedded Sand

Observation of the three outcrops shows that facies Sh lies unconformably above Str (Fig. 13). According to Miall (1977, 1978), bedding of Sh is massive to laminated, with grain-sizes ranging from very-fine to very-coarse sand, with the possible presence of granules. Sh is interpreted to have formed under planar bed flow conditions with medium to high rates of flow.

Sh occurs at all three outcrop locations. Deposition is thought to be the result of an increase in water flowing from the mesa; however, peak flow from the melting ice cap probably had not been reached. Grain-sizes in the study area range from very-fine to very-coarse sand, with some granules. Examination of figures 22 and 23 shows that laminations were present in most units; however, some bedding is massive. Bed thicknesses range from ~10 to 60 cm (~4 to 24 in.).

The contact between laminated Sh and cross-bedded Str is nearly horizontal (Fig. 23), and this contact is thought to mark a flood between normal flow and flood stage flow. If this boundary was not the marker between a normal flow and flood flow, then the contact would have followed the top of the trough cross-bedding in Str, rather than eroding a near horizontal contact through the bedform. A highly irregular erosional boundary marks the top of Sh and suggests that there is missing section that has been scoured away by overriding deposits.

Fig. 22. Laminated bedding of Sh at Redlands Mesa Grade (August 2009).

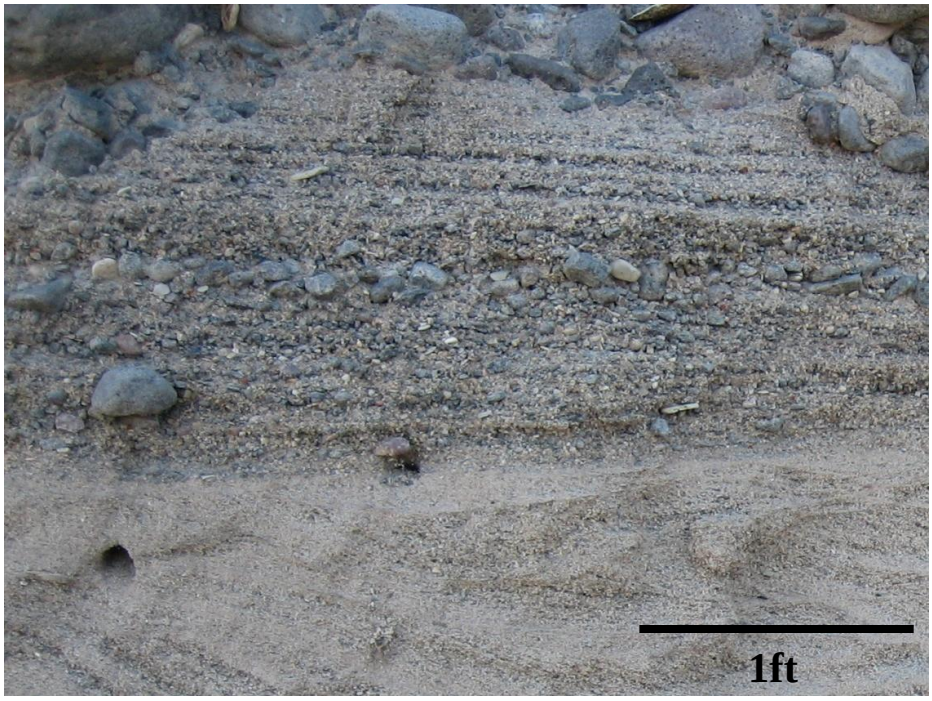

Fig. 23. Near horizontal contact between Str and Sh at Cory Grade (August 2009).

5.5.4 Facies Gm: Massive or Crudely Bedded Gravel

Facies Gm lies unconformably above Sh (Fig. 22). Clast grain-sizes range from granule to boulder, with faint horizontal bedding present in some locations. Deposits are commonly orthoconglomerates (Fig. 24), with a silty-sandy matrix likely deposited in the open matrix framework after deposition of the gravel clasts. Interpretation of this sequence suggests that Gm is probably a flood deposit resulting from glacial outburst melting. Arrows identifying flooding sequences are shown in figure 24. Coarse-grained material is at the base and fines upward, as flooding waned. Bedding structures include imbrication and interbedded lenses of fine-grained material.

Field mapping of the three outcrops shows Gm is in all three outcrops, and comprises the largest portion of each outcrop (~50%). It is assumed that deposition of Gm is from glacial outburst flooding during peak climatic warming, with grain-sizes ranging from granule to boulder.

Study of figures 24 and 25 shows that horizontal bedding of Gm is crude. Most of the units show massive bedding. Grain imbrication (Fig. 25) and interbedded sand lenses occur at all outcrops. Gm is composed entirely of orthoconglomerates, with a sand matrix. Bed thicknesses range from ~0.5 to 4 m (~1.6 to 13 feet). Field examination (Fig. 13) suggests that the lower contact with Sh is a highly irregular erosional contact.

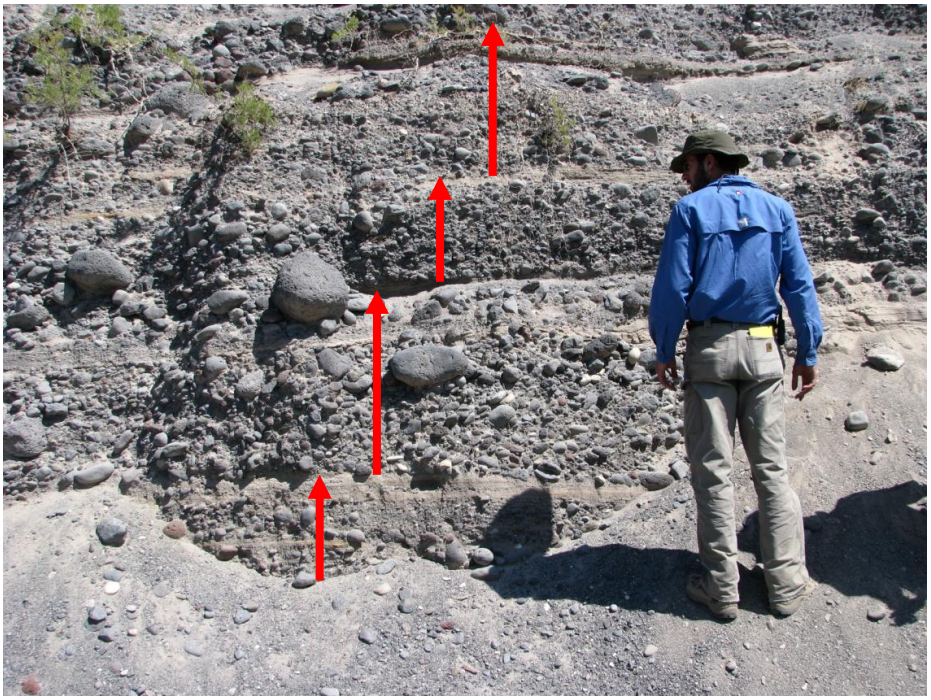

Fig. 24. Orthoconglomerate of Gm at Cory Grade showing flood cycles (flood cycles depicted by arrows) (August 2009).

Fig. 25. Imbrication in Gm at Cory Grade (August 2009).

5.5.5 Facies Gms: Massive Matrix-supported Gravel

The interpretation of Gms is based on Rust's (1978) description of these type facies. Thus, examination of figure 26 shows a matrix-supported, very-coarse sand to boulder conglomerate that is very poorly sorted, and has no sedimentary structures or bedforms. The matrix ranges from mud to very-fine sand, and is assumed to be deposited syn-depositionaly with the clasts. It is assumed that Gms formed by debris flow processes.

Gms facies are found at all three outcrops; however, the facies does not have a specific placement in the depositional sequence because of the irregular nature of debris flows. It is assumed that debris flows occurred when soils became super-saturated with melt-water, and "flowed" down the flanks of Grand Mesa. The flow transported clasts of all sizes from the upper slopes of the mesa.

Field mapping showed no sedimentary structures or bedforms to occur in Gms. Unit thicknesses ranged from ~0.1 to 1.0 m (~0.3 to 3.3 ft) at Cory Grade and Redlands Mesa Grade, respectively. Hotchkiss Grade contained one example of Gms that is ~3 to 4 m (~10 to 13 ft).

Each outcrop appeared to have a large Gms deposit that constituted the top ~3 to 4 m (~10 to 13 ft) of the outcrop. Samples were not collected at Cedar Mesa Grade because permission from the land owner was not granted; however, photographic analysis suggests that Cedar Mesa Grade is composed of many Gms deposits.

Fig. 26. Paraconglomerate of Gms at Cedar Mesa Grade (August 2009).

5.6 Stratigraphic Sequence

A stratigraphic sequence was constructed based on the five facies that were identified at the study sites. Four (Fl, Str, Sh, and Gm) appear to follow a repeatable vertical succession in the outcrops, a result of multiple melting events. The fifth facies, Gms, repeats; however, because of the irregular nature of debris flows, no repeatability occurs in the vertical succession of deposits. Each vertical succession of repeating facies is believed to be an individual flood. Table 12 (adapted from Miall; 1977, 1978) gives a brief description of each facies present in the study area.

The highly variable vertical distribution of grain-sizes, varying sedimentary structures, and abundant scour surfaces are evidence for highly fluctuating discharge rates (Miller, 2006). During times of outburst flooding, deposition is thought to

resemble a present day high-energy braided fluvial or braidplain system (Miller, 2006). According to various authors (Eyles and Miall, 1984; Nemec and Steel, 1984; Rust and Koster, 1984; Miller, 2006), a braided fluvial/braidplain depositional system would deposit a fining upward sequence (coarse gravels to boulders fining to very-fine sands and silts) in the geologic record, if erosion was not a factor.

Table 12. Summary of facies in the study area.

Facies Identifier	Lithofacies	Sedimentary Structures	Interpretation
Gms	massive, matrix supported gravel	none	debris flow deposits
Gm	gravel, massive or crudely bedded, minor sand, silt, or clay lenses	grain imbrication, gravel cross-beds, ripple marks in fine grained lenses	glacial outburst flood deposits
St	very fine to very coarse sand, may contain granules	trough cross-beds, planar cross-beds	braided river deposits, low to medium flow regime
Sr	very fine to very coarse sand	ripple marks of all kinds, including climbing ripples	braided river deposits, low to medium flow regime
Sh	very fine to very coarse sand, may contain granules	horizontal lamination	boundary between normal braided river flow regimes and glacial outburst flow regimes
Fl	very fine sand, silt, mud, interbedded	massive bedding, possible laminations and faint ripples	over bank waning flood deposits

*** Table adapted from Miall (1977, 1978).**

An idealized sequence, based on a braided fluvial, fining upward sequence experiencing no erosion, was constructed (Fig. 27). The idealized sequence in figure 27 represents the five repeatable facies (Fl, Str, Sh, Gm, Gms) from the study area in the assumed depositional relationship. Figure 27 shows Gms at the base of the sequence. Above Gms is Gm, fining upward into Sh, Str, and then Fl, respectively. It is highly possible that other units (most likely fines) were deposited above Fl, and subsequently eroded and are not present in the outcrops. The idealized sequence was not measured because depositional thicknesses are unknown. Because of the lateral discontinuity of these deposits (Fig. 28), these units are not able to be correlated. Very few units extend continuously for more than ~100 m (~330 ft), with most only extending ~10 to 20 m (~35 to 65 ft). Note that the lateral discontinuity is considered a result of braidplain deposition, with multiple channels.

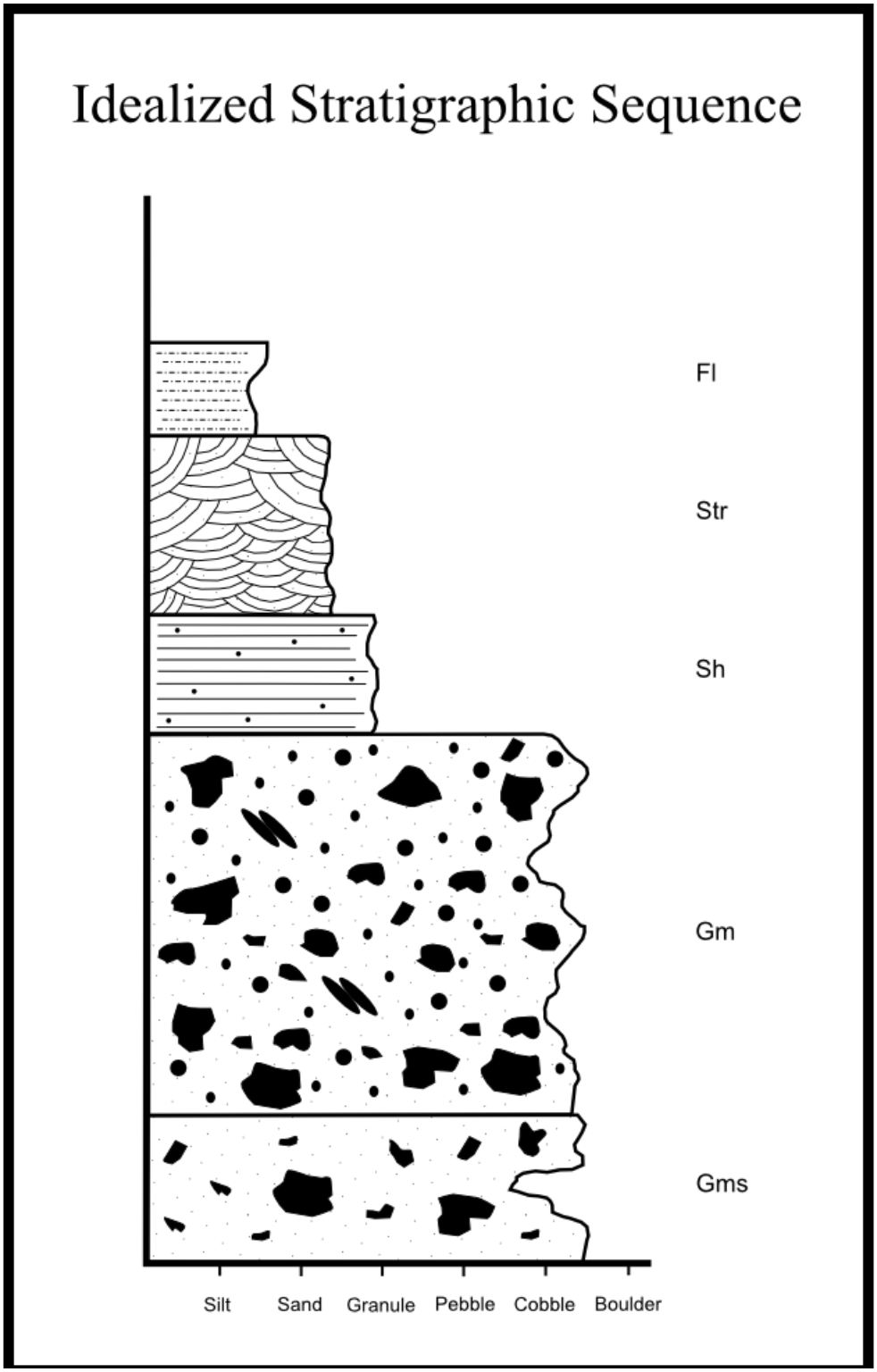

Fig. 27. Stratigraphic column showing idealized sequence in the study area.

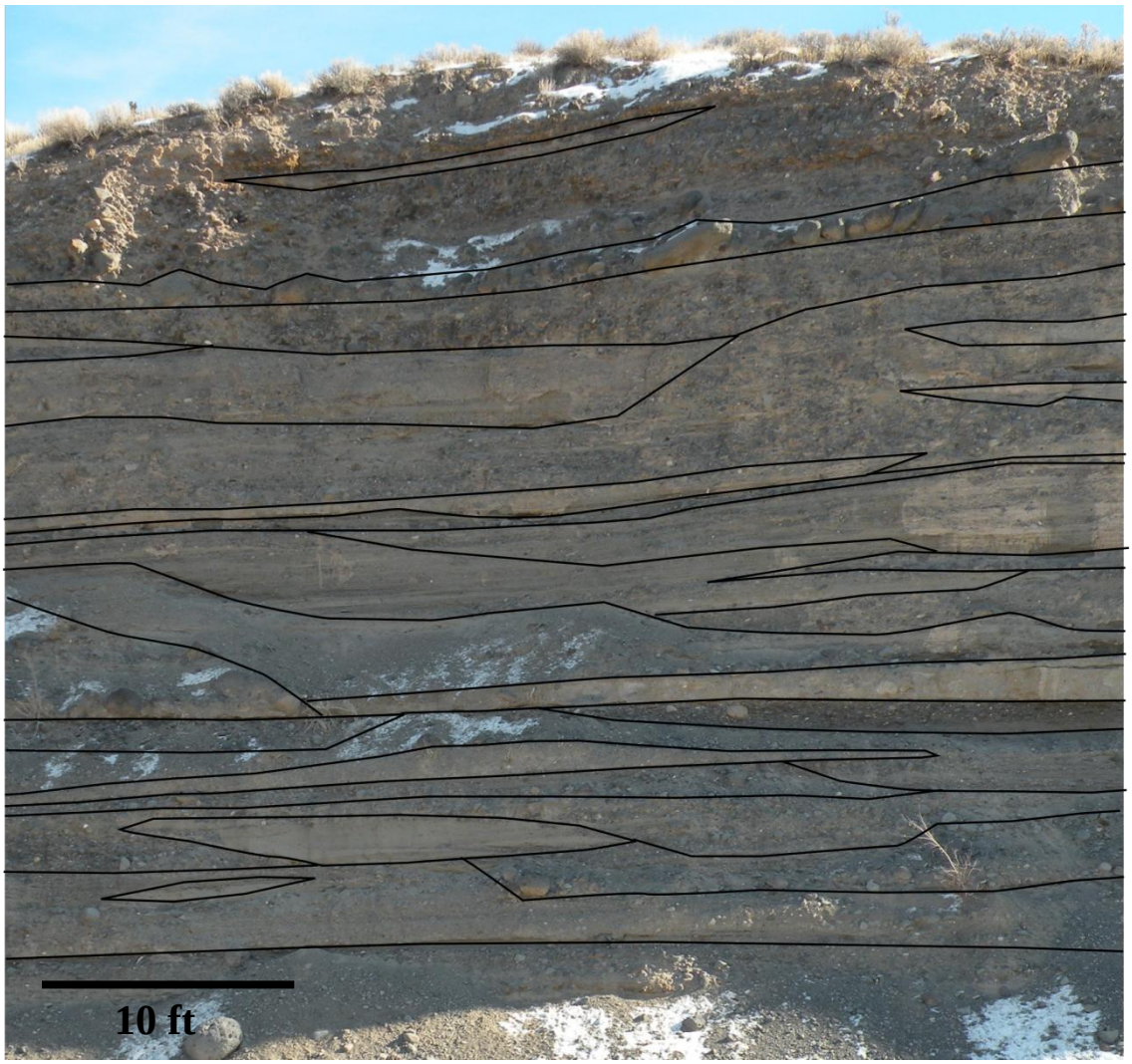

Fig. 28. Photograph at Cory Grade showing the lateral discontinuity of beds.

As previously discussed, a braided fluvial/braidplain depositional sequence should fine upward from coarse gravels to boulders at the base, to very fine sands and silts at the top. After detailed examination of the outcrops in the field, no instances of a fining upward sequence were observed. Grain-size and photographic analysis revealed a coarsening upward sequence, with all units bounded by erosional surfaces.

A generalized sequence (Fig. 29) was created to portray what was observed in the field. Figure 29 shows the generalized sequence coarsening upward, transitioning from silt and fine sand at the base to granule and boulder at the top. Contacts between facies are erosional, and, therefore, an unknown amount of geologic time is assumed to be missing in the record. Fine-grained deposits are highly susceptible to erosion (Fig. 19) and can be scoured away during the deposition of overlying coarse-grained material (Miller, 2006).

The lowest facies in the sequence is Fl. Fl is assumed to have been deposited during waning flow conditions, and grain-sizes range from silt to fine sand, with faint laminations and ripples (Fig. 13). The second facies in the sequence is Str, which is coarser-grained than Fl and assumed to scour away Fl units during deposition. Evidence of scour in Fl is seen in figure 13. Deposition of Str is assumed to have occurred during times of higher flow regimes than Fl, and, therefore, is coarse to very-coarse sand with trough cross-bedding. Above Str is Sh. Sh is probably a flood deposit that marks the boundary between normal flow and high flow conditions. Sh is characterized by very-coarse sand with the presence of some granules, laminated bedding, and a horizontal erosional contact with Str.

The last facies identified in the sequence, Gm, is a massive to crudely horizontally-bedded orthoconglomerate with clasts ranging from granule to boulder, and a silty-sandy matrix. Imbricated beds are common, and some interbedded sand lenses are present. Gms is a paraconglomerate with poorly sorted clasts ranging from sand to boulders and a matrix of silt to very fine sand. Gms was probably deposited by debris flows and has no predictable repeatability in the stratigraphic succession. Because Gms was not deposited directly by outwash flood waters, no set position occurs where one would find it in the depositional sequence like the other four facies in the study area.

The best exposures of the complete generalized sequence are at Cory Grade; incomplete sequences are at Hotchkiss Grade and Redlands Mesa Grade. Sequences that are incomplete are missing Fl, and occasionally Str from assumed scouring of overlying deposits. The following figures (Fig. 30, 31, 32, and 33) are examples of the generalized depositional sequences at Cory Grade and Redlands Mesa Grade.

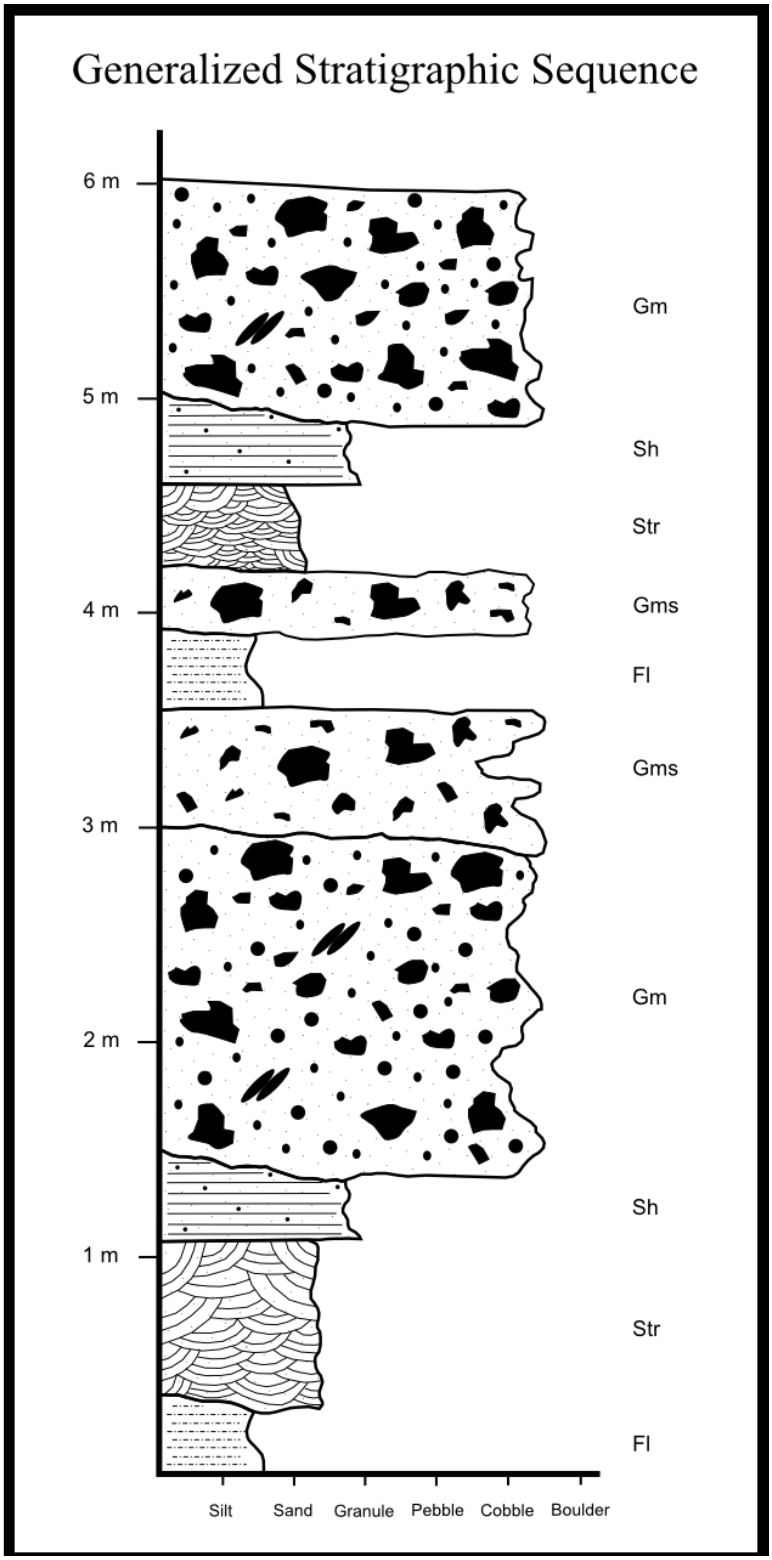

Fig. 29. Stratigraphic column showing generalized sequence in the study area.

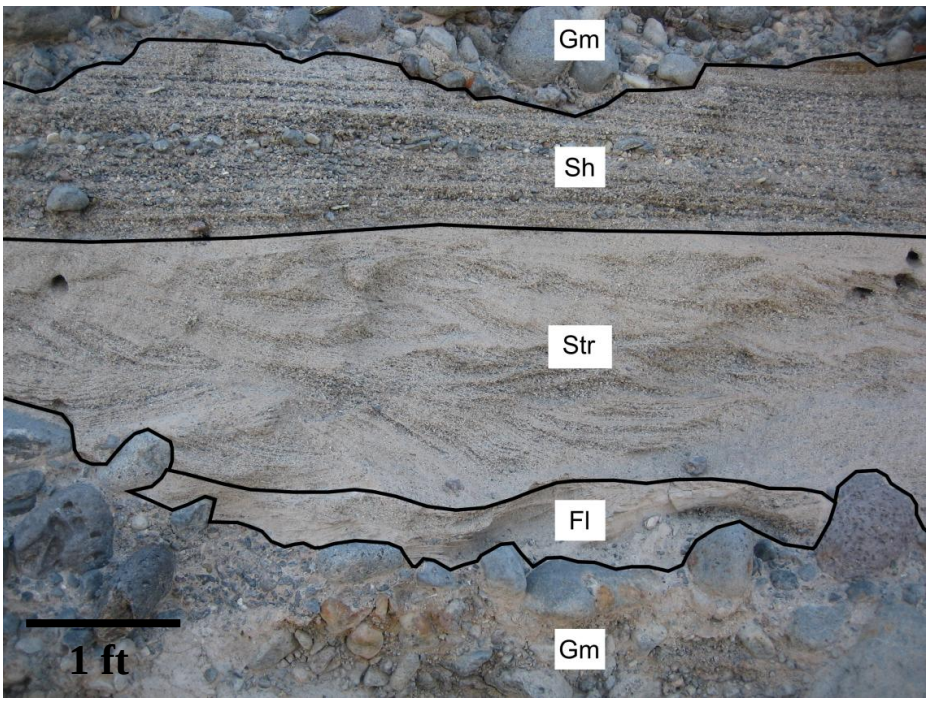

Fig. 30. Example of generalized sequence at Cory Grade (August 2009).

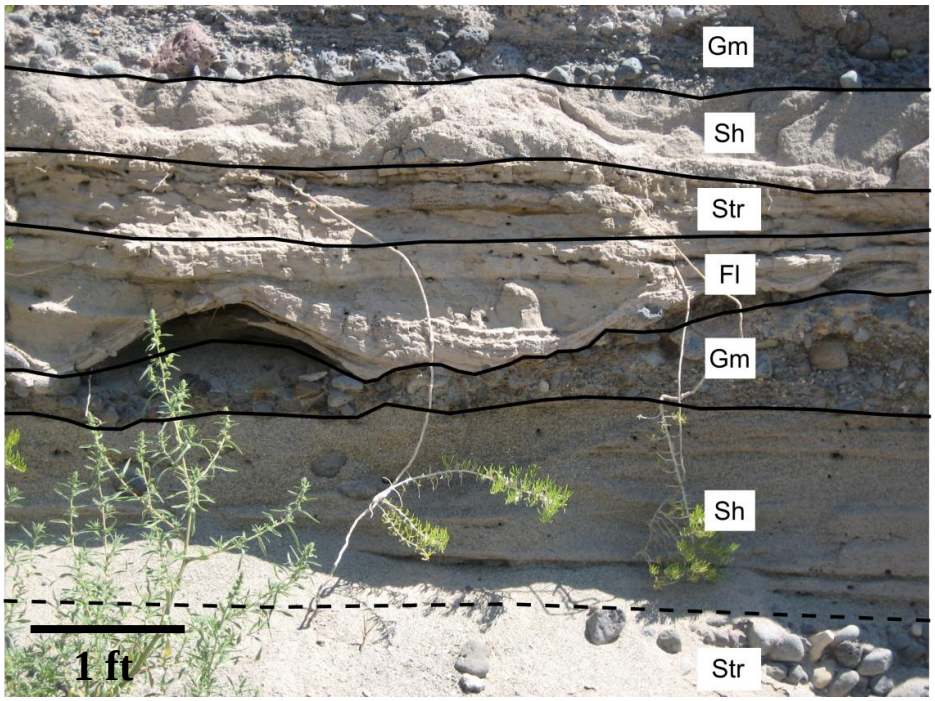

Fig. 31. A second example of generalized sequence at Cory Grade (August 2009).

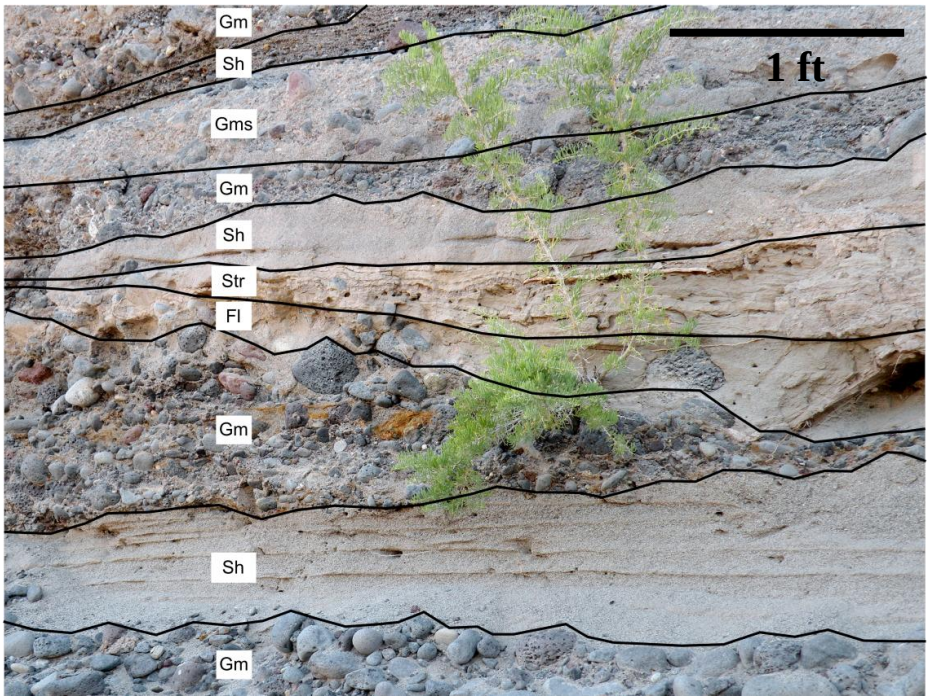

Fig. 32. A third example of generalized sequence at Cory Grade (August 2009).

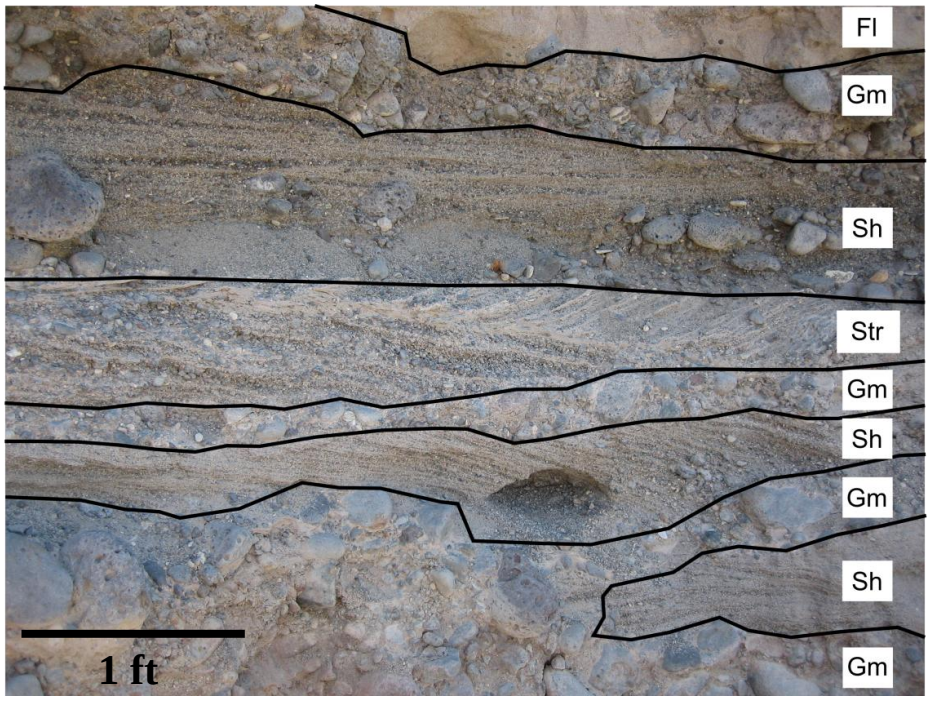

Fig. 33. Example of generalized sequence at Redlands Mesa Grade (August 2009).

5.7 Geomorphic Interpretation

The geomorphic evolution of Grand Mesa is separated into four stages for discussion in this thesis: (1) Ice cap glaciation; (2) Event one melting; (3) Event two melting; and (4) Present day. The four stages are designed to simplify, interpret, and explain the depositional environments and geomorphic history of Grand Mesa. The stages represent a brief overview of the geomorphic change that has occurred from Pleistocene to present along the southern flanks of Grand Mesa.

5.7.1 Ice Cap Glaciation

Grand Mesa was covered by a series of ice sheets during the Pleistocene; ranging from Pre-Bull Lake to Pinedale. Discussion has addressed whether three or four periods of ice sheet development occurred (Retzer, 1954; Richmond, 1965; Robinson and Dea, 1981; Richmond, 1986; Armour et al., 2002). Because the deposits that are the focus of this thesis are all related to late Pleistocene warming, the discussion of the number of ice sheet development events are extraneous to the discussion. The interpretation of Grand Mesa during the initial glacial advancement is portrayed in figure 34.

During early stages of glaciation, ice covered the entire expanse of the basalt cap and extended hundreds of meters down the flanks of Grand Mesa. The flanks of the mesa were assumed to have had a gentle gradient with little evidence of any prior erosional topography. During the first event, erosion was enhanced by low-energy, melt-waters from the ice cap. Thus, it is assumed that as the climate slowly began to warm, melting increased, and the ice cap began to recede. Climatic warming lead to an

increased amount of glacial melting, increasing the amount of glacial outburst flooding, and, therefore, increasing the amount of erosion on the southern flanks of the mesa.

Figure 34 characterizes the Grand Mesa ice cap draped over the top of the mesa and down onto the uppermost slopes of the southern flanks. The extent of the ice is based on field mapping of terminal moraines in the area. It is assumed that as the initial run-off from melt-water flowed, it eroded into the flanks and resulted in the initial formation of small ridges and finger mesas, depicted as lines trending approximately north-south on the diagram.

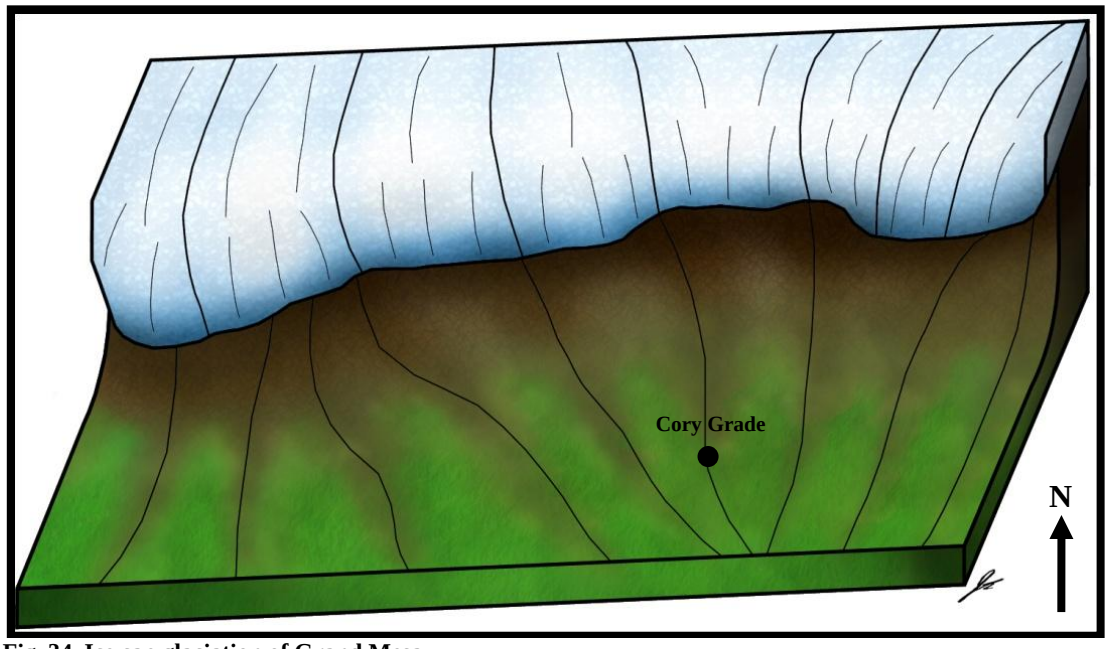

Fig. 34. Ice cap glaciation of Grand Mesa.

5.7.2 Event One Melting

One can logically state that the Grand Mesa ice cap experienced a significant amount of melt between the initial event (Fig. 34) and event one (Fig. 35) because of increased climatic warming. The ice cap logically retreated several hundred meters up the flanks of the mesa and covered only the basalt cap. As the ice cap receded, it deposited moraines, depicted in figure 35 as a single line below black circles. The moraines, which have been identified in the field, mark the lowest elevations that the ice reached. Three sets of moraines are depicted in figure 35 adjacent to the lowest extent of the ice cap.

During event one of melting, the erosion/deposition process is transitioning from normal melt conditions to glacial outburst flooding associated with climatic warming. Down cutting associated with increased flow regimes has increased, further developing the ridge and finger mesa system from the previous event (Fig. 34). The ridge and finger mesa landforms are portrayed in figure 35 as a series of branching lines that trend approximately north-south. As down cutting increased, the drainages from the mesa continued to develop, and began to merge towards the center of the area, near Cory Grade. As the ice cap continued to recede, erosion continued to increase, and the ridges, and subsequent drainages, continued to develop.

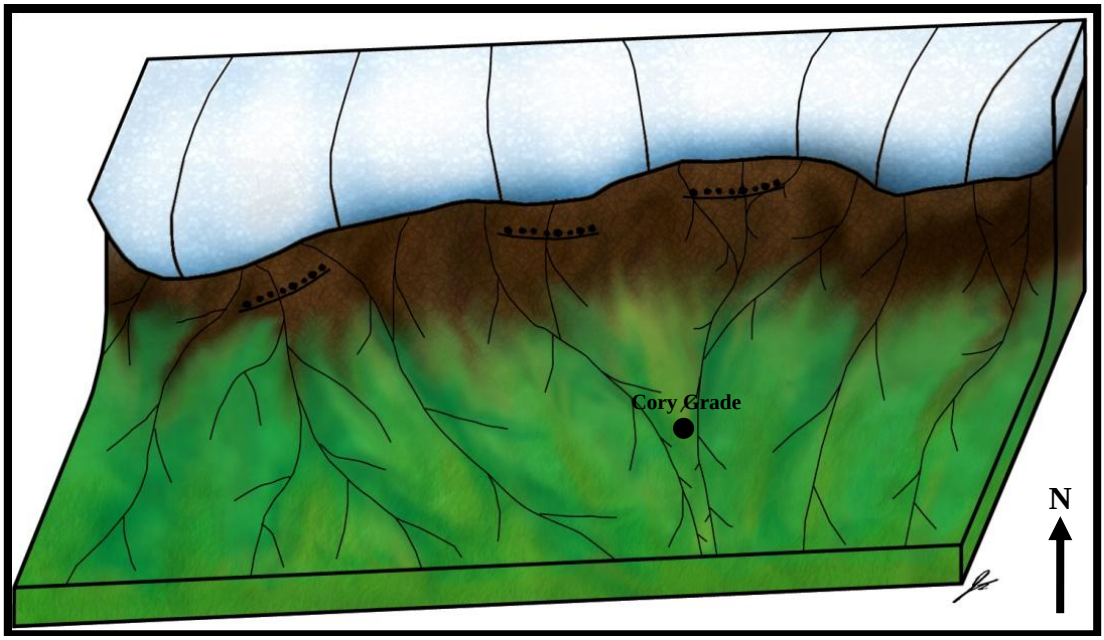

Fig. 35. Event one melting of Grand Mesa ice cap.

5.7.3 Event Two Melting

Significant retreat of the ice cap exposed the southern border of the basaltic mesa cap during stage two of melting (Fig. 36). Stage two melting represented a period of continuous outburst floods from the remaining ice on Grand Mesa. Drainage patterns became more complex and interconnected during this stage.

High-energy glacial outburst floods were frequent during this event, as the ice cap continued to degrade. Climatic warming had significantly increased during this event (Zhuang, 2010, per. comm.), resulting in more frequent outburst floods. Drainages from the mesa occurred in the form of a series of high-energy, braided fluvial systems or braid plains. Distinctive drainage pathways underwent significant development from the previous event. The ridge system in figure 36 (portrayed as a set of branching lines trending approximately north-south) continued to develop through down-cutting and

began to merge towards Cory Grade. Flood waters were channeled within existing pathways, and draining the western and eastern portions of the study area drained towards Cory Grade. Ultimately, all melt-water reached the Gunnison River, which is not depicted on these figures.

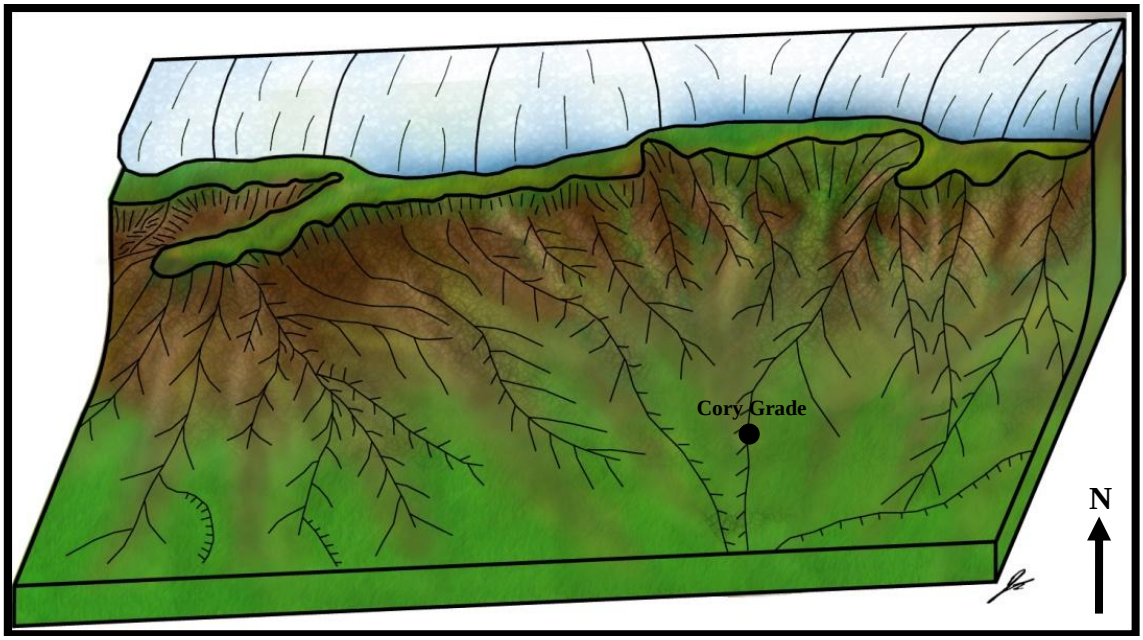

Fig. 36. Event two melting of Grand Mesa ice cap.

5.7.4 Present Day Grand Mesa

A representation of the current state of Grand Mesa (Fig. 37) depicts the heavily forested basaltic cap. Features of glaciation occur around the top of the mesa, as documented by Henderson (1923).

Small "finger" mesas (Redlands mesa, Cedar Mesa, Rogers Mesa, etc.) have fully developed as a result of continued down cutting and extend out from Grand Mesa. Figure 37 shows the extensive dendritic ridge system that channeled the melt-water during event two melting. The ridge system continued to merge towards Cory Grade. Valleys on the east and west side of Cory Grade served as the main pathways for melt-water during maximum glacial outburst flooding, which occurred during event two.

First-order streams (Surface Creek, Youngs Creek, Cottonwood Creek, Horse Creek, etc.) have subsequently developed in the former outwash pathway and flow into the modern Gunnison River. These streams are likely remnants of the ancient braided system responsible for sediment transportation during major melting events.

The landscape to the west of Cory Grade is composed entirely of Cretaceous Mancos Shale. Limited outcrops of Mancos Shale can be found to the east of Cory Grade; however, the majority of the landscape is covered by Quaternary alluvium associated with melt-water events. It is hypothesized that the lack of Quaternary alluvium west of Cory Grade is a result of either steeper gradients, which resulted in higher velocity flows that eroded rather than deposited, or no melt-water channels impacted this area. And, thus, the erosional landscape that is seen today is the result of post-glacial erosion. It is also hypothesized that the main drainage off Grand Mesa was

along the State Highway 65 corridor, widening into a broad alluvial fan. With a large percentage of outwash traveling along this pathway, it is highly unlikely that deposition would have occurred west of this drainage corridor.

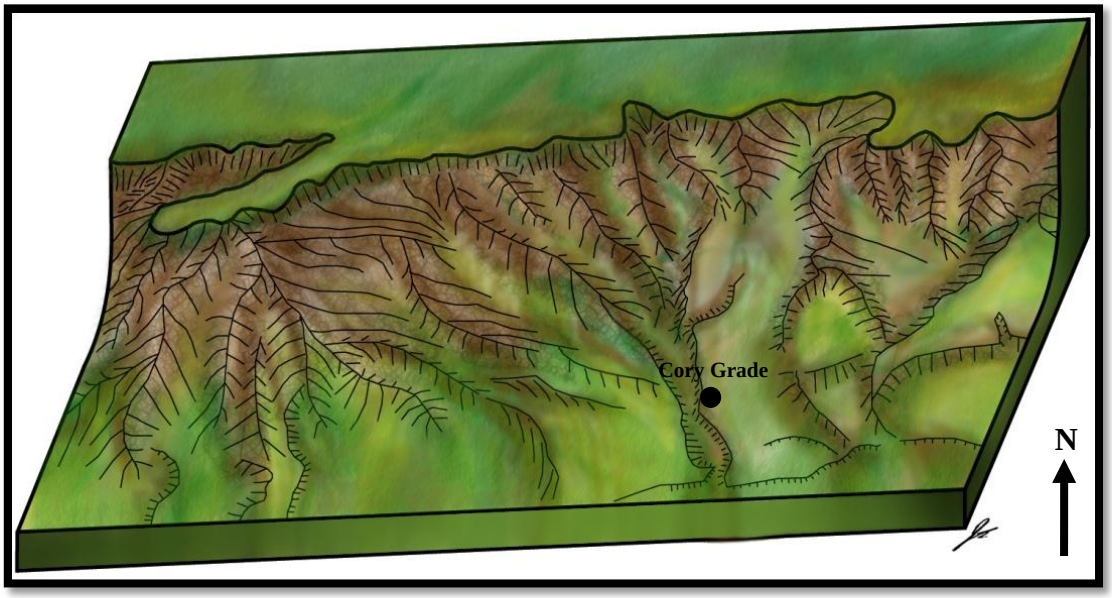

Fig. 37. Present day Grand Mesa.

5.8 Outcrop Morphology

All four outcrops in this study are the result of glacio-fluvial processes, each possessing its own unique morphology. Outcrop morphology varies because of elevation, slope morphology, drainage pathways, and distance from the sediment source. The positions of all outcrops in the study area south of Grand Mesa are shown in figure 38, and the morphology of each outcrop is discussed in the following sections.

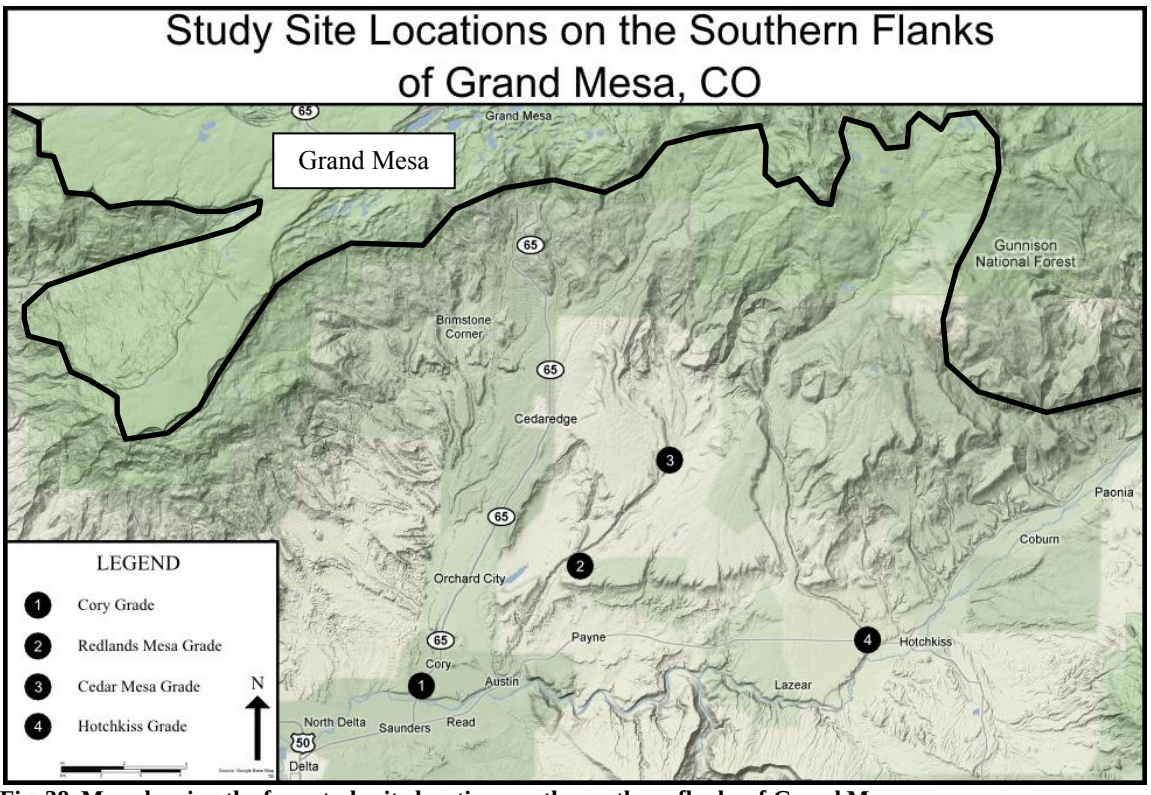

Fig. 38. Map showing the four study site locations on the southern flanks of Grand Mesa.

5.8.1 Cory Grade

Cory Grade is the major outcrop for this thesis study. The outcrop is located along the east side of State Highway 65, ~4 km (~2.5 mi) north of State Highway 92 and

has a total exposure distance of ~1 km (~0.6 mi). Cory Grade has the lowest elevation of the four outcrops, ranging from ~1,542 m (~5,060 ft) at the southern end to 1,570 m (~5,150 ft) at the northern extent. Exposed thicknesses of the outcrop are consistent at approximately ~20 m (~65 ft) for its entire extent (Fig. 39).

Cory Grade is the southernmost outcrop (Fig. 38) and has the longest drainage pathway from the mesa, ~30 km (~19 mi). The drainage pathway for the melt-water followed the corridor of State Highway 65 until north of Cedaredge, where it connected to a drainage pathway flowing off of Grand Mesa (Fig. 40).

The initial gradient from Grand Mesa is relatively high, but quickly decreases as it approaches State Highway 65, allowing for stream development in a broad fan starting at the edge of the mesa and widening southward between State Highway 65 and Hotchkiss. Based on field work, it is hypothesized that the initial melt-water streams were high-energy braided fluvial environments as the result of rapid release of glacial melt during climatic warming. High-energy braided streams transitioned to low-energy fluvial systems during periods of steady-state melting.

Clasts at Cory Grade are predominantly massive and vesicular basalt (~95%). Other clasts from unknown sources include quartzite, felsic igneous rocks, and chert. Cohesive clay clasts, ranging from very-coarse sand to cobble, are common in this outcrop and were likely sourced by the underlying Mancos Shale.

Five facies containing specific sedimentary structures were identified at Cory Grade. The lower portion of the outcrop is granule to cobble braided fluvial deposits of Gm. Imbrication and crude horizontal bedding occur in this facies. As discussed earlier,

imbrication shows a paleocurrent direction from Grand Mesa, indicating the source is to the north, and not associated with the ancestral Gunnison River.

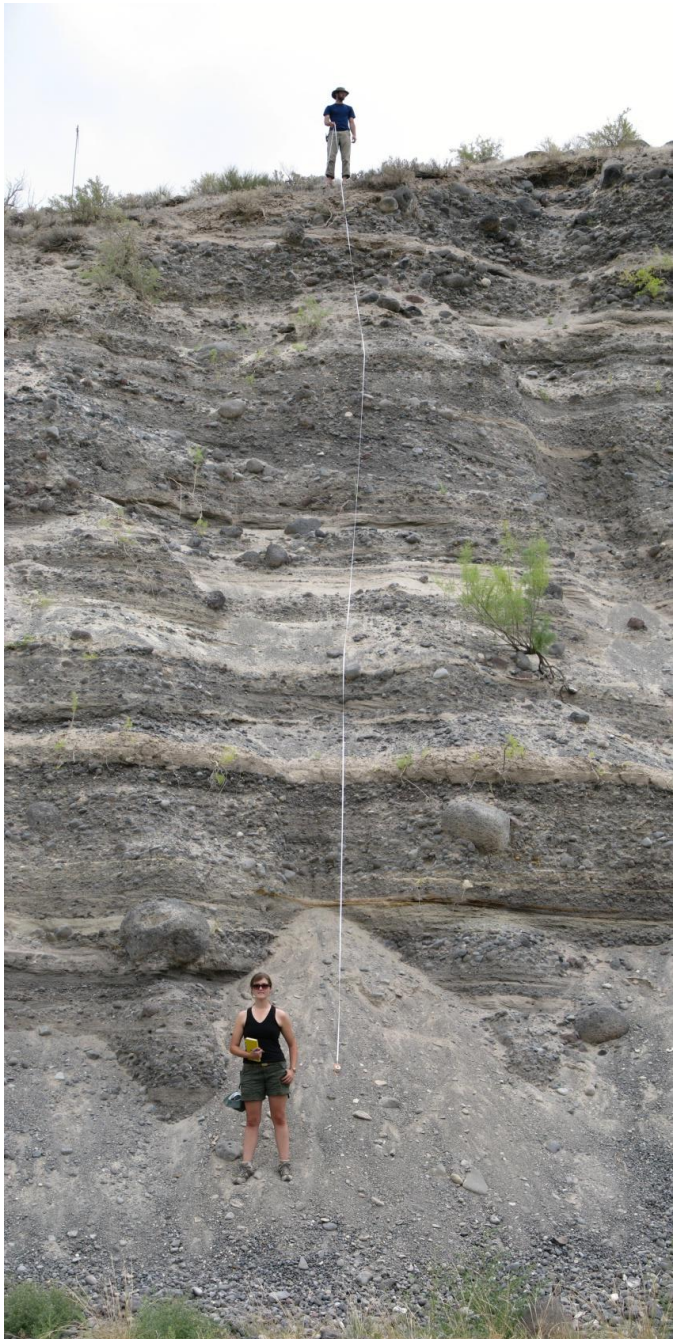

Fig. 39. Photograph showing approximate outcrop height of Cory Grade (~20 m; ~65 ft) (August 2009).

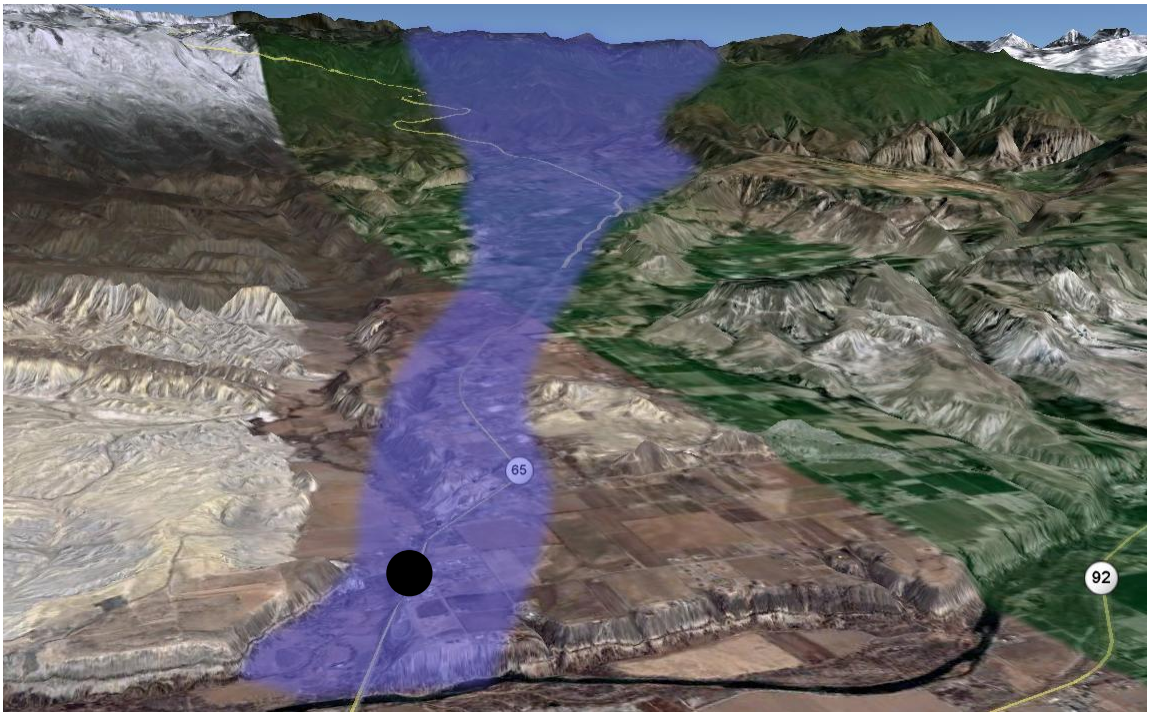

Fig. 40. Vertically exaggerated Google image showing proposed drainage pathway for Cory Grade. The black circle represents the approximate location of Cory Grade.

A large percentage of coarse to very-coarse fluvial sand units of Str and Sh are at Cory Grade. These units have varying amounts of cross-bedding and laminations, as well as laminated pebble and sand beds. It is assumed that the boundary between Str and Sh represents the boundary between normal flow regimes of seasonal melting and high-energy flow regimes from climatic warming.

Deposits from debris flows at Cory Grade are stratigraphically thinner (~0.5 m; ~1.5 ft) than at other outcrops within this study area. Thinning of the beds is assumed to be the result of the outcrop distance from the source (i.e., Grand Mesa), a total distance of ~30 km (~19 mi). The top ~3 to 4 m (~10 to 13 ft) of outcrop is a massive debris flow

(Gms). Clasts within this unit range from granule to boulder, some exceeding ~1 m (~3.3 ft) in diameter.

The two most prevalent facies at Cory Grade are Str and Gm. A large percentage of the outcrop is medium- to high-energy fluvial deposits, indicating this area was the main drainage conduit for melt-water flowing from the mesa. Cory Grade is the farthest outcrop from Grand Mesa, and, therefore, should contain finer-grained material because of the transport distances. This is not the case, however, as evidenced by the large fraction of granule to boulder sized material in Gm and Gms deposits. Thus, an alternative explanation might be that these coarse-grained deposits could be a result of ice damming on the upper slopes, collecting coarse material, and then breaking out in a large release flows.

5.8.2 Redlands Mesa Grade

Redlands Mesa Grade is ~10 km (~6 mi) to the northeast of Cory Grade. The outcrop is ~300 m (~985 ft) long and trends in a west-east direction. The western elevation is ~1,775 m (~5,825 ft) and rises to ~1,790 m (~5,875 ft) at its eastern extent. Redlands Mesa Grade outcrop is the second highest in elevation in the study area.

Redlands Mesa Grade is located on the southern flank of a small finger mesa. Units similar to those on Redlands Mesa occur on other mesas in the general vicinity. The drainage pathway for this outcrop flowed along stream valleys of Dry and Currant Creeks (Fig. 41). The Redlands Mesa Grade drainage is the second longest drainage in the study area at ~ 23 km (~14 mi).

The gradient associated with Redlands Mesa Grade is very similar to the gradient at Cory Grade. The gradient is high adjacent to Grand Mesa, and quickly decreases as it moves away from Grand Mesa. Because the drainage is confined to stream beds, channels did not braid, and Gm does not occur in high percentages in the outcrop.

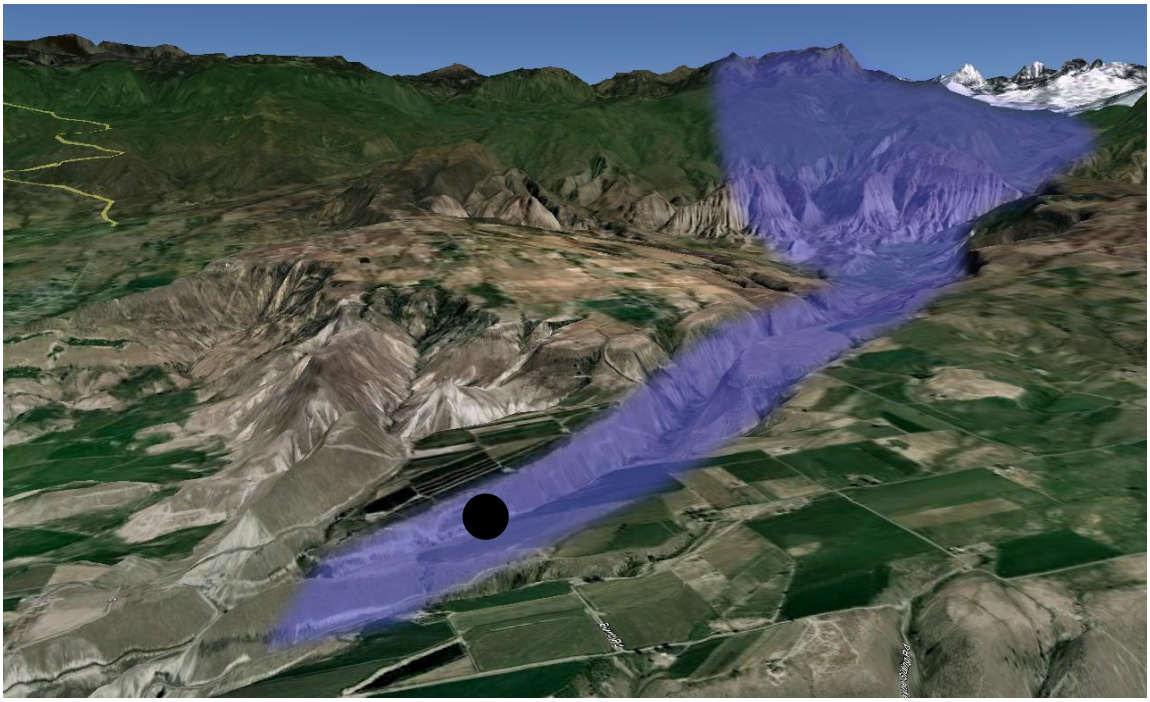

Fig. 41. Vertically exaggerated Google image showing proposed drainage pathway for Redlands Mesa Grade. The black circle represents the approximate location of Redlands Mesa Grade.

Clasts at Redlands Mesa Grade are dominated by massive and vesicular basalt (~95%). Other clasts from unknown sources include quartzite, felsic igneous rocks, and chert. Cohesive clay clasts are common and the underlying Mancos Shale probably served as the source area.

All five facies are present at Redlands Mesa Grade; however, the most common are Gms, Str, and Sh, respectively. This outcrop is composed primarily of very-coarse

sand and granules. Imbrication is not common, and the outcrop is dominated by a variety of ripple cross-laminations and cross-bedding structures, as well as laminated sands and granule beds. Fl is not common in this outcrop because of scour from the overlying coarse to very-coarse sand fluvial deposits. A complete depositional sequence is not present at Redlands Mesa Grade.

A large percentage of debris flow deposits of Gms occur at Redlands Mesa Grade (Fig. 42). Bed thicknesses of Gms are ~1 m (~3.3 ft) thick. The top ~3 to 4 m (~10 to 13 ft) of the outcrop, based on field mapping, appears to be one continuous debris flow deposit (Gms). Small interspersed granule to pebble beds exist; however, no boulders were identified at this outcrop.

The lowest visible portion of this outcrop is alternating units of granule, very-coarse sand, and debris flow deposits. The very-coarse sands have complex cross-bedding structures indicative of a high-energy fluvial environment. The cross-bedding structures here are the largest of any outcrop studied. Because this outcrop is located on the perimeter of a stream valley, it is possible that oversaturation of the surrounding soils during outwash events resulted in debris flows down the sides of the stream valleys. This sequence of events would account for the repetitious intervals of Gms, which was not observed at other outcrops.

Fig. 42. Alternating units of Gms, Str, and Sh at Redlands Mesa Grade (August 2009).

5.8.3 Cedar Mesa Grade

Cedar Mesa Grade is ~18 km (~11 mi) to the northeast of Cory Grade. The outcrop is ~100 m (~330 ft) long and trends in a north-south direction. Cedar Mesa Grade is located at the highest elevation of the four study sites, with a northern elevation of ~1,935 m (~6,350 ft) sloping to ~1,925 m (~6,315 ft) at its southern extent.

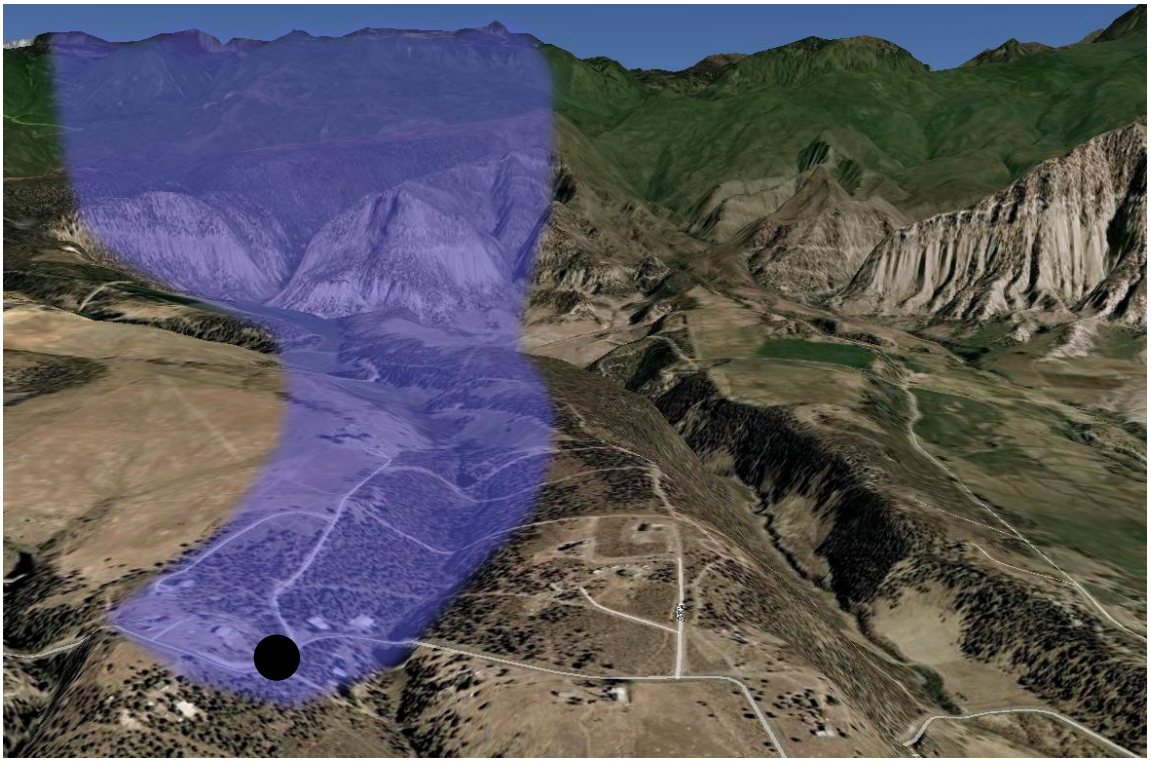

Fig. 43. Vertically exaggerated Google image showing proposed drainage pathway for Cedar Mesa Grade. The black circle represents the approximate location of Cedar Mesa Grade.

This outcrop is located on the southern tip of a small finger mesa extending from Grand Mesa. It is located ~9 km (~5.6 mi) from the edge of Grand Mesa (Fig. 43). The drainage pathway for this outcrop follows a drainage pathway from Grand Mesa. It is likely that sheet flow and mass movement (debris flow) were the depositional processes

responsible for the formation of this outcrop, based on the surrounding topography. Unlike the previously discussed outcrops, Cedar Mesa Grade does not have a large drainage system that served as a conduit for melt-waterss.

The gradient associated with Cedar Mesa Grade is relatively low except adjacent to the base of Grand Mesa. No confining barriers existed to direct the flow of water like the previous outcrops, and, therefore, debris flows were likely the only mode of deposition for this outcrop.

Fig. 44. Cedar Mesa Grade (August 2009).

Clasts are dominated by basalt pebbles, cobbles, and boulders (~95%). Analysis of the outcrop photographs suggests the dominant facies present is Gms (Fig. 44). Visual inspection of the outcrop shows grain-size is much coarser (pebble to boulder) than the other outcrops, and deposits are matrix-supported conglomerates, indicative of Gms. Boulder-sized clasts greater than one meter occur frequently in the outcrop (Fig. 45). These clasts are too large to be transported by most flow regimes and, therefore, they must have been deposited as debris flows. No sedimentary structures were identified.

Fig. 45. Photograph at Cedar Mesa Grade showing boulders within Gms (August 2009).

Because of the orientation of the outcrop and the mesa in which the outcrop is located, it is highly unlikely that braided or meandering activity played a role in its formation. During field mapping, no evidence of the occurrence of distinctive channels that would have contained the flow were found; therefore, melt-water could have flowed across the lands surface as sheet wash or in a braid plain. It is further suggested that over-saturation of the soils created unstable conditions, and large slump blocks failed and moved down the gentle gradient. Gms deposits at Cedar Mesa Grade are much thicker than the other outcrops, and, therefore, probably formed from a few large slumps rather than a combination of many small debris flows.

5.8.4 Hotchkiss Grade

Hotchkiss Grade is located ~23 km (~14 mi) to the east of Cory Grade on State Highway 92 just to the west of downtown Hotchkiss. The outcrop is ~75 m (~245 ft) long and trends in a northwest-southeast direction. The northwestern elevation is ~1,675 m (~5,500 ft) and rises to ~1,669 m (~5,475 ft) at its southeastern extent.

The drainage pathway for this outcrop is from the southeastern side of Grand Mesa, unlike the other three outcrops whose drainages were from the southern edge. It is hypothesized that the drainage followed a path similar to the present day pathway of Leroux Creek draining to the southeast, where it merged with a secondary drainage flowing from Grand Mesa in a northeasterly direction (Fig. 46). The length of the drainage pathway is ~9 km (~5.6 mi) long.

The gradient for this drainage is the lowest of the four outcrops. Field mapping in this area suggested that the flow probably was confined to stream channels and braiding was held to a minimum, and Gm deposits were not prevalent at this outcrop.

Grain-size analysis of Hotchkiss Grade indicates a wide range of sediment sizes from silt and very-fine sand to pebble and boulder. The largest clast was found at the base of the outcrop and measured greater than one meter in diameter (Fig. 47). Clasts were composed of massive and vesicular basalt (~95%). Some exotic clasts were found (quartzite, felsic igneous rocks, and chert).

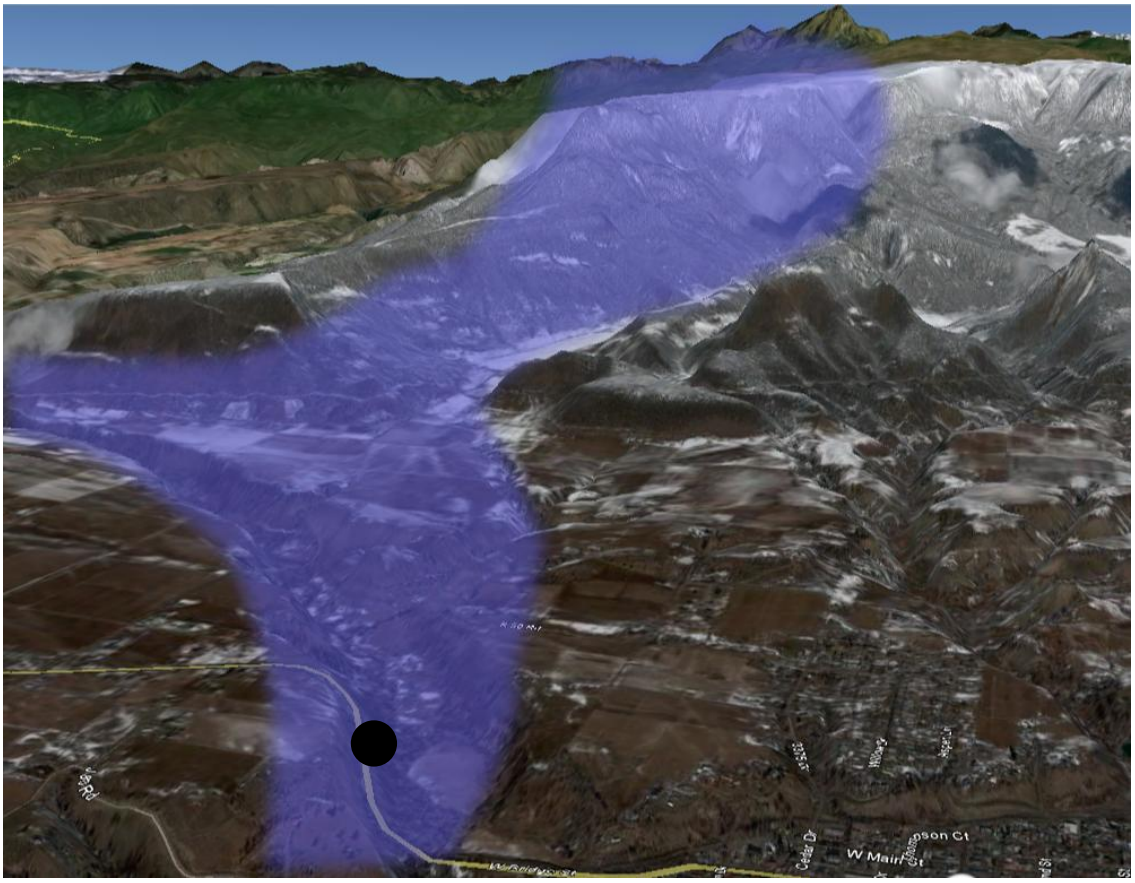

Fig. 46. Vertically exaggerated Google image showing proposed drainage pathway for Hotchkiss Grade. The black circle represents the approximate location of Hotchkiss Grade.

Detailed field mapping and analysis suggests that all five facies are present at Hotchkiss Grade; however, the site is dominated by Gms and Str. Based on the analysis, the lower portion of the outcrop probably is a large braided fluvial deposit of Gm and is the only deposit in the outcrop. It is granule to cobble in size and imbrication is present suggesting flow from Grand Mesa. Numerous repeating units of Str containing trough cross-bedding are present. Several small debris flow deposits (~0.1 to 0.75 m; ~0.3 to 2.5 ft), are present and the last deposit is ~3 to 4 m (~10 to 13 ft), a large debris flow that has clasts ranging from coarse sand to boulder (Fig. 48).

Fig. 47. Photo showing the largest clast found at Hotchkiss Grade. The basalt clast is >1m in diameter (August 2009).

Melt-waters must have been confined to stream valleys, as flow occurred from Grand Mesa. Fluvial processes have played a major role in outcrop formation and morphology, with Str making up a large percentage of the outcrop. Fluvial deposits of Str and Sh are present and exhibit well defined cross-bedding structures. The largest example of Gm is preserved at the base of the outcrop (~1.5 m; ~5 ft exposed). It is assumed that this was the result of initial glacial outburst flooding. Several small discontinuous debris flow deposits are present. In addition, a large deposit comprising the upper ~3 to 4 m (~10 to 13 ft) of the outcrop is present. Fl is rare in this outcrop, and no complete depositional sequences occur at Hotchkiss Grade.

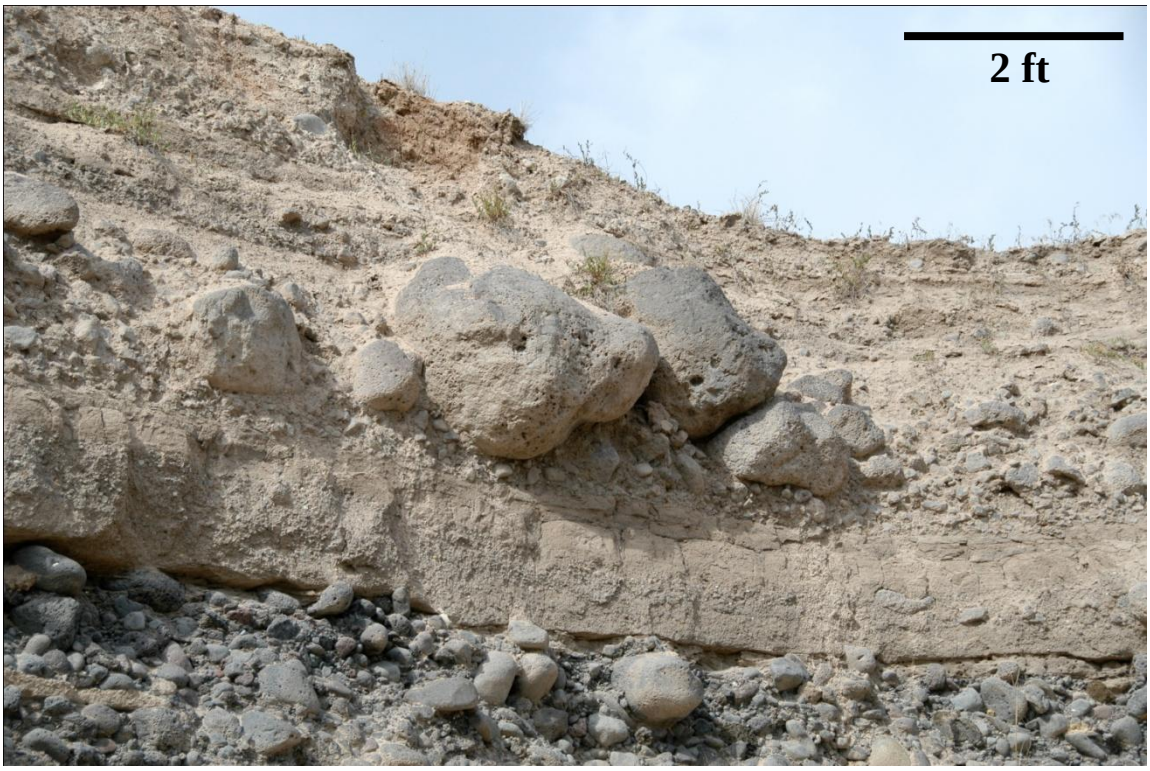

Fig. 48. Debris flow (Gms) showing grain-size variability (August 2009).

6. CONCLUSIONS

The question posed for this research was: Are these glacio-fluvial deposits associated with the melting of the ice cap or are they fluvial terraces associated with the evolution of the ancestral Gunnison River? From that question three objectives were established:

1) Map the aerial extent of the deposits to identify sediment sources.
2) Determine the depositional environments associated with the strata in the deposits, and
3) Determine the depositional sequence of events recorded in the deposits and correlate over space.

The research was driven by the hypothesis:

H_1: The deposits are glacio-fluvial and associated with melting of the ice cap from Pleistocene climatic warming.

The null hypothesis was:

H_0: The deposits are not glacio-fluvial and area associated with the ancestral Gunnison River drainage.

Sieve analysis revealed that two major depositional environments occurred during Pleistocene melting of the Grand Mesa ice cap: (1) glacio-fluvial outwash, and (2) debris flows. Deposits were divided into four grain-size categories based on the Udden-Wentworth grain scale; $\geq 0\ \Phi$; 0 to -1 Φ; -1 to -2 Φ; and $\leq -2\ \Phi$. Grain-size variability was highest at Cory Grade and Hotchkiss Grade, ranging from silt to boulder.

Redlands Mesa Grade was noticeably coarser, with the dominant grain-size being very-coarse sand, but with no clasts larger than pebble. Unfortunately, only one sample was collected at Cedar Mesa Grade because of land access issues, and grain-size analysis was not completed for this outcrop. Nevertheless, photographic analysis suggests that Cedar Mesa Grade is the coarsest of the four outcrops with most clasts ranging from pebble to boulder.

Clast composition is estimated to be greater than 95% basalt in the deposits of all four outcrops. Debris flow deposits contained a wide variety of clasts including basalt, rip-up mud clasts, and other foreign igneous and sedimentary rock fragments. The only source of basalt in the area is the Tertiary basaltic mesa cap, supporting the hypothesis that these deposits are a result of melt-water flowing from the mesa during Pleistocene climatic warming, and depositing basalt sediments on the southern flanks of Grand Mesa. It is highly unlikely that the Gunnison River transported very-coarse sand to boulder basalt clasts because of the source of basalt. However, terraces indicate that the ancestral Gunnison River was much higher in the Pleistocene, and therefore, possibly reworked sediments associated with ice cap melting.

Sedimentary structures were examined in the field and documented with photographs. The most prominent structure showing paleocurrent direction was imbricated bedding. Imbrication indicates a paleocurrent flow direction of S25W at Cory Grade and Redlands Mesa Grade, and S40E at Hotchkiss Grade. All three of these paleocurrent directions suggest flow from Grand Mesa. No imbrication was found that paralleled the flow direction of the ancestral Gunnison River.

Facies analysis shows that five major facies are present in the study area. Fl is the finest grained and is composed of silt to very-fine sand. It contains fine laminations and ripples, and is a result of melting of the Grand Mesa ice cap. Fl is not present in all the outcrops because of scouring. Its full stratigraphic thickness is unknown. Str is composed of coarse sand, contains trough cross-bedding, planar cross-bedding. This facies was deposited by a higher rate of flow than Fl and had a large source of sediment and quick burial for the preservation of abundant ripples. Facies Sh is representative of the transition from low flow regimes of seasonal melting to high flow regimes associated with climatic warming. Evidence for this transition occurs in the near horizontal contact between Str and Sh. Laminated, very-coarse sands to granules were deposited in this facies. Gm overlies Sh and is a granule to boulder orthoconglomerate. It is poorly sorted with silt to sand matrix. Imbricated bedding and crude horizontal bedding occurs in this facies. Gms is the fifth facies in the study area. It is a paraconglomerate, with a mud to very-fine sand matrix and clast sizes ranging from granule to boulder.

A depositional sequence of facies was identified in the study area. Observations in the field and grain-size analyses suggest that the sequence is coarsening upward. A generalized stratigraphic column was created to portray this observed coarsening upward sequence. The generalized sequence coarsens upward from silt and fine sand at the base to pebble and boulder at the top. Because of the nature of debris flows, these deposits are random in the stratigraphic record and so are placed randomly within the sequence. It appears that Fl was commonly scoured away during deposition of Str, and is commonly missing from the sequence. The only complete sequences are at Cory Grade.

The reason for this is thought to be the distance Cory Grade is from Grand Mesa, allowing flow to subside, and limiting the scour of Fl.

An idealized stratigraphic sequence was constructed based on braided fluvial systems fining upward, rather than coarsening upward. The study area is assumed to have once had many fine-grained units, which were subsequently eroded away during the deposition of overlying coarse-grained units. The idealized sequence fines upwards from Gm and Gms at the base, to Sh, Str, and Fl, respectively.

Each outcrop exhibits a unique morphology because of drainage pathways from Grand Mesa, outcrop distance from Grand Mesa, elevation of the outcrops, and gradient over which the outwash traveled. Cory Grade and Hotchkiss Grade, being the farthest from the mesa, contain each of the five facies in the study area. Redlands Mesa Grade is composed of coarse and very-coarse sand with few deposits containing pebbles and boulders. After photographic analysis, it was observed that Cedar Mesa Grade is composed almost entirely of debris flow deposits.

Several complications were overcome to complete this study. Careful sampling was used to collect only sediment from one unit at a time; however, the disaggregation of the outcrop complicated sampling fidelity. Limited outcrop availability and unstable conditions of the outcrops limited sampling to no more than the length of an arm high on the outcrop. A more detailed analysis of the entire vertical succession of the outcrops is needed to clarify questions such as how many melting events can be described in the outcrop, and do differences exist in seasonal melt deposits versus outwash deposits? A

more detailed sequence could be compiled if it were possible to sample the entire vertical sequences of the outcrops.

In conclusion, the deposits are glacio-fluvial associated with the melting of the ice cap and not fluvial terraces associated with the evolution of the ancestral Gunnison River.

- First, the source of sediment is from Grand Mesa and is granule, pebble, cobble, and boulder sized clasts in all outcrops, and composed of ~95% basalt. Coarse and very-coarse sands are composed of a mixture of basalt and quartz. The only source of basalt in the region is the basaltic cap of Grand Mesa.
- Second, the deposits are probably glacio-fluvial and debris flows associated with Pleistocene melting of the Grand Mesa ice cap. Sedimentary structures found on the outcrops include varying degrees of cross-bedding, sand and pebble laminae, imbricated bedding, and others. Paleocurrent directions determined from grain imbrications indicate flow from Grand Mesa during outwash events. Paraconglomerate debris flows were identified at all outcrops. The debris flows have no sedimentary structures and are thought to be a result of oversaturation of soil during times of glacial outburst flooding.
- Thus, one can conclude that the deposits are not associated with deposition by the Gunnison River. Clast composition indicates the source of sediment is from the basaltic cap of Grand Mesa, the only basalt source in the region. Sedimentary structures indicate paleocurrent flow directions from Grand Mesa, not parallel to the ancestral Gunnison River. The ancestral Gunnison River did

not transport boulder sized, basalt clasts to the current location. If the ancestral Gunnison River was responsible for deposition, imbrications would indicate paleocurrent directions in an east-west direction, following the flow of the river.

REFERENCES

Aslan, A., Cole, R., 2002. Sedimentological comparison of two new Lava Creek B Ash occurrences in western Colorado. Geological Society of America Denver Annual Meeting Paper No. 58-6.

Aslan, A., Quigley, J., Cole, T., Grubbs, D., Kellerby, D., Meunier, Y., Polson, J., Rodriguez, T., Stover, J., 2005. Geological mapping of Quaternary Colorado and Gunnison River terraces in the Grand Valley, Western Colorado. Rocky Mountain Section - 57th Annual Meeting Paper No. 11-7.

Armour, J., Fawcett, P.J., Geissman, J.W., 2002. 15 k.y. paleoclimatic and glacial record from northern New Mexico. Geology. 30(8), 723-726.

Baker, F., 2002. Weathering rinds on Quaternary basalt gravels from Grand Mesa moraines and terraces. M.S. Thesis, Mesa State College, Grand Junction.

Baker, F., Rundell, J., Hasebi, K., Cole, R., Aslan, A., 2002. Geomorphic evolution of Grand Mesa, Western Colorado. Geological Society of America Annual Meeting Paper No. 207-1.

Balsillie, J. H., Donoghue, J. F., Butler, K. M., Koch, J. L., 2002. Plotting equations for Gaussian percentiles and a spreadsheet program for generating probability plots. Journal of Sedimentary Research. 72(6), 929-943.

Brodzikowski, K., van Loon, A. J., 1991. Glacigenic Sediments. Elsevier Science Publishing Company Inc., New York.

Cole, J. P., King, C. A. M., 1968. Quantitative Geography, John Wiley & Sons Ltd, London.

Cole, R. D., Sexton, J. L., 1981. Pleistocene surficial deposits of the Grand Mesa, Colorado. New Mexico Geological Society Guidebook, 32nd Field Conference, Western Slope Colorado, pp. 121-126.

Cole, R. D., 2001. Late Cenozoic erosional history of Grand Mesa, Western Colorado. Rocky Mountain (53rd) and South-Central (35th) Sections, Geological Society of America, Joint Annual Meeting Session No. 13.

Collinson, J. D., 2006. Alluvial sediments. In: Reading, H.G. (ed.), Sedimentary Environments: Processes, Facies and Stratigraphy. Blackwell Publishing, Malden, MA, pp. 37-82.

Collinson, J. D., Thompson, D. B., 1982. Sedimentary Structures. George Allen & Unwin, London.

Compton, R. R., 1985. Geology in the Field. John Wiley & Sons, Inc., New York.

Crofts, R. S., 1981. Mapping techniques in geomorphology. In: Richards, K. S. (ed.), Geomorphological Techniques. George Allen & Unwin, London, pp. 66-75.

Dalsgaard, K., Jensen, J. L., Sorensen, M., 1991. Methodology of sieving small samples and calibration of sieve set. In: Syvitski, J. P. M. (ed.), Principles, Methods, and Applications of Particle Size Analysis. Cambridge University Press, Cambridge, pp. 64-75.

Darling, A., Rider, K., Gloyd, J., Cole, R., 2007a. Sedimentological characteristics of Late Cenozoic gravel-armored surfaces on the southwestern flank of Grand Mesa, Western Colorado. Geological Society of America Annual Meeting Paper No. 113-7.

Darling, A., Aslan, A., Betton, C. W., Cole, R., Karlstrom, K., 2007b. Late Quaternary incision rates and drainage evolution of the confluence of the Uncompahgre and Gunnison Rivers based on terraces dated with lava Creek B Ash, Western Colorado. Geological Society of America Annual Meeting Paper No. 113-4.

Darling, A., Karlstrom, K. E., Aslan, A., Cole, R., Betton, C., Wan, E., 2009. Quaternary incision rates and drainage evolution of the Uncompahgre and Gunnison Rivers, western Colorado, as calibrated by the Lava Creek B Ash. Rocky Mountain Geology. 44(1), 71-83.

Davis, J. C., 1973. Statistics and Data Analysis in Geology. John Wiley & Sons, Inc., New York.

Eyles, N., Miall, A.D., 1984. Glacial facies. In: Walker, R. G. (ed.), Facies Models. Geological Association of Canada, Toronto, Ontario, pp. 15-38.

Folk, R. L., 1974. Petrology of Sedimentary Rocks. Hemphill Publishing Co., Austin, TX.

Graham, J., 1988. Collection and analysis of field data. In: Tucker, M. (ed.), Techniques in Sedimentology. Blackwell Science, Osney Mead, Oxford, pp. 5-62.

Henderson, J., 1923. The glacial geology of Grand Mesa, Colorado. Journal of Geology. 31(8), 676-678.

High Plains Regional Climate Center. 1971-2000 Monthly Climate Summary: Cedaredge, CO (051440). http://www.hprcc.unl.edu/cgi-bin/cli_perl_lib/cliMAIN.pl?co1440 (accessed on 9/29/2009).

King, C. A. M., 1967. Techniques in Geomorphology. Edward Arnold Ltd., London.

Krumbein, W. C., 1934. Size frequency distributions of sediments. Journal of Sedimentary Petrology. 4, 65-77.

McCave, I. N., Syvitski, J. P. M., 1991. Principles and methods of geological particle size analysis. In: Syvitski, J. P. M., (ed.), Principles, Methods, and Applications of Particle Size Analysis. Cambridge University Press, Cambridge, pp. 1-21.

McManus, J., 1988. Grain-size determination and interpretation. In: Tucker, M. (ed.), Techniques in Sedimentology. Blackwell Science, Osney Mead, Oxford, pp. 63-85.

Miall, A. D., 1977. A review of the braided-river depositional environment. Earth Science Reviews. 13, 1-62.

Miall, A. D., 1978. Lithofacies types and vertical profile models in braided-river deposits: A summary. In: Miall, A. D. (ed.), Fluvial Sedimentology. Canadian Society of Petroleum Geologists, Calgary, pp. 597-604.

Miller, J. M. G., 2006. Glacial sediments. In: Reading, H. G. (ed.), Sedimentary Environments: Processes, Facies and Stratigraphy. Blackwell Publishing, Malden, MA, pp. 454-484.

Mutel, C. F., Emerick, J. C., 1992. From Grassland to Glacier. Johnson Publishing, Boulder, CO.

Nemec, W., Steel, R. J., 1984. Alluvial and coastal conglomerates: Their significant features and some comments on gravelly mass-flow deposits. In: Koster, E. H., Steel, R. J (eds.), Sedimentology of Gravels and Conglomerates. Canadian Society of Petroleum Geologists, Calgary. Memoir 10, pp. 1-31.

Pettijohn, F. J., 1975. Sedimentary Rocks. Harper & Row, Publishers, New York.

Ramaley, F., 1927. Colorado Plant Life. University of Colorado, Boulder, CO.

Reineck, H.-E., Singh, I. B., 1973. Depositional Sedimentary Environments. Springer-Verlag, New York.

Retzer, J. L., 1954. Glacial advances and soil development, Grand Mesa, CO. American Journal of Science. 252, 26-37.

Richmond, G.M., 1965. Glaciation of the Rocky Mountains. In: Wright, H.E. Jr., Frey, D.G. (eds.), The Quaternary of the United States. Princeton University Press, Princeton, New Jersey, pp. 217-230.

Richmond, G.M., 1986. Stratigraphy and correlation of glacial deposits of the Rocky Mountains, the Colorado Plateau, and the ranges of the Great Basin. In: Sibrava, V., Bowen, D.Q. and Richmond, G.M. (eds.), Quaternary Glaciations in the Northern Hemisphere. Pergamon Press, New York, pp. 99-127.

Rider, K., Darling, A., Gloyd, J., Cole, R., 2006. Relative ages and origins of Late Cenozoic pediments on the south flank of Grand Mesa, Colorado. Rocky Mountain Section - 58th Annual Meeting Paper No. 16-5.

Ritter, D. F., Kochel, R. C., Miller, J. R., 2002. Process Geomorphology. Waveland Press, Inc. Long Grove, IL.

Robinson, C., Dea, P., 1981. Quaternary glacial and slope-failure deposits of the Crested Butte area, Gunnison County, Colorado. New Mexico Geological Society Guidebook, 32nd Field Conference, Western Slope Colorado, pp. 155-163.

Rust, B. R., 1978. Depositional models for braided alluvium. In: Miall, A. D. (ed.), Fluvial Sedimentology. Canadian Society of Petroleum Geologists, Calgary, pp. 605-626.

Rust, B. R., Koster, E. H., 1984. Coarse alluvial deposits. In: Walker, R. G. (ed.), Facies Models. Geological Association of Canada, Toronto, Ontario, pp. 53-69.

Sahu, B. K., 1964. Depositional mechanisms from the size analysis of clastic sediments. Journal of Sedimentary Petrology. 34, 73-83.

Sandoval, M. M., 2007. Quaternary incision history of the Black Canyon of the Gunnison, Colorado. M.S. thesis, The University of New Mexico, Albuquerque.

Sinnock, S., 1978. Geomorphology of the Uncompahgre Plateau and Grand Valley, Western Colorado, U.S.A. Ph.D. dissertation, Purdue University, West Lafayette.

Sinnock, S., 1981. Glacial moraines, terraces and pediments of Grand Valley, Western Colorado. New Mexico Geological Society Guidebook, 32nd Field Conference, Western Slope Colorado, pp. 113-120.

Yeend, W. E., 1965. Quaternary geology of the Grand Mesa area, Western Colorado. Ph.D. dissertation, University of Wisconsin, Madison.

APPENDIX A

ANALYSIS OF GRAIN-SIZE DATA

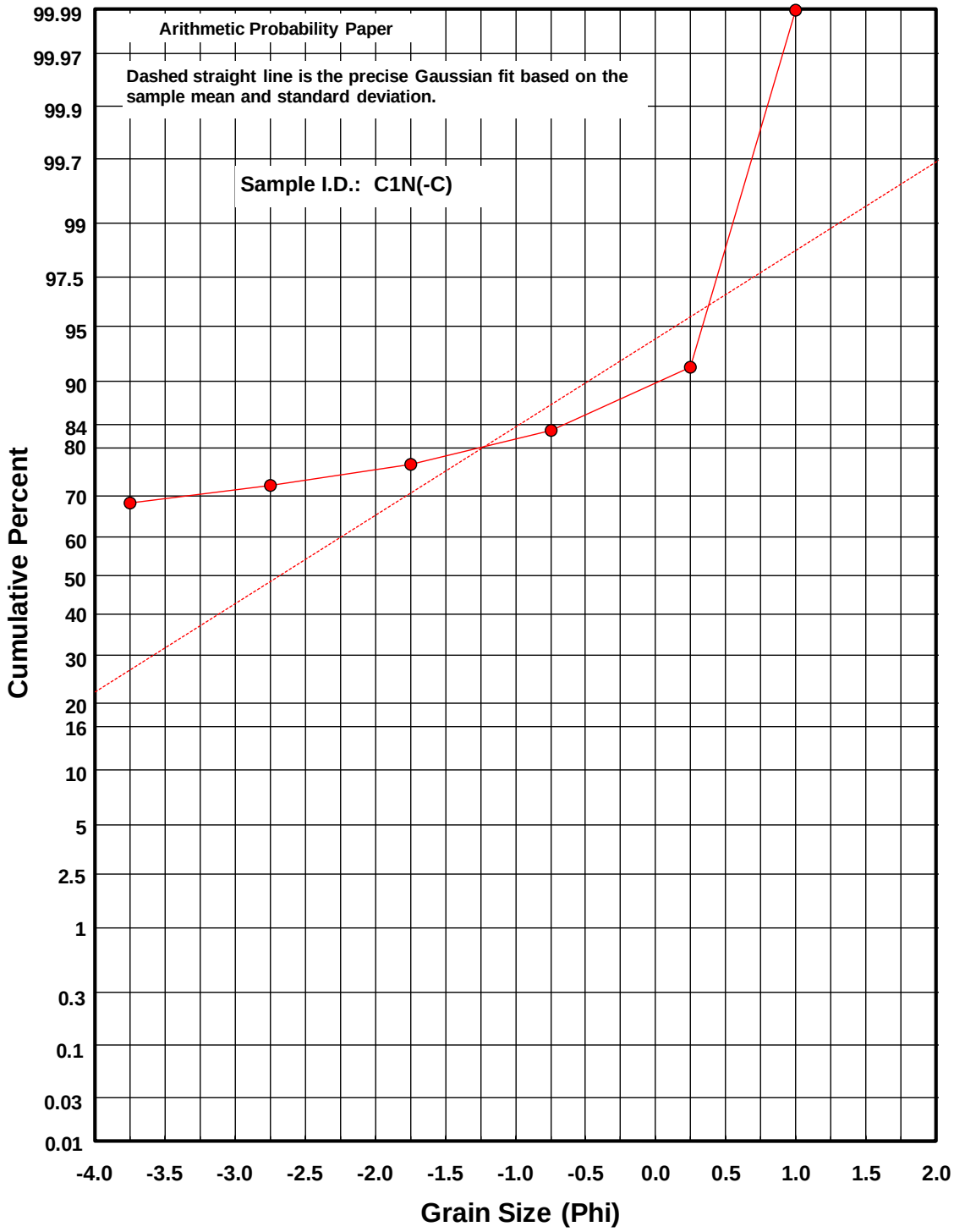
Arithmetic Probability Paper
Dashed straight line is the precise Gaussian fit based on the sample mean and standard deviation.
Sample I.D.: C1N(-C)
Cumulative Percent
99.99
99.97
99.9
99.7
99
97.5
95
90
84
80
70
60
50
40
30
20
16
10
5
2.5
1
0.3
0.1
0.03
0.01
-4.0
-3.5
-3.0
-2.5
-2.0
-1.5
-1.0
-0.5
0.0
0.5
1.0
1.5
2.0
Grain Size (Phi)

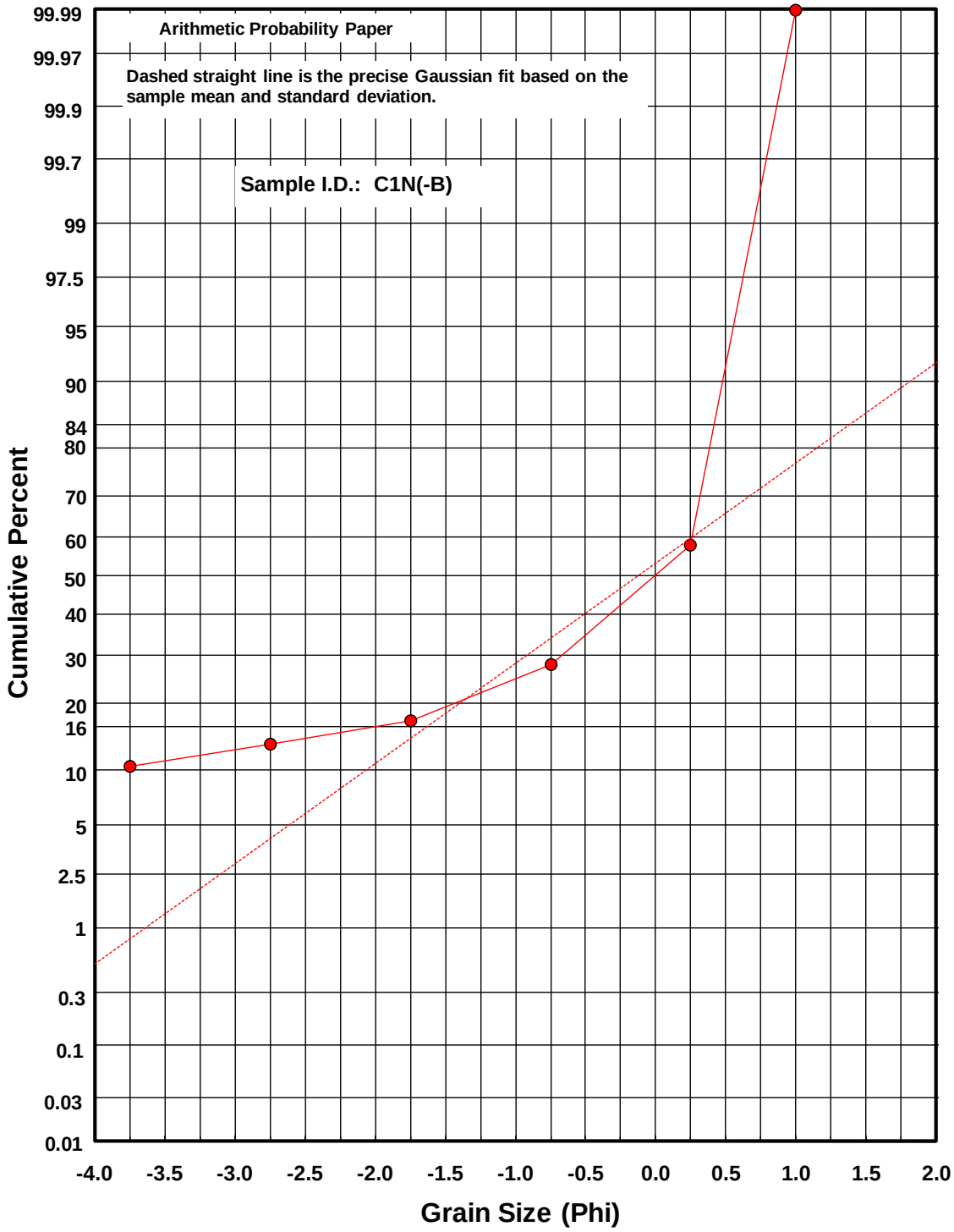
Arithmetic Probability Paper
Dashed straight line is the precise Gaussian fit based on the sample mean and standard deviation.
Sample I.D.: C1N(-B)
Cumulative Percent
99.99
99.97
99.9
99.7
99
97.5
95
90
84
80
70
60
50
40
30
20
16
10
5
2.5
1
0.3
0.1
0.03
0.01
-4.0
-3.5
-3.0
-2.5
-2.0
-1.5
-1.0
-0.5
0.0
0.5
1.0
1.5
2.0
Grain Size (Phi)

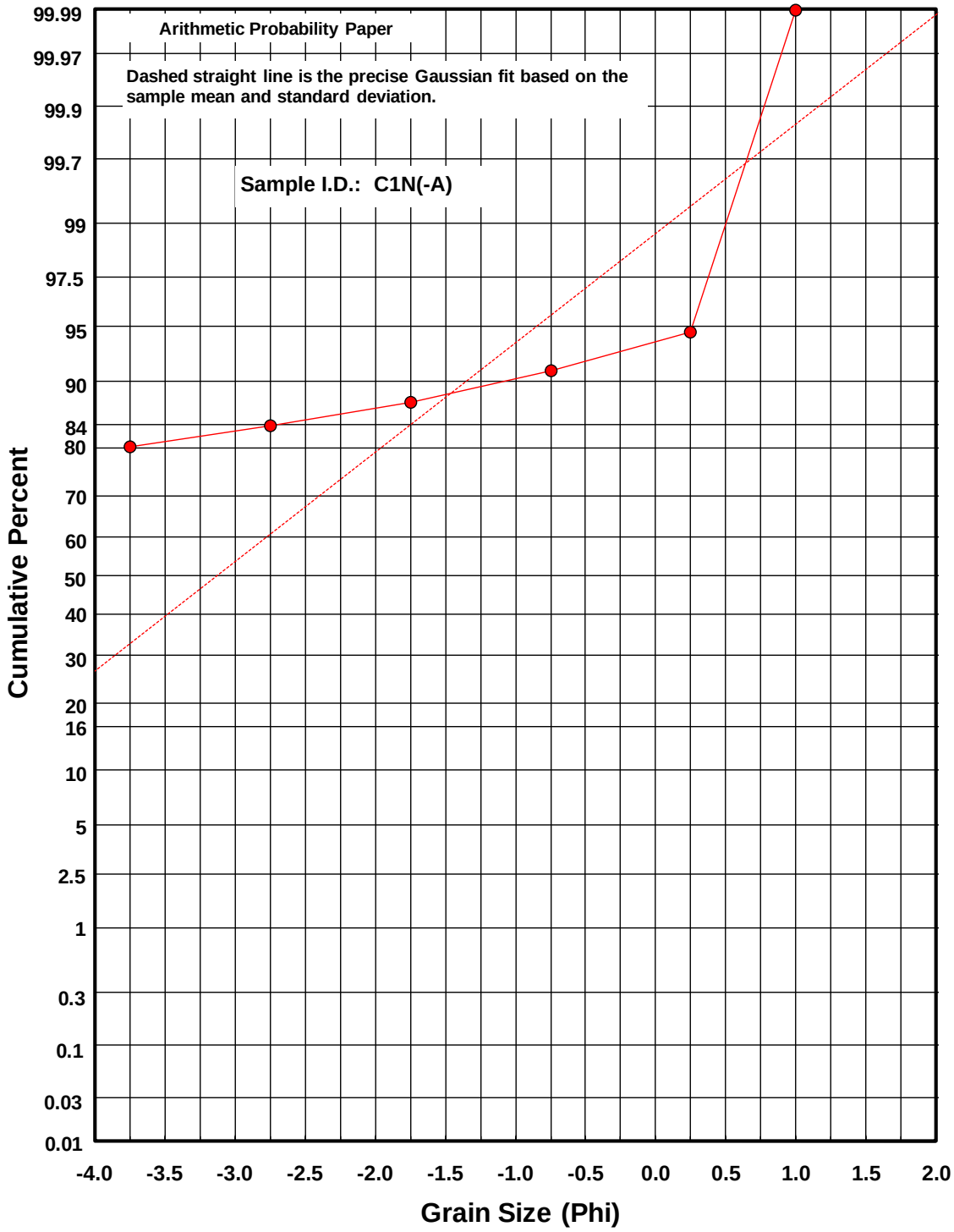
Arithmetic Probability Paper
Dashed straight line is the precise Gaussian fit based on the sample mean and standard deviation.
Sample I.D.: C1N(-A)
Cumulative Percent
99.99
99.97
99.9
99.7
99
97.5
95
90
84
80
70
60
50
40
30
20
16
10
5
2.5
1
0.3
0.1
0.03
0.01
-4.0
-3.5
-3.0
-2.5
-2.0
-1.5
-1.0
-0.5
0.0
0.5
1.0
1.5
2.0
Grain Size (Phi)

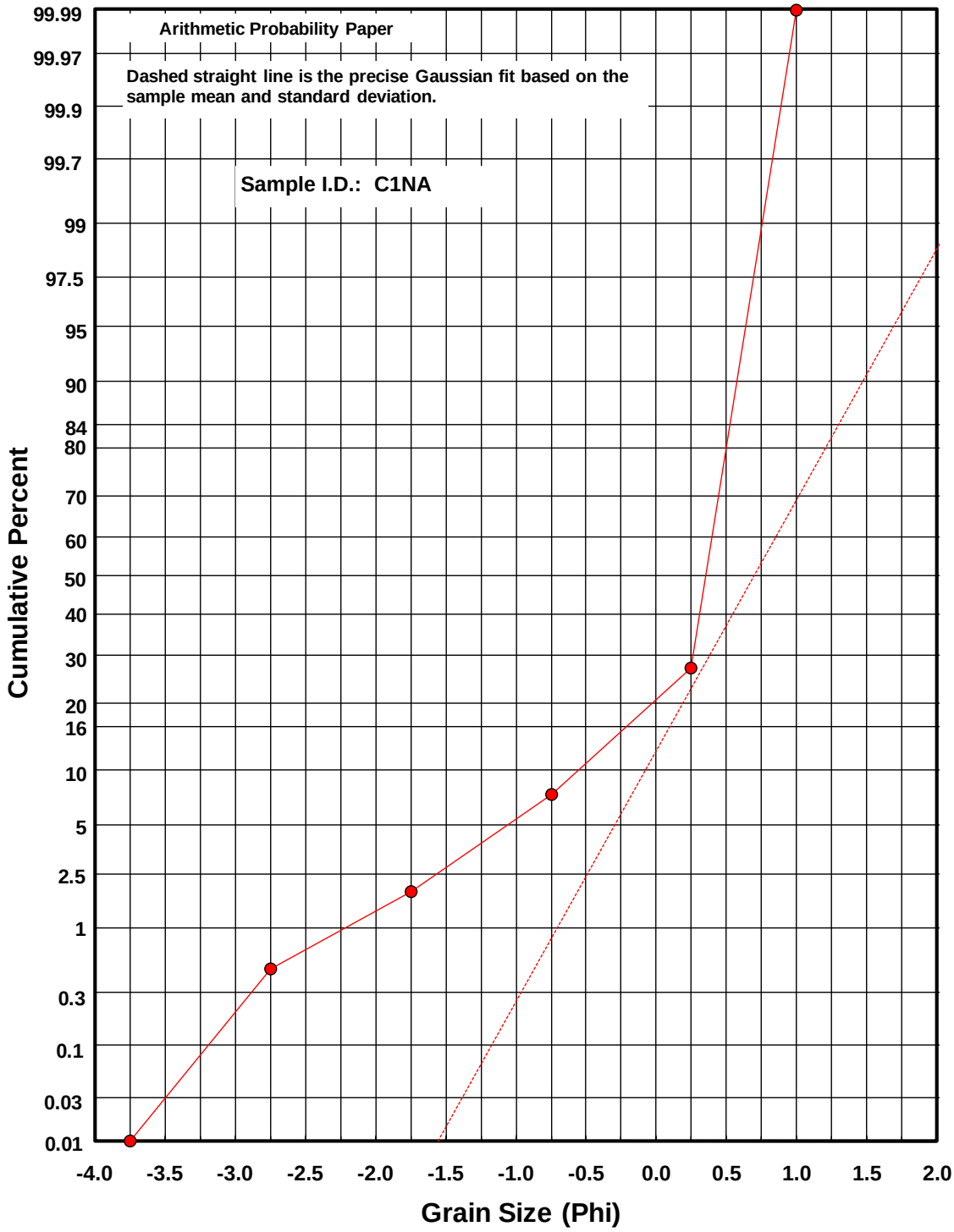
Arithmetic Probability Paper
Dashed straight line is the precise Gaussian fit based on the sample mean and standard deviation.
Sample I.D.: C1NA
Cumulative Percent
99.99
99.97
99.9
99.7
99
97.5
95
90
84
80
70
60
50
40
30
20
16
10
5
2.5
1
0.3
0.1
0.03
0.01
-4.0
-3.5
-3.0
-2.5
-2.0
-1.5
-1.0
-0.5
0.0
0.5
1.0
1.5
2.0
Grain Size (Phi)

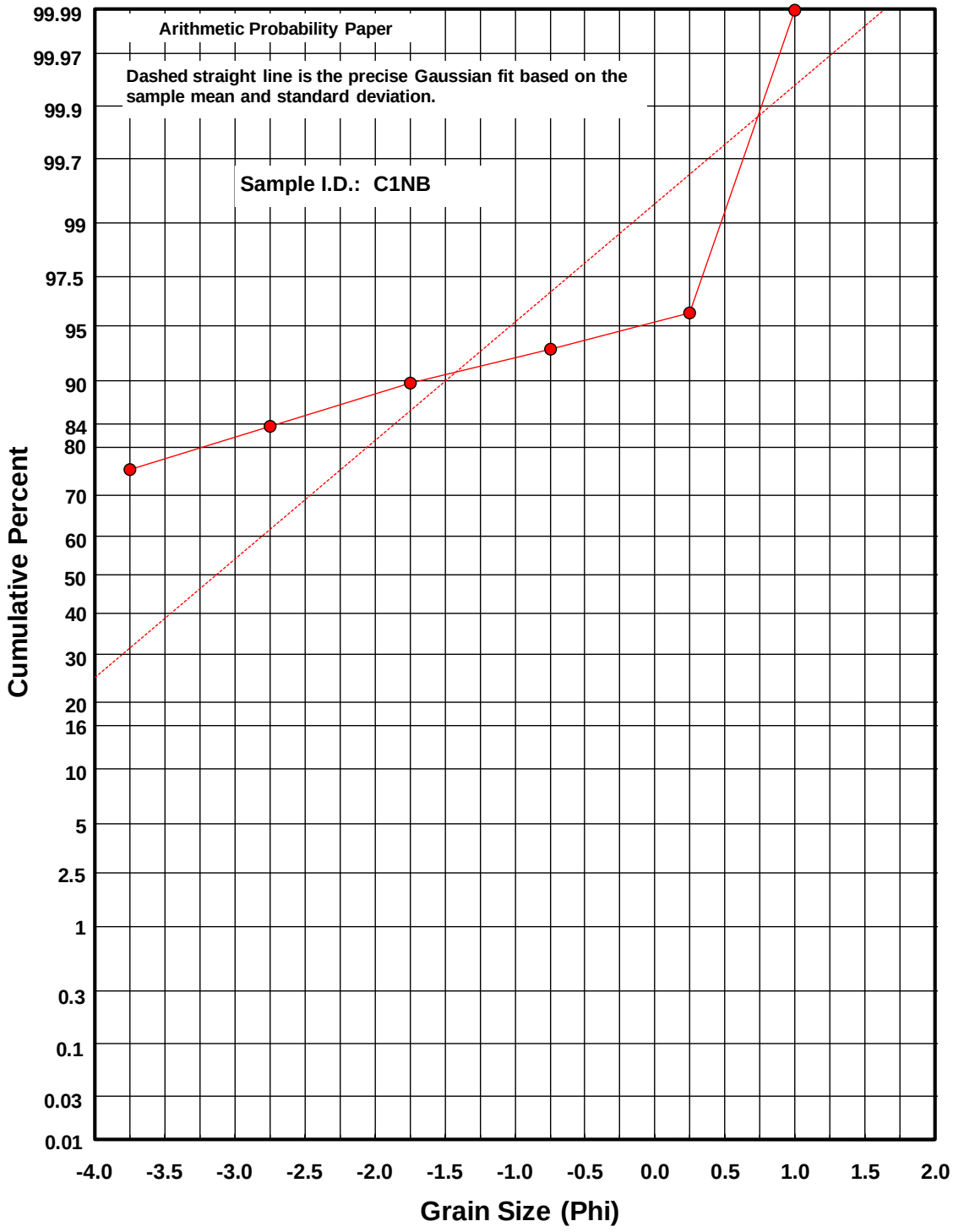
Arithmetic Probability Paper
Dashed straight line is the precise Gaussian fit based on the sample mean and standard deviation.
Sample I.D.: C1NB
Cumulative Percent
99.99
99.97
99.9
99.7
99
97.5
95
90
84
80
70
60
50
40
30
20
16
10
5
2.5
1
0.3
0.1
0.03
0.01
-4.0
-3.5
-3.0
-2.5
-2.0
-1.5
-1.0
-0.5
0.0
0.5
1.0
1.5
2.0
Grain Size (Phi)

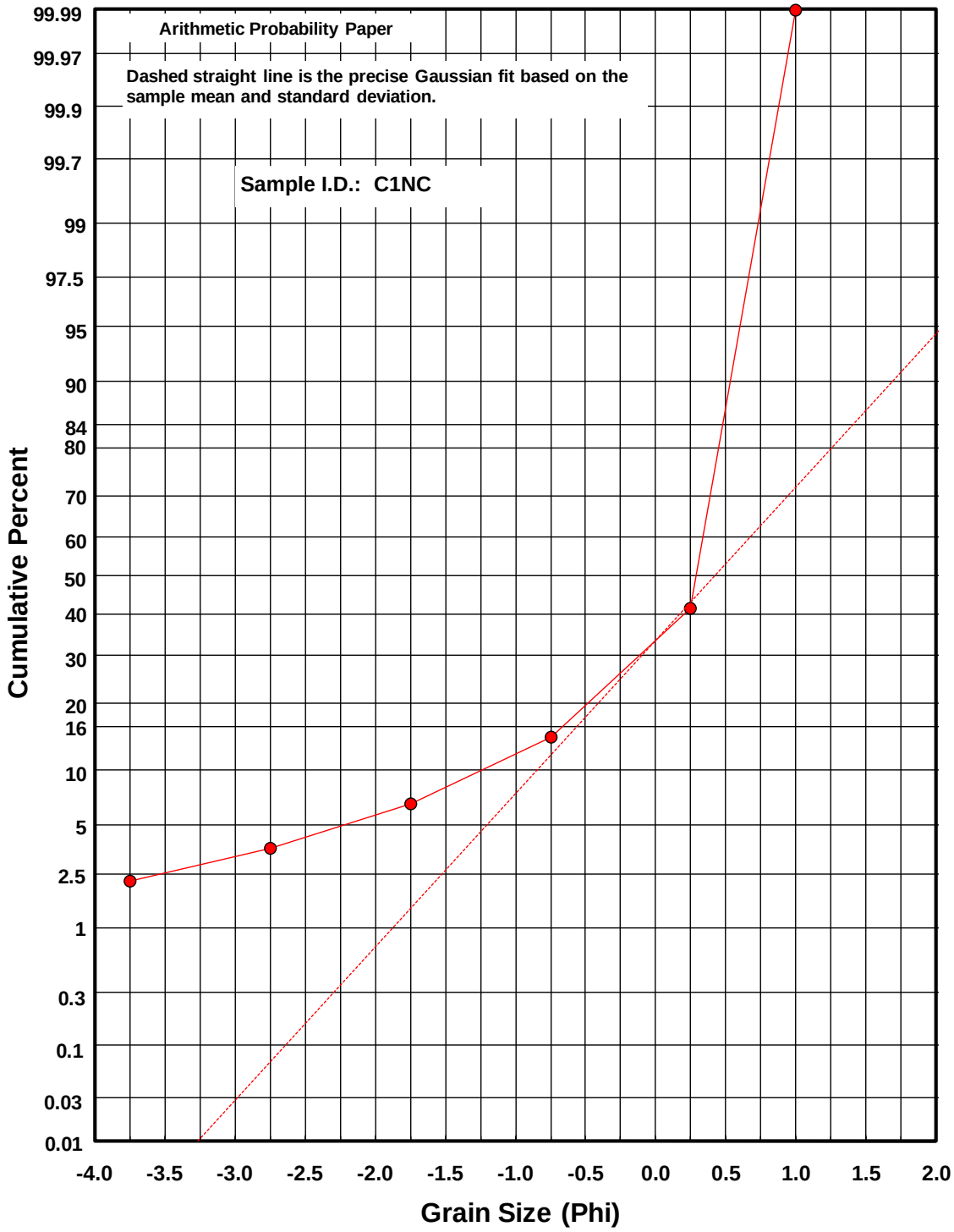
Arithmetic Probability Paper
Dashed straight line is the precise Gaussian fit based on the sample mean and standard deviation.
Sample I.D.: C1NC
Cumulative Percent
99.99
99.97
99.9
99.7
99
97.5
95
90
84
80
70
60
50
40
30
20
16
10
5
2.5
1
0.3
0.1
0.03
0.01
-4.0
-3.5
-3.0
-2.5
-2.0
-1.5
-1.0
-0.5
0.0
0.5
1.0
1.5
2.0
Grain Size (Phi)

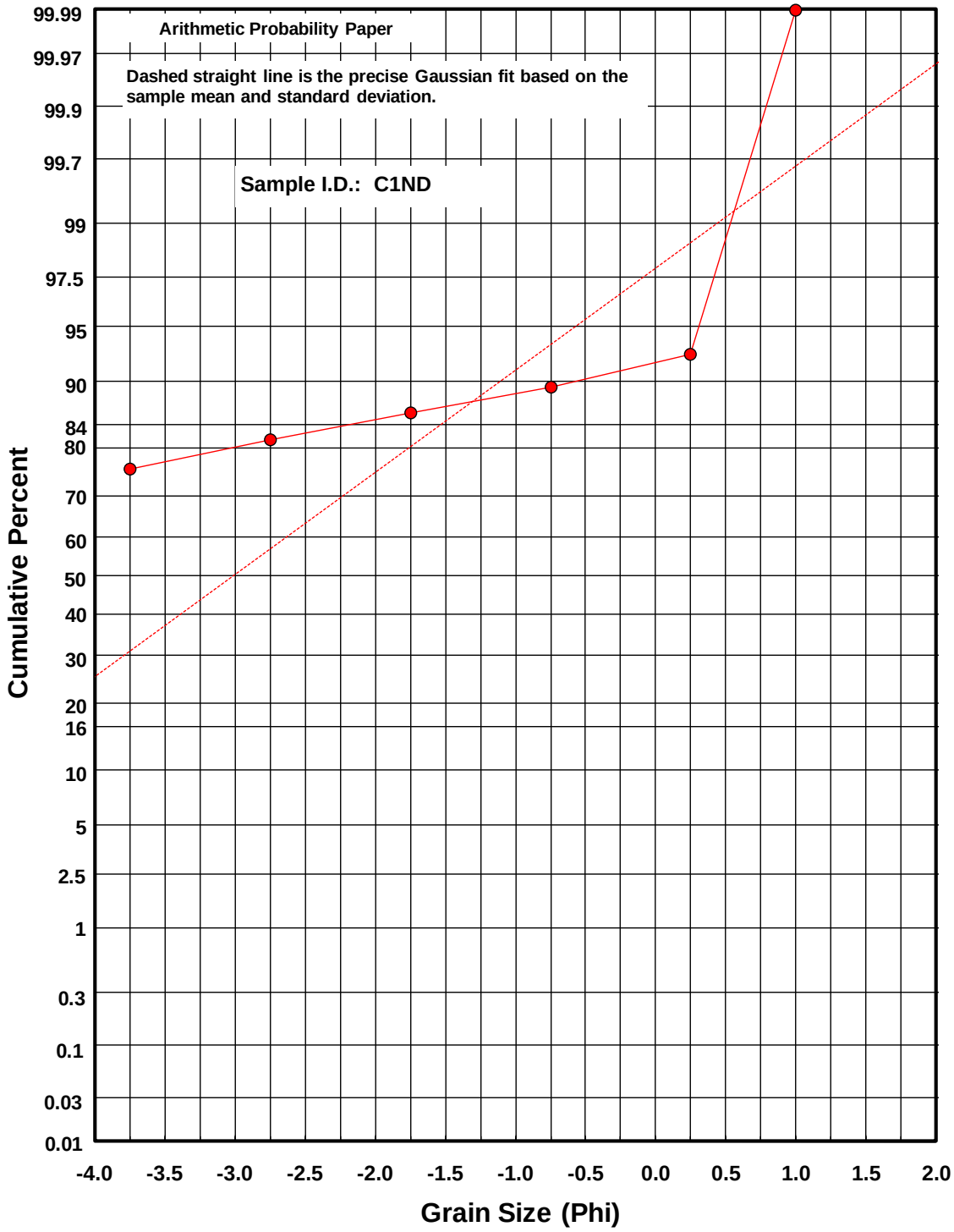
Arithmetic Probability Paper
Dashed straight line is the precise Gaussian fit based on the sample mean and standard deviation.
Sample I.D.: C1ND
Cumulative Percent
99.99
99.97
99.9
99.7
99
97.5
95
90
84
80
70
60
50
40
30
20
16
10
5
2.5
1
0.3
0.1
0.03
0.01
-4.0
-3.5
-3.0
-2.5
-2.0
-1.5
-1.0
-0.5
0.0
0.5
1.0
1.5
2.0
Grain Size (Phi)

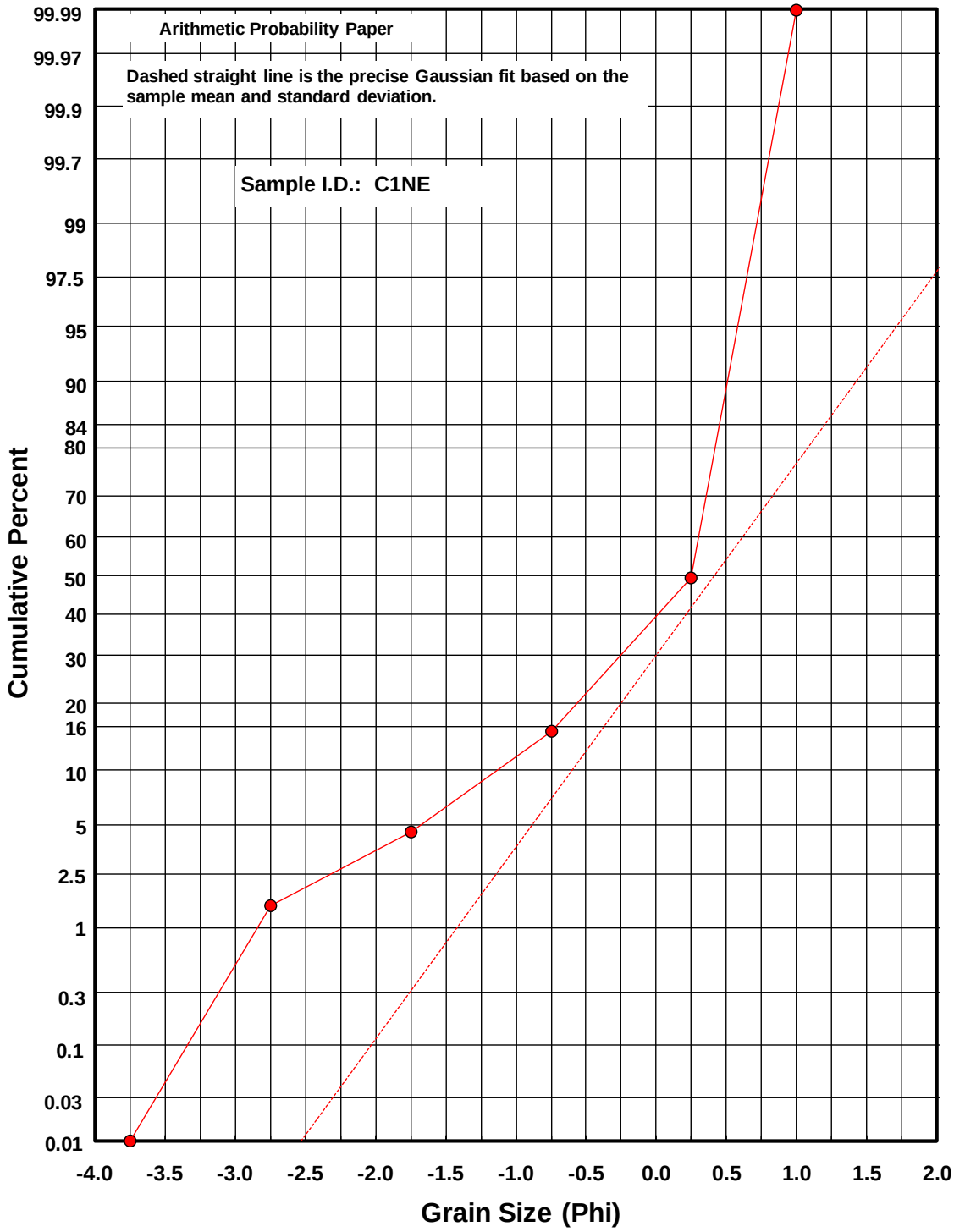
Arithmetic Probability Paper
Dashed straight line is the precise Gaussian fit based on the sample mean and standard deviation.
Sample I.D.: C1NE
Cumulative Percent
99.99
99.97
99.9
99.7
99
97.5
95
90
84
80
70
60
50
40
30
20
16
10
5
2.5
1
0.3
0.1
0.03
0.01
-4.0
-3.5
-3.0
-2.5
-2.0
-1.5
-1.0
-0.5
0.0
0.5
1.0
1.5
2.0
Grain Size (Phi)

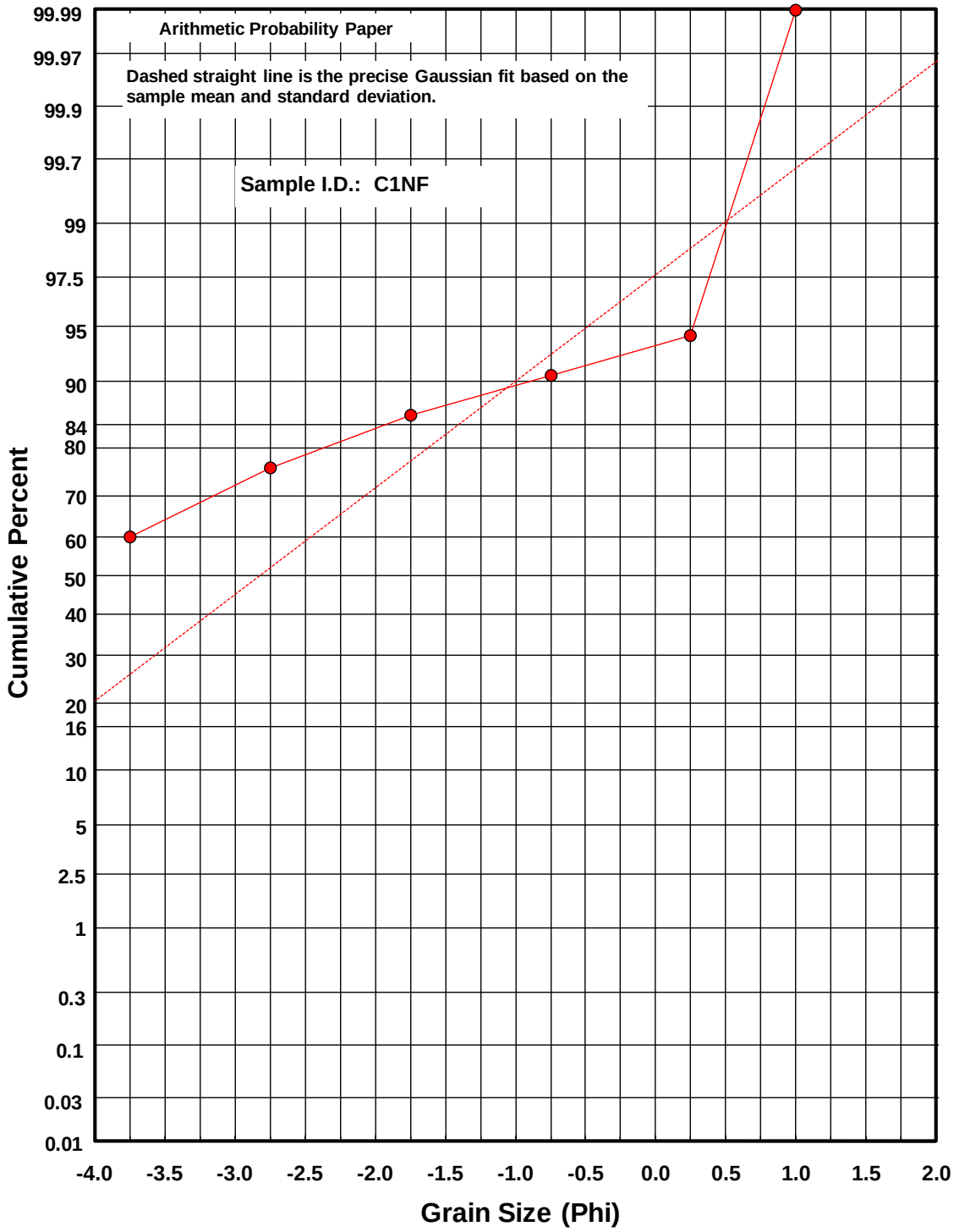
Arithmetic Probability Paper
Dashed straight line is the precise Gaussian fit based on the sample mean and standard deviation.
Sample I.D.: C1NF
Cumulative Percent
99.99
99.97
99.9
99.7
99
97.5
95
90
84
80
70
60
50
40
30
20
16
10
5
2.5
1
0.3
0.1
0.03
0.01
-4.0
-3.5
-3.0
-2.5
-2.0
-1.5
-1.0
-0.5
0.0
0.5
1.0
1.5
2.0
Grain Size (Phi)

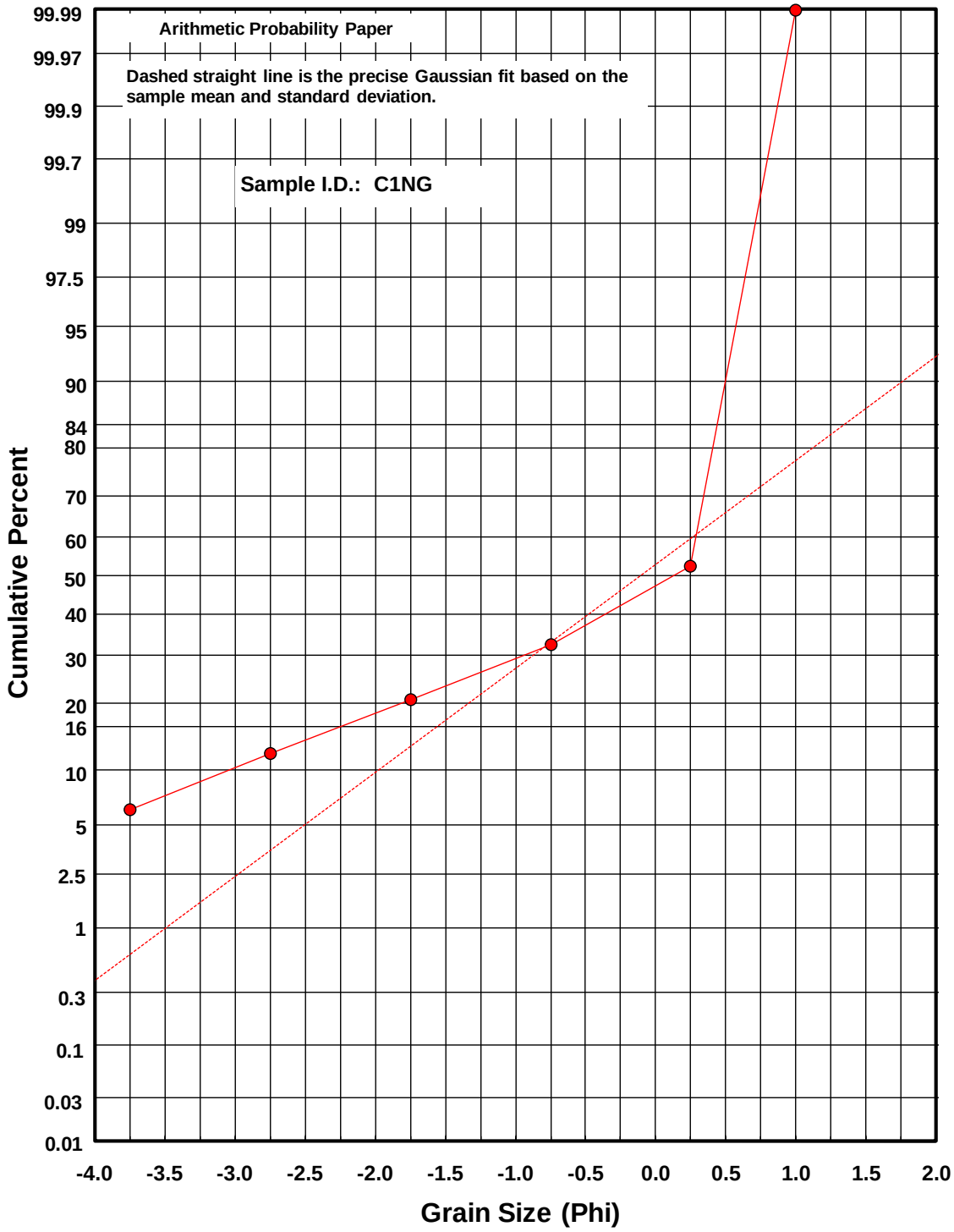
Arithmetic Probability Paper
Dashed straight line is the precise Gaussian fit based on the sample mean and standard deviation.
Sample I.D.: C1NG
Cumulative Percent
99.99
99.97
99.9
99.7
99
97.5
95
90
84
80
70
60
50
40
30
20
16
10
5
2.5
1
0.3
0.1
0.03
0.01
-4.0
-3.5
-3.0
-2.5
-2.0
-1.5
-1.0
-0.5
0.0
0.5
1.0
1.5
2.0
Grain Size (Phi)

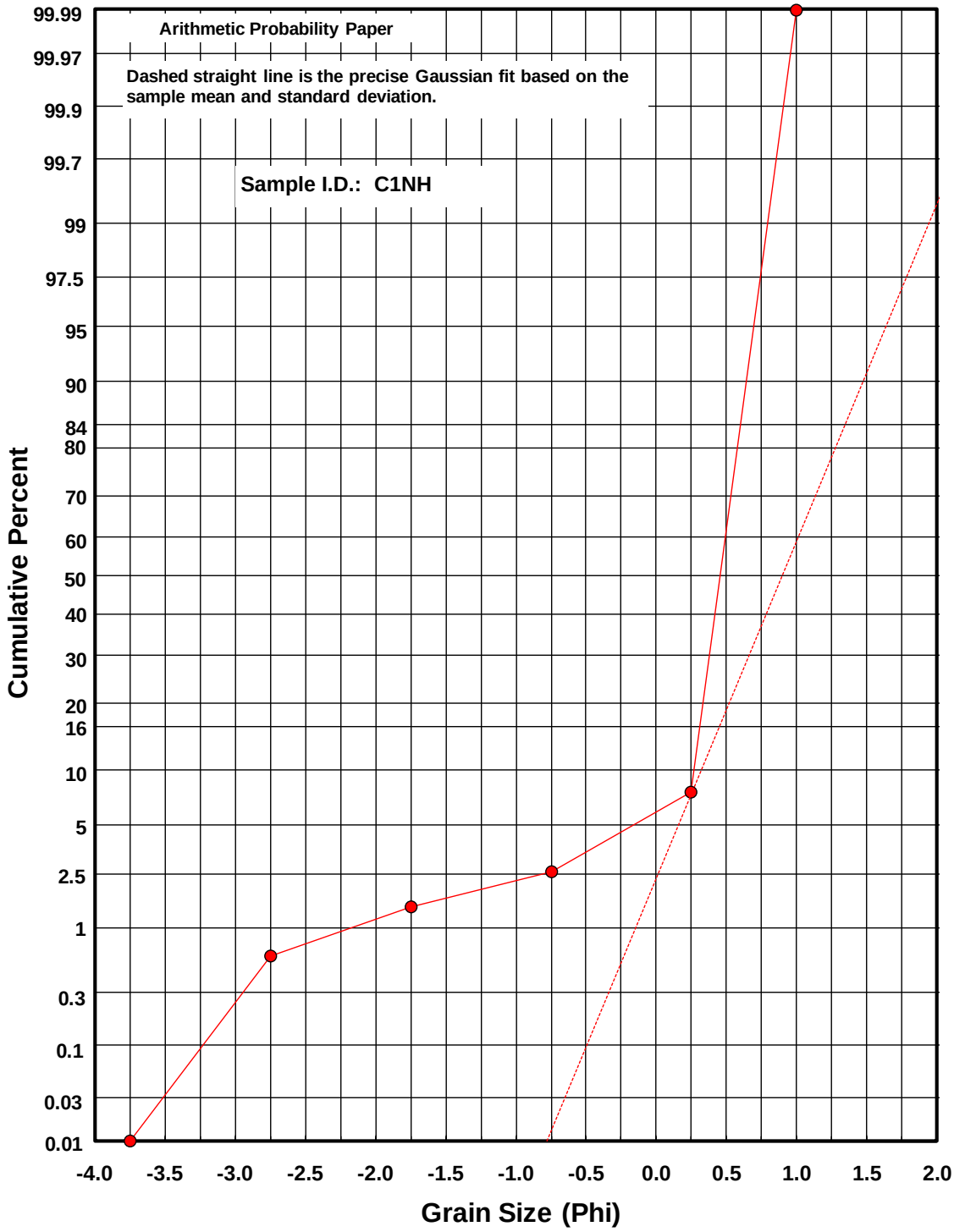
Arithmetic Probability Paper
Dashed straight line is the precise Gaussian fit based on the sample mean and standard deviation.
Sample I.D.: C1NH
Cumulative Percent
99.99
99.97
99.9
99.7
99
97.5
95
90
84
80
70
60
50
40
30
20
16
10
5
2.5
1
0.3
0.1
0.03
0.01
-4.0
-3.5
-3.0
-2.5
-2.0
-1.5
-1.0
-0.5
0.0
0.5
1.0
1.5
2.0
Grain Size (Phi)

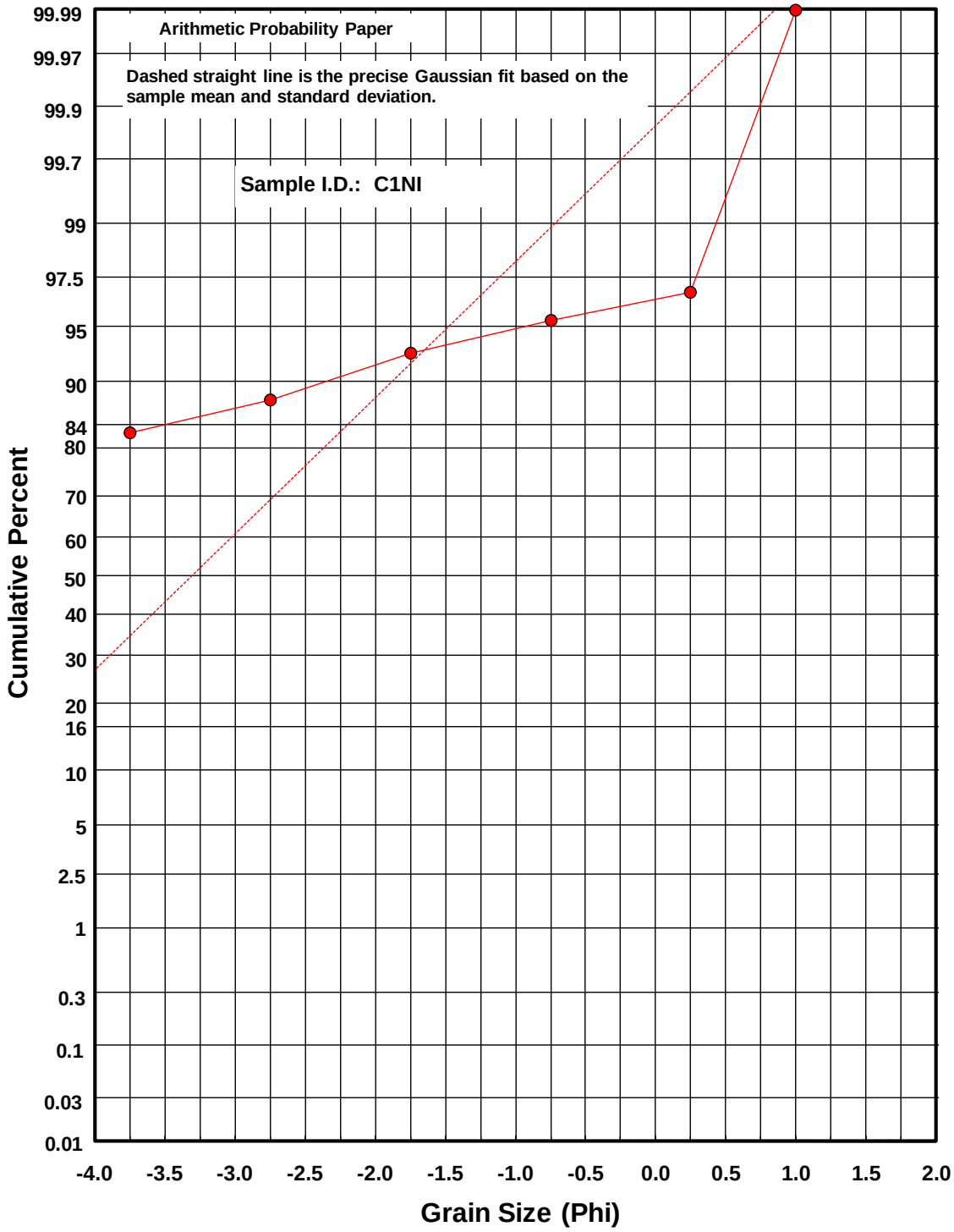
Arithmetic Probability Paper
Dashed straight line is the precise Gaussian fit based on the sample mean and standard deviation.
Sample I.D.: C1NI
Cumulative Percent
99.99
99.97
99.9
99.7
99
97.5
95
90
84
80
70
60
50
40
30
20
16
10
5
2.5
1
0.3
0.1
0.03
0.01
-4.0
-3.5
-3.0
-2.5
-2.0
-1.5
-1.0
-0.5
0.0
0.5
1.0
1.5
2.0
Grain Size (Phi)

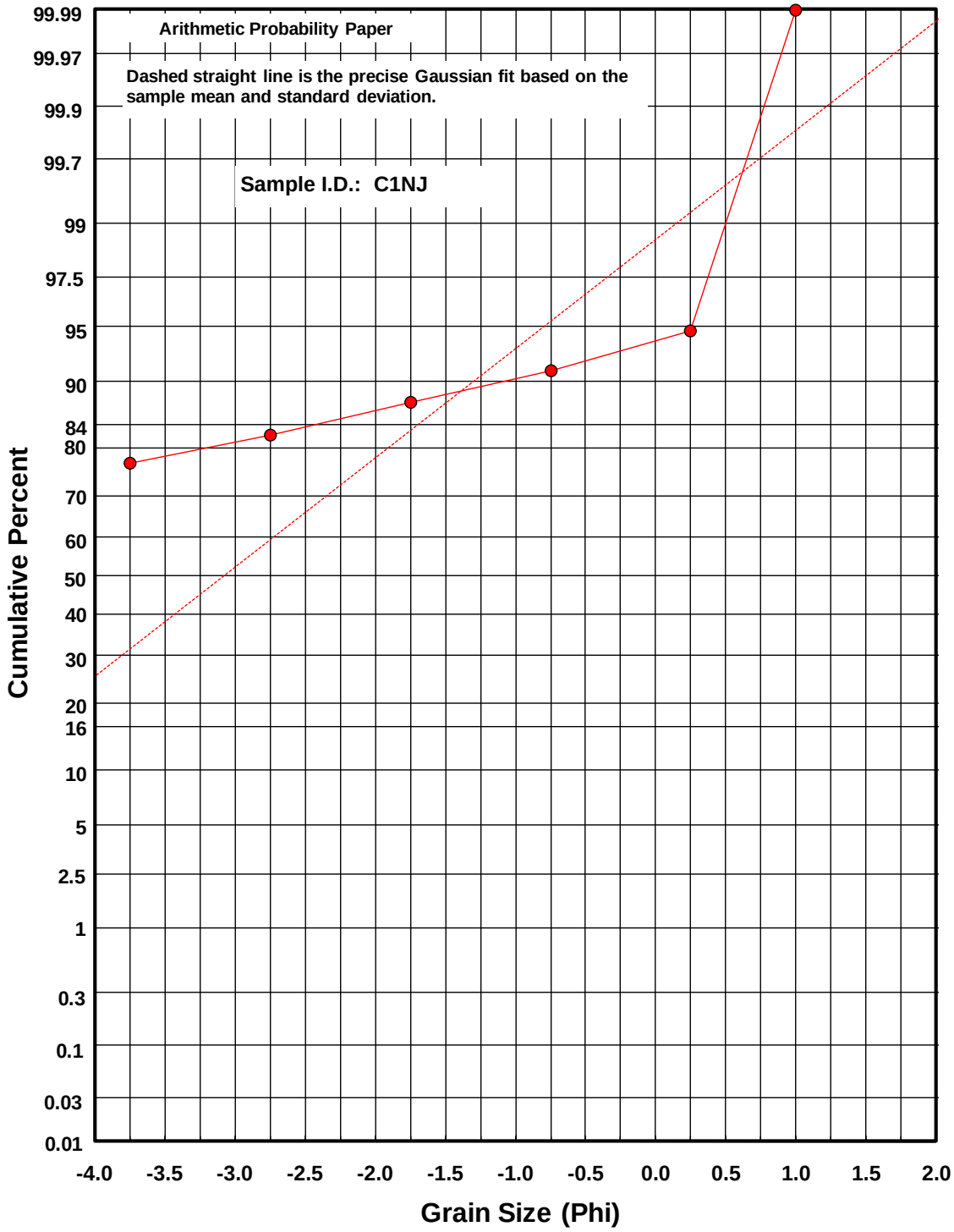
Arithmetic Probability Paper
Dashed straight line is the precise Gaussian fit based on the sample mean and standard deviation.
Sample I.D.: C1NJ
Cumulative Percent
99.99
99.97
99.9
99.7
99
97.5
95
90
84
80
70
60
50
40
30
20
16
10
5
2.5
1
0.3
0.1
0.03
0.01
-4.0
-3.5
-3.0
-2.5
-2.0
-1.5
-1.0
-0.5
0.0
0.5
1.0
1.5
2.0
Grain Size (Phi)

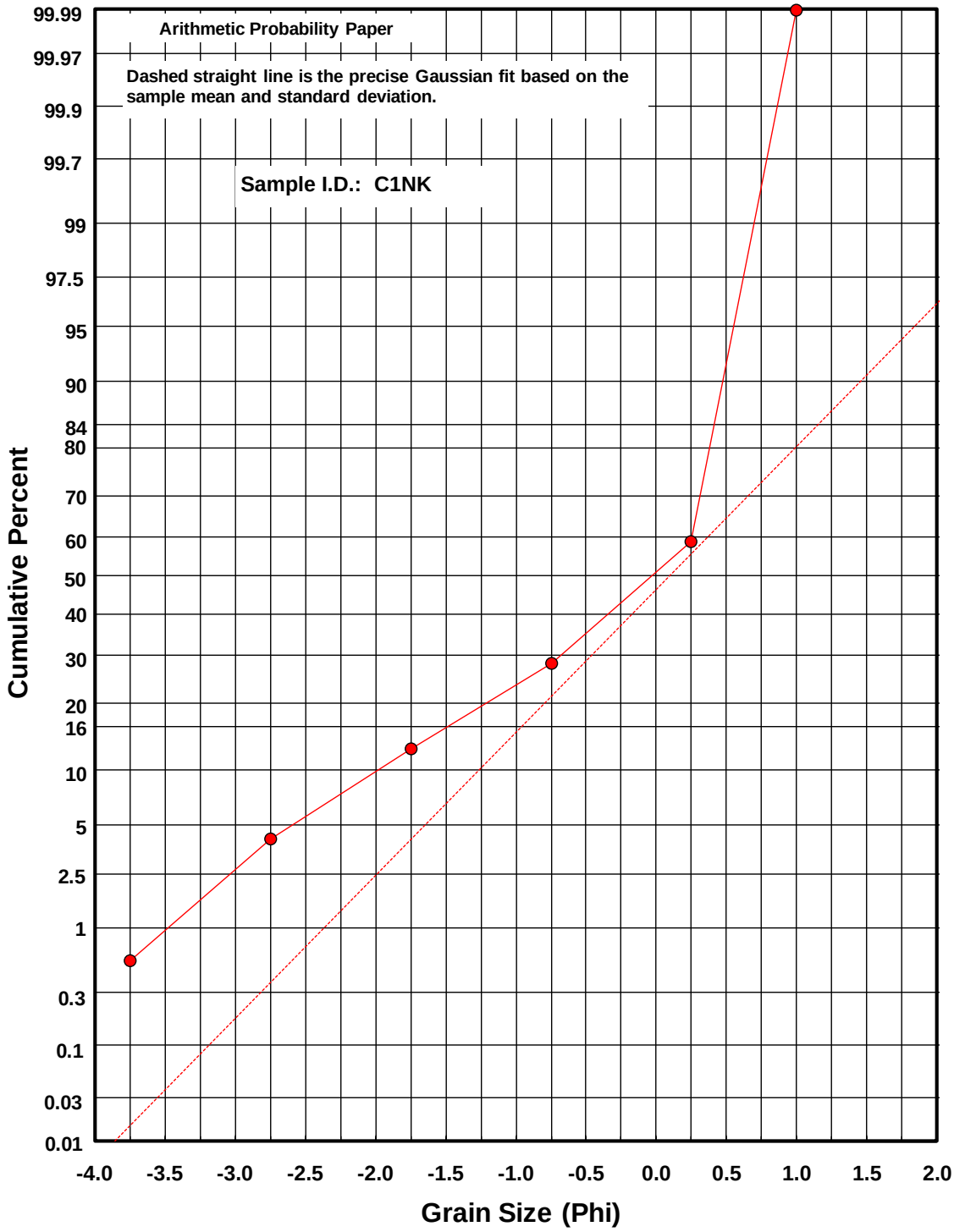
Arithmetic Probability Paper
Dashed straight line is the precise Gaussian fit based on the sample mean and standard deviation.
Sample I.D.: C1NK
Cumulative Percent
99.99
99.97
99.9
99.7
99
97.5
95
90
84
80
70
60
50
40
30
20
16
10
5
2.5
1
0.3
0.1
0.03
0.01
-4.0
-3.5
-3.0
-2.5
-2.0
-1.5
-1.0
-0.5
0.0
0.5
1.0
1.5
2.0
Grain Size (Phi)

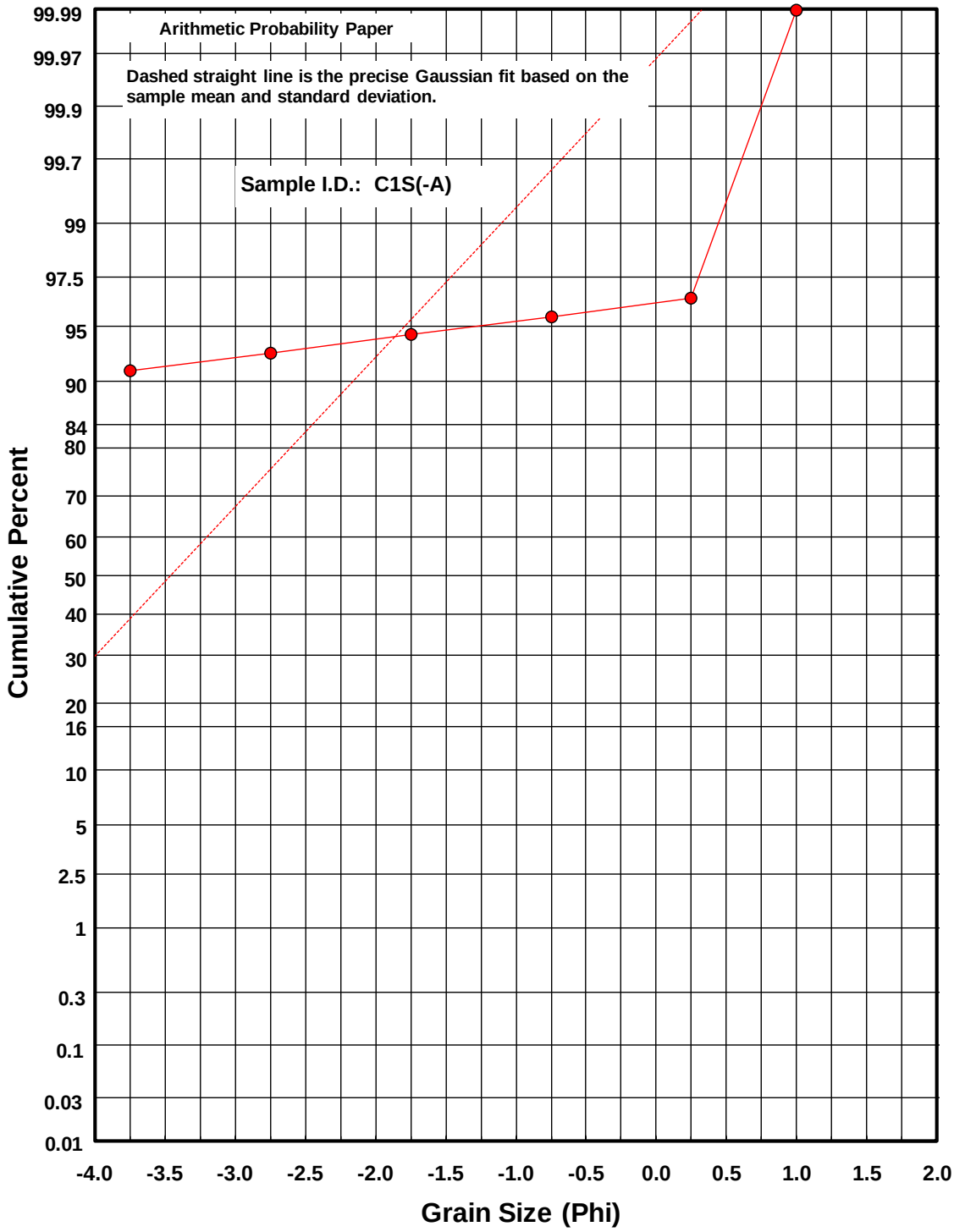
Arithmetic Probability Paper
Dashed straight line is the precise Gaussian fit based on the sample mean and standard deviation.
Sample I.D.: C1S(-A)
Cumulative Percent
99.99
99.97
99.9
99.7
99
97.5
95
90
84
80
70
60
50
40
30
20
16
10
5
2.5
1
0.3
0.1
0.03
0.01
-4.0
-3.5
-3.0
-2.5
-2.0
-1.5
-1.0
-0.5
0.0
0.5
1.0
1.5
2.0
Grain Size (Phi)

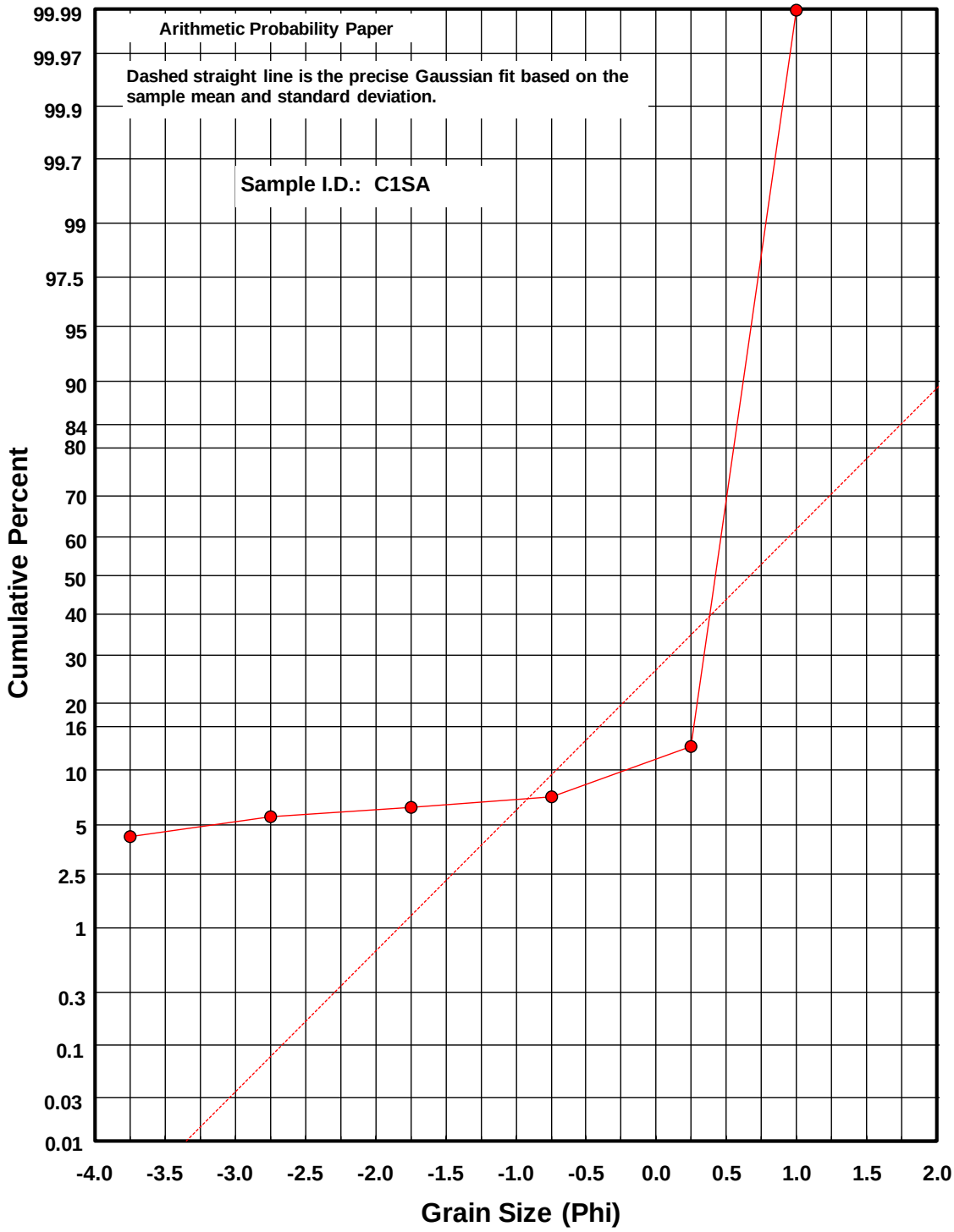
Arithmetic Probability Paper
Dashed straight line is the precise Gaussian fit based on the sample mean and standard deviation.
Sample I.D.: C1SA
Cumulative Percent
99.99
99.97
99.9
99.7
99
97.5
95
90
84
80
70
60
50
40
30
20
16
10
5
2.5
1
0.3
0.1
0.03
0.01
-4.0
-3.5
-3.0
-2.5
-2.0
-1.5
-1.0
-0.5
0.0
0.5
1.0
1.5
2.0
Grain Size (Phi)

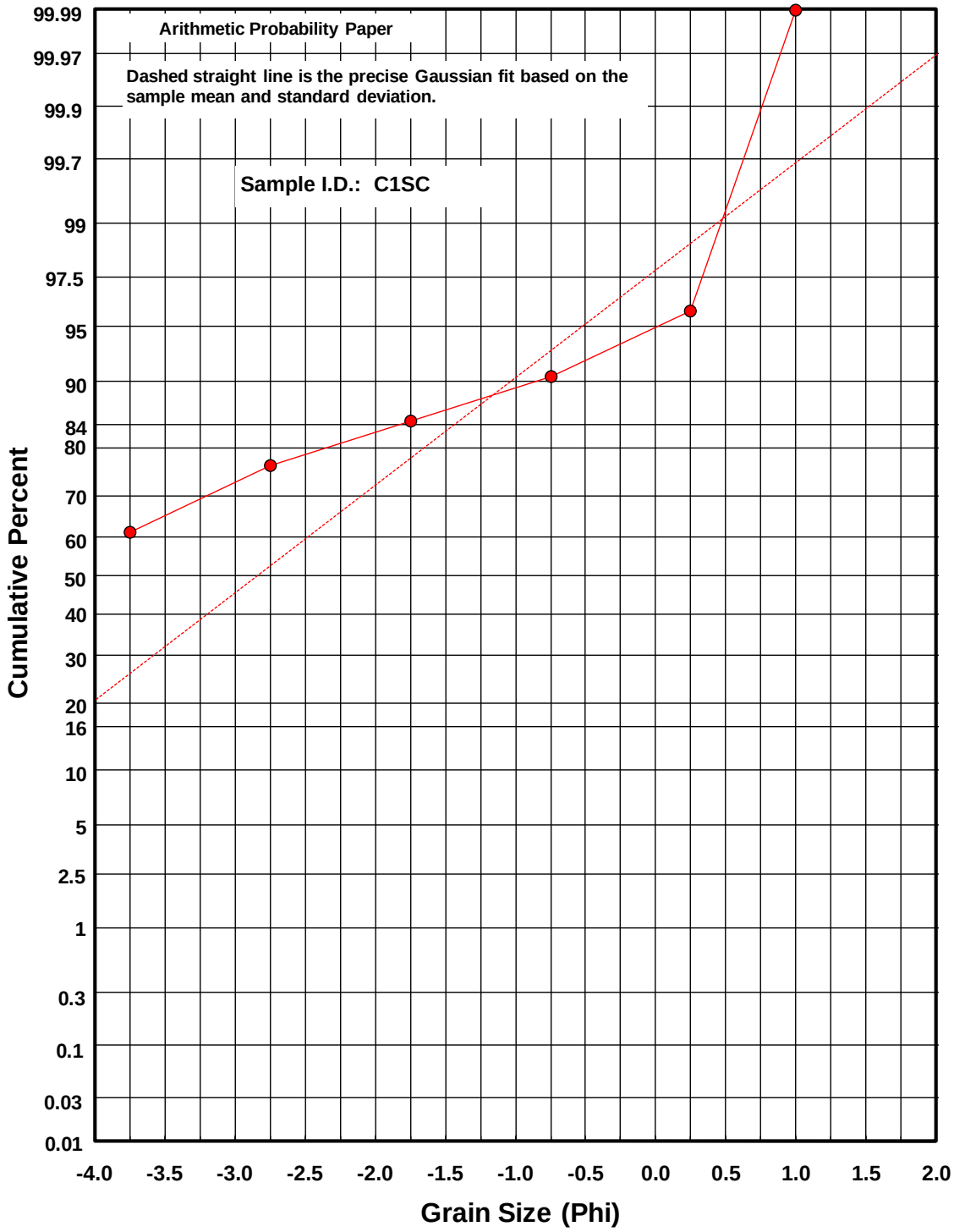
Arithmetic Probability Paper
Dashed straight line is the precise Gaussian fit based on the sample mean and standard deviation.
Sample I.D.: C1SC
Cumulative Percent
99.99
99.97
99.9
99.7
99
97.5
95
90
84
80
70
60
50
40
30
20
16
10
5
2.5
1
0.3
0.1
0.03
0.01
-4.0
-3.5
-3.0
-2.5
-2.0
-1.5
-1.0
-0.5
0.0
0.5
1.0
1.5
2.0
Grain Size (Phi)

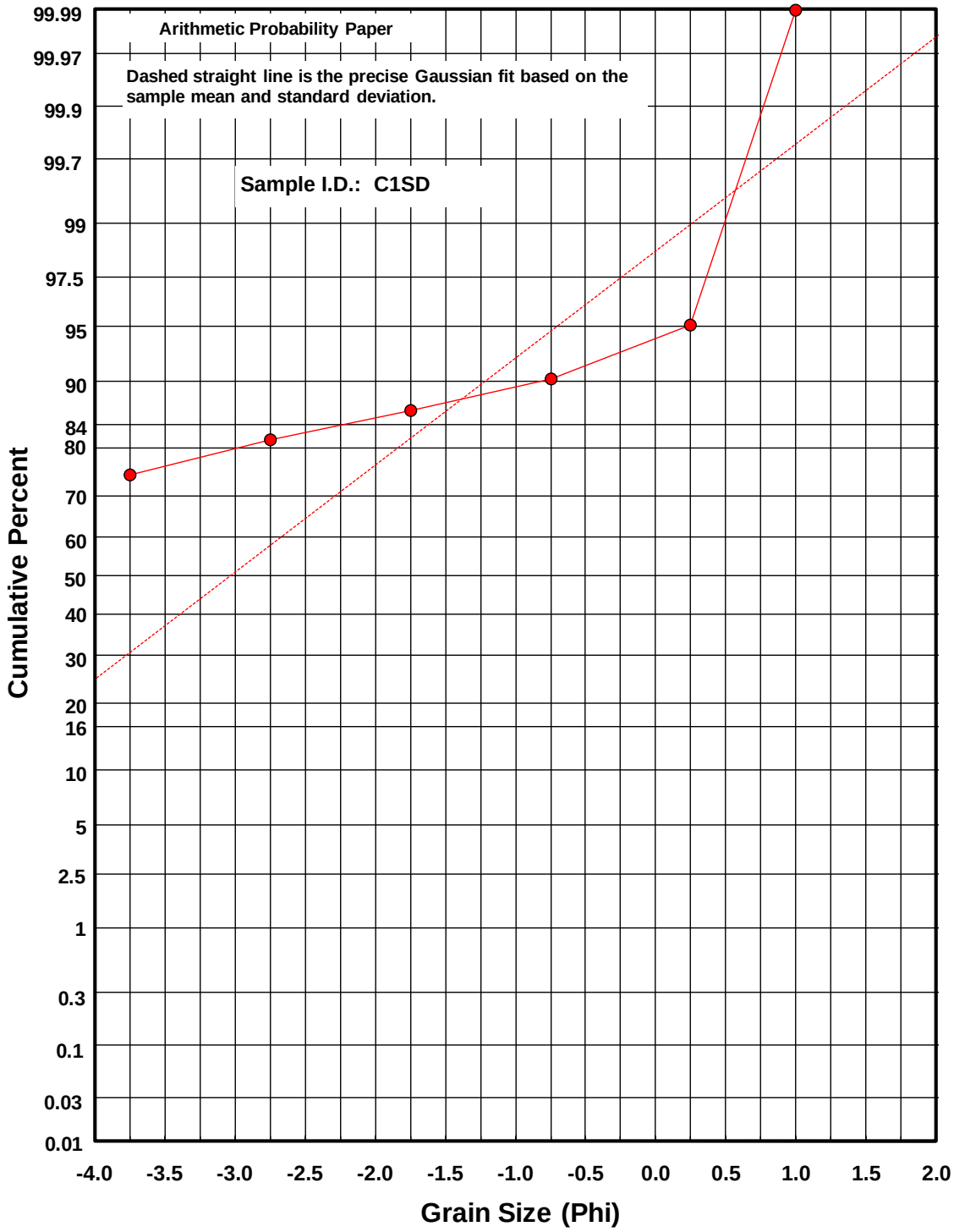
Arithmetic Probability Paper
Dashed straight line is the precise Gaussian fit based on the sample mean and standard deviation.
Sample I.D.: C1SD
Cumulative Percent
99.99
99.97
99.9
99.7
99
97.5
95
90
84
80
70
60
50
40
30
20
16
10
5
2.5
1
0.3
0.1
0.03
0.01
-4.0
-3.5
-3.0
-2.5
-2.0
-1.5
-1.0
-0.5
0.0
0.5
1.0
1.5
2.0
Grain Size (Phi)

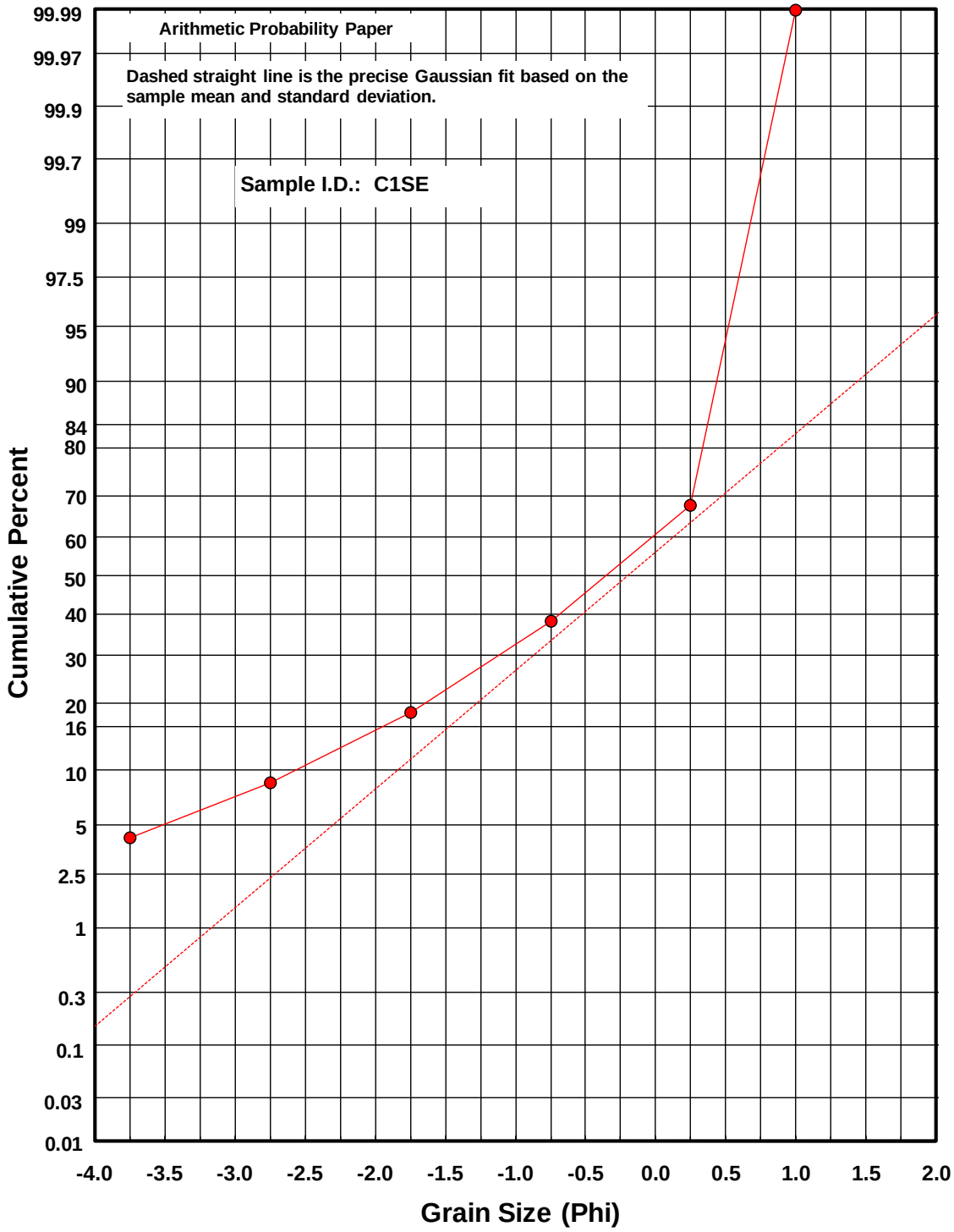
Arithmetic Probability Paper
Dashed straight line is the precise Gaussian fit based on the sample mean and standard deviation.
Sample I.D.: C1SE
Cumulative Percent
99.99
99.97
99.9
99.7
99
97.5
95
90
84
80
70
60
50
40
30
20
16
10
5
2.5
1
0.3
0.1
0.03
0.01
-4.0
-3.5
-3.0
-2.5
-2.0
-1.5
-1.0
-0.5
0.0
0.5
1.0
1.5
2.0
Grain Size (Phi)

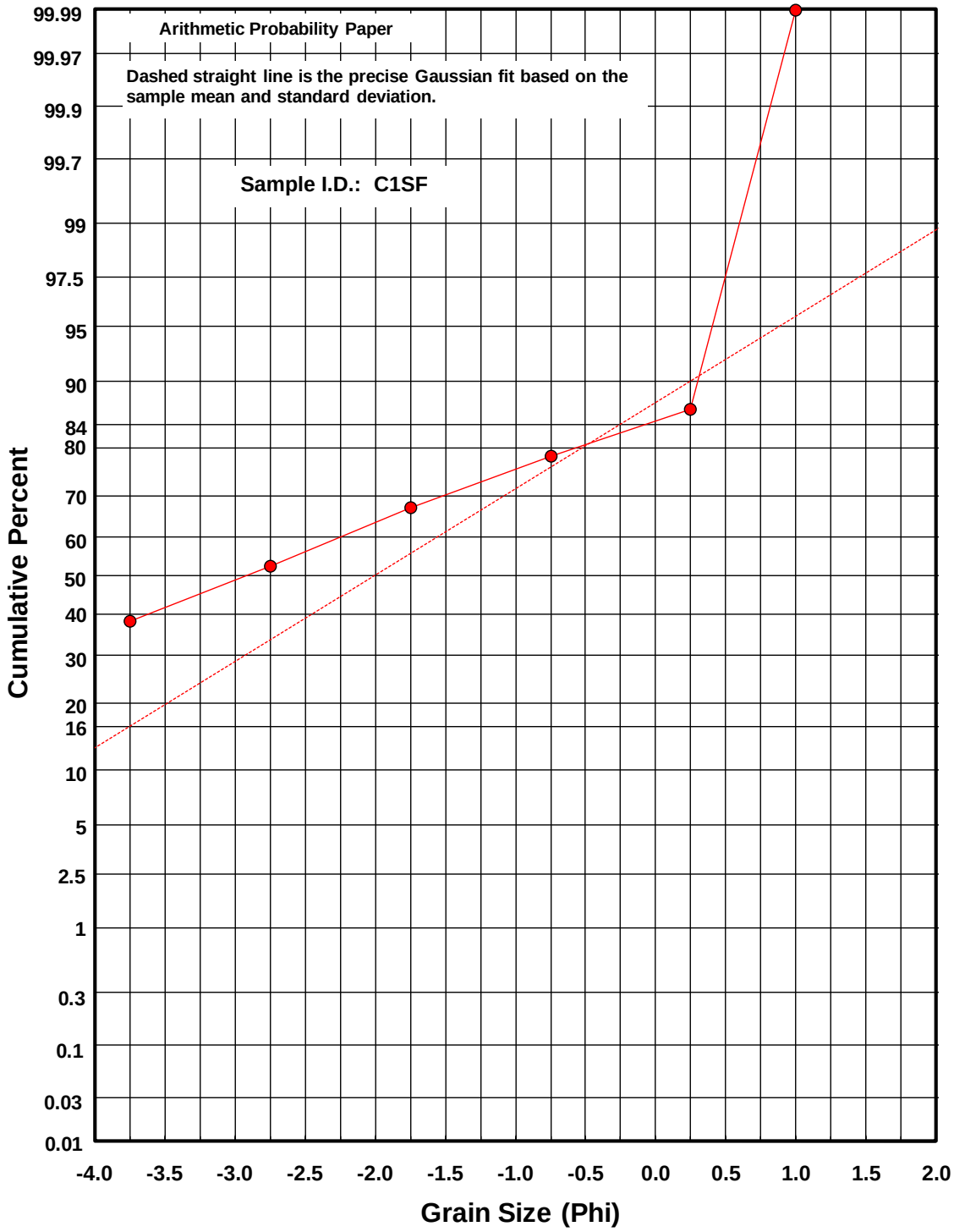
Arithmetic Probability Paper
Dashed straight line is the precise Gaussian fit based on the sample mean and standard deviation.
Sample I.D.: C1SF
Cumulative Percent
99.99
99.97
99.9
99.7
99
97.5
95
90
84
80
70
60
50
40
30
20
16
10
5
2.5
1
0.3
0.1
0.03
0.01
-4.0
-3.5
-3.0
-2.5
-2.0
-1.5
-1.0
-0.5
0.0
0.5
1.0
1.5
2.0
Grain Size (Phi)

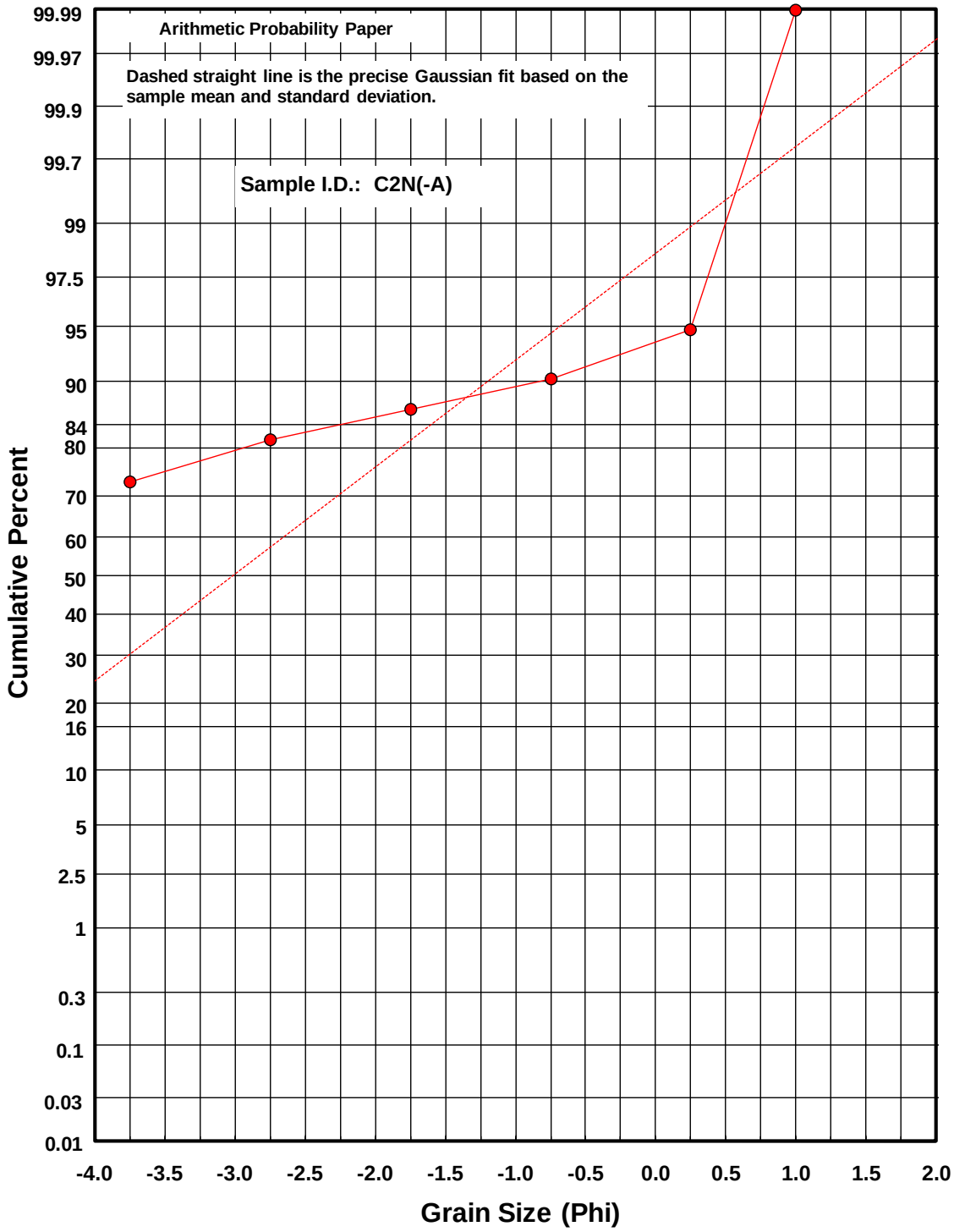
Arithmetic Probability Paper
Dashed straight line is the precise Gaussian fit based on the sample mean and standard deviation.
Sample I.D.: C2N(-A)
Cumulative Percent
99.99
99.97
99.9
99.7
99
97.5
95
90
84
80
70
60
50
40
30
20
16
10
5
2.5
1
0.3
0.1
0.03
0.01
-4.0
-3.5
-3.0
-2.5
-2.0
-1.5
-1.0
-0.5
0.0
0.5
1.0
1.5
2.0
Grain Size (Phi)

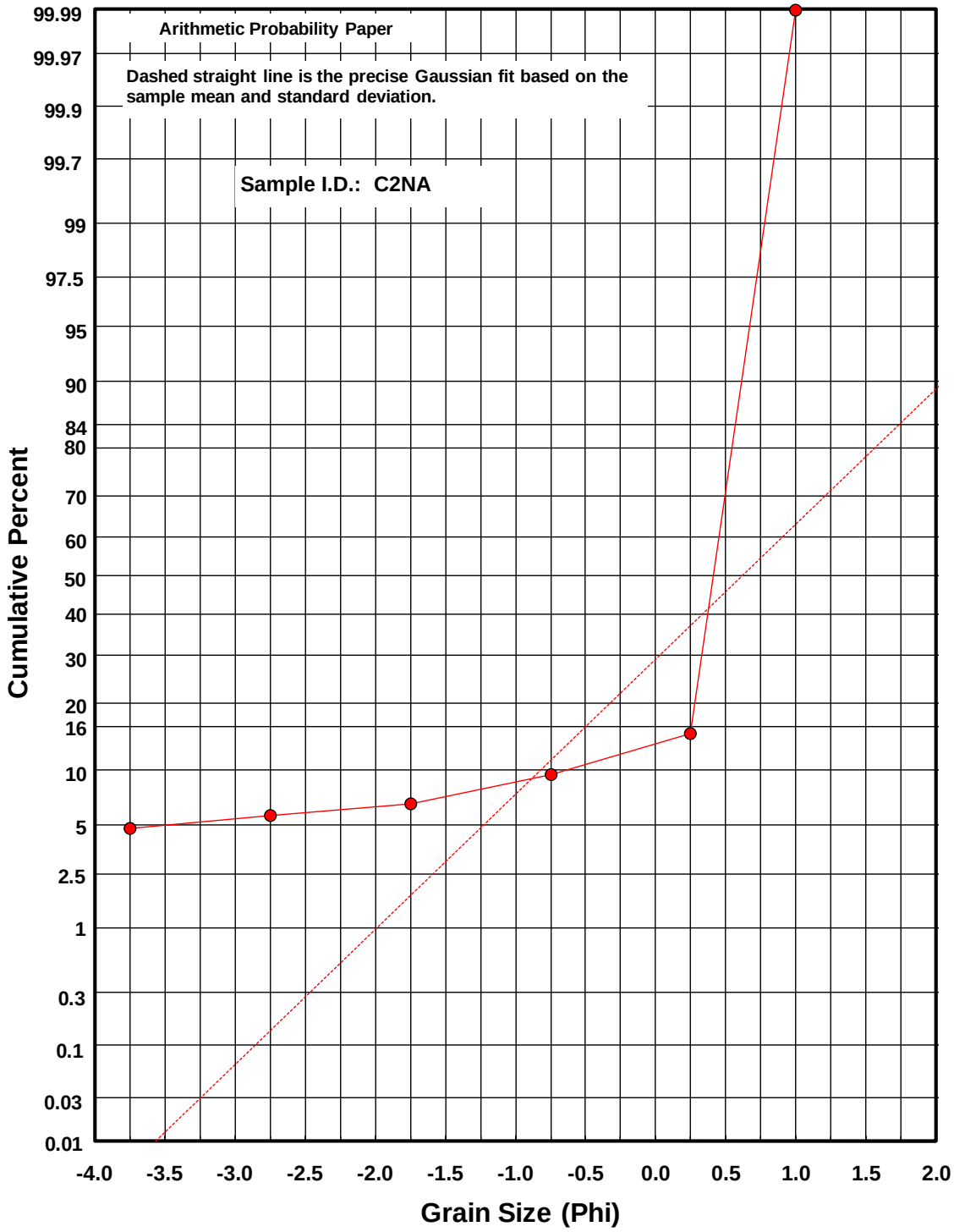
Arithmetic Probability Paper
Dashed straight line is the precise Gaussian fit based on the sample mean and standard deviation.
Sample I.D.: C2NA
Cumulative Percent
99.99
99.97
99.9
99.7
99
97.5
95
90
84
80
70
60
50
40
30
20
16
10
5
2.5
1
0.3
0.1
0.03
0.01
-4.0
-3.5
-3.0
-2.5
-2.0
-1.5
-1.0
-0.5
0.0
0.5
1.0
1.5
2.0
Grain Size (Phi)

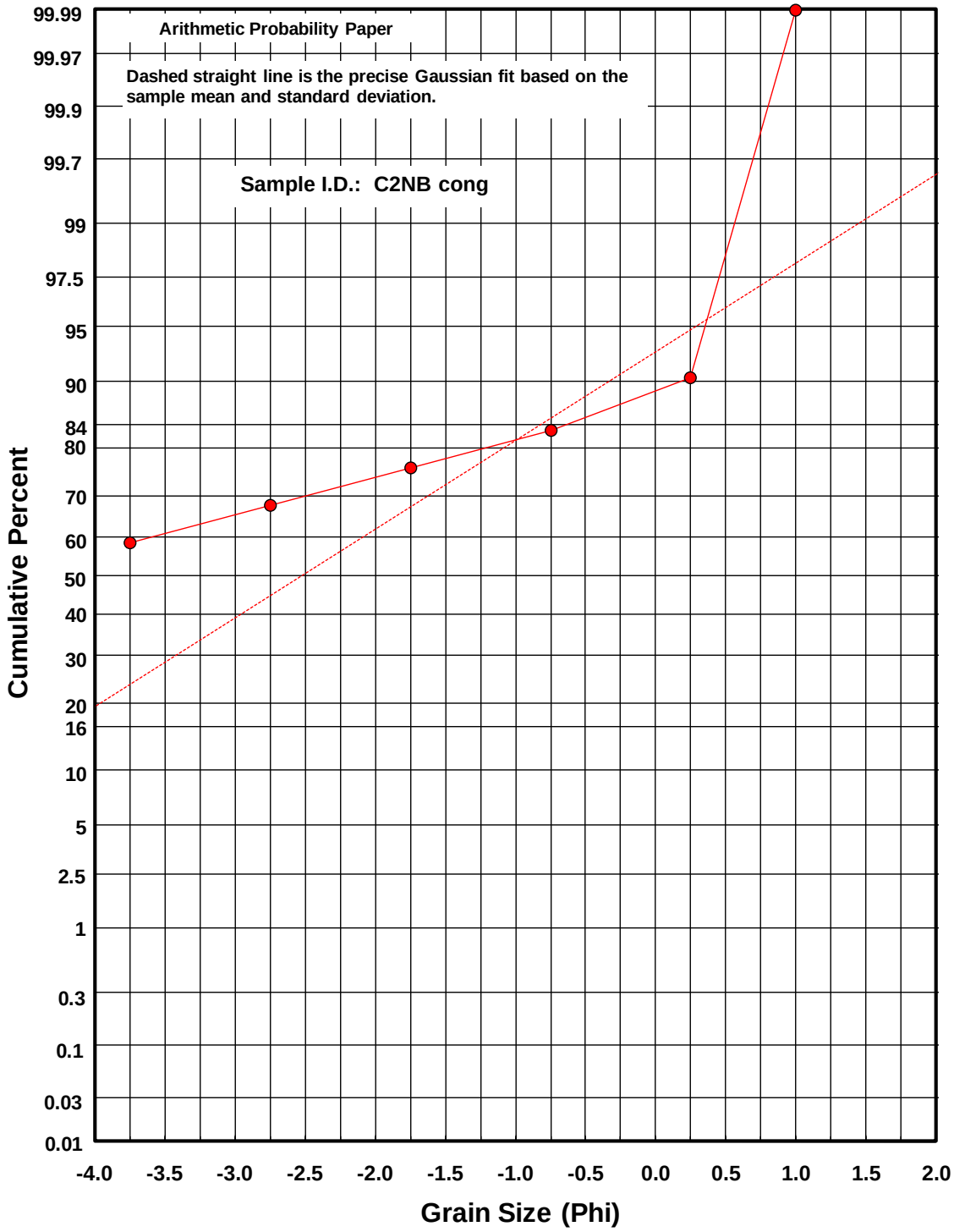
Arithmetic Probability Paper
Dashed straight line is the precise Gaussian fit based on the sample mean and standard deviation.
Sample I.D.: C2NB cong
Cumulative Percent
99.99
99.97
99.9
99.7
99
97.5
95
90
84
80
70
60
50
40
30
20
16
10
5
2.5
1
0.3
0.1
0.03
0.01
-4.0
-3.5
-3.0
-2.5
-2.0
-1.5
-1.0
-0.5
0.0
0.5
1.0
1.5
2.0
Grain Size (Phi)

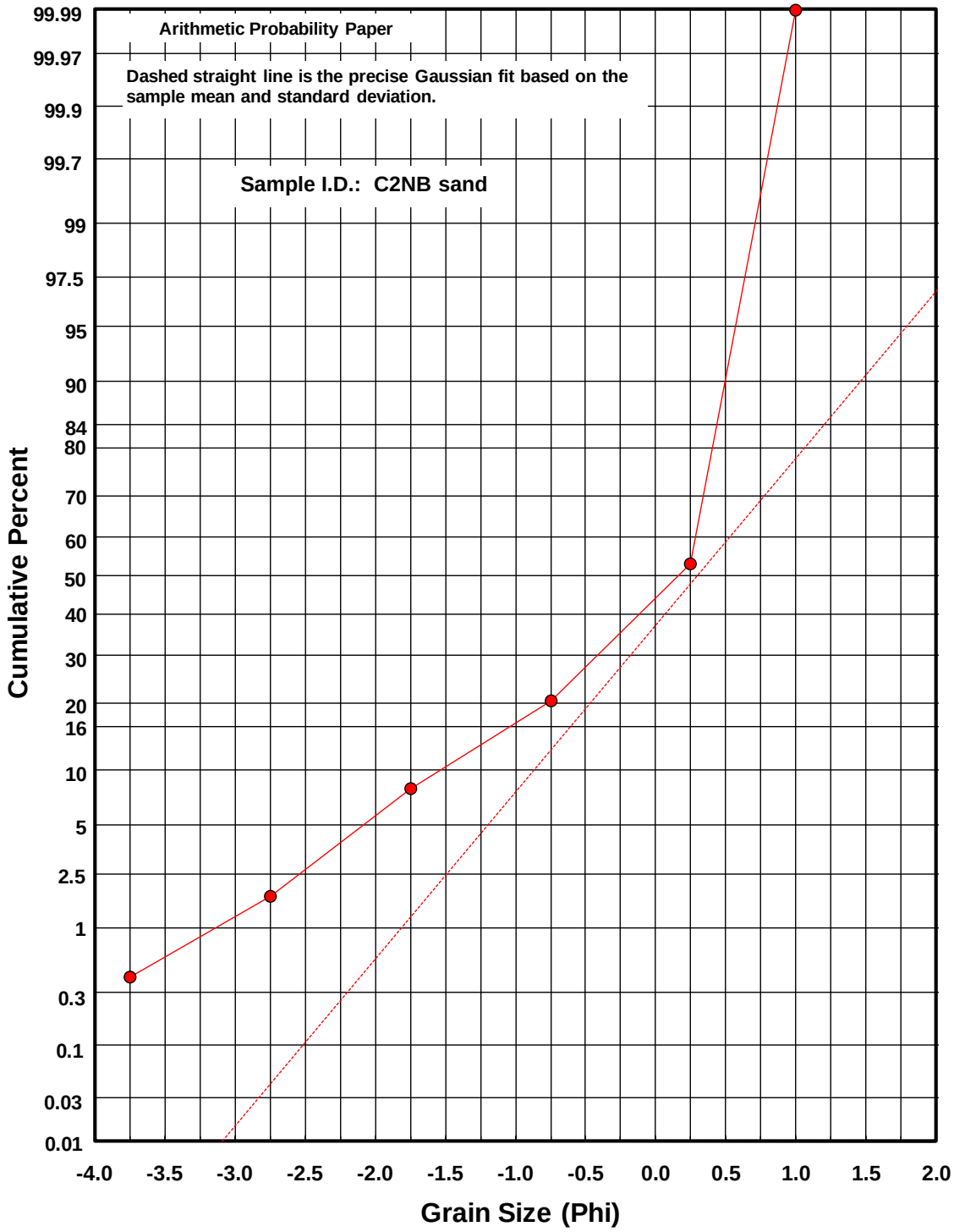
Arithmetic Probability Paper
Dashed straight line is the precise Gaussian fit based on the sample mean and standard deviation.
Sample I.D.: C2NB sand
Cumulative Percent
99.99
99.97
99.9
99.7
99
97.5
95
90
84
80
70
60
50
40
30
20
16
10
5
2.5
1
0.3
0.1
0.03
0.01
-4.0
-3.5
-3.0
-2.5
-2.0
-1.5
-1.0
-0.5
0.0
0.5
1.0
1.5
2.0
Grain Size (Phi)

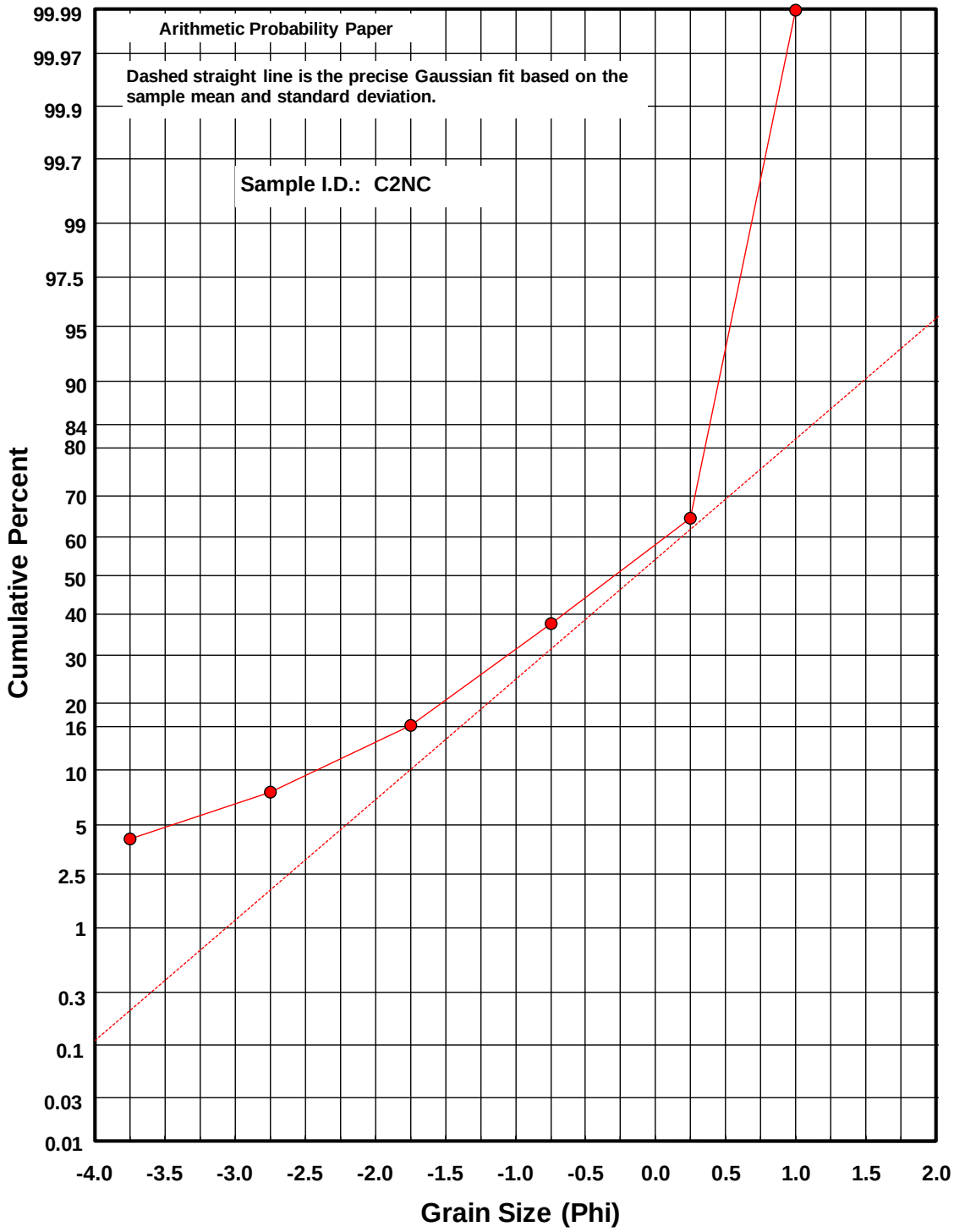
Arithmetic Probability Paper
Dashed straight line is the precise Gaussian fit based on the sample mean and standard deviation.
Sample I.D.: C2NC
Cumulative Percent
99.99
99.97
99.9
99.7
99
97.5
95
90
84
80
70
60
50
40
30
20
16
10
5
2.5
1
0.3
0.1
0.03
0.01
-4.0
-3.5
-3.0
-2.5
-2.0
-1.5
-1.0
-0.5
0.0
0.5
1.0
1.5
2.0
Grain Size (Phi)

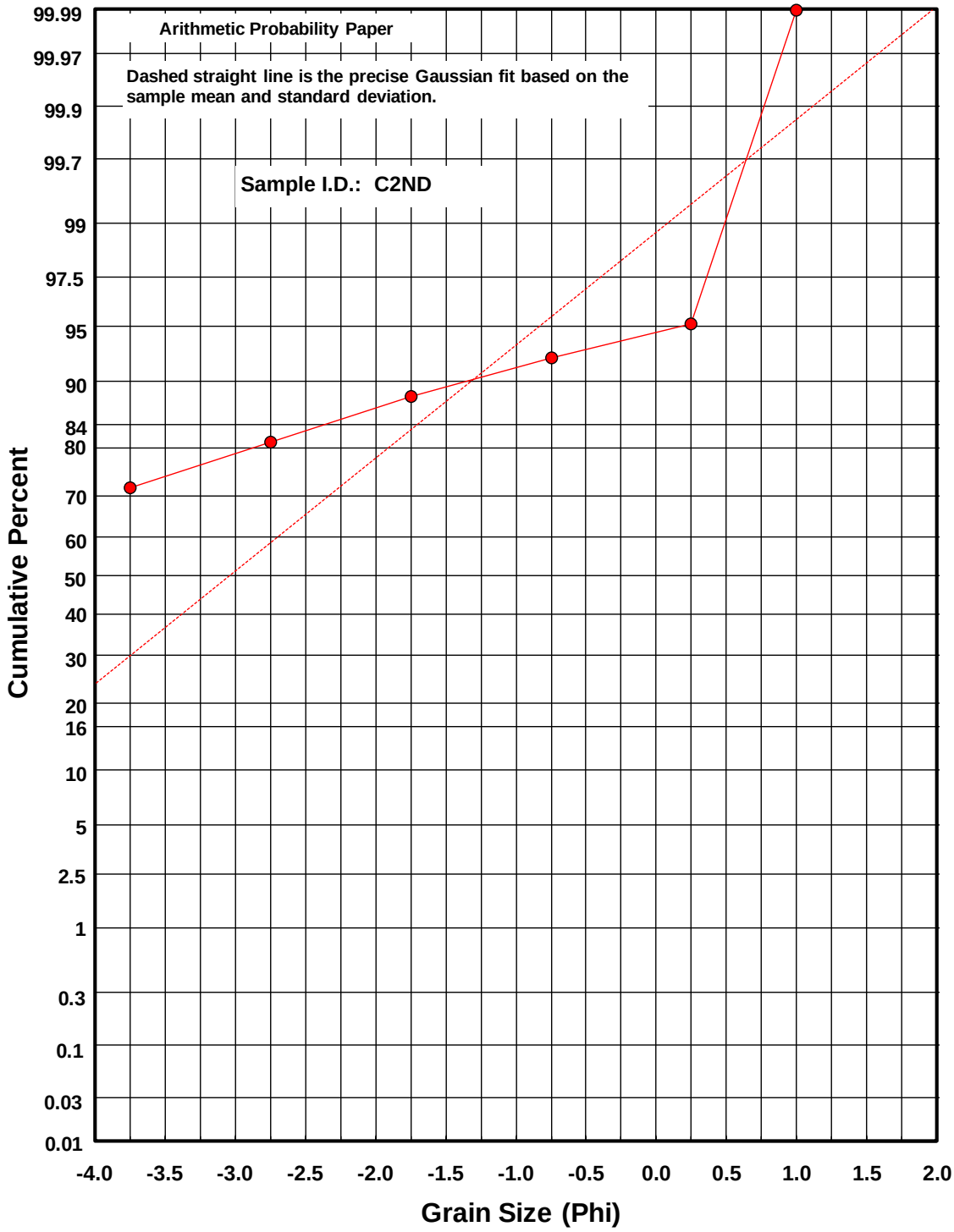
Arithmetic Probability Paper
Dashed straight line is the precise Gaussian fit based on the sample mean and standard deviation.
Sample I.D.: C2ND
Cumulative Percent
99.99
99.97
99.9
99.7
99
97.5
95
90
84
80
70
60
50
40
30
20
16
10
5
2.5
1
0.3
0.1
0.03
0.01
-4.0
-3.5
-3.0
-2.5
-2.0
-1.5
-1.0
-0.5
0.0
0.5
1.0
1.5
2.0
Grain Size (Phi)

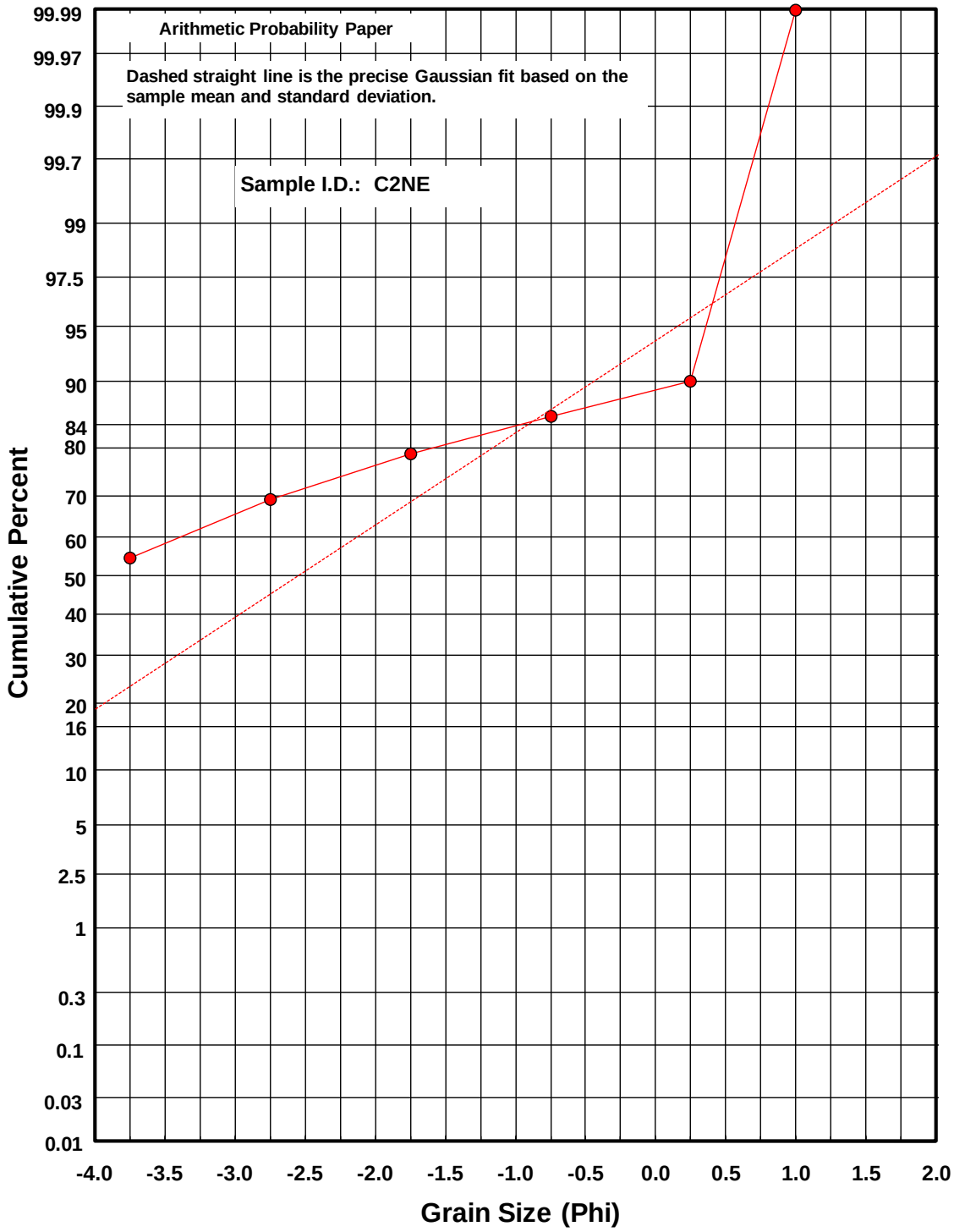
Arithmetic Probability Paper
Dashed straight line is the precise Gaussian fit based on the sample mean and standard deviation.
Sample I.D.: C2NE
Cumulative Percent
99.99
99.97
99.9
99.7
99
97.5
95
90
84
80
70
60
50
40
30
20
16
10
5
2.5
1
0.3
0.1
0.03
0.01
-4.0
-3.5
-3.0
-2.5
-2.0
-1.5
-1.0
-0.5
0.0
0.5
1.0
1.5
2.0
Grain Size (Phi)

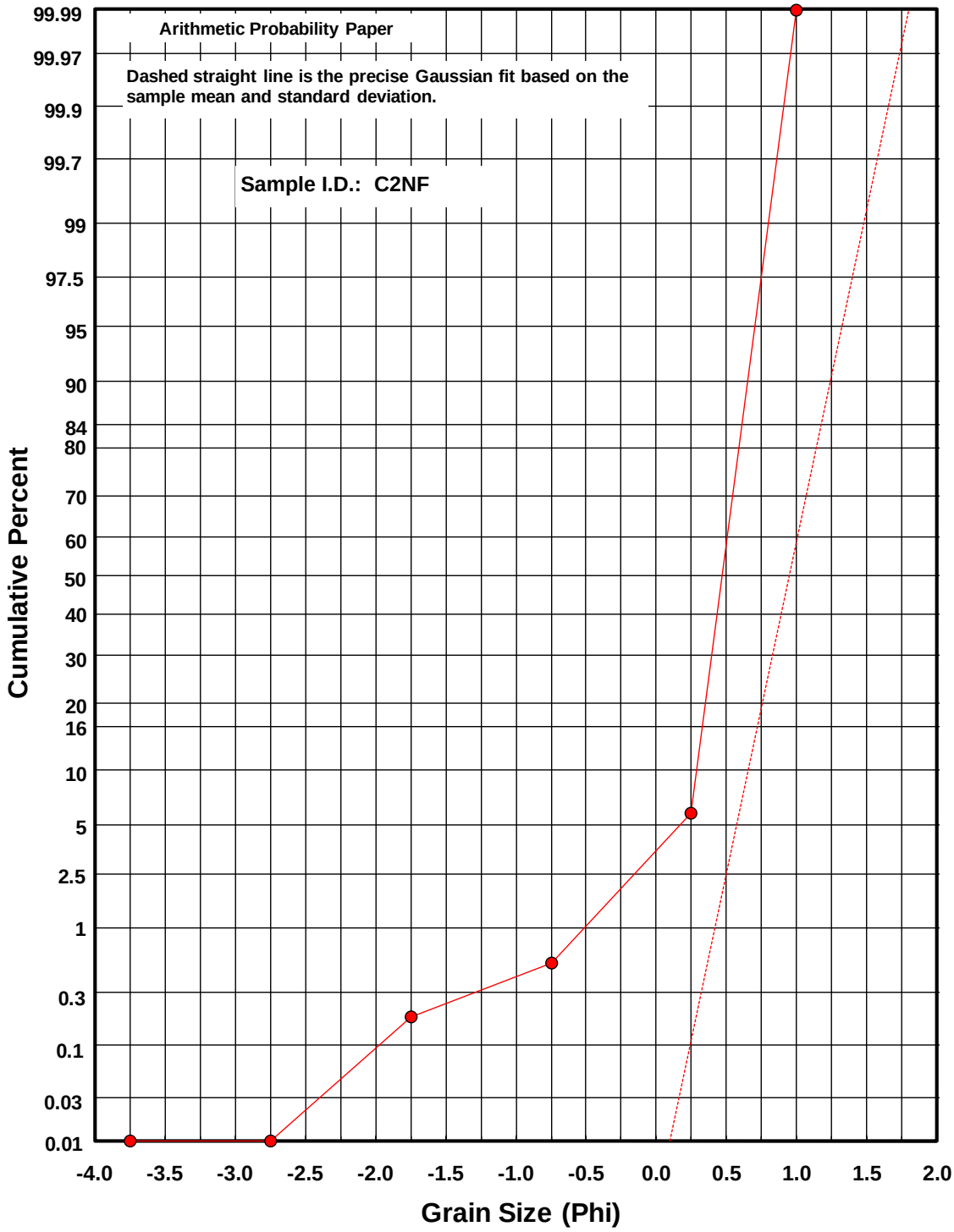
Arithmetic Probability Paper
Dashed straight line is the precise Gaussian fit based on the sample mean and standard deviation.
Sample I.D.: C2NF
Cumulative Percent
99.99
99.97
99.9
99.7
99
97.5
95
90
84
80
70
60
50
40
30
20
16
10
5
2.5
1
0.3
0.1
0.03
0.01
-4.0
-3.5
-3.0
-2.5
-2.0
-1.5
-1.0
-0.5
0.0
0.5
1.0
1.5
2.0
Grain Size (Phi)

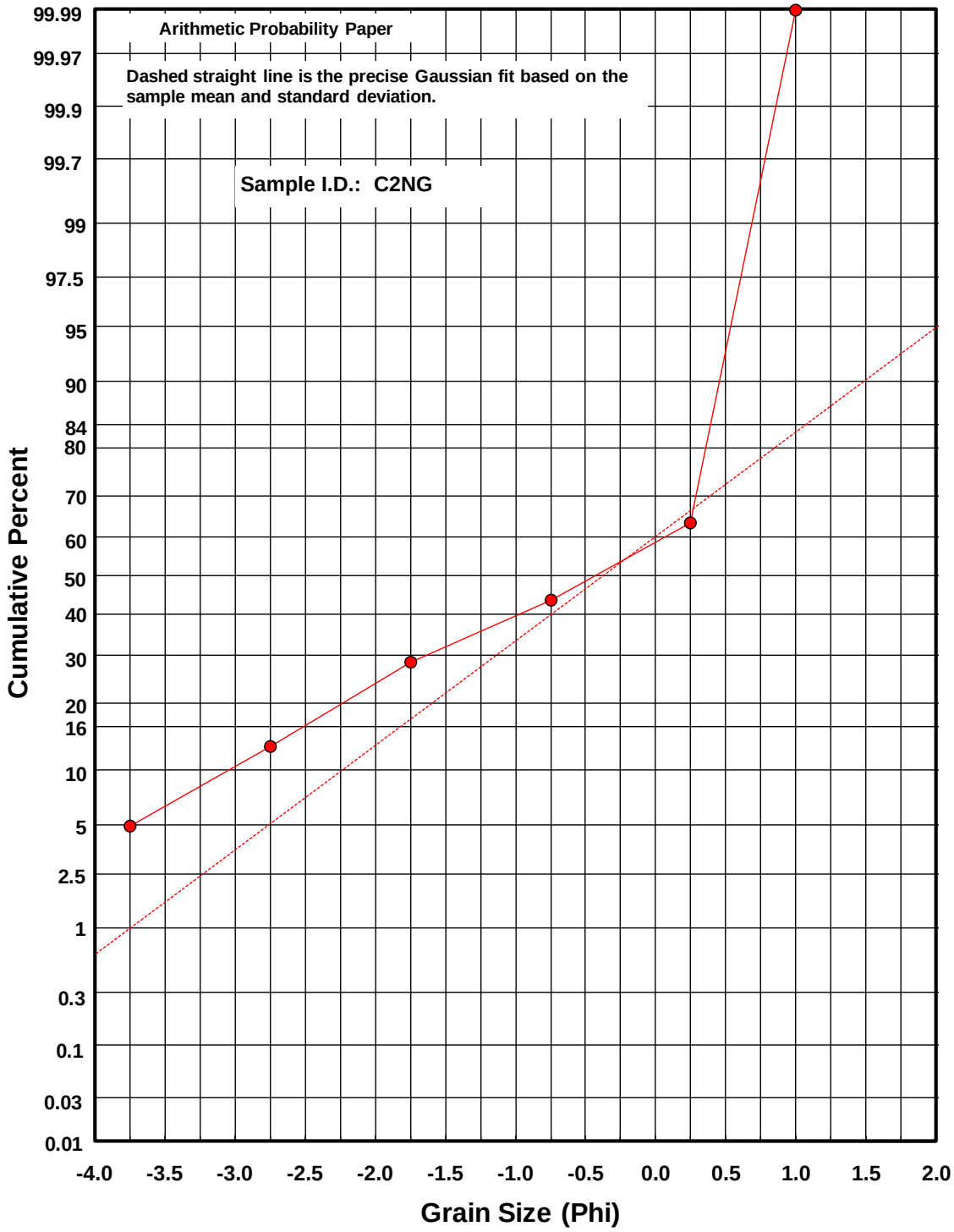
Arithmetic Probability Paper
Dashed straight line is the precise Gaussian fit based on the sample mean and standard deviation.
Sample I.D.: C2NG
Cumulative Percent
99.99
99.97
99.9
99.7
99
97.5
95
90
84
80
70
60
50
40
30
20
16
10
5
2.5
1
0.3
0.1
0.03
0.01
-4.0
-3.5
-3.0
-2.5
-2.0
-1.5
-1.0
-0.5
0.0
0.5
1.0
1.5
2.0
Grain Size (Phi)

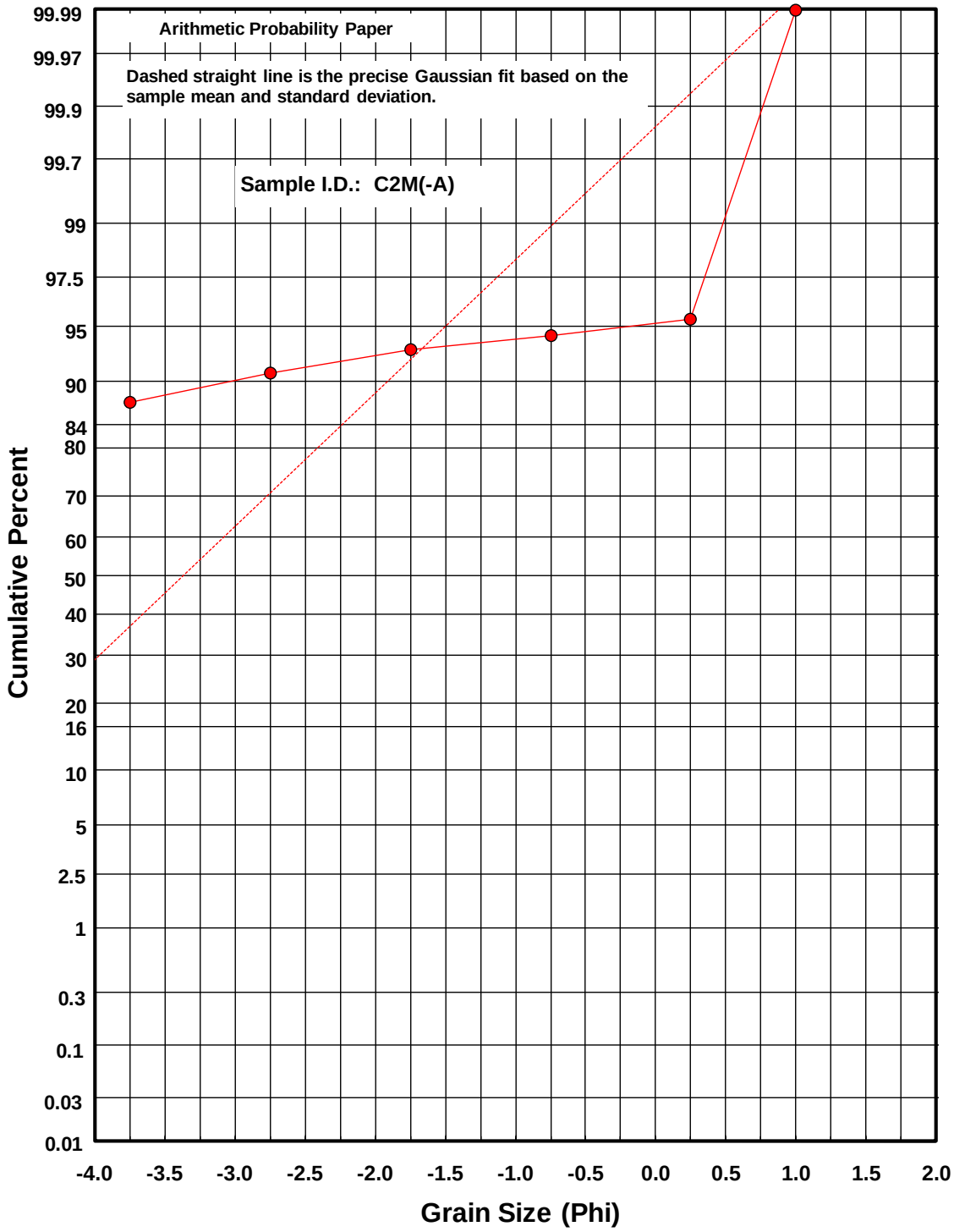
Arithmetic Probability Paper
Dashed straight line is the precise Gaussian fit based on the sample mean and standard deviation.
Sample I.D.: C2M(-A)
Cumulative Percent
99.99
99.97
99.9
99.7
99
97.5
95
90
84
80
70
60
50
40
30
20
16
10
5
2.5
1
0.3
0.1
0.03
0.01
-4.0
-3.5
-3.0
-2.5
-2.0
-1.5
-1.0
-0.5
0.0
0.5
1.0
1.5
2.0
Grain Size (Phi)

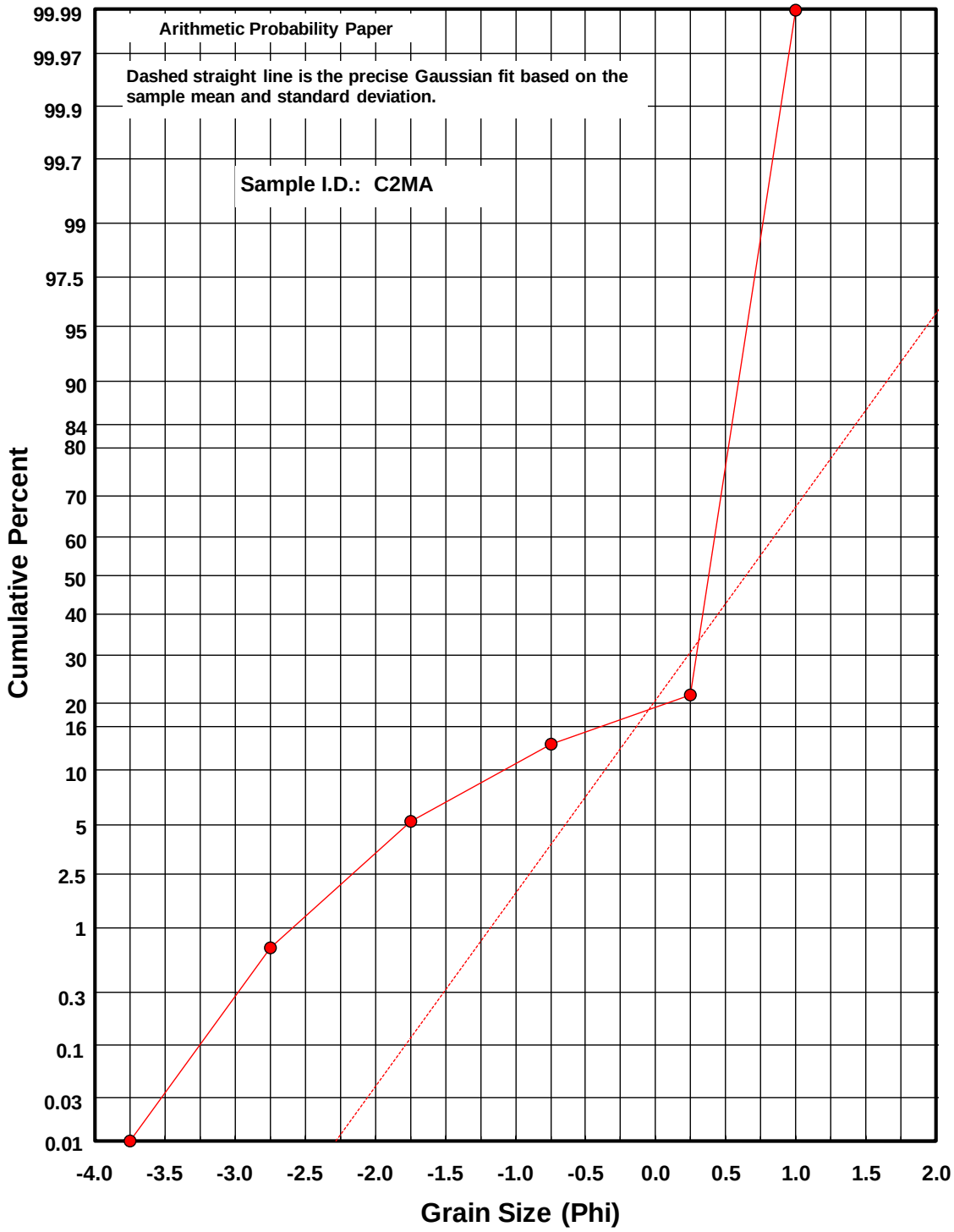
Arithmetic Probability Paper
Dashed straight line is the precise Gaussian fit based on the sample mean and standard deviation.
Sample I.D.: C2MA
Cumulative Percent
99.99
99.97
99.9
99.7
99
97.5
95
90
84
80
70
60
50
40
30
20
16
10
5
2.5
1
0.3
0.1
0.03
0.01
-4.0
-3.5
-3.0
-2.5
-2.0
-1.5
-1.0
-0.5
0.0
0.5
1.0
1.5
2.0
Grain Size (Phi)

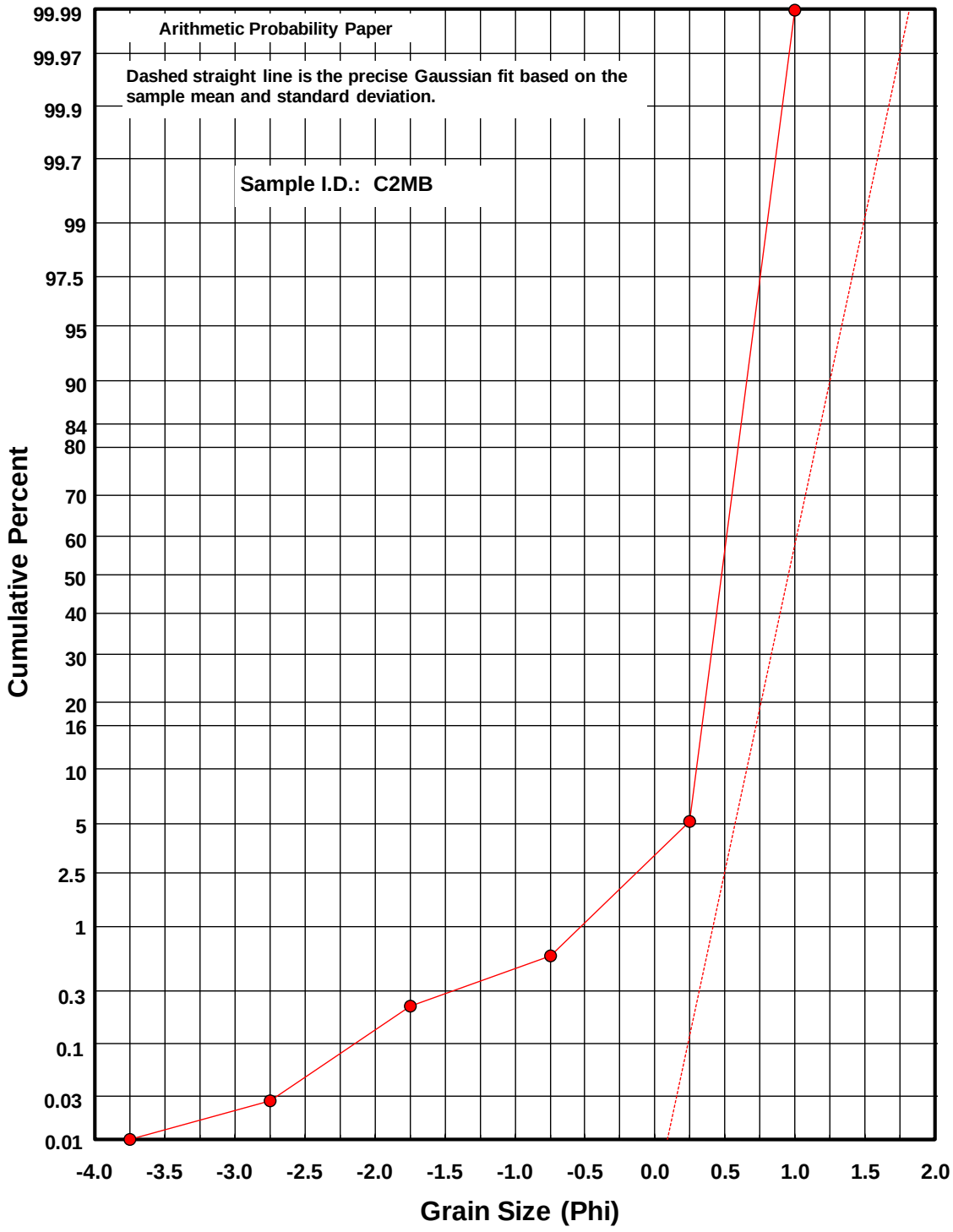
Arithmetic Probability Paper
Dashed straight line is the precise Gaussian fit based on the sample mean and standard deviation.
Sample I.D.: C2MB
Cumulative Percent
99.99
99.97
99.9
99.7
99
97.5
95
90
84
80
70
60
50
40
30
20
16
10
5
2.5
1
0.3
0.1
0.03
0.01
-4.0
-3.5
-3.0
-2.5
-2.0
-1.5
-1.0
-0.5
0.0
0.5
1.0
1.5
2.0
Grain Size (Phi)

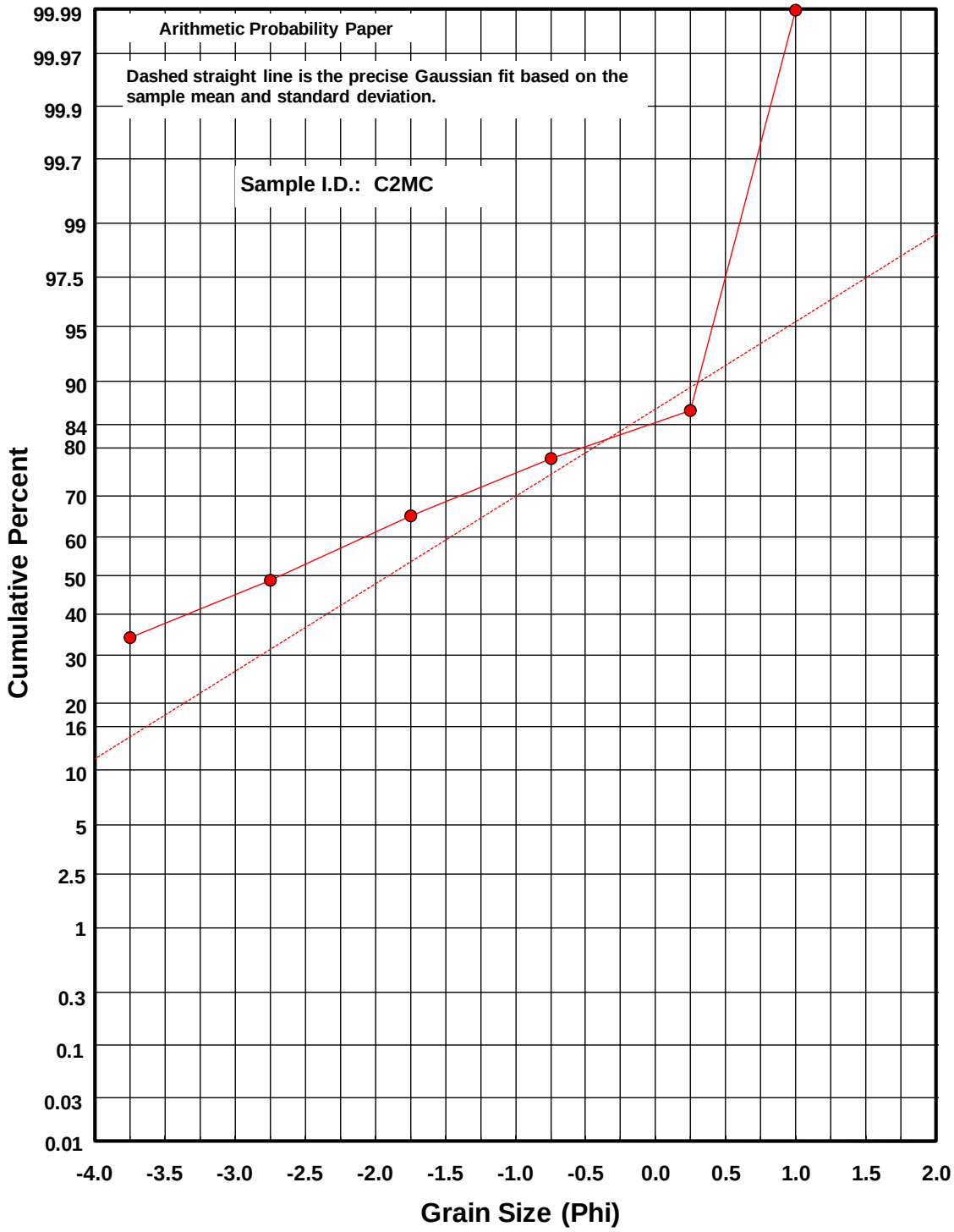
Arithmetic Probability Paper
Dashed straight line is the precise Gaussian fit based on the sample mean and standard deviation.
Sample I.D.: C2MC
Cumulative Percent
99.99
99.97
99.9
99.7
99
97.5
95
90
84
80
70
60
50
40
30
20
16
10
5
2.5
1
0.3
0.1
0.03
0.01
-4.0
-3.5
-3.0
-2.5
-2.0
-1.5
-1.0
-0.5
0.0
0.5
1.0
1.5
2.0
Grain Size (Phi)

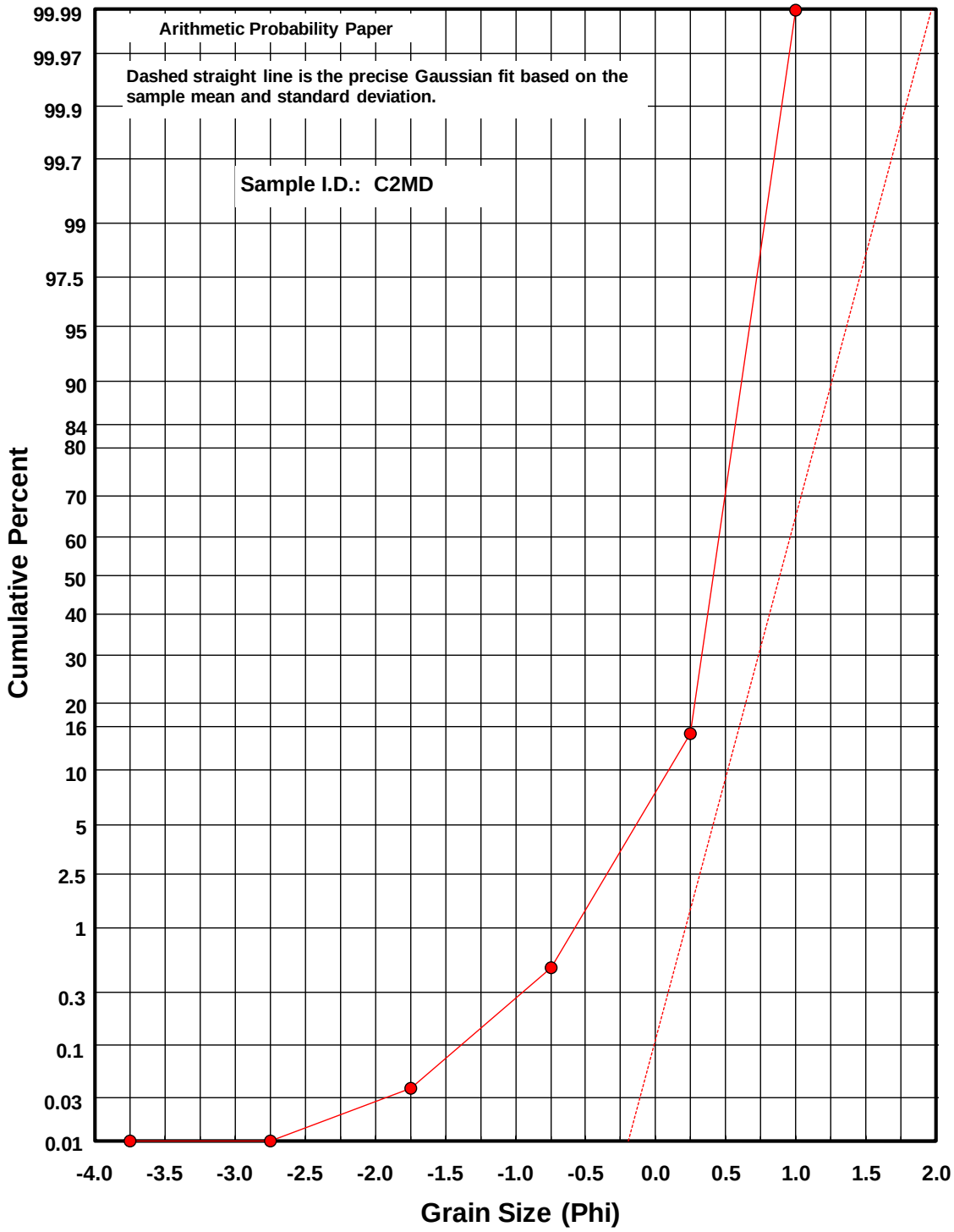
Arithmetic Probability Paper
Dashed straight line is the precise Gaussian fit based on the sample mean and standard deviation.
Sample I.D.: C2MD
Cumulative Percent
99.99
99.97
99.9
99.7
99
97.5
95
90
84
80
70
60
50
40
30
20
16
10
5
2.5
1
0.3
0.1
0.03
0.01
-4.0
-3.5
-3.0
-2.5
-2.0
-1.5
-1.0
-0.5
0.0
0.5
1.0
1.5
2.0
Grain Size (Phi)

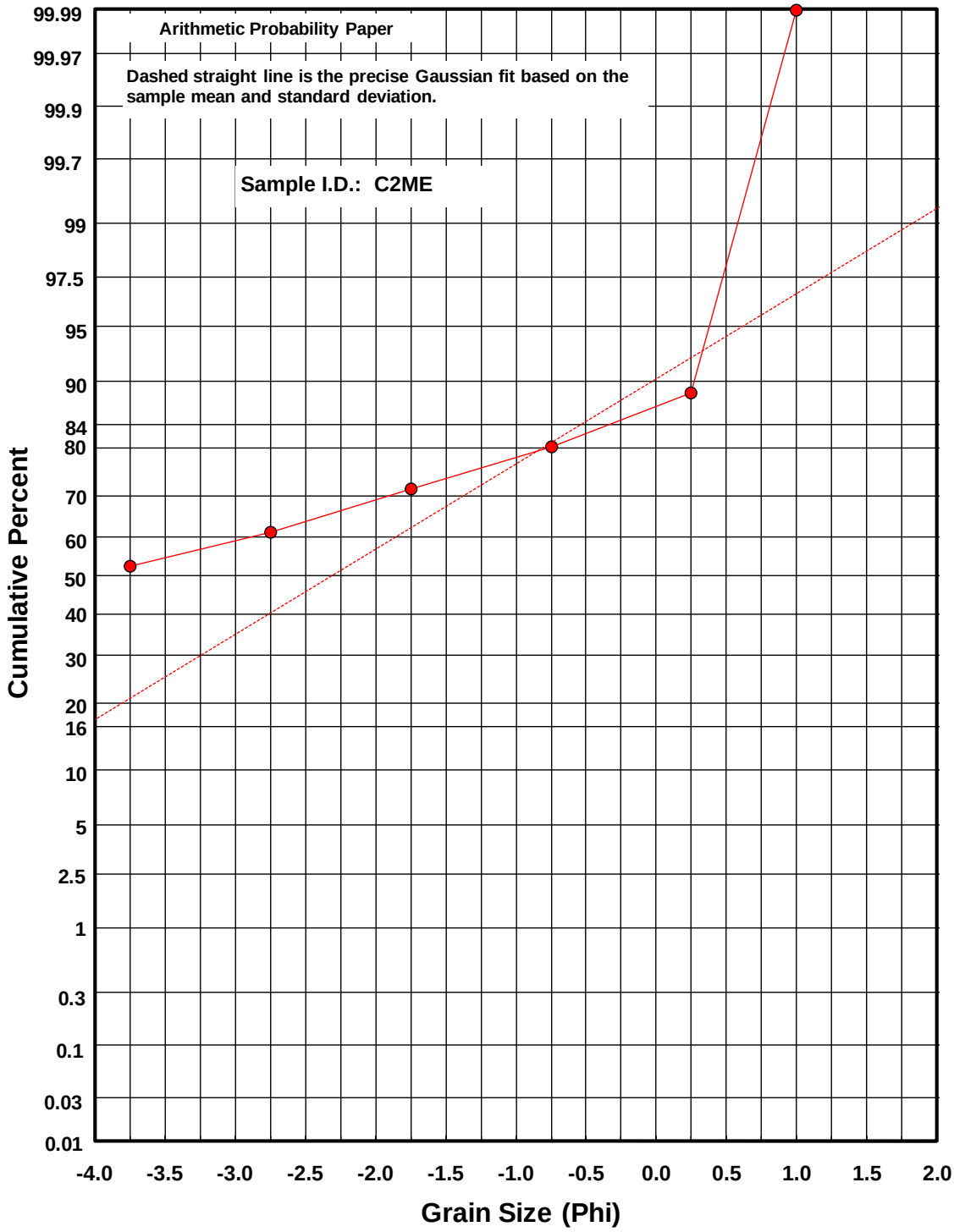
Arithmetic Probability Paper
Dashed straight line is the precise Gaussian fit based on the sample mean and standard deviation.
Sample I.D.: C2ME
Cumulative Percent
99.99
99.97
99.9
99.7
99
97.5
95
90
84
80
70
60
50
40
30
20
16
10
5
2.5
1
0.3
0.1
0.03
0.01
-4.0
-3.5
-3.0
-2.5
-2.0
-1.5
-1.0
-0.5
0.0
0.5
1.0
1.5
2.0
Grain Size (Phi)

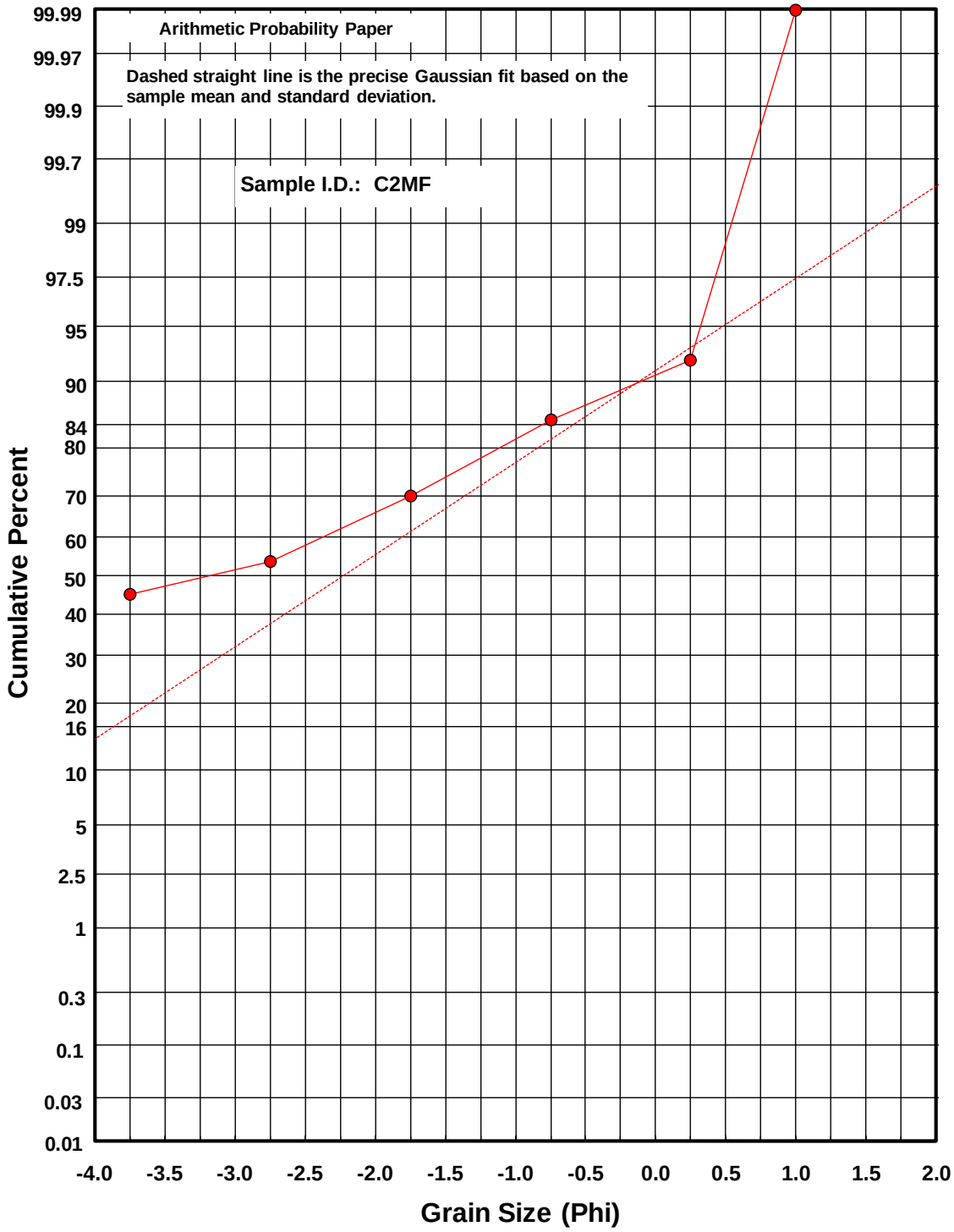
Arithmetic Probability Paper
Dashed straight line is the precise Gaussian fit based on the sample mean and standard deviation.
Sample I.D.: C2MF
Cumulative Percent
99.99
99.97
99.9
99.7
99
97.5
95
90
84
80
70
60
50
40
30
20
16
10
5
2.5
1
0.3
0.1
0.03
0.01
-4.0
-3.5
-3.0
-2.5
-2.0
-1.5
-1.0
-0.5
0.0
0.5
1.0
1.5
2.0
Grain Size (Phi)

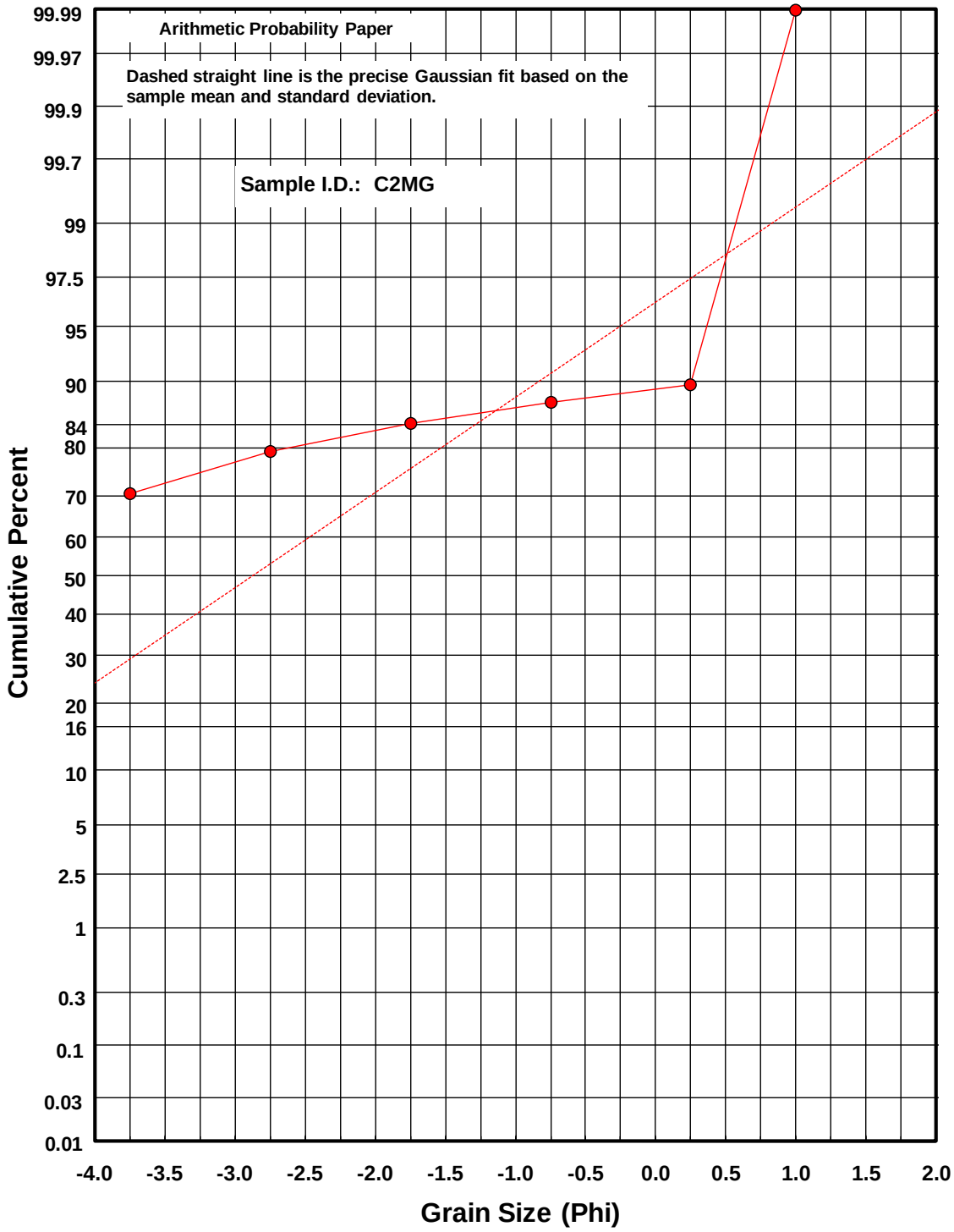
Arithmetic Probability Paper
Dashed straight line is the precise Gaussian fit based on the sample mean and standard deviation.
Sample I.D.: C2MG
Cumulative Percent
99.99
99.97
99.9
99.7
99
97.5
95
90
84
80
70
60
50
40
30
20
16
10
5
2.5
1
0.3
0.1
0.03
0.01
-4.0
-3.5
-3.0
-2.5
-2.0
-1.5
-1.0
-0.5
0.0
0.5
1.0
1.5
2.0
Grain Size (Phi)

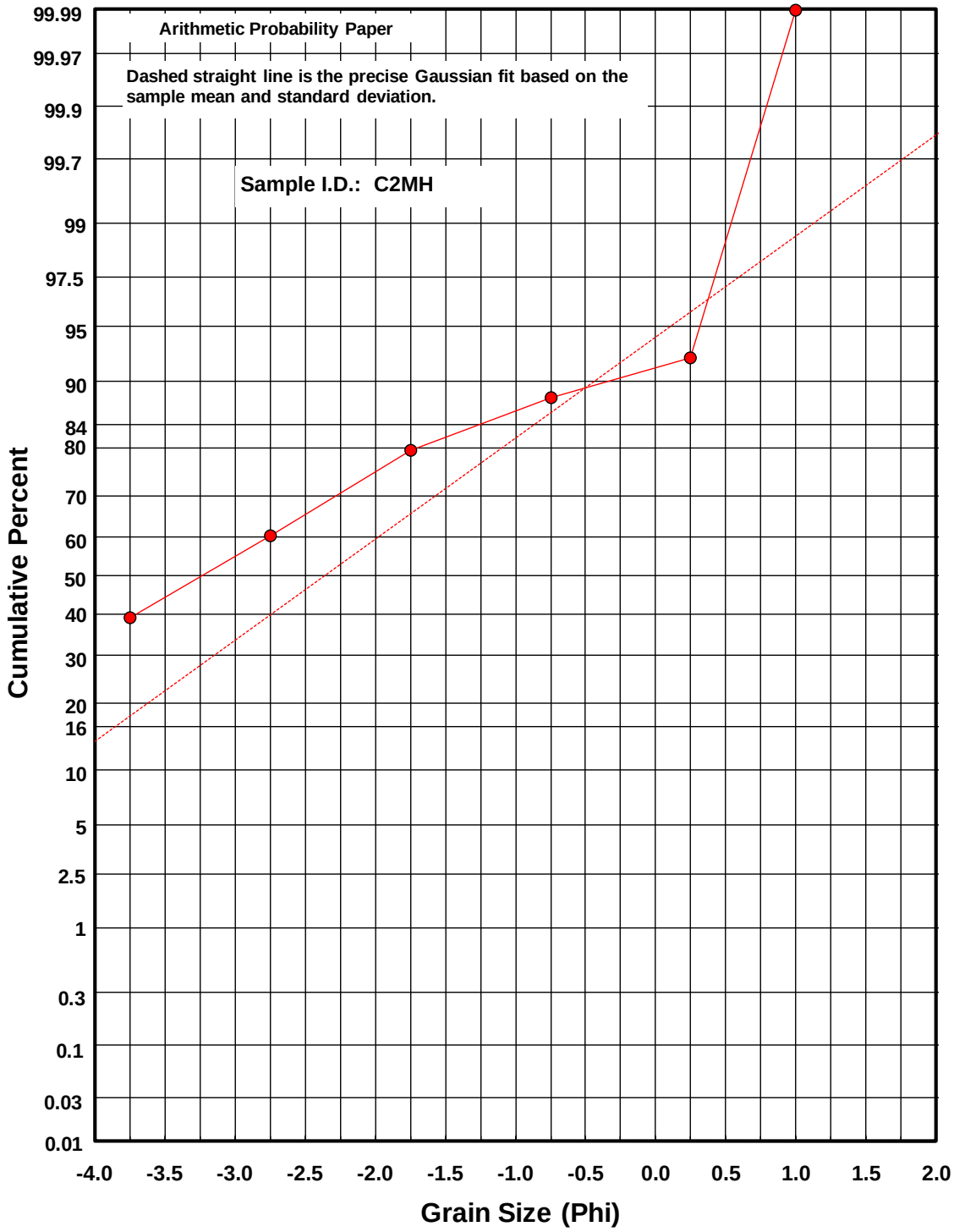
Arithmetic Probability Paper
Dashed straight line is the precise Gaussian fit based on the sample mean and standard deviation.
Sample I.D.: C2MH
Cumulative Percent
99.99
99.97
99.9
99.7
99
97.5
95
90
84
80
70
60
50
40
30
20
16
10
5
2.5
1
0.3
0.1
0.03
0.01
-4.0
-3.5
-3.0
-2.5
-2.0
-1.5
-1.0
-0.5
0.0
0.5
1.0
1.5
2.0
Grain Size (Phi)

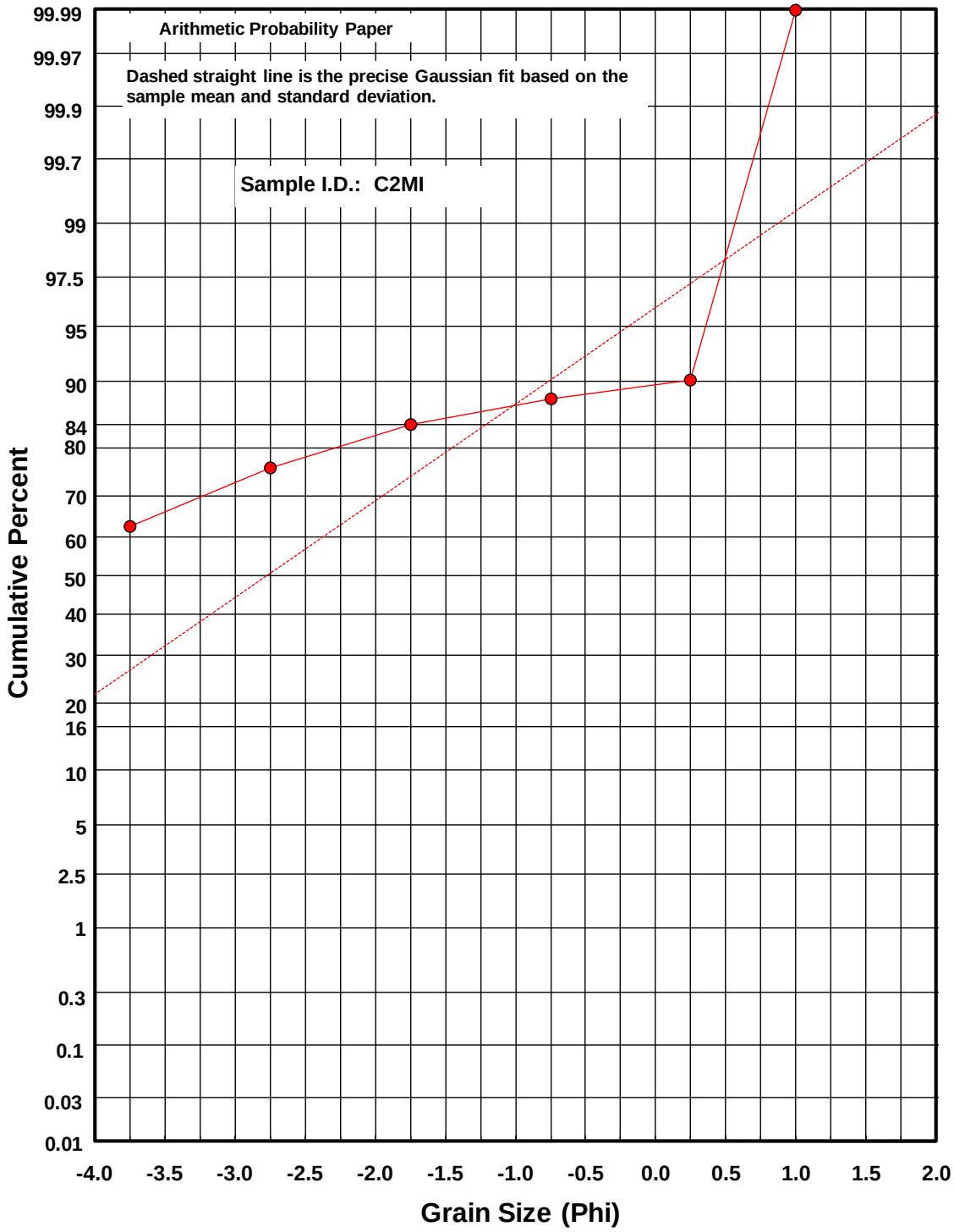
Arithmetic Probability Paper
Dashed straight line is the precise Gaussian fit based on the sample mean and standard deviation.
Sample I.D.: C2MI
Cumulative Percent
99.99
99.97
99.9
99.7
99
97.5
95
90
84
80
70
60
50
40
30
20
16
10
5
2.5
1
0.3
0.1
0.03
0.01
-4.0
-3.5
-3.0
-2.5
-2.0
-1.5
-1.0
-0.5
0.0
0.5
1.0
1.5
2.0
Grain Size (Phi)

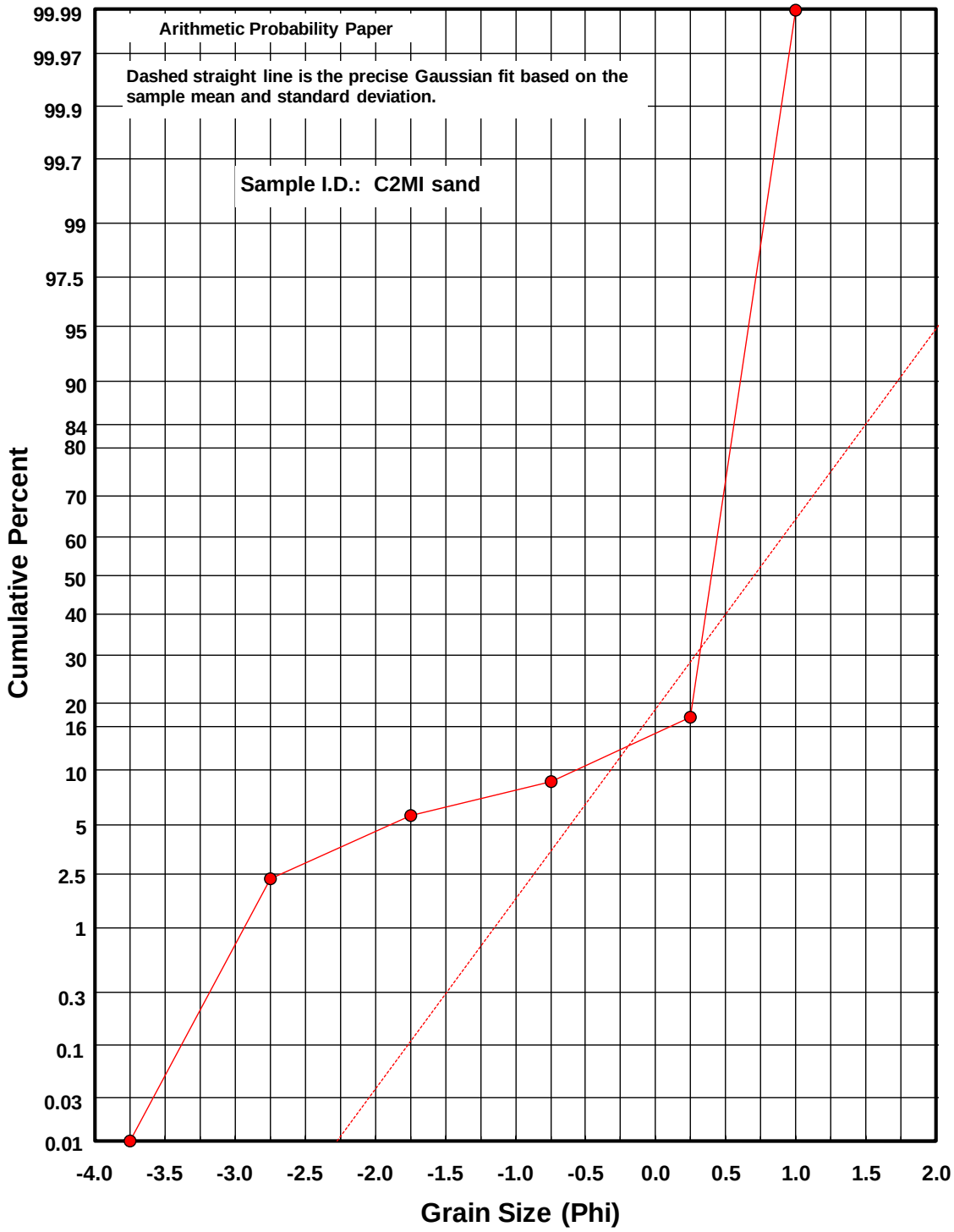
Arithmetic Probability Paper
Dashed straight line is the precise Gaussian fit based on the sample mean and standard deviation.
Sample I.D.: C2MI sand
Cumulative Percent
99.99
99.97
99.9
99.7
99
97.5
95
90
84
80
70
60
50
40
30
20
16
10
5
2.5
1
0.3
0.1
0.03
0.01
-4.0
-3.5
-3.0
-2.5
-2.0
-1.5
-1.0
-0.5
0.0
0.5
1.0
1.5
2.0
Grain Size (Phi)

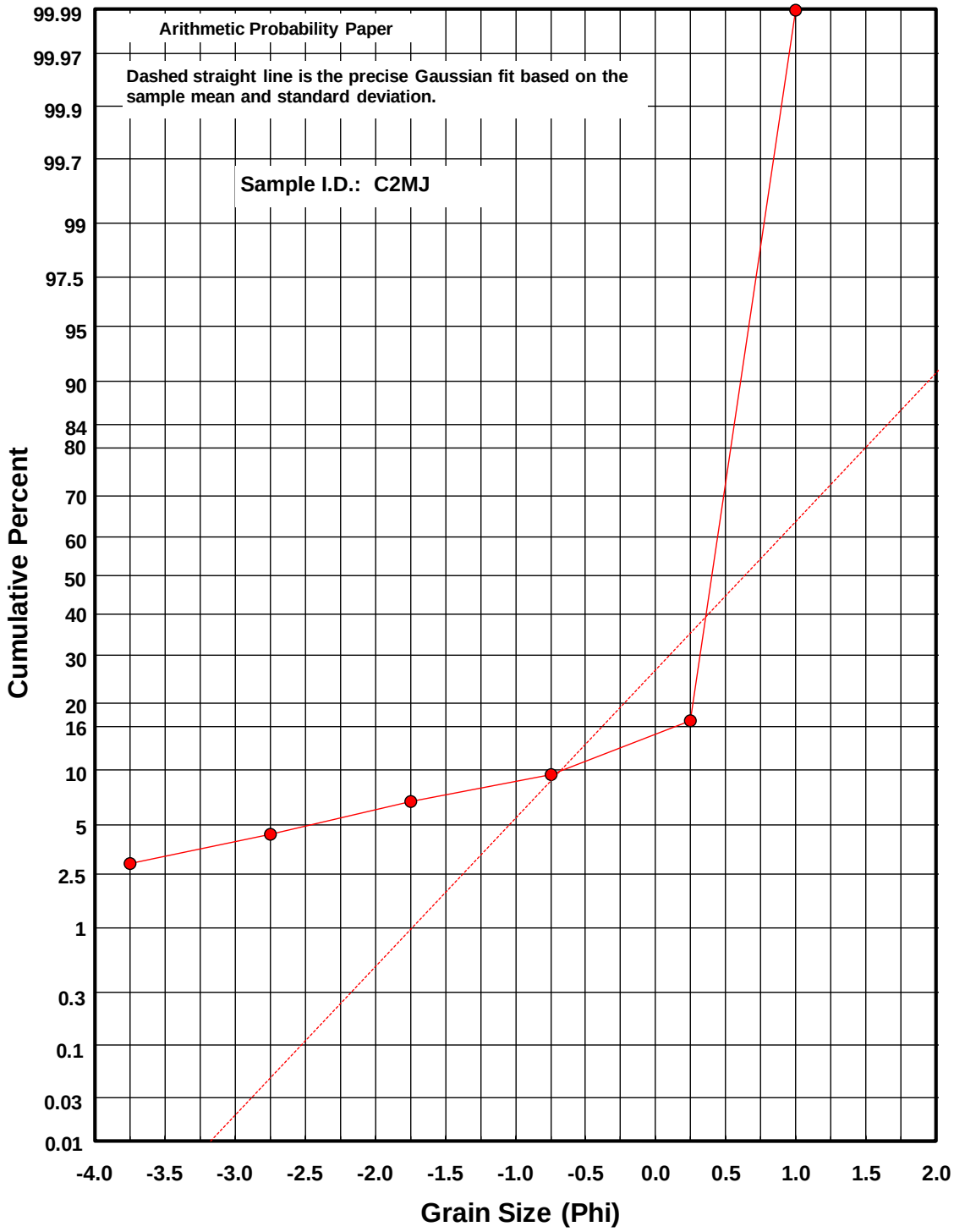
Arithmetic Probability Paper
Dashed straight line is the precise Gaussian fit based on the sample mean and standard deviation.
Sample I.D.: C2MJ
Cumulative Percent
99.99
99.97
99.9
99.7
99
97.5
95
90
84
80
70
60
50
40
30
20
16
10
5
2.5
1
0.3
0.1
0.03
0.01
-4.0
-3.5
-3.0
-2.5
-2.0
-1.5
-1.0
-0.5
0.0
0.5
1.0
1.5
2.0
Grain Size (Phi)

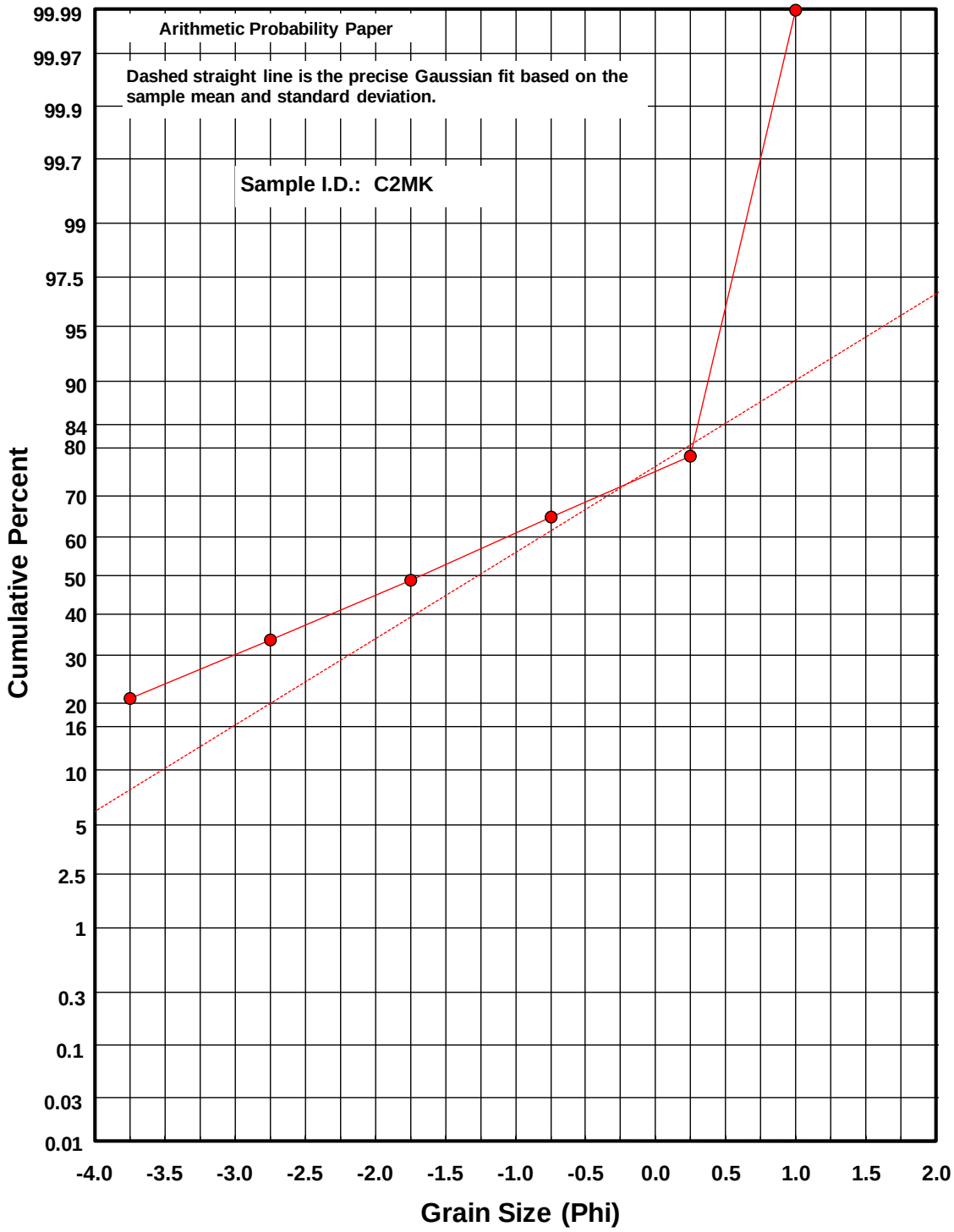
Arithmetic Probability Paper
Dashed straight line is the precise Gaussian fit based on the sample mean and standard deviation.
Sample I.D.: C2MK
Cumulative Percent
99.99
99.97
99.9
99.7
99
97.5
95
90
84
80
70
60
50
40
30
20
16
10
5
2.5
1
0.3
0.1
0.03
0.01
-4.0
-3.5
-3.0
-2.5
-2.0
-1.5
-1.0
-0.5
0.0
0.5
1.0
1.5
2.0
Grain Size (Phi)

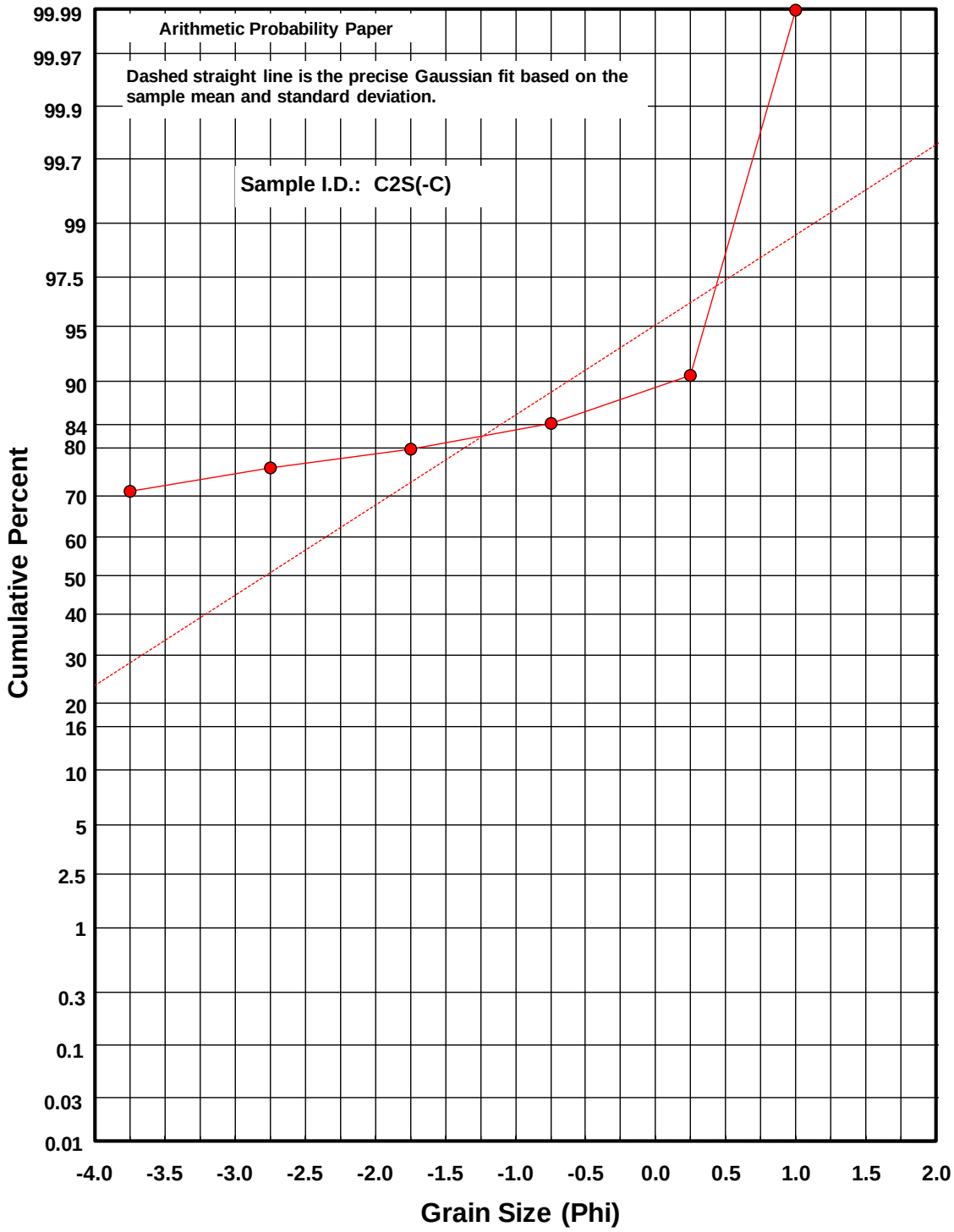
Arithmetic Probability Paper
Dashed straight line is the precise Gaussian fit based on the sample mean and standard deviation.
Sample I.D.: C2S(-C)
Cumulative Percent
99.99
99.97
99.9
99.7
99
97.5
95
90
84
80
70
60
50
40
30
20
16
10
5
2.5
1
0.3
0.1
0.03
0.01
-4.0
-3.5
-3.0
-2.5
-2.0
-1.5
-1.0
-0.5
0.0
0.5
1.0
1.5
2.0
Grain Size (Phi)

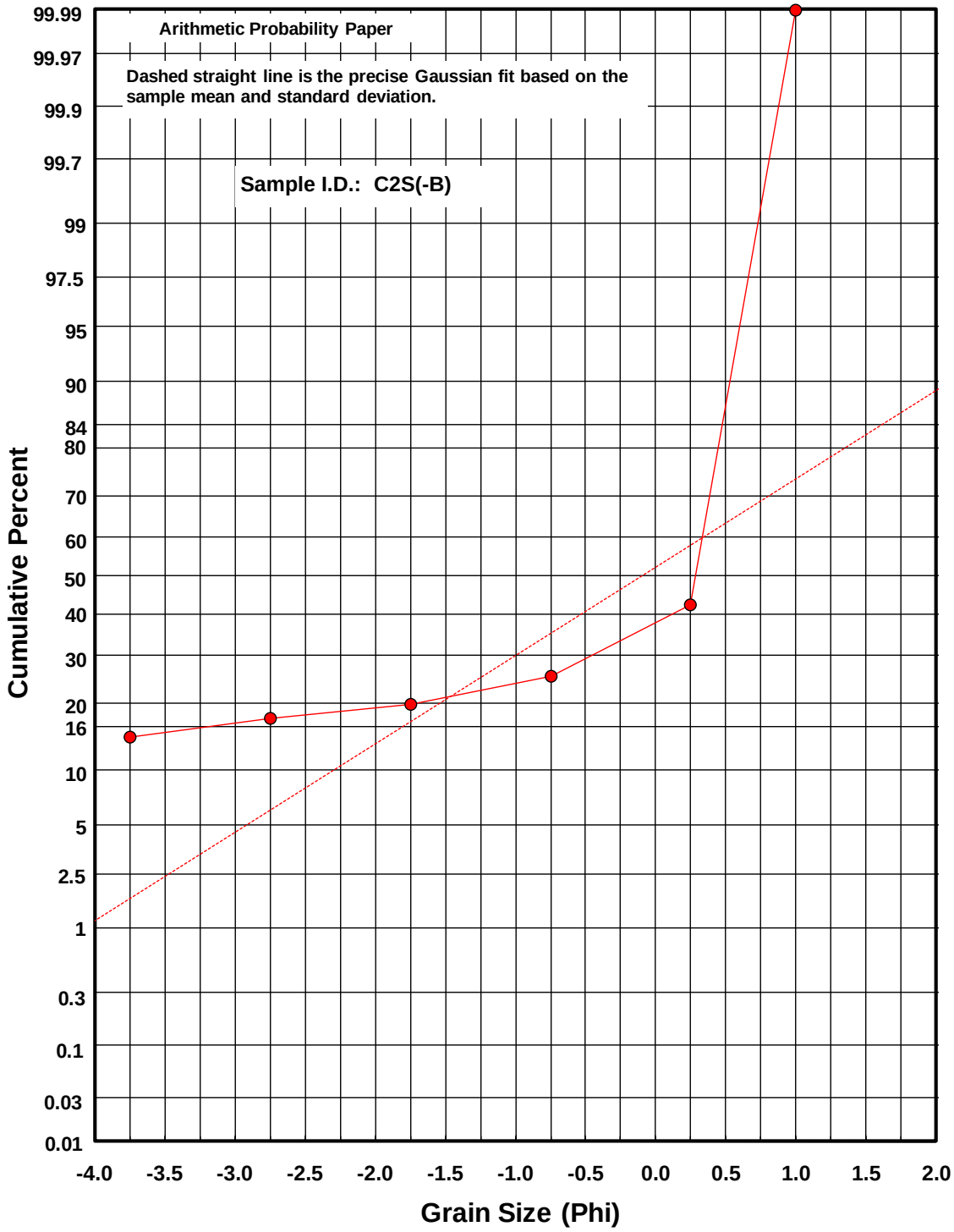
Arithmetic Probability Paper
Dashed straight line is the precise Gaussian fit based on the sample mean and standard deviation.
Sample I.D.: C2S(-B)
Cumulative Percent
99.99
99.97
99.9
99.7
99
97.5
95
90
84
80
70
60
50
40
30
20
16
10
5
2.5
1
0.3
0.1
0.03
0.01
-4.0
-3.5
-3.0
-2.5
-2.0
-1.5
-1.0
-0.5
0.0
0.5
1.0
1.5
2.0
Grain Size (Phi)

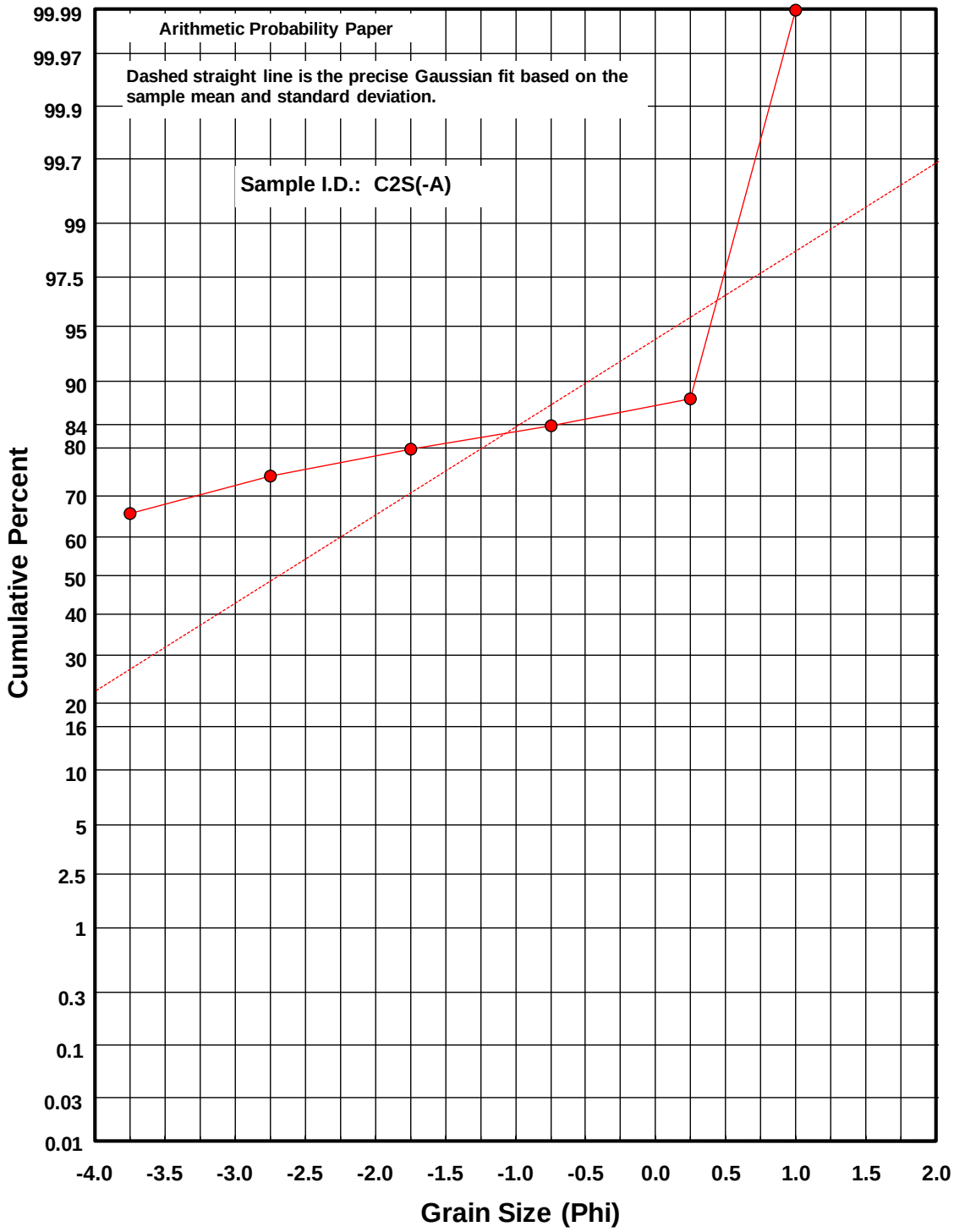
Arithmetic Probability Paper
Dashed straight line is the precise Gaussian fit based on the sample mean and standard deviation.
Sample I.D.: C2S(-A)
Cumulative Percent
99.99
99.97
99.9
99.7
99
97.5
95
90
84
80
70
60
50
40
30
20
16
10
5
2.5
1
0.3
0.1
0.03
0.01
-4.0
-3.5
-3.0
-2.5
-2.0
-1.5
-1.0
-0.5
0.0
0.5
1.0
1.5
2.0
Grain Size (Phi)

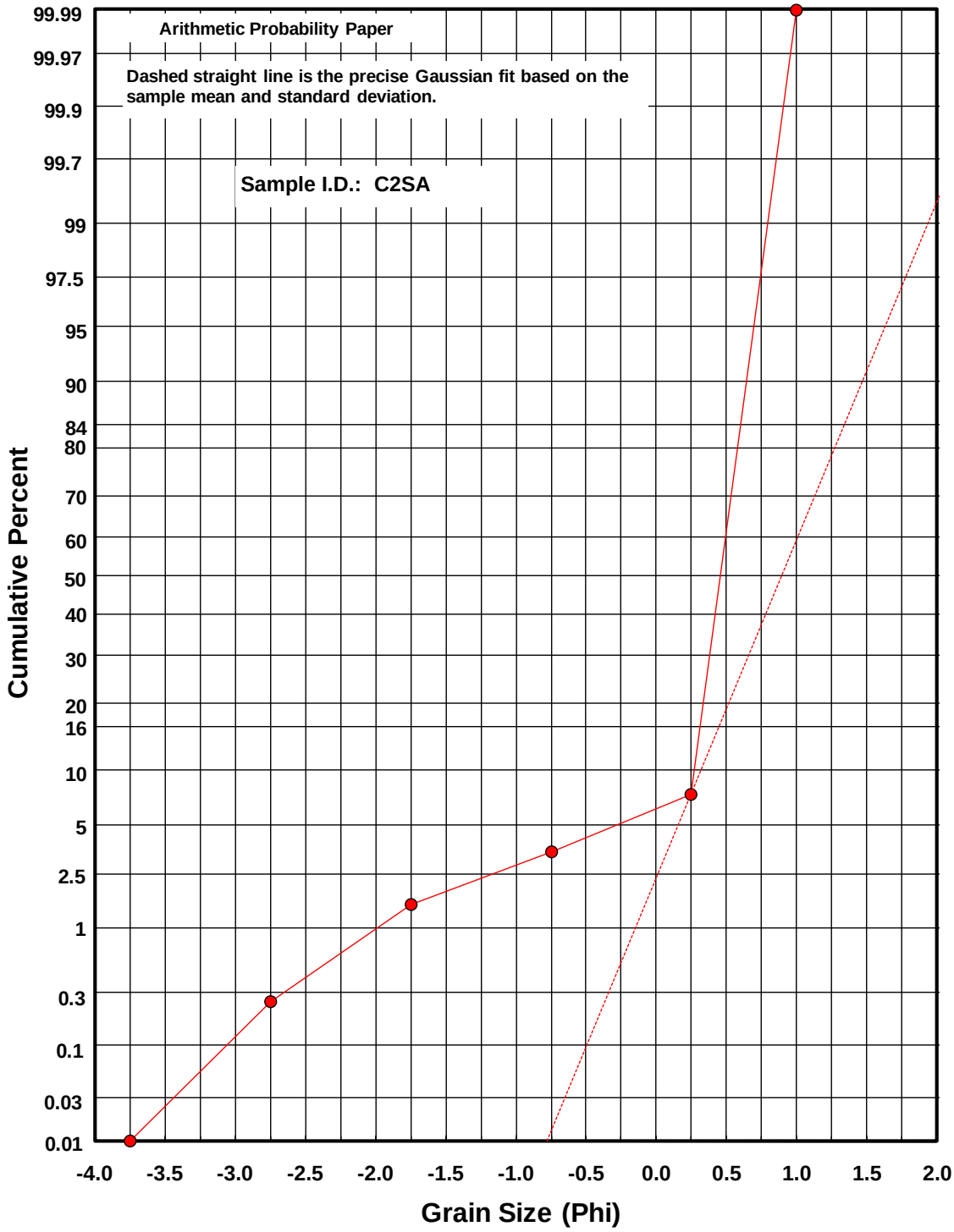
Arithmetic Probability Paper
Dashed straight line is the precise Gaussian fit based on the sample mean and standard deviation.
Sample I.D.: C2SA
Cumulative Percent
99.99
99.97
99.9
99.7
99
97.5
95
90
84
80
70
60
50
40
30
20
16
10
5
2.5
1
0.3
0.1
0.03
0.01
-4.0
-3.5
-3.0
-2.5
-2.0
-1.5
-1.0
-0.5
0.0
0.5
1.0
1.5
2.0
Grain Size (Phi)

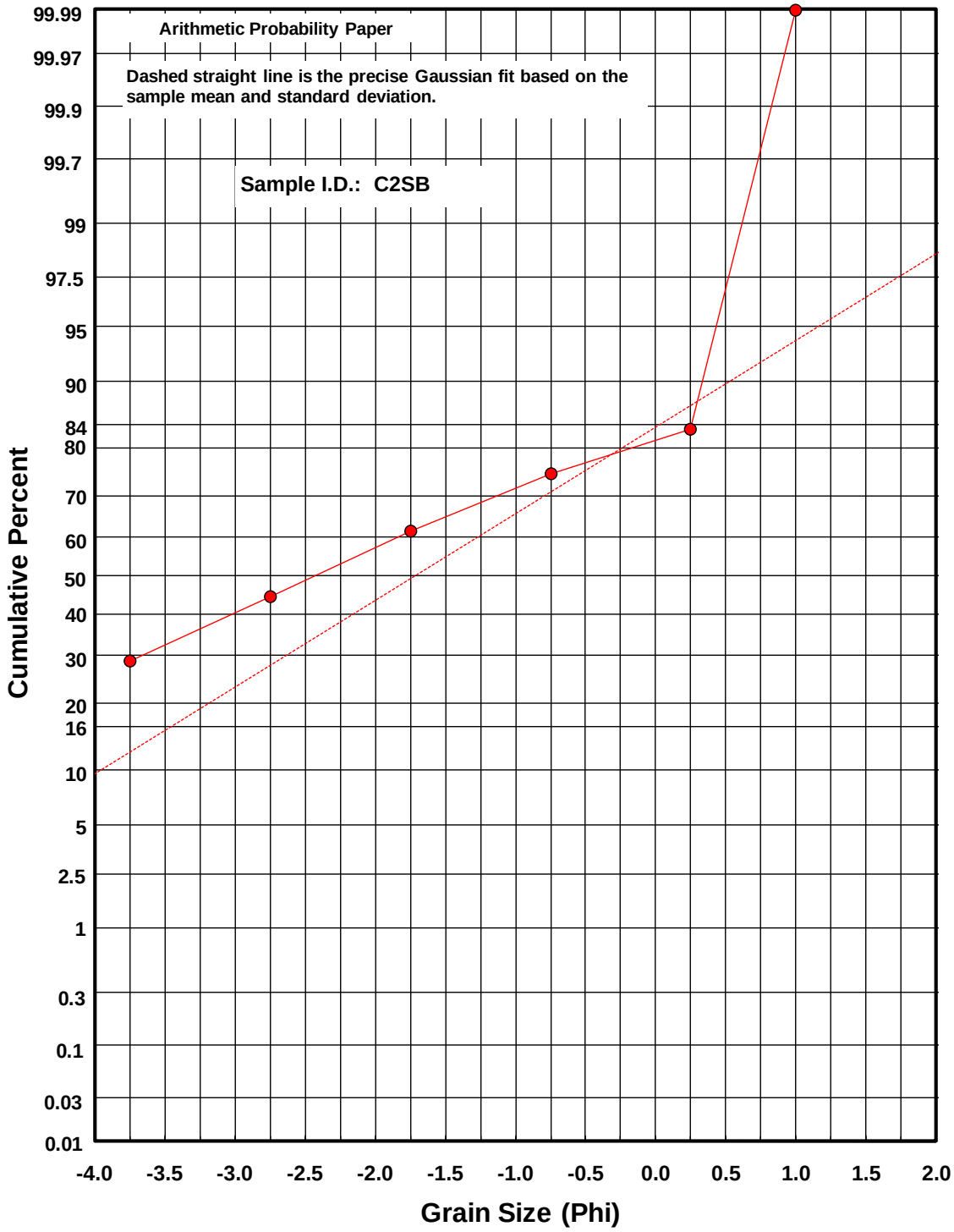
Arithmetic Probability Paper
Dashed straight line is the precise Gaussian fit based on the sample mean and standard deviation.
Sample I.D.: C2SB
Cumulative Percent
99.99
99.97
99.9
99.7
99
97.5
95
90
84
80
70
60
50
40
30
20
16
10
5
2.5
1
0.3
0.1
0.03
0.01
-4.0
-3.5
-3.0
-2.5
-2.0
-1.5
-1.0
-0.5
0.0
0.5
1.0
1.5
2.0
Grain Size (Phi)

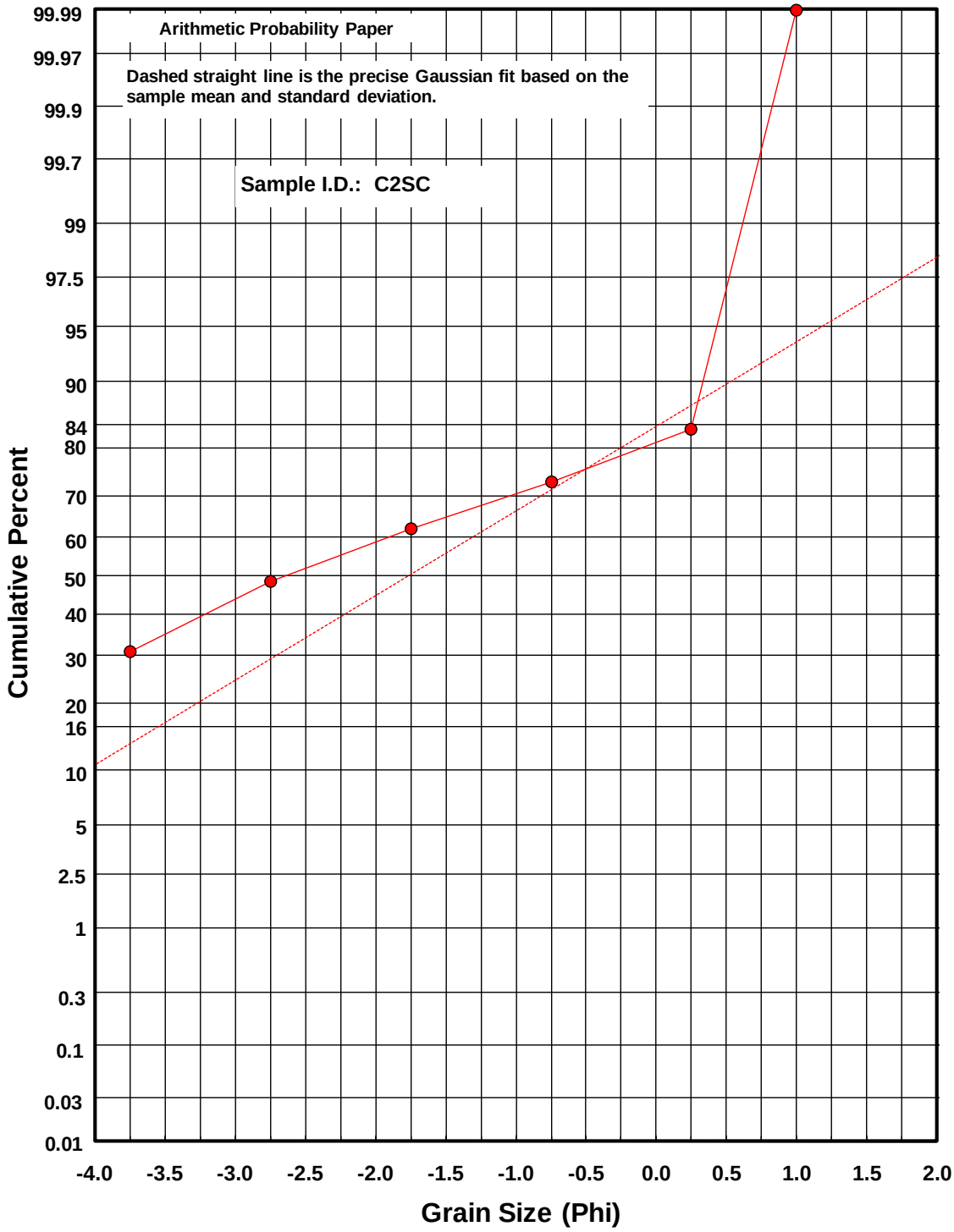
Arithmetic Probability Paper
Dashed straight line is the precise Gaussian fit based on the sample mean and standard deviation.
Sample I.D.: C2SC
Cumulative Percent
99.99
99.97
99.9
99.7
99
97.5
95
90
84
80
70
60
50
40
30
20
16
10
5
2.5
1
0.3
0.1
0.03
0.01
-4.0
-3.5
-3.0
-2.5
-2.0
-1.5
-1.0
-0.5
0.0
0.5
1.0
1.5
2.0
Grain Size (Phi)

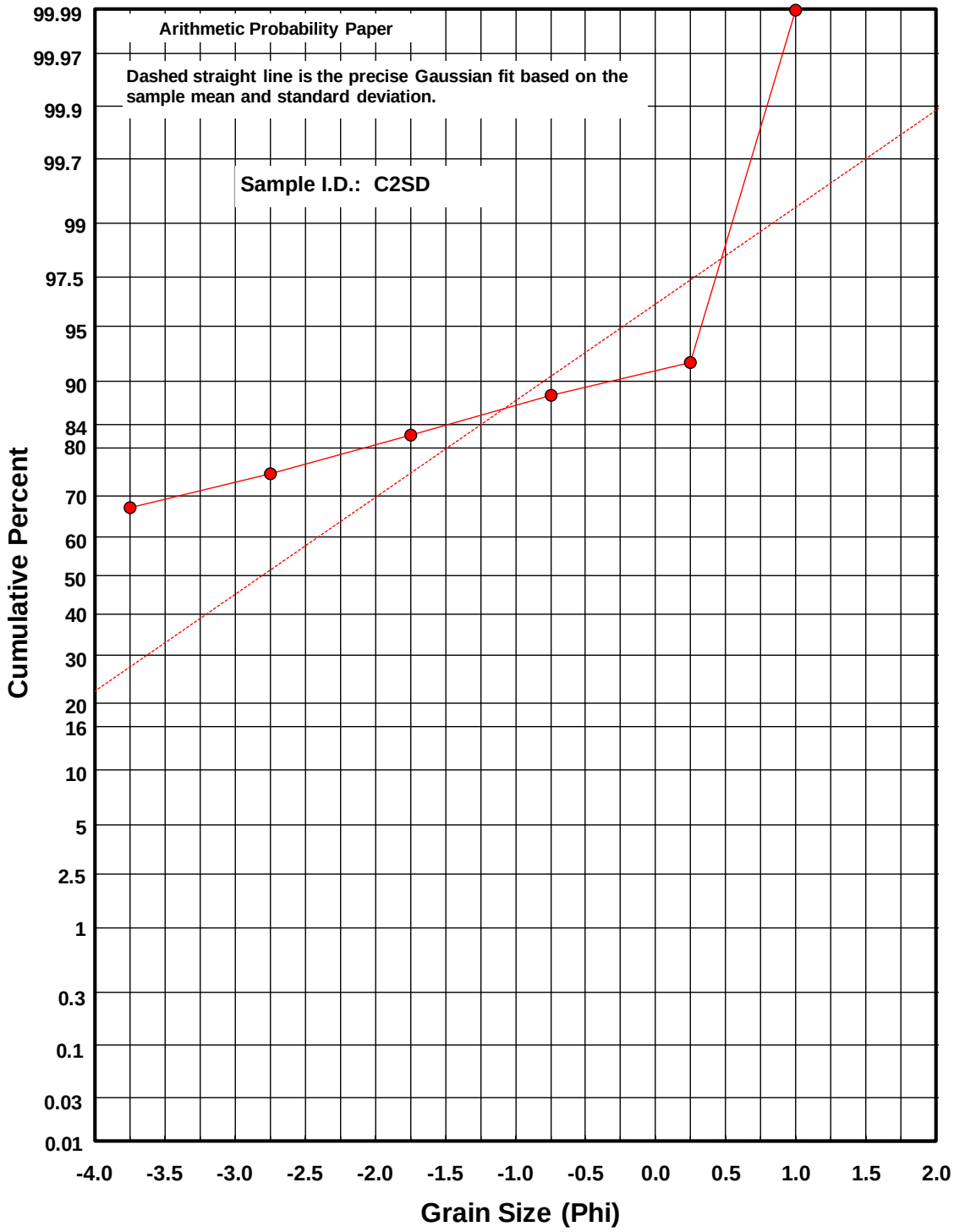
Arithmetic Probability Paper
Dashed straight line is the precise Gaussian fit based on the sample mean and standard deviation.
Sample I.D.: C2SD
Cumulative Percent
99.99
99.97
99.9
99.7
99
97.5
95
90
84
80
70
60
50
40
30
20
16
10
5
2.5
1
0.3
0.1
0.03
0.01
-4.0
-3.5
-3.0
-2.5
-2.0
-1.5
-1.0
-0.5
0.0
0.5
1.0
1.5
2.0
Grain Size (Phi)

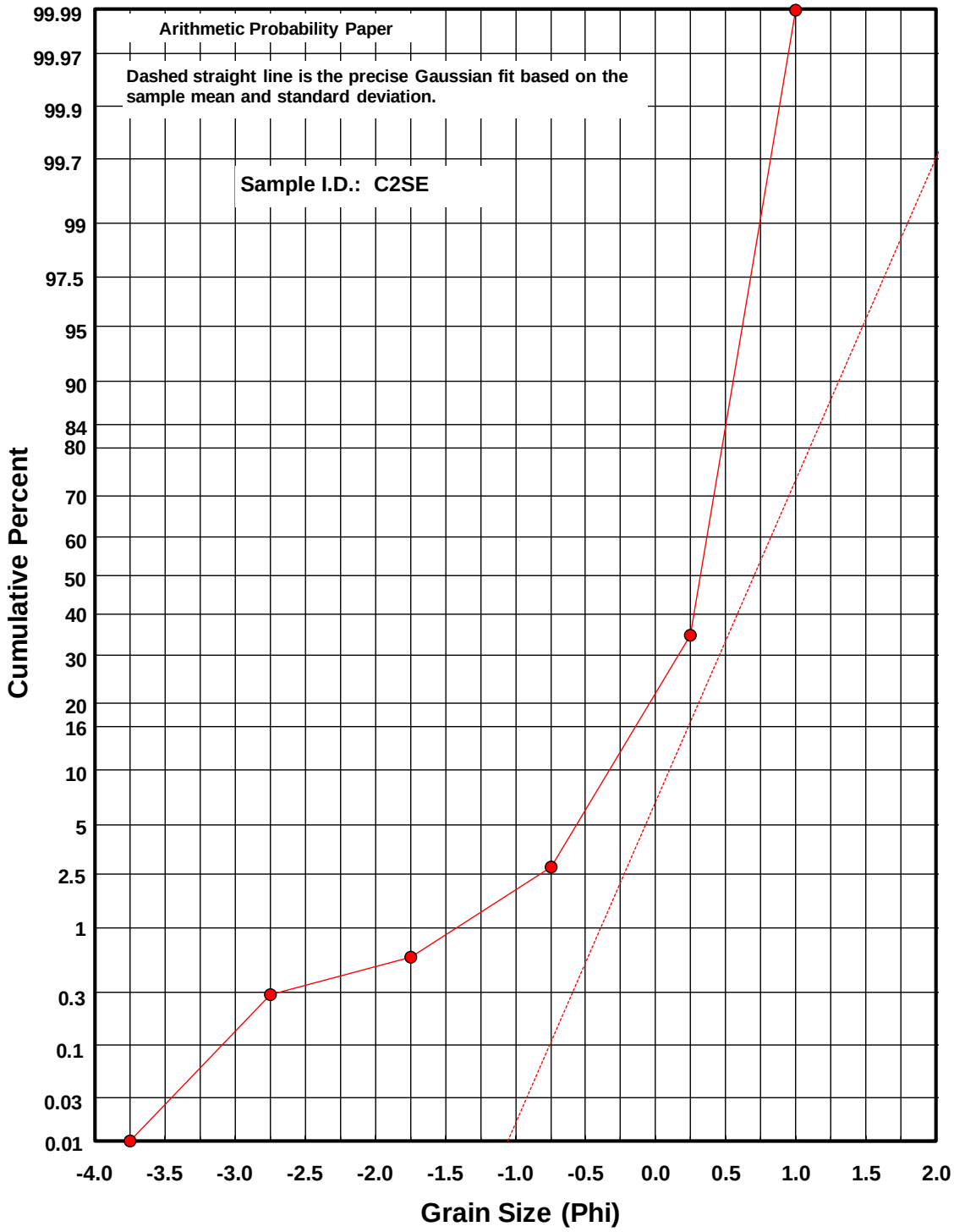
Arithmetic Probability Paper
Dashed straight line is the precise Gaussian fit based on the sample mean and standard deviation.
Sample I.D.: C2SE
Cumulative Percent
99.99
99.97
99.9
99.7
99
97.5
95
90
84
80
70
60
50
40
30
20
16
10
5
2.5
1
0.3
0.1
0.03
0.01
-4.0
-3.5
-3.0
-2.5
-2.0
-1.5
-1.0
-0.5
0.0
0.5
1.0
1.5
2.0
Grain Size (Phi)

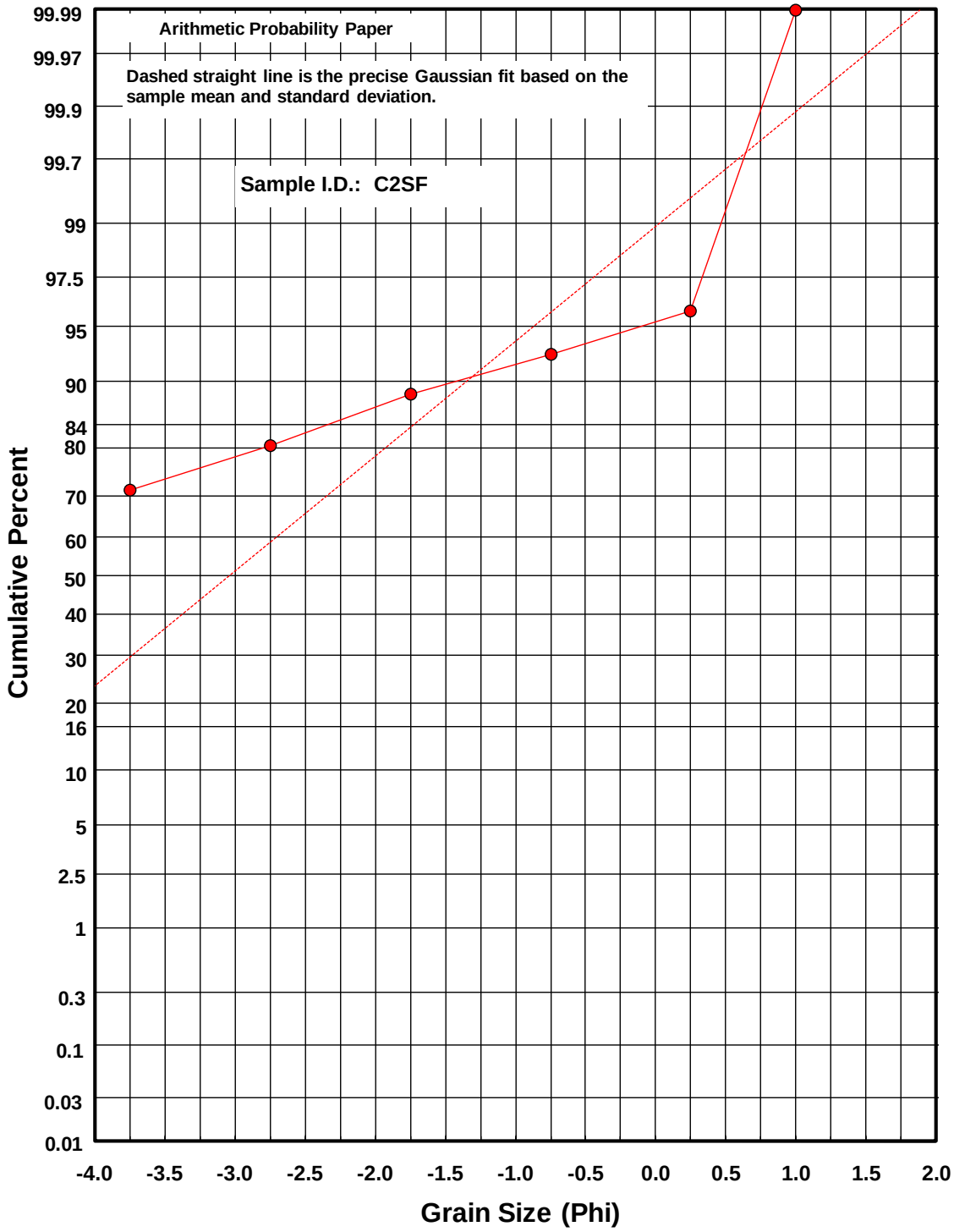
Arithmetic Probability Paper
Dashed straight line is the precise Gaussian fit based on the sample mean and standard deviation.
Sample I.D.: C2SF
Cumulative Percent
99.99
99.97
99.9
99.7
99
97.5
95
90
84
80
70
60
50
40
30
20
16
10
5
2.5
1
0.3
0.1
0.03
0.01
-4.0
-3.5
-3.0
-2.5
-2.0
-1.5
-1.0
-0.5
0.0
0.5
1.0
1.5
2.0
Grain Size (Phi)

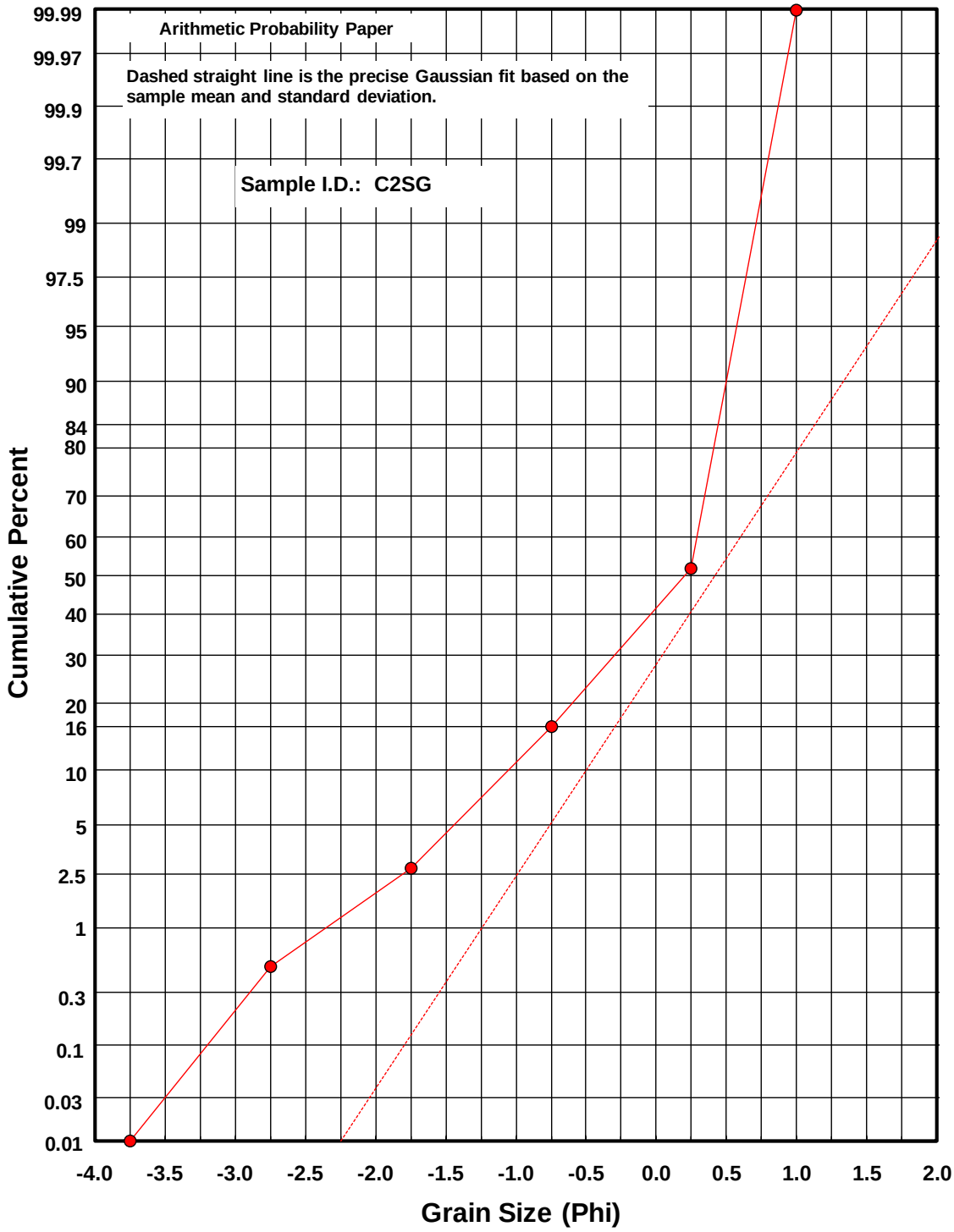
Arithmetic Probability Paper
Dashed straight line is the precise Gaussian fit based on the sample mean and standard deviation.
Sample I.D.: C2SG
Cumulative Percent
99.99
99.97
99.9
99.7
99
97.5
95
90
84
80
70
60
50
40
30
20
16
10
5
2.5
1
0.3
0.1
0.03
0.01
-4.0
-3.5
-3.0
-2.5
-2.0
-1.5
-1.0
-0.5
0.0
0.5
1.0
1.5
2.0
Grain Size (Phi)

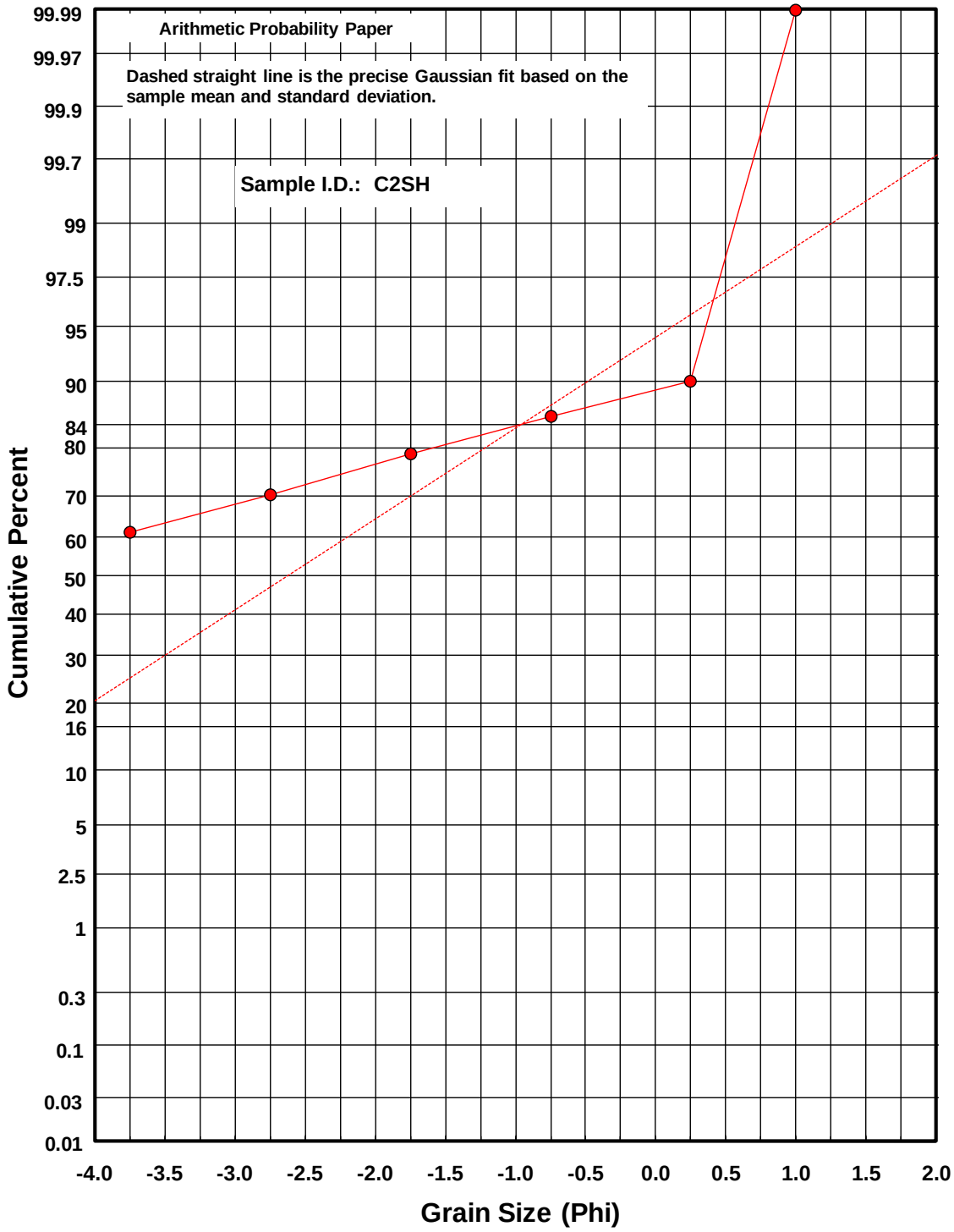
Arithmetic Probability Paper
Dashed straight line is the precise Gaussian fit based on the sample mean and standard deviation.
Sample I.D.: C2SH
Cumulative Percent
99.99
99.97
99.9
99.7
99
97.5
95
90
84
80
70
60
50
40
30
20
16
10
5
2.5
1
0.3
0.1
0.03
0.01
-4.0
-3.5
-3.0
-2.5
-2.0
-1.5
-1.0
-0.5
0.0
0.5
1.0
1.5
2.0
Grain Size (Phi)

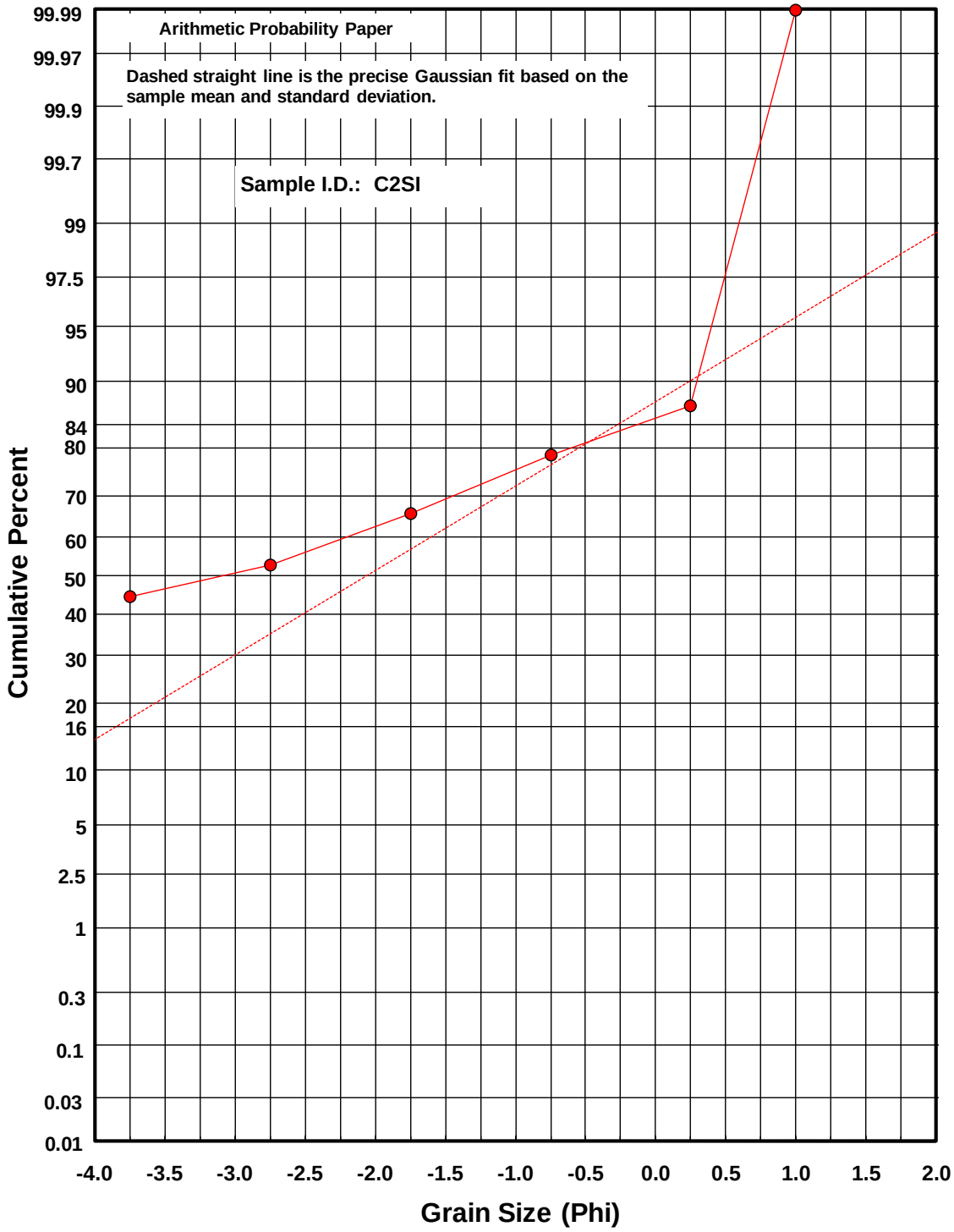
Arithmetic Probability Paper
Dashed straight line is the precise Gaussian fit based on the sample mean and standard deviation.
Sample I.D.: C2SI
Cumulative Percent
99.99
99.97
99.9
99.7
99
97.5
95
90
84
80
70
60
50
40
30
20
16
10
5
2.5
1
0.3
0.1
0.03
0.01
-4.0
-3.5
-3.0
-2.5
-2.0
-1.5
-1.0
-0.5
0.0
0.5
1.0
1.5
2.0
Grain Size (Phi)

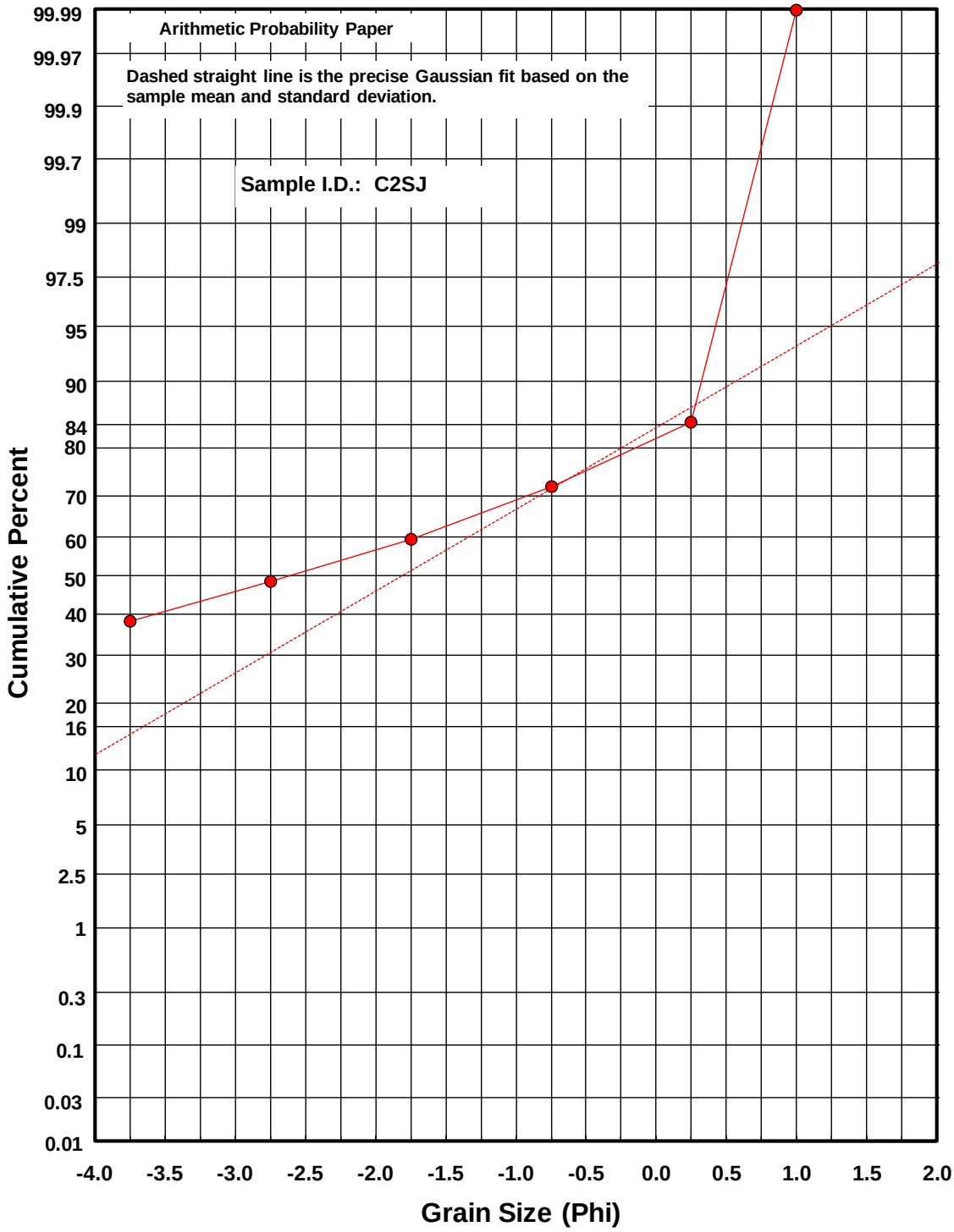
Arithmetic Probability Paper
Dashed straight line is the precise Gaussian fit based on the sample mean and standard deviation.
Sample I.D.: C2SJ
Cumulative Percent
99.99
99.97
99.9
99.7
99
97.5
95
90
84
80
70
60
50
40
30
20
16
10
5
2.5
1
0.3
0.1
0.03
0.01
-4.0
-3.5
-3.0
-2.5
-2.0
-1.5
-1.0
-0.5
0.0
0.5
1.0
1.5
2.0
Grain Size (Phi)

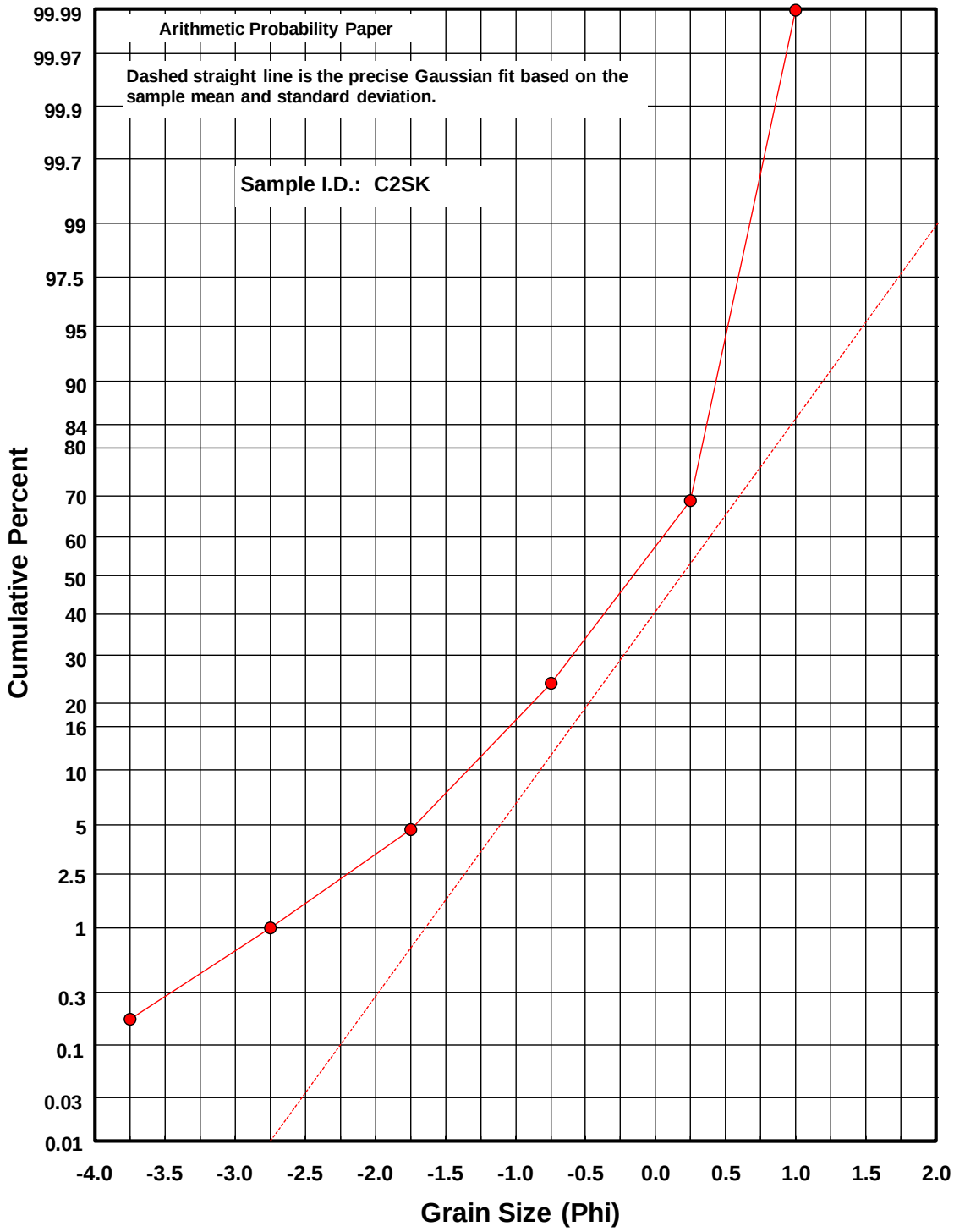
Arithmetic Probability Paper
Dashed straight line is the precise Gaussian fit based on the sample mean and standard deviation.
Sample I.D.: C2SK
Cumulative Percent
99.99
99.97
99.9
99.7
99
97.5
95
90
84
80
70
60
50
40
30
20
16
10
5
2.5
1
0.3
0.1
0.03
0.01
-4.0
-3.5
-3.0
-2.5
-2.0
-1.5
-1.0
-0.5
0.0
0.5
1.0
1.5
2.0
Grain Size (Phi)

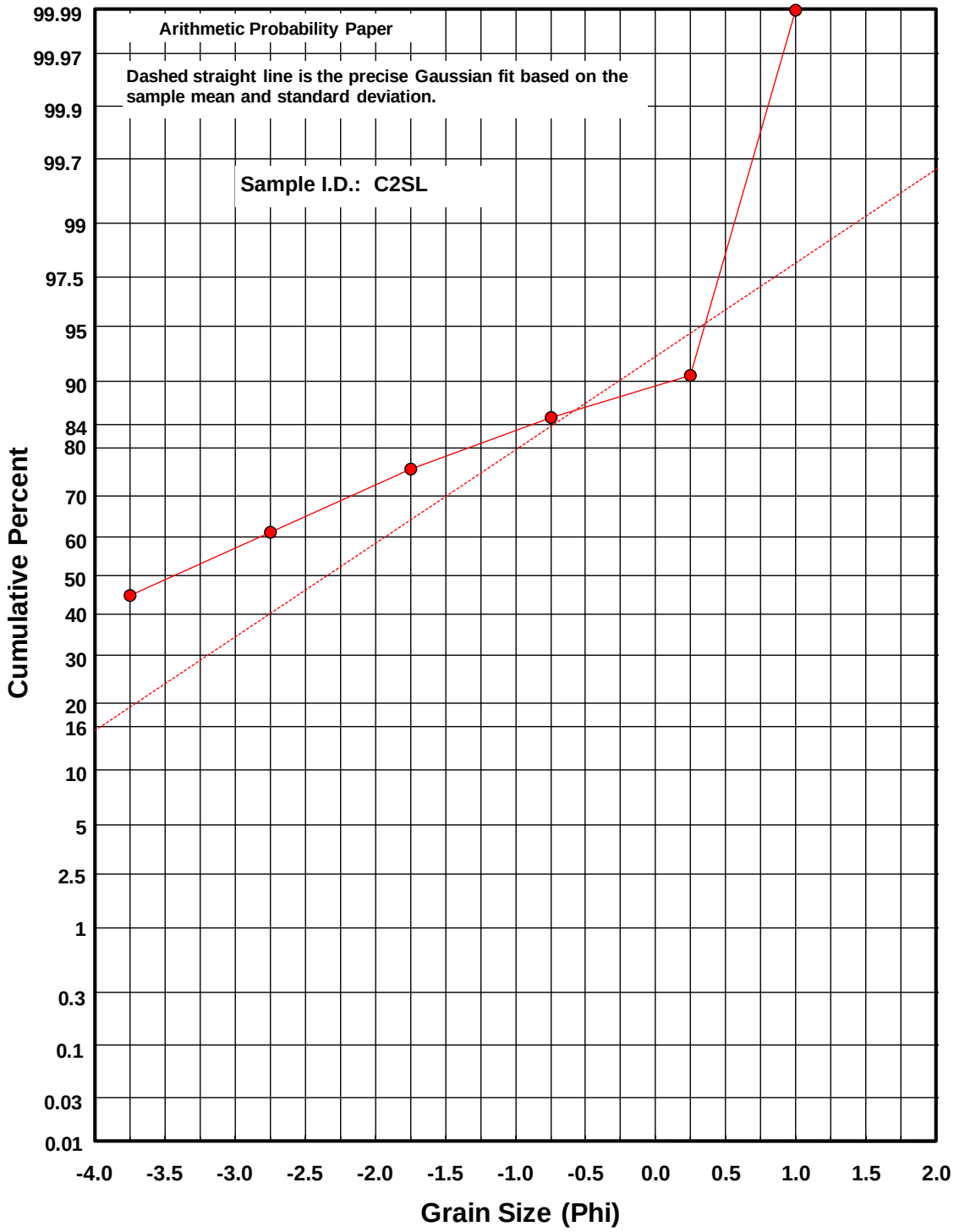
Arithmetic Probability Paper
Dashed straight line is the precise Gaussian fit based on the sample mean and standard deviation.
Sample I.D.: C2SL
Cumulative Percent
99.99
99.97
99.9
99.7
99
97.5
95
90
84
80
70
60
50
40
30
20
16
10
5
2.5
1
0.3
0.1
0.03
0.01
-4.0
-3.5
-3.0
-2.5
-2.0
-1.5
-1.0
-0.5
0.0
0.5
1.0
1.5
2.0
Grain Size (Phi)

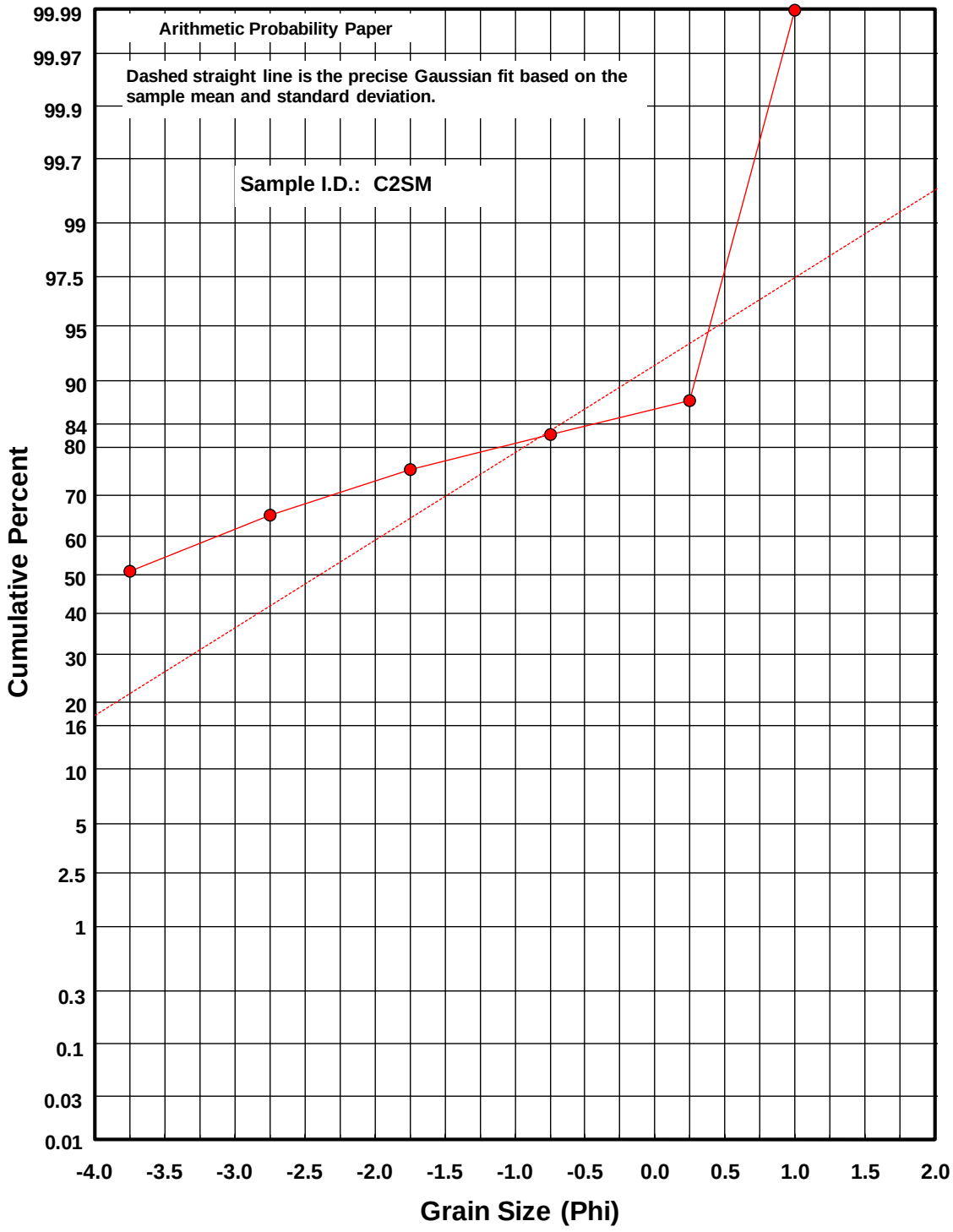
Arithmetic Probability Paper
Dashed straight line is the precise Gaussian fit based on the sample mean and standard deviation.
Sample I.D.: C2SM
Cumulative Percent
99.99
99.97
99.9
99.7
99
97.5
95
90
84
80
70
60
50
40
30
20
16
10
5
2.5
1
0.3
0.1
0.03
0.01
-4.0
-3.5
-3.0
-2.5
-2.0
-1.5
-1.0
-0.5
0.0
0.5
1.0
1.5
2.0
Grain Size (Phi)

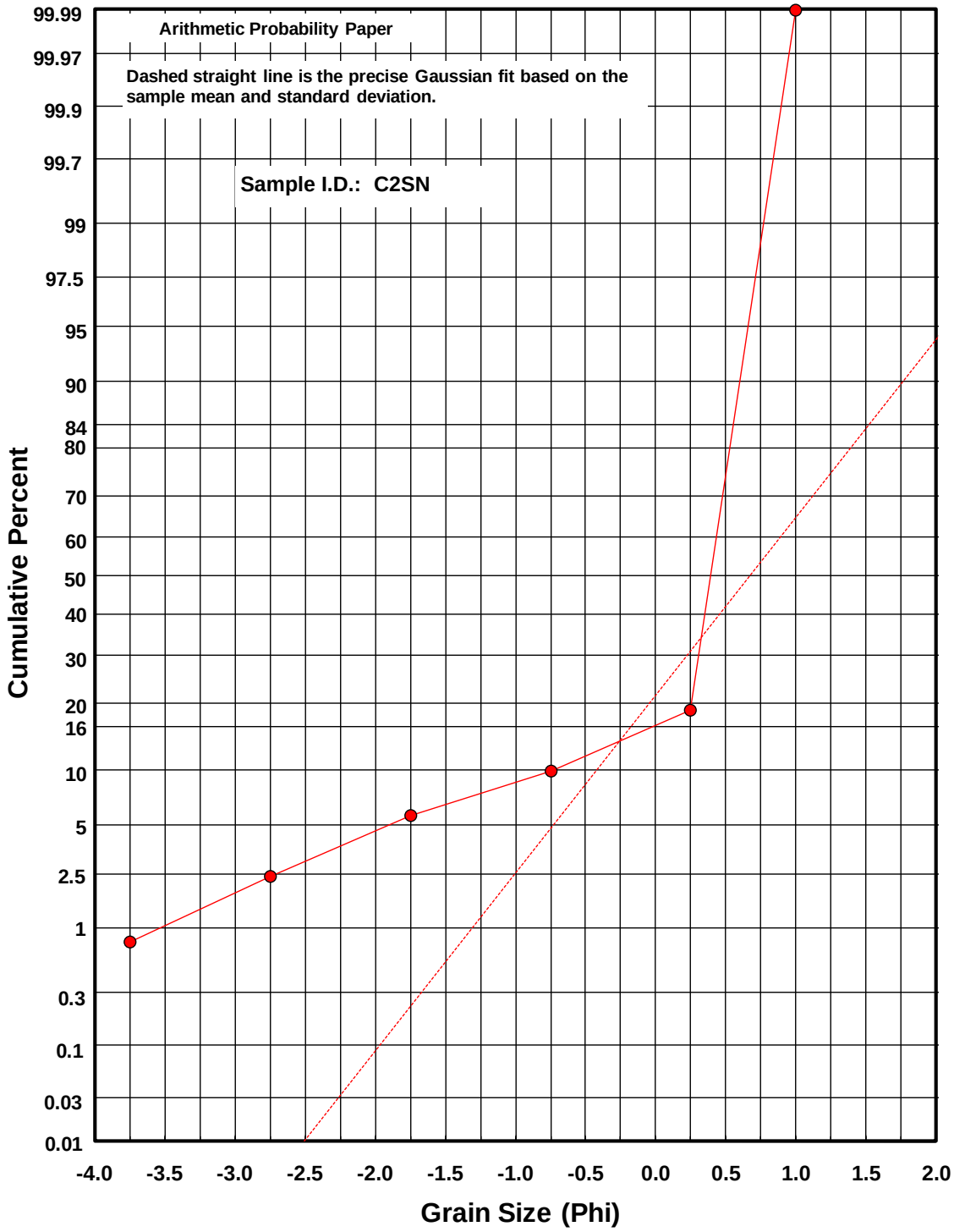
Arithmetic Probability Paper
Dashed straight line is the precise Gaussian fit based on the sample mean and standard deviation.
Sample I.D.: C2SN
Cumulative Percent
99.99
99.97
99.9
99.7
99
97.5
95
90
84
80
70
60
50
40
30
20
16
10
5
2.5
1
0.3
0.1
0.03
0.01
-4.0
-3.5
-3.0
-2.5
-2.0
-1.5
-1.0
-0.5
0.0
0.5
1.0
1.5
2.0
Grain Size (Phi)

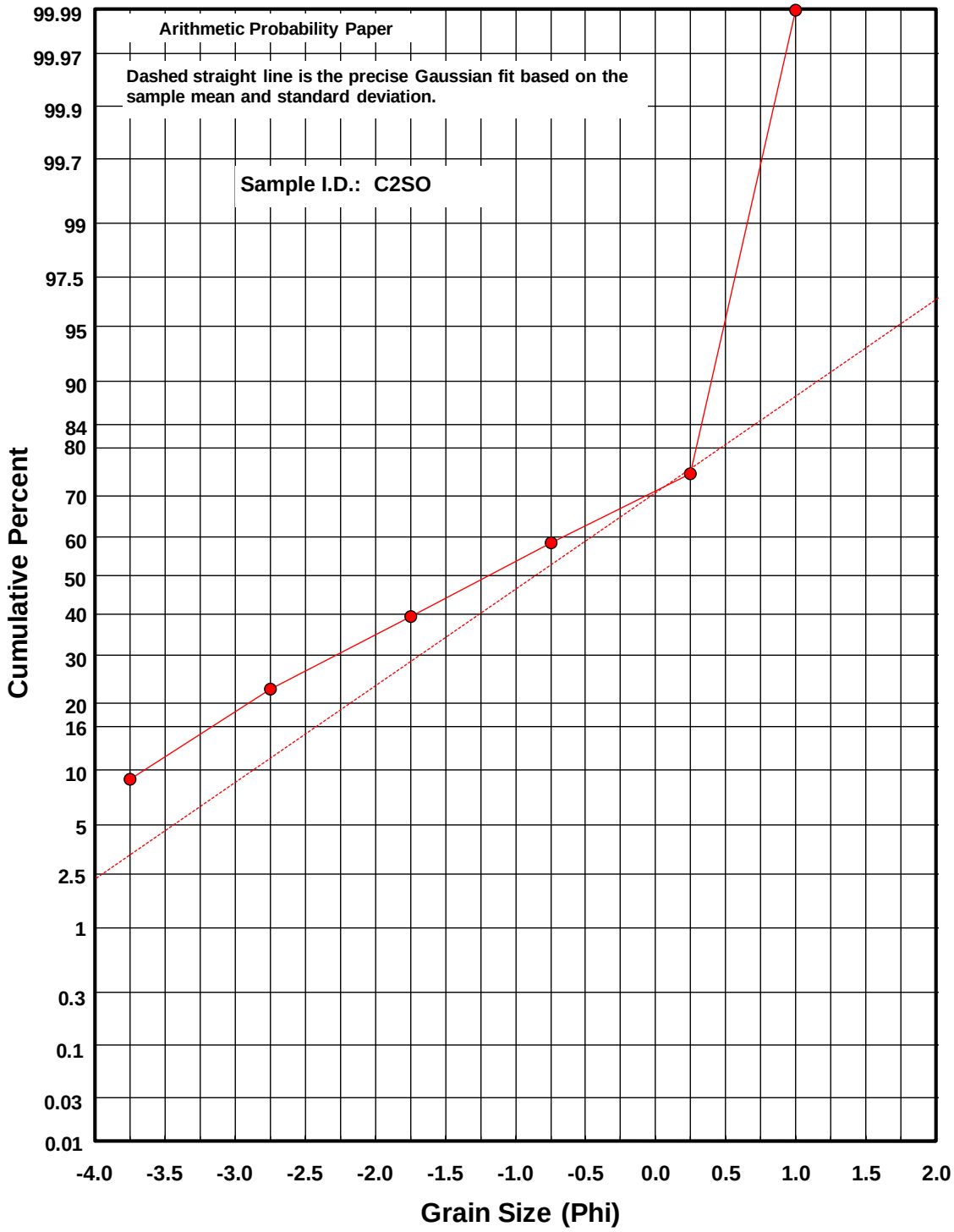
Arithmetic Probability Paper
Dashed straight line is the precise Gaussian fit based on the sample mean and standard deviation.
Sample I.D.: C2SO
Cumulative Percent
99.99
99.97
99.9
99.7
99
97.5
95
90
84
80
70
60
50
40
30
20
16
10
5
2.5
1
0.3
0.1
0.03
0.01
-4.0
-3.5
-3.0
-2.5
-2.0
-1.5
-1.0
-0.5
0.0
0.5
1.0
1.5
2.0
Grain Size (Phi)

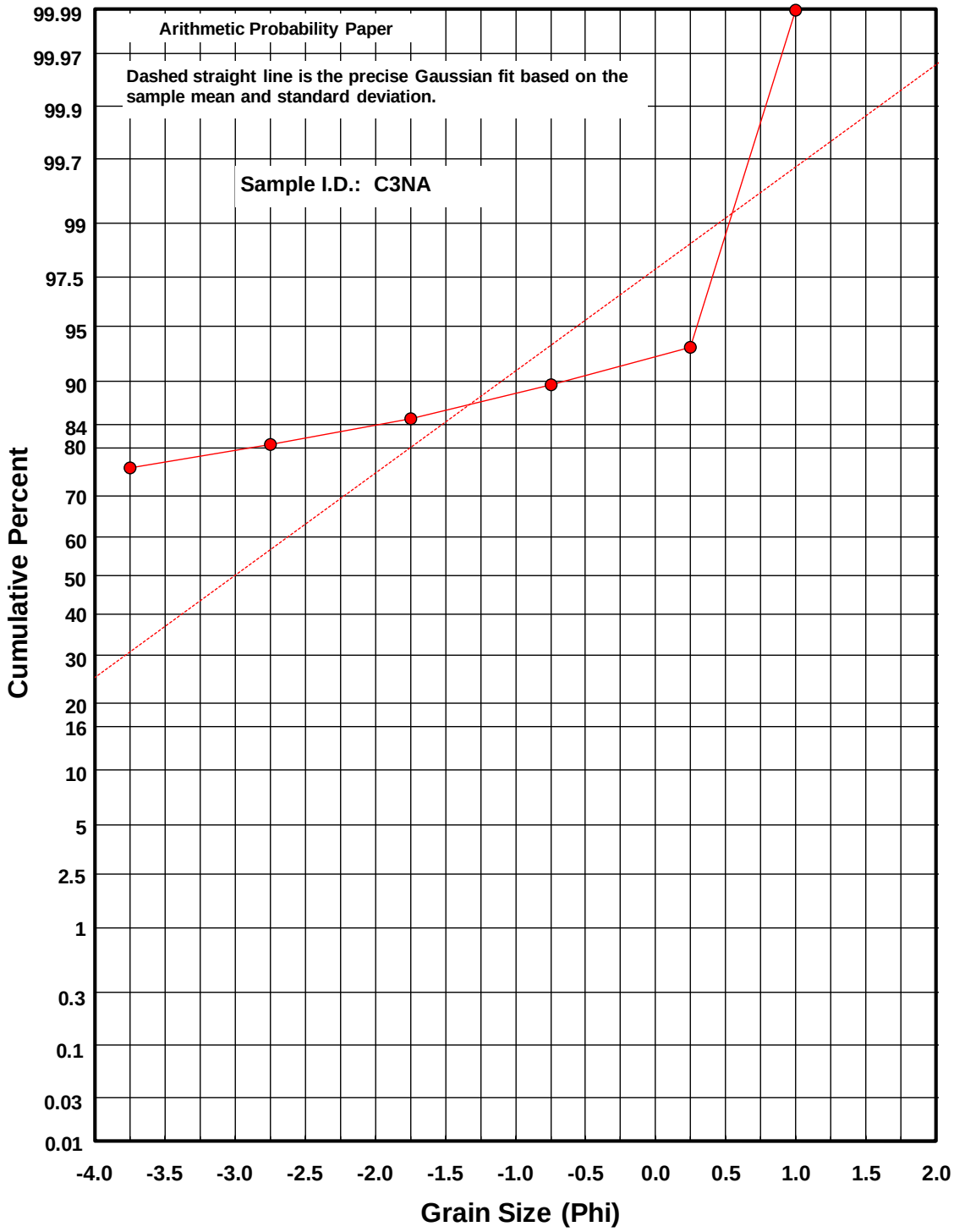
Arithmetic Probability Paper
Dashed straight line is the precise Gaussian fit based on the sample mean and standard deviation.
Sample I.D.: C3NA
Cumulative Percent
99.99
99.97
99.9
99.7
99
97.5
95
90
84
80
70
60
50
40
30
20
16
10
5
2.5
1
0.3
0.1
0.03
0.01
-4.0
-3.5
-3.0
-2.5
-2.0
-1.5
-1.0
-0.5
0.0
0.5
1.0
1.5
2.0
Grain Size (Phi)

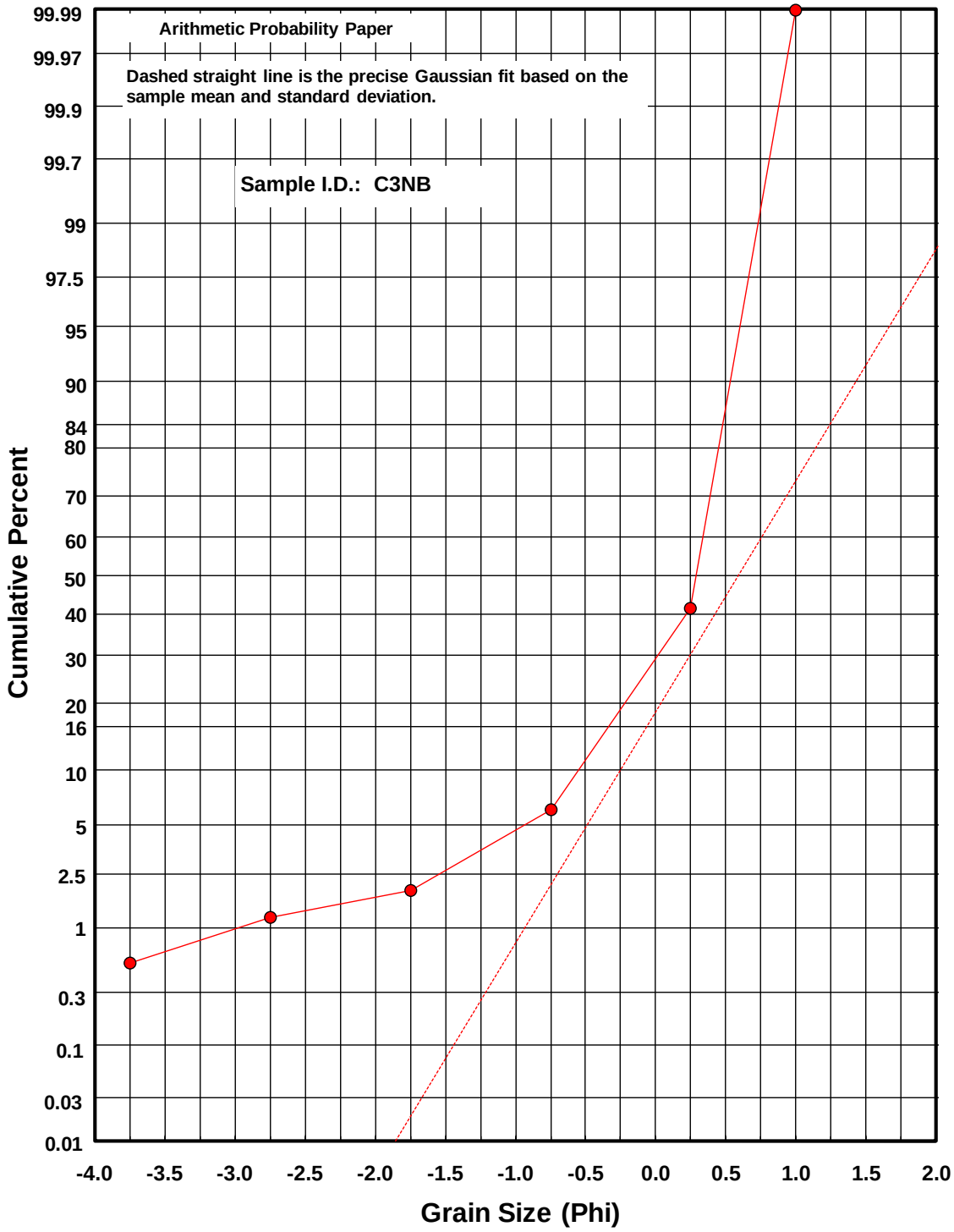
Arithmetic Probability Paper
Dashed straight line is the precise Gaussian fit based on the sample mean and standard deviation.
Sample I.D.: C3NB
Cumulative Percent
99.99
99.97
99.9
99.7
99
97.5
95
90
84
80
70
60
50
40
30
20
16
10
5
2.5
1
0.3
0.1
0.03
0.01
-4.0
-3.5
-3.0
-2.5
-2.0
-1.5
-1.0
-0.5
0.0
0.5
1.0
1.5
2.0
Grain Size (Phi)

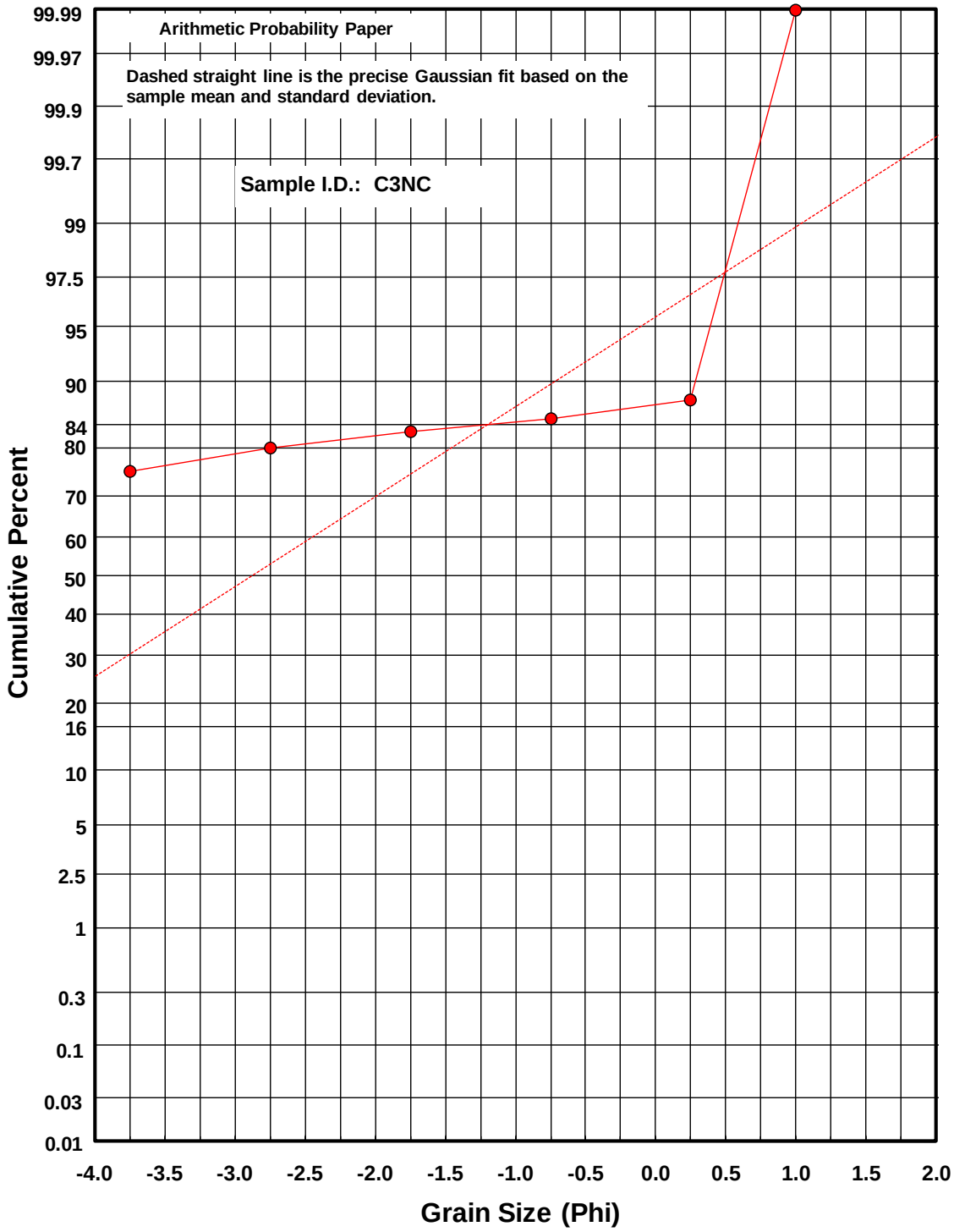
Arithmetic Probability Paper
Dashed straight line is the precise Gaussian fit based on the sample mean and standard deviation.
Sample I.D.: C3NC
Cumulative Percent
99.99
99.97
99.9
99.7
99
97.5
95
90
84
80
70
60
50
40
30
20
16
10
5
2.5
1
0.3
0.1
0.03
0.01
-4.0
-3.5
-3.0
-2.5
-2.0
-1.5
-1.0
-0.5
0.0
0.5
1.0
1.5
2.0
Grain Size (Phi)

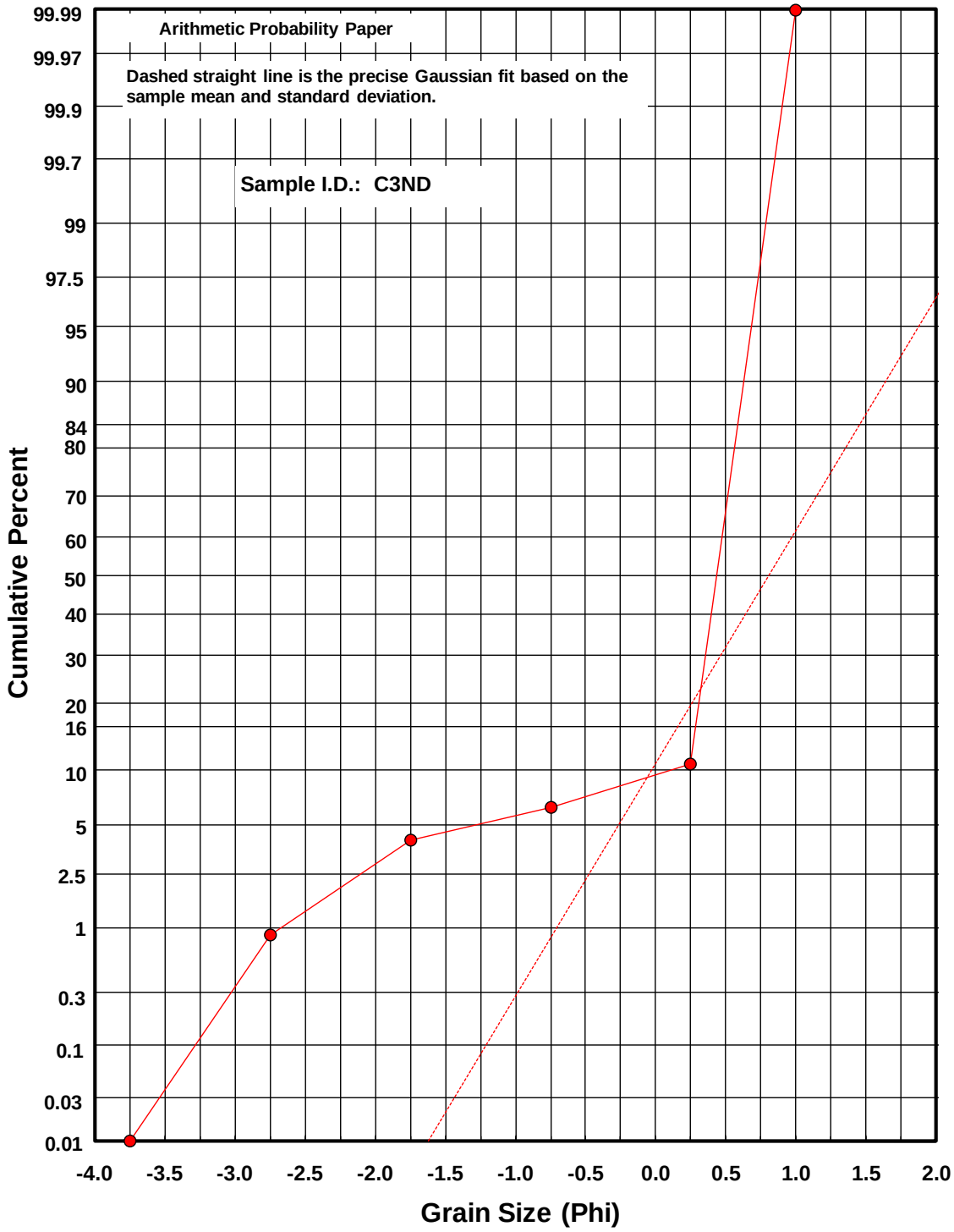
Arithmetic Probability Paper
Dashed straight line is the precise Gaussian fit based on the sample mean and standard deviation.
Sample I.D.: C3ND
Cumulative Percent
99.99
99.97
99.9
99.7
99
97.5
95
90
84
80
70
60
50
40
30
20
16
10
5
2.5
1
0.3
0.1
0.03
0.01
-4.0
-3.5
-3.0
-2.5
-2.0
-1.5
-1.0
-0.5
0.0
0.5
1.0
1.5
2.0
Grain Size (Phi)

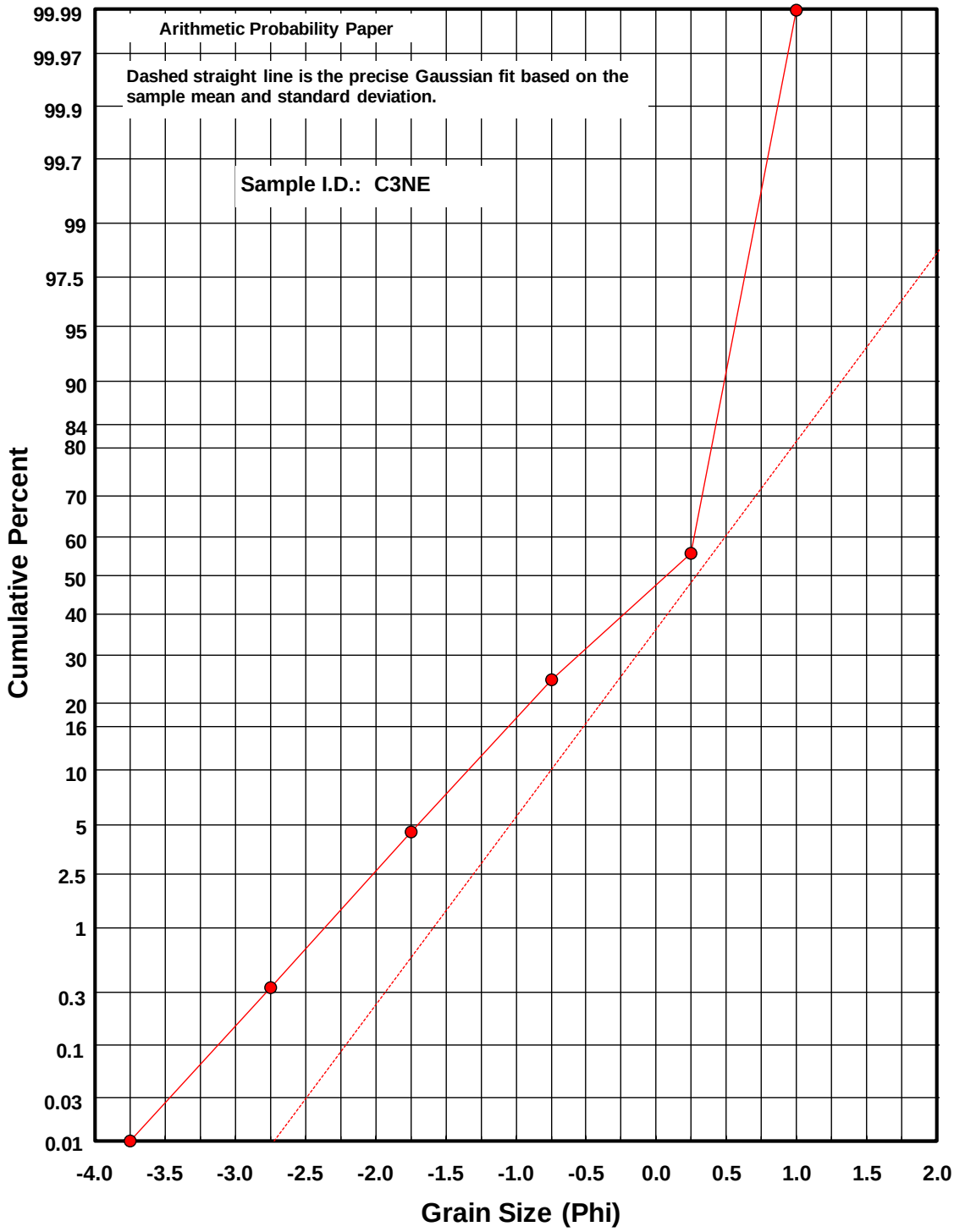
Arithmetic Probability Paper
Dashed straight line is the precise Gaussian fit based on the sample mean and standard deviation.
Sample I.D.: C3NE
Cumulative Percent
99.99
99.97
99.9
99.7
99
97.5
95
90
84
80
70
60
50
40
30
20
16
10
5
2.5
1
0.3
0.1
0.03
0.01
-4.0
-3.5
-3.0
-2.5
-2.0
-1.5
-1.0
-0.5
0.0
0.5
1.0
1.5
2.0
Grain Size (Phi)

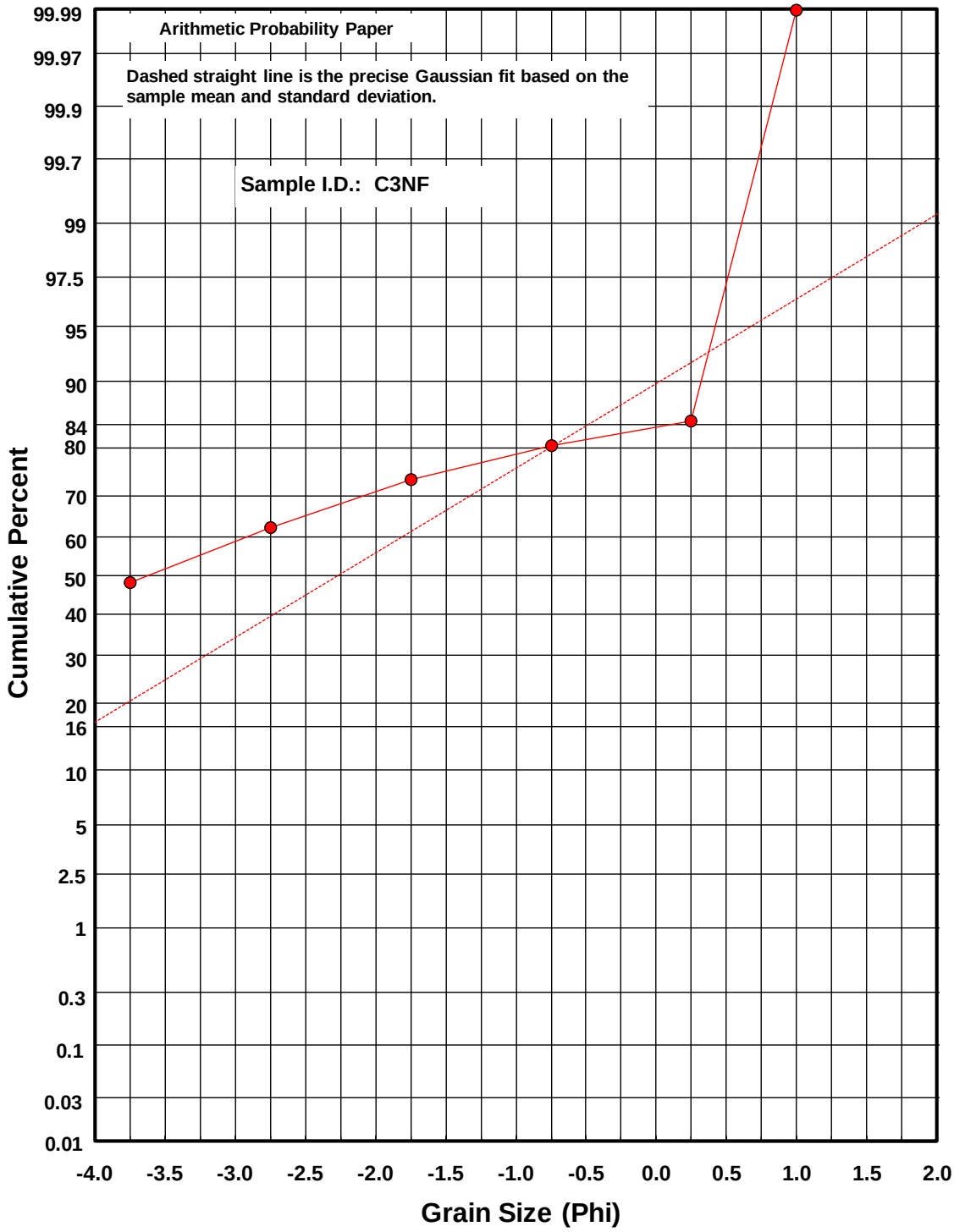
Arithmetic Probability Paper
Dashed straight line is the precise Gaussian fit based on the sample mean and standard deviation.
Sample I.D.: C3NF
Cumulative Percent
99.99
99.97
99.9
99.7
99
97.5
95
90
84
80
70
60
50
40
30
20
16
10
5
2.5
1
0.3
0.1
0.03
0.01
-4.0
-3.5
-3.0
-2.5
-2.0
-1.5
-1.0
-0.5
0.0
0.5
1.0
1.5
2.0
Grain Size (Phi)

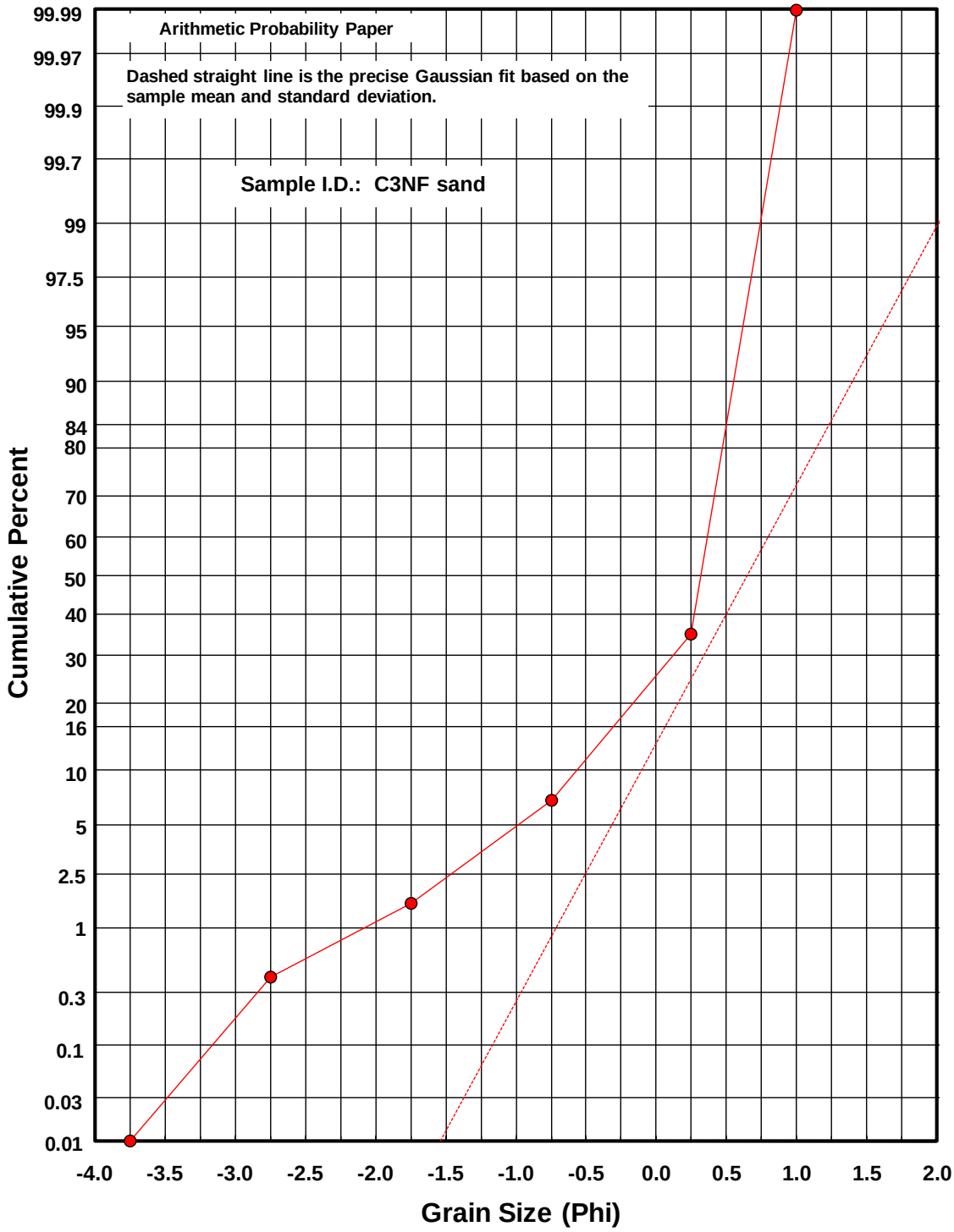
Arithmetic Probability Paper
Dashed straight line is the precise Gaussian fit based on the sample mean and standard deviation.
Sample I.D.: C3NF sand
Cumulative Percent
99.99
99.97
99.9
99.7
99
97.5
95
90
84
80
70
60
50
40
30
20
16
10
5
2.5
1
0.3
0.1
0.03
0.01
-4.0
-3.5
-3.0
-2.5
-2.0
-1.5
-1.0
-0.5
0.0
0.5
1.0
1.5
2.0
Grain Size (Phi)

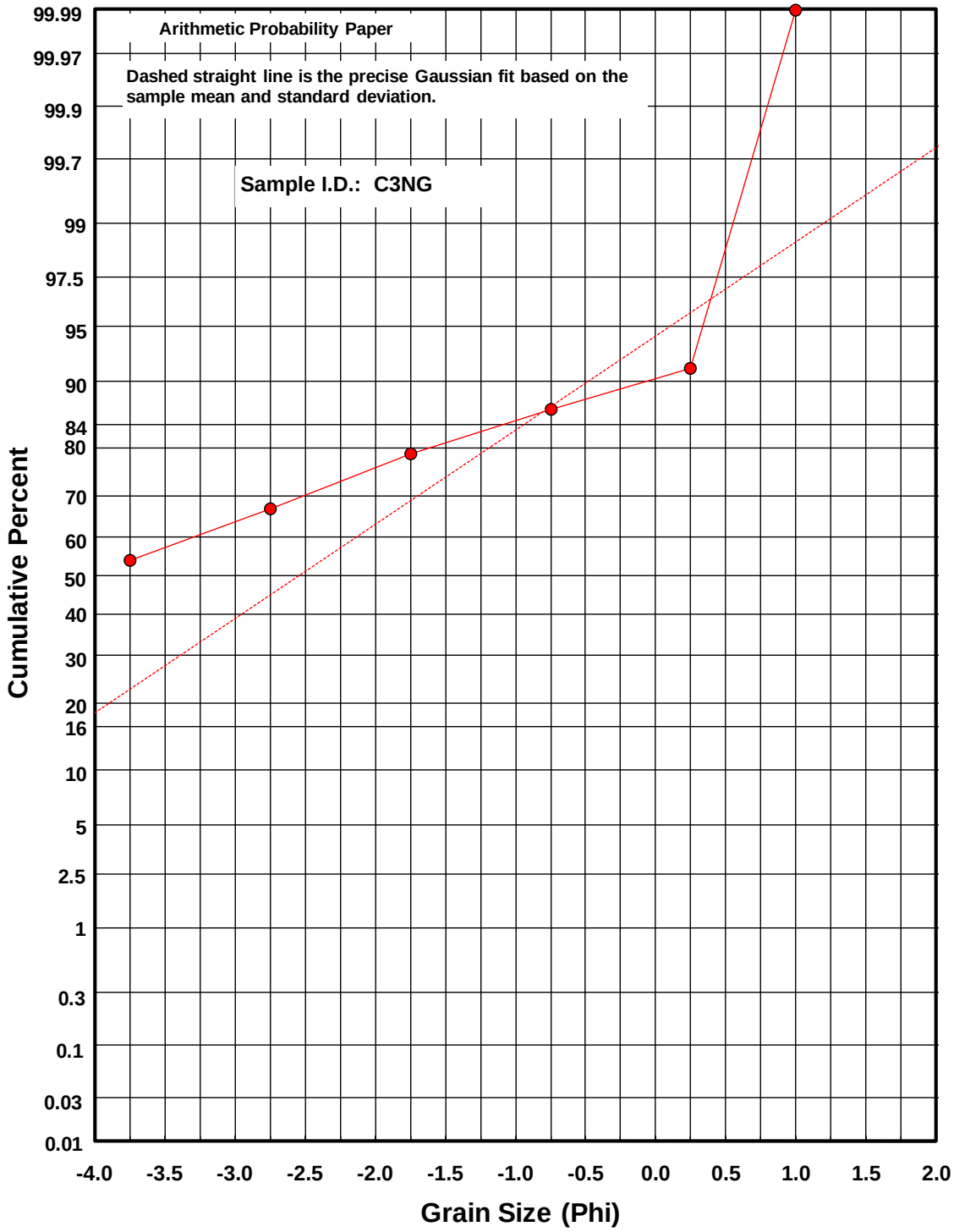
Arithmetic Probability Paper
Dashed straight line is the precise Gaussian fit based on the sample mean and standard deviation.
Sample I.D.: C3NG
Cumulative Percent
99.99
99.97
99.9
99.7
99
97.5
95
90
84
80
70
60
50
40
30
20
16
10
5
2.5
1
0.3
0.1
0.03
0.01
-4.0
-3.5
-3.0
-2.5
-2.0
-1.5
-1.0
-0.5
0.0
0.5
1.0
1.5
2.0
Grain Size (Phi)

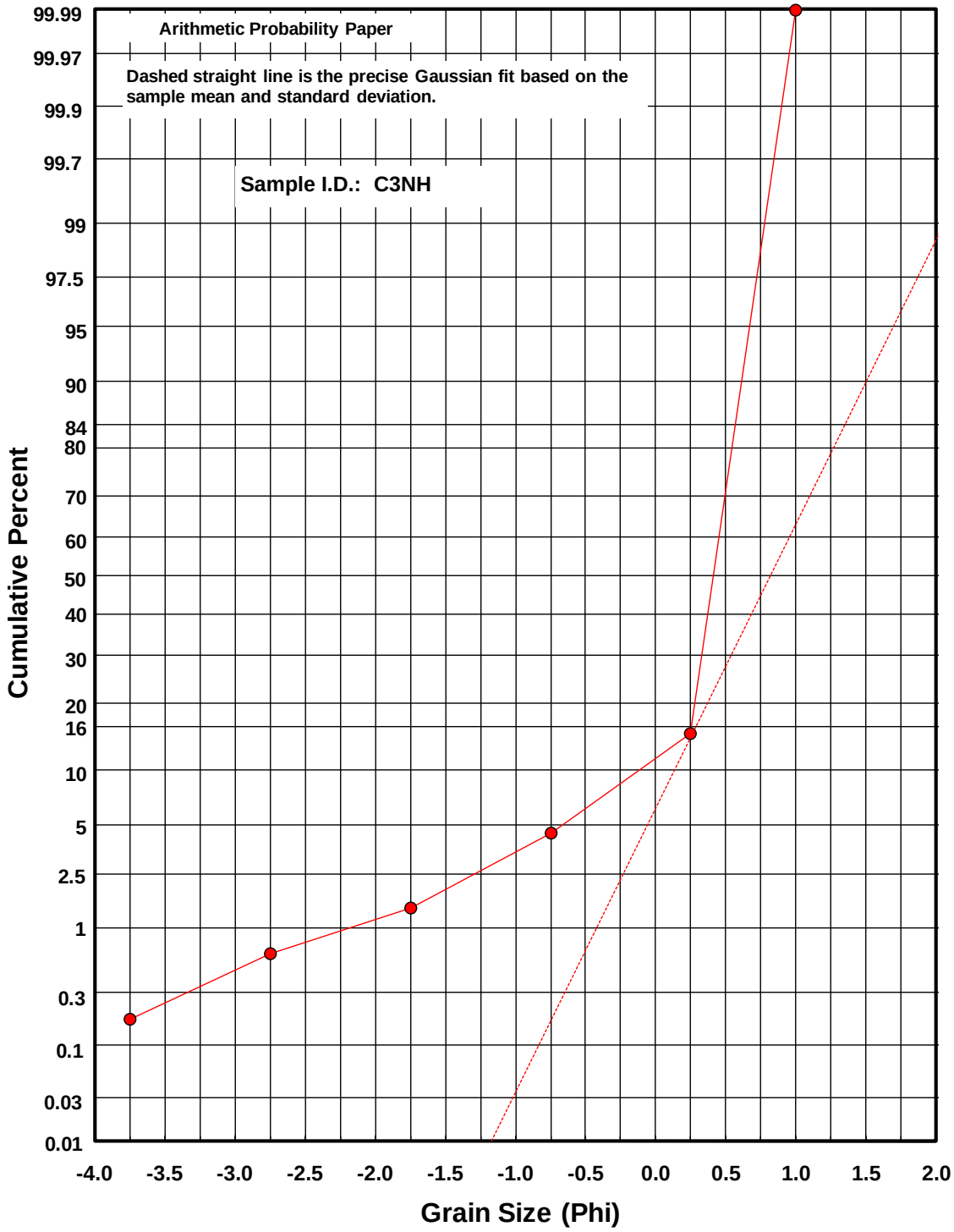
Arithmetic Probability Paper
Dashed straight line is the precise Gaussian fit based on the sample mean and standard deviation.
Sample I.D.: C3NH
Cumulative Percent
99.99
99.97
99.9
99.7
99
97.5
95
90
84
80
70
60
50
40
30
20
16
10
5
2.5
1
0.3
0.1
0.03
0.01
-4.0
-3.5
-3.0
-2.5
-2.0
-1.5
-1.0
-0.5
0.0
0.5
1.0
1.5
2.0
Grain Size (Phi)

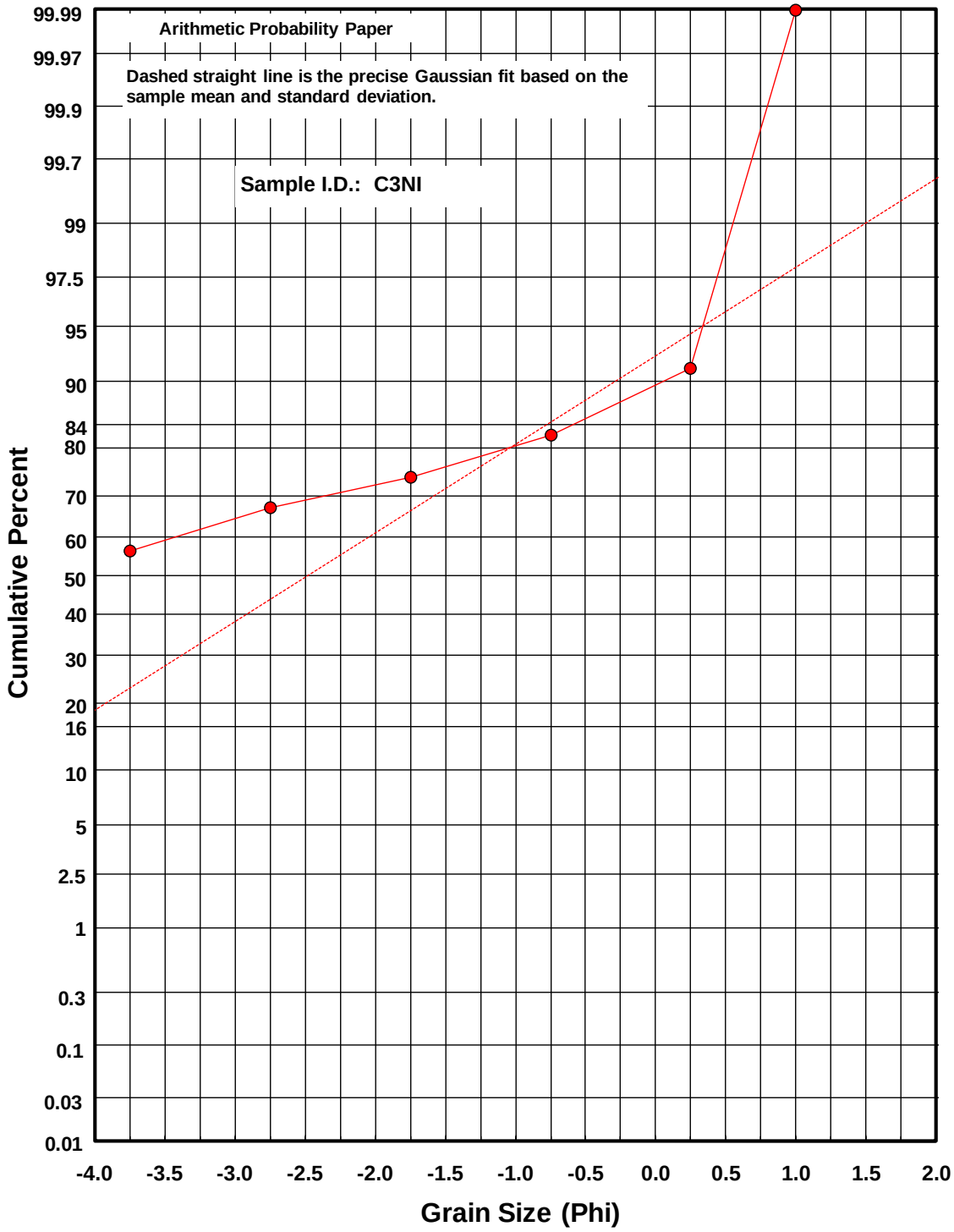
Arithmetic Probability Paper
Dashed straight line is the precise Gaussian fit based on the sample mean and standard deviation.
Sample I.D.: C3NI
Cumulative Percent
99.99
99.97
99.9
99.7
99
97.5
95
90
84
80
70
60
50
40
30
20
16
10
5
2.5
1
0.3
0.1
0.03
0.01
-4.0
-3.5
-3.0
-2.5
-2.0
-1.5
-1.0
-0.5
0.0
0.5
1.0
1.5
2.0
Grain Size (Phi)

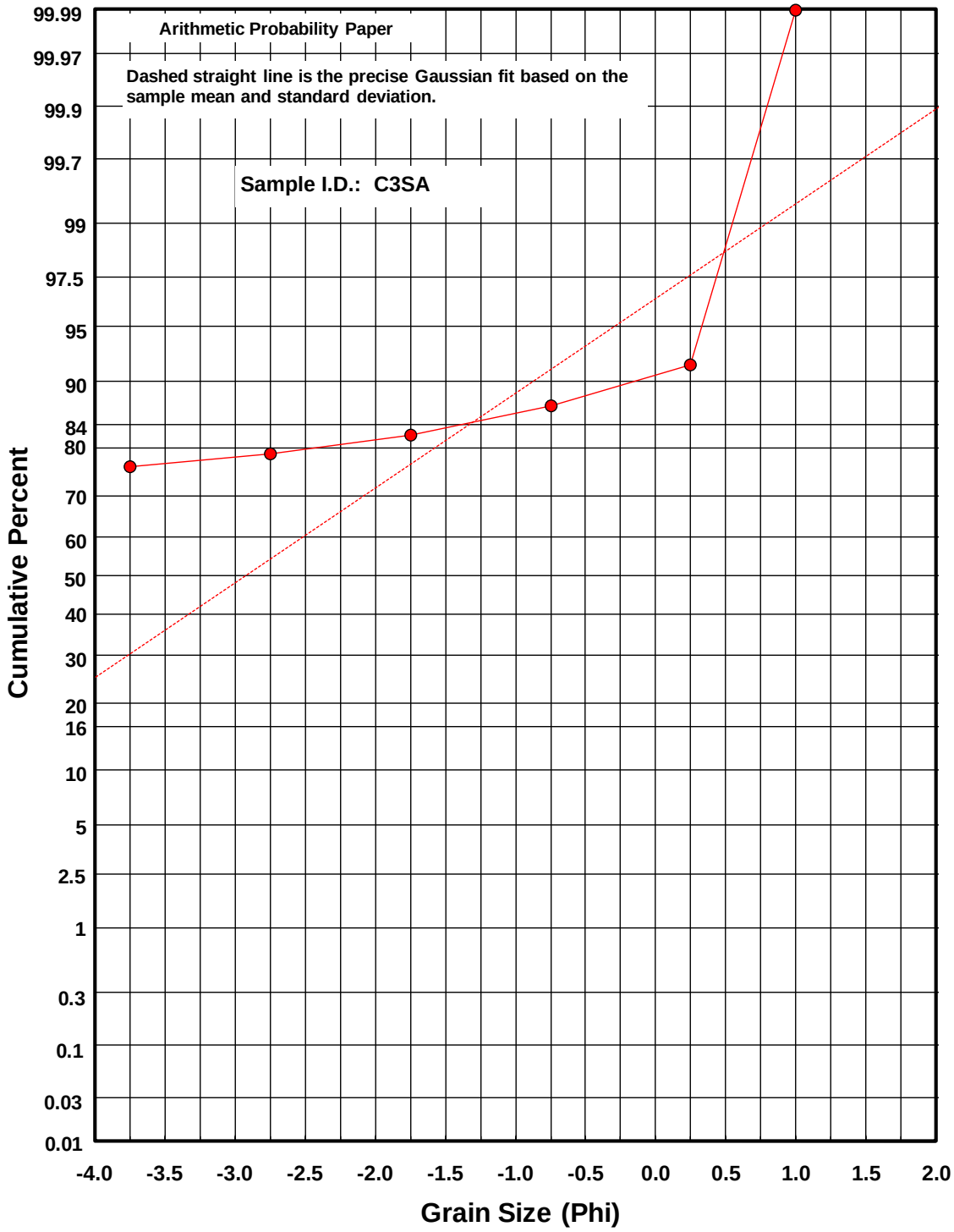
Arithmetic Probability Paper
Dashed straight line is the precise Gaussian fit based on the sample mean and standard deviation.
Sample I.D.: C3SA
Cumulative Percent
99.99
99.97
99.9
99.7
99
97.5
95
90
84
80
70
60
50
40
30
20
16
10
5
2.5
1
0.3
0.1
0.03
0.01
-4.0
-3.5
-3.0
-2.5
-2.0
-1.5
-1.0
-0.5
0.0
0.5
1.0
1.5
2.0
Grain Size (Phi)

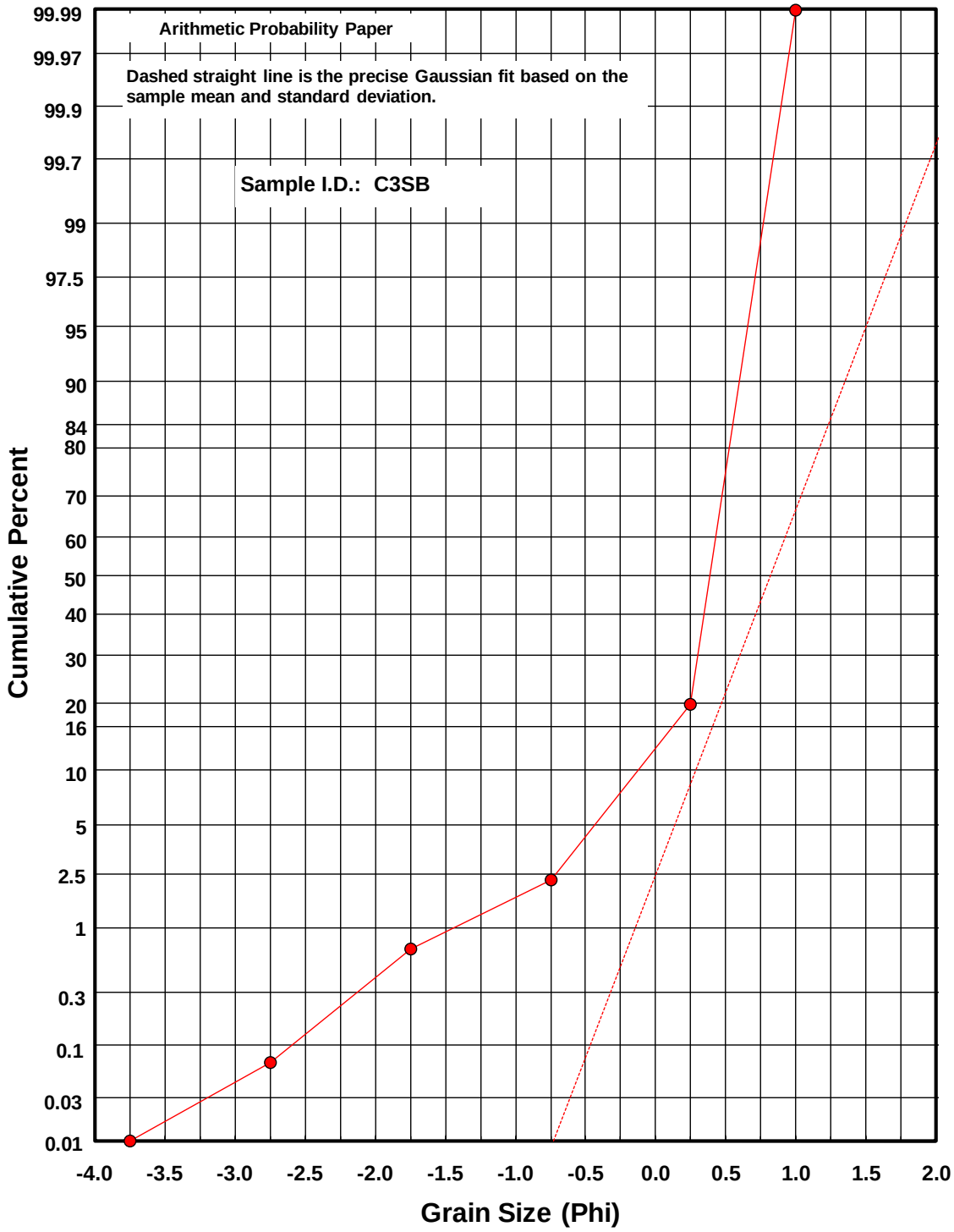
Arithmetic Probability Paper
Dashed straight line is the precise Gaussian fit based on the sample mean and standard deviation.
Sample I.D.: C3SB
Cumulative Percent
99.99
99.97
99.9
99.7
99
97.5
95
90
84
80
70
60
50
40
30
20
16
10
5
2.5
1
0.3
0.1
0.03
0.01
-4.0
-3.5
-3.0
-2.5
-2.0
-1.5
-1.0
-0.5
0.0
0.5
1.0
1.5
2.0
Grain Size (Phi)

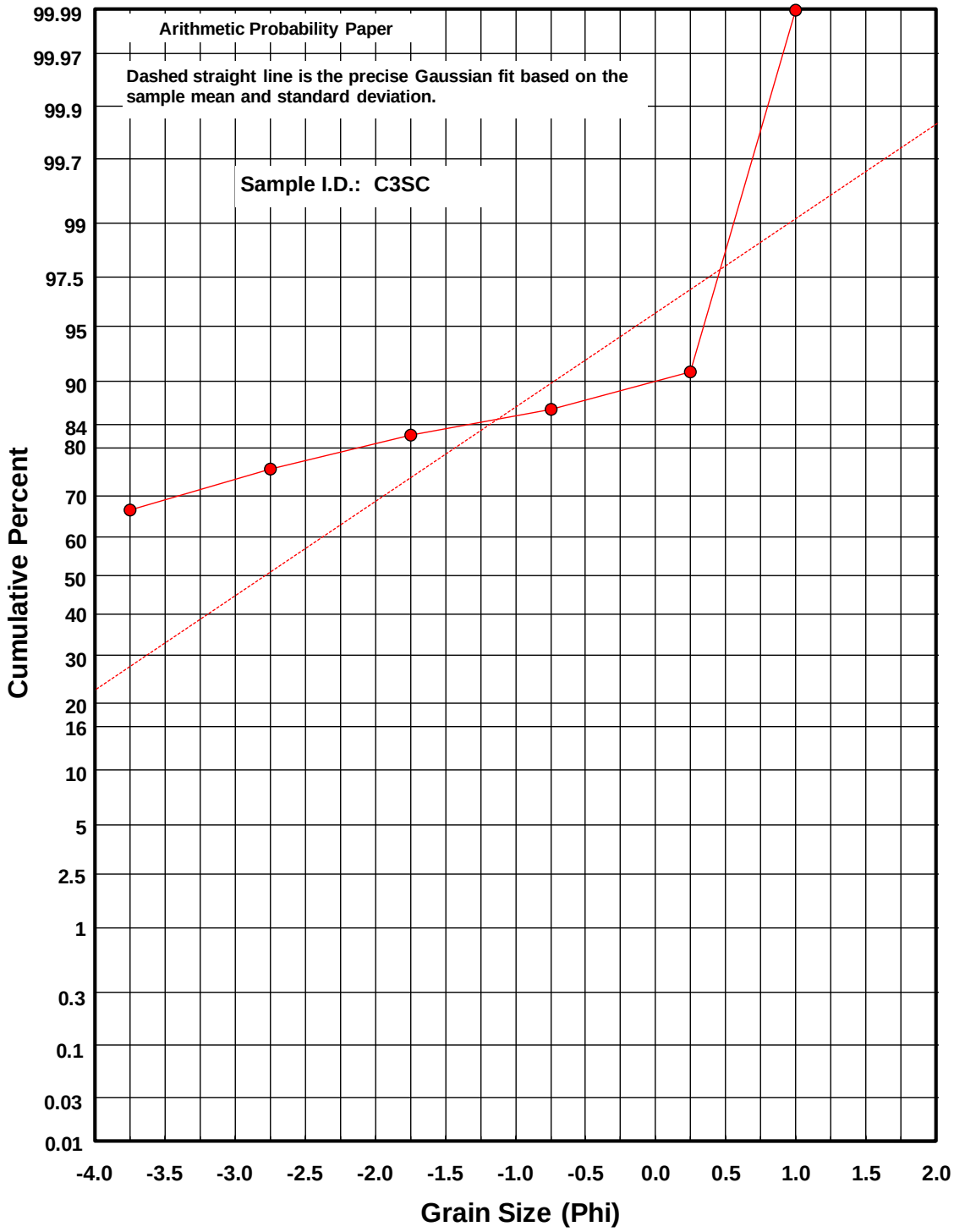
Arithmetic Probability Paper
Dashed straight line is the precise Gaussian fit based on the sample mean and standard deviation.
Sample I.D.: C3SC
Cumulative Percent
99.99
99.97
99.9
99.7
99
97.5
95
90
84
80
70
60
50
40
30
20
16
10
5
2.5
1
0.3
0.1
0.03
0.01
-4.0
-3.5
-3.0
-2.5
-2.0
-1.5
-1.0
-0.5
0.0
0.5
1.0
1.5
2.0
Grain Size (Phi)

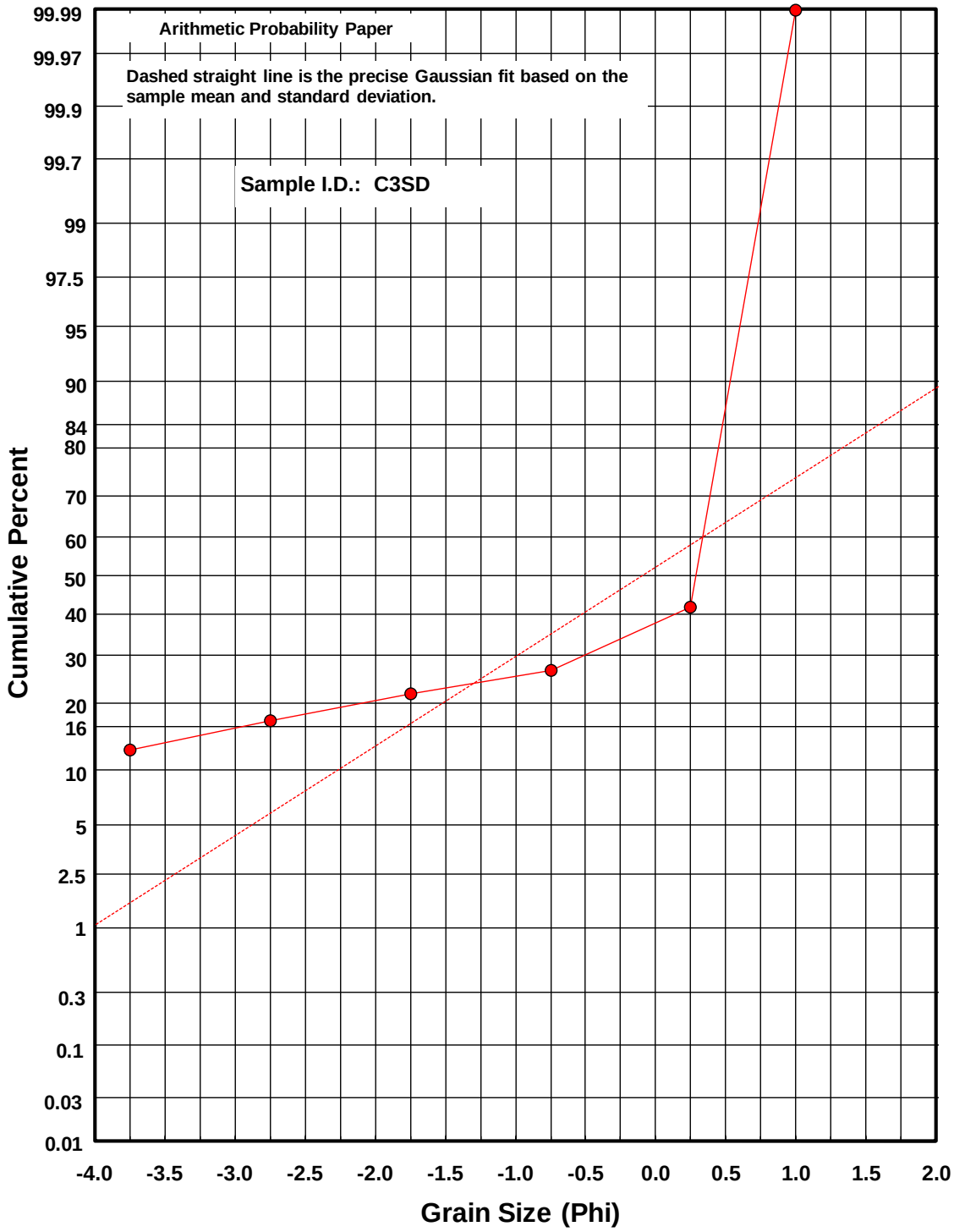
Arithmetic Probability Paper
Dashed straight line is the precise Gaussian fit based on the sample mean and standard deviation.
Sample I.D.: C3SD
Cumulative Percent
99.99
99.97
99.9
99.7
99
97.5
95
90
84
80
70
60
50
40
30
20
16
10
5
2.5
1
0.3
0.1
0.03
0.01
-4.0
-3.5
-3.0
-2.5
-2.0
-1.5
-1.0
-0.5
0.0
0.5
1.0
1.5
2.0
Grain Size (Phi)

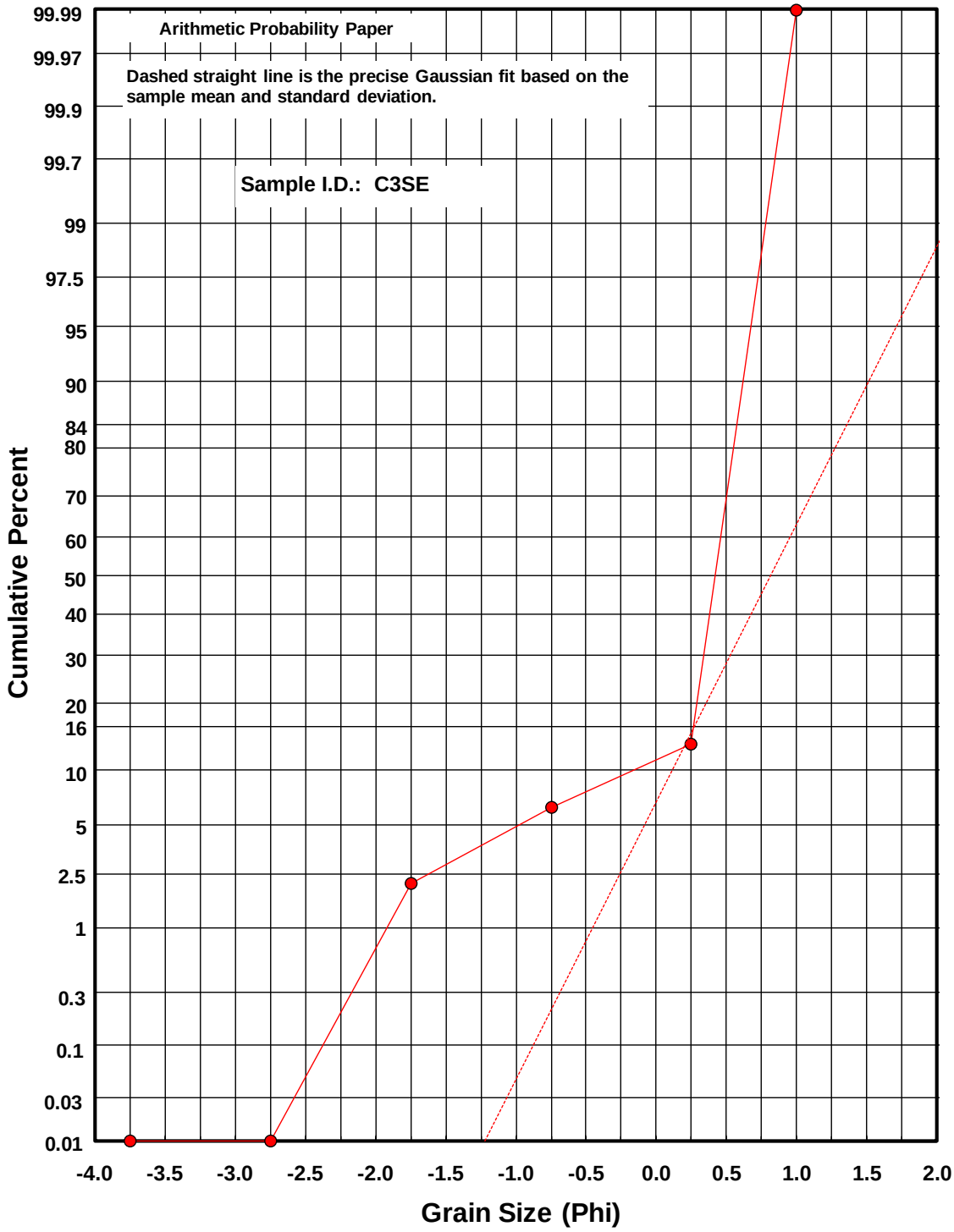
Arithmetic Probability Paper
Dashed straight line is the precise Gaussian fit based on the sample mean and standard deviation.
Sample I.D.: C3SE
Cumulative Percent
99.99
99.97
99.9
99.7
99
97.5
95
90
84
80
70
60
50
40
30
20
16
10
5
2.5
1
0.3
0.1
0.03
0.01
-4.0
-3.5
-3.0
-2.5
-2.0
-1.5
-1.0
-0.5
0.0
0.5
1.0
1.5
2.0
Grain Size (Phi)

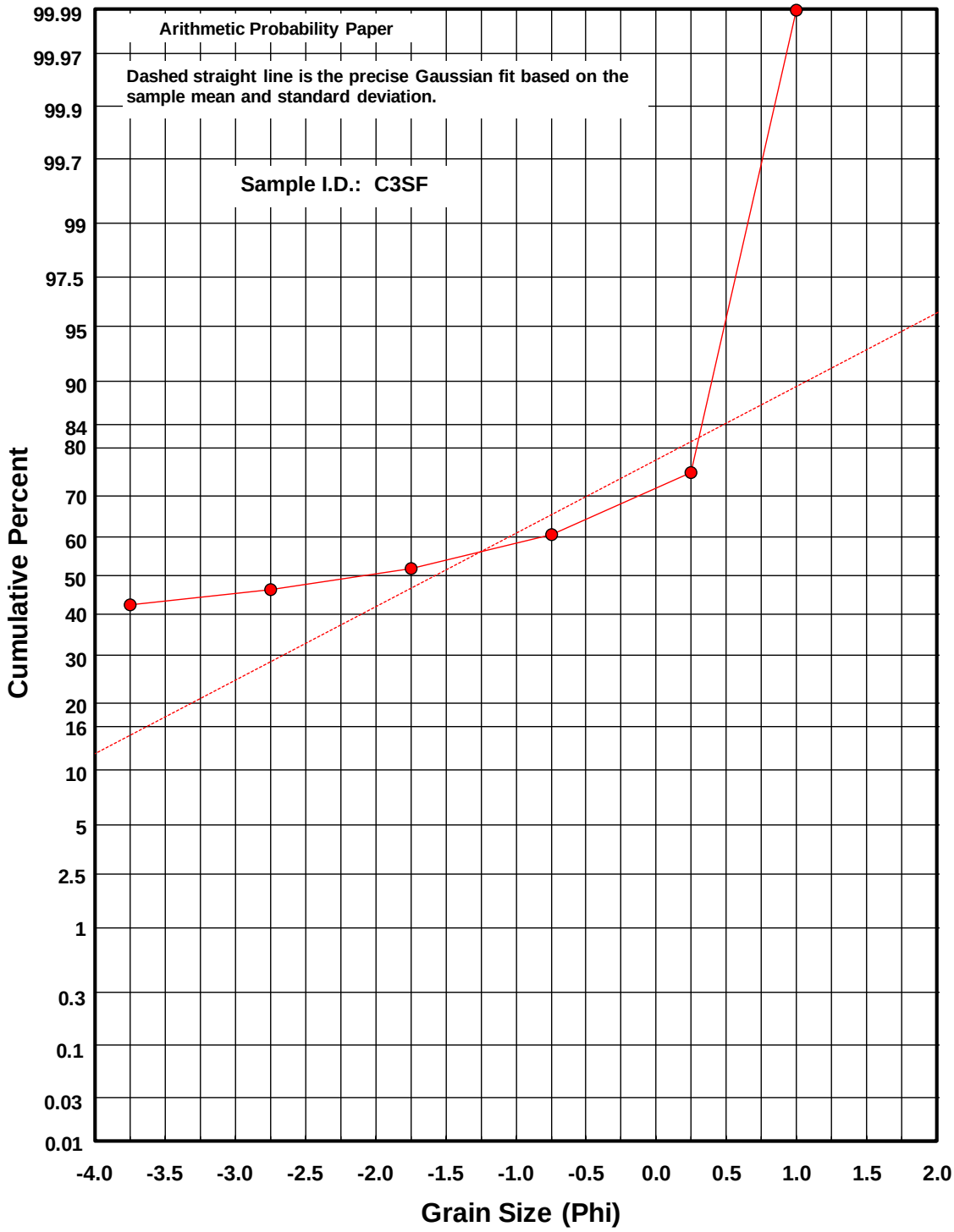
Arithmetic Probability Paper
Dashed straight line is the precise Gaussian fit based on the sample mean and standard deviation.
Sample I.D.: C3SF
Cumulative Percent
99.99
99.97
99.9
99.7
99
97.5
95
90
84
80
70
60
50
40
30
20
16
10
5
2.5
1
0.3
0.1
0.03
0.01
-4.0
-3.5
-3.0
-2.5
-2.0
-1.5
-1.0
-0.5
0.0
0.5
1.0
1.5
2.0
Grain Size (Phi)

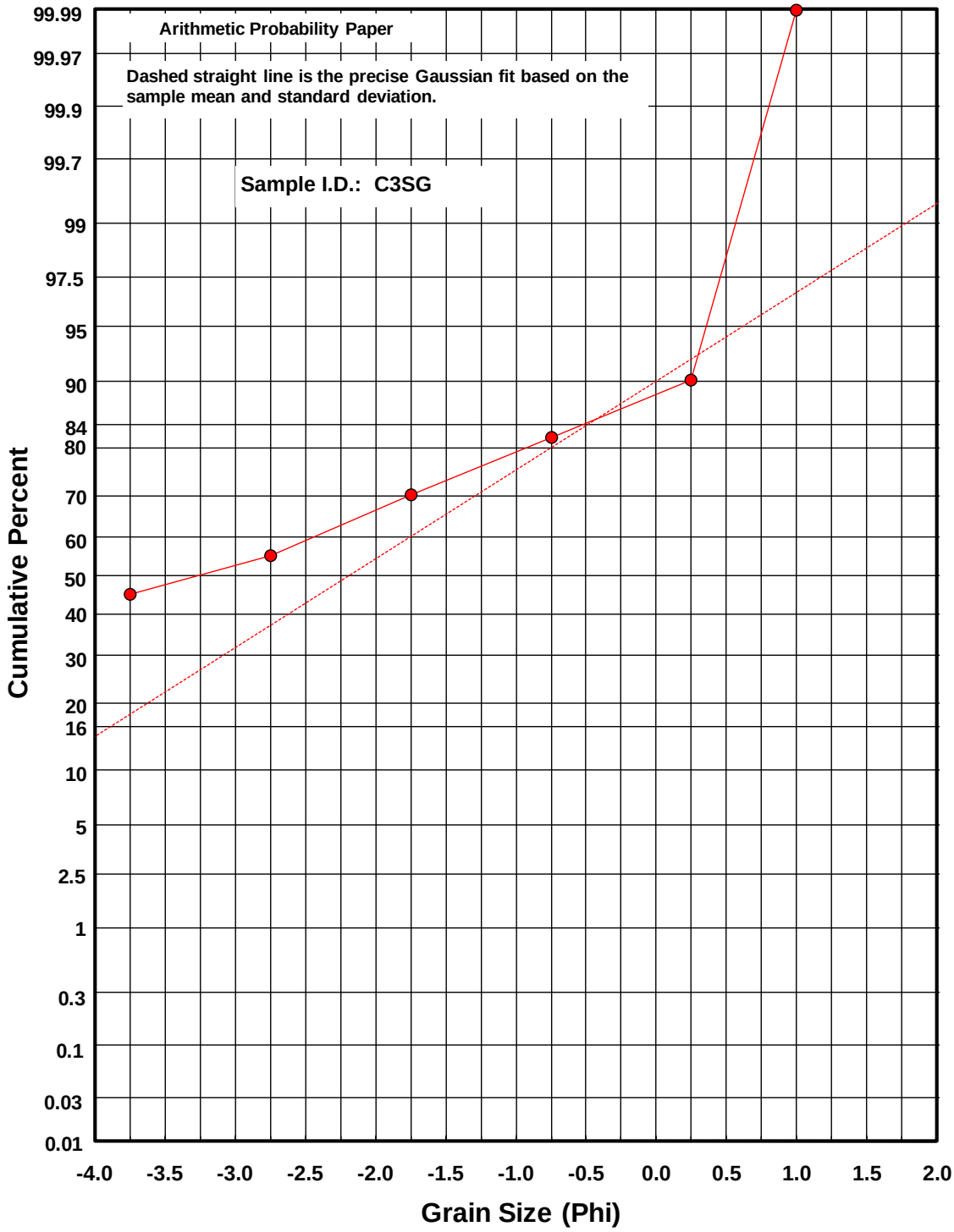
Arithmetic Probability Paper
Dashed straight line is the precise Gaussian fit based on the sample mean and standard deviation.
Sample I.D.: C3SG
Cumulative Percent
99.99
99.97
99.9
99.7
99
97.5
95
90
84
80
70
60
50
40
30
20
16
10
5
2.5
1
0.3
0.1
0.03
0.01
-4.0
-3.5
-3.0
-2.5
-2.0
-1.5
-1.0
-0.5
0.0
0.5
1.0
1.5
2.0
Grain Size (Phi)

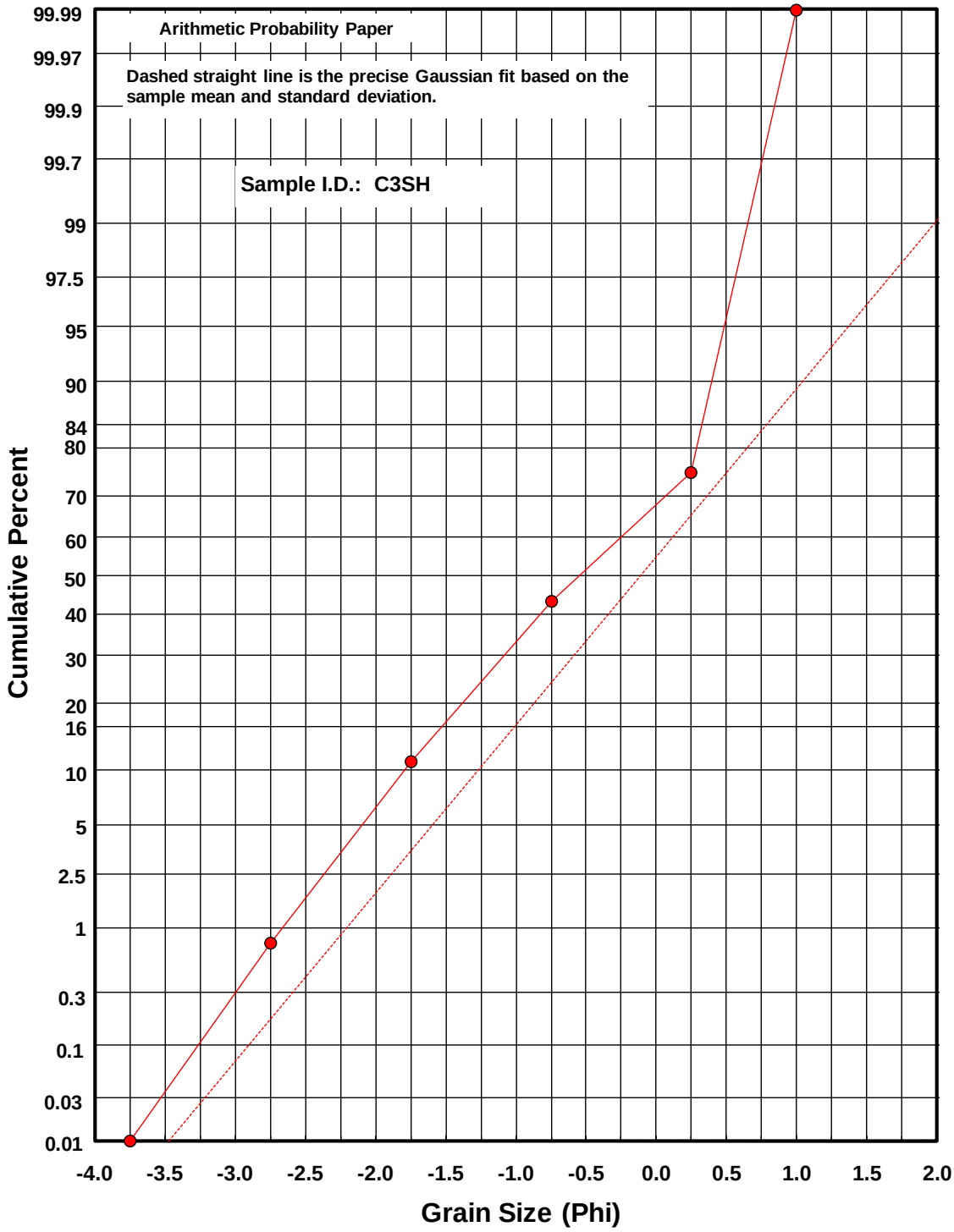
Arithmetic Probability Paper
Dashed straight line is the precise Gaussian fit based on the sample mean and standard deviation.
Sample I.D.: C3SH
Cumulative Percent
99.99
99.97
99.9
99.7
99
97.5
95
90
84
80
70
60
50
40
30
20
16
10
5
2.5
1
0.3
0.1
0.03
0.01
-4.0
-3.5
-3.0
-2.5
-2.0
-1.5
-1.0
-0.5
0.0
0.5
1.0
1.5
2.0
Grain Size (Phi)

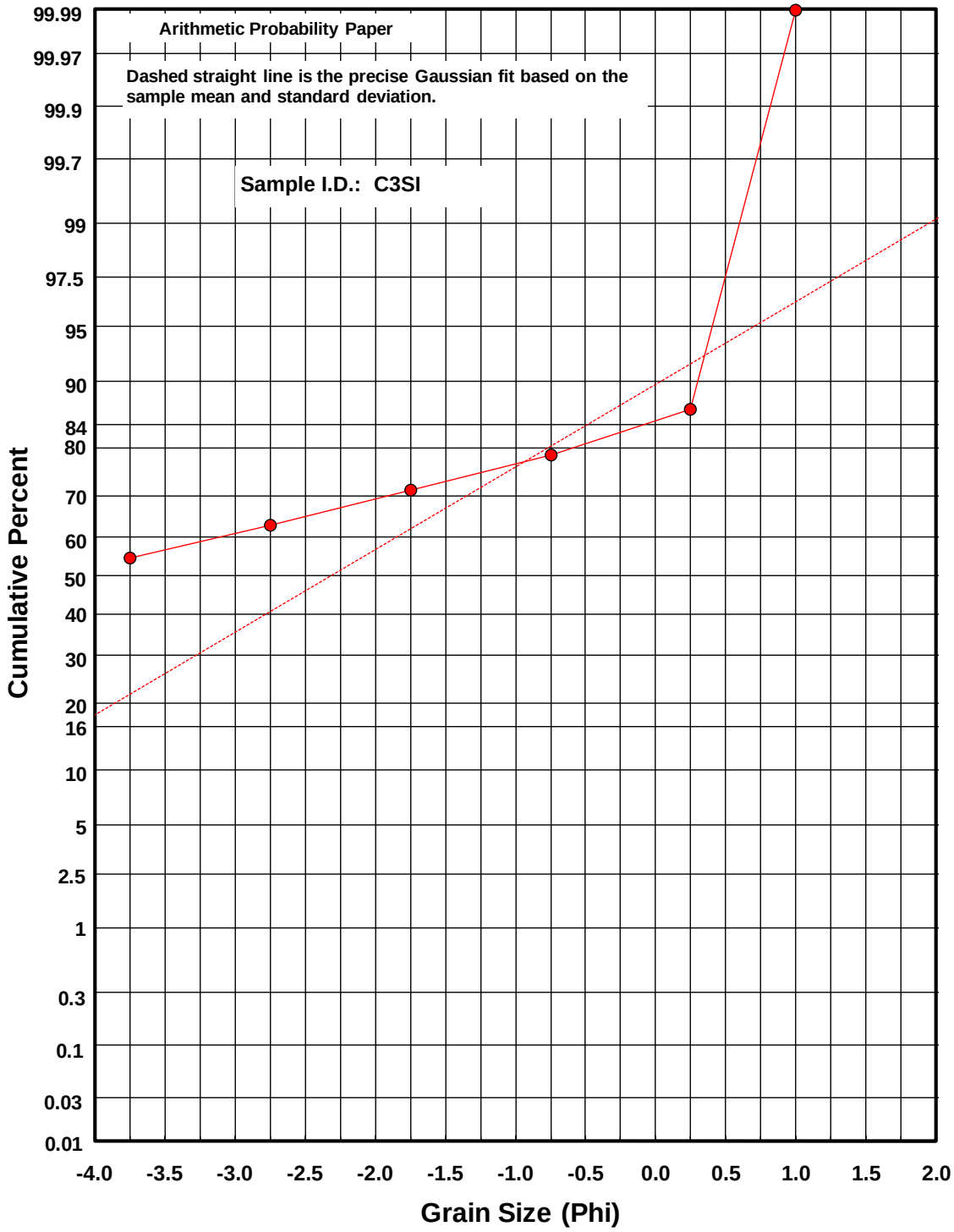
Arithmetic Probability Paper
Dashed straight line is the precise Gaussian fit based on the sample mean and standard deviation.
Sample I.D.: C3SI
Cumulative Percent
99.99
99.97
99.9
99.7
99
97.5
95
90
84
80
70
60
50
40
30
20
16
10
5
2.5
1
0.3
0.1
0.03
0.01
-4.0
-3.5
-3.0
-2.5
-2.0
-1.5
-1.0
-0.5
0.0
0.5
1.0
1.5
2.0
Grain Size (Phi)

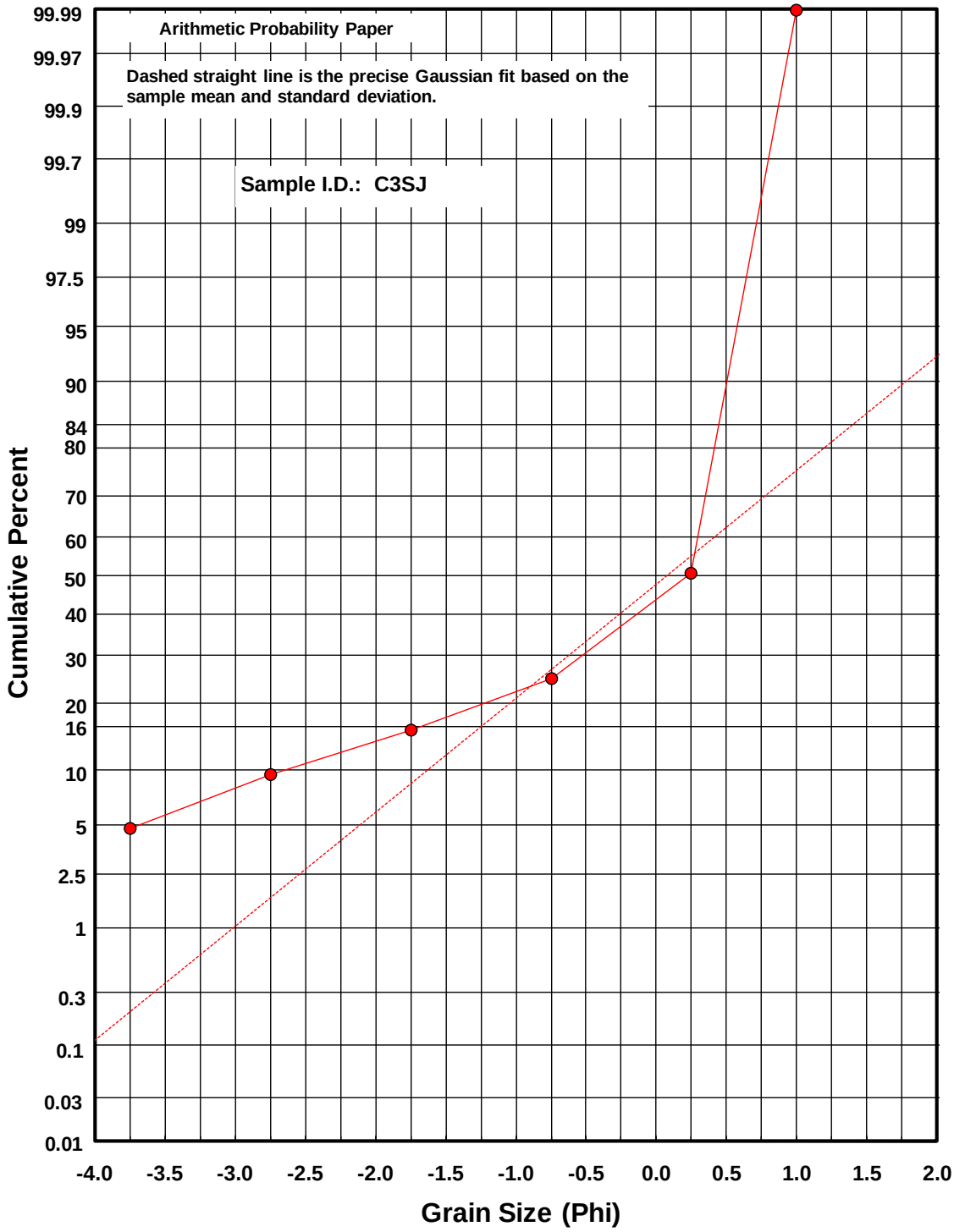
Arithmetic Probability Paper
Dashed straight line is the precise Gaussian fit based on the sample mean and standard deviation.
Sample I.D.: C3SJ
Cumulative Percent
99.99
99.97
99.9
99.7
99
97.5
95
90
84
80
70
60
50
40
30
20
16
10
5
2.5
1
0.3
0.1
0.03
0.01
-4.0
-3.5
-3.0
-2.5
-2.0
-1.5
-1.0
-0.5
0.0
0.5
1.0
1.5
2.0
Grain Size (Phi)

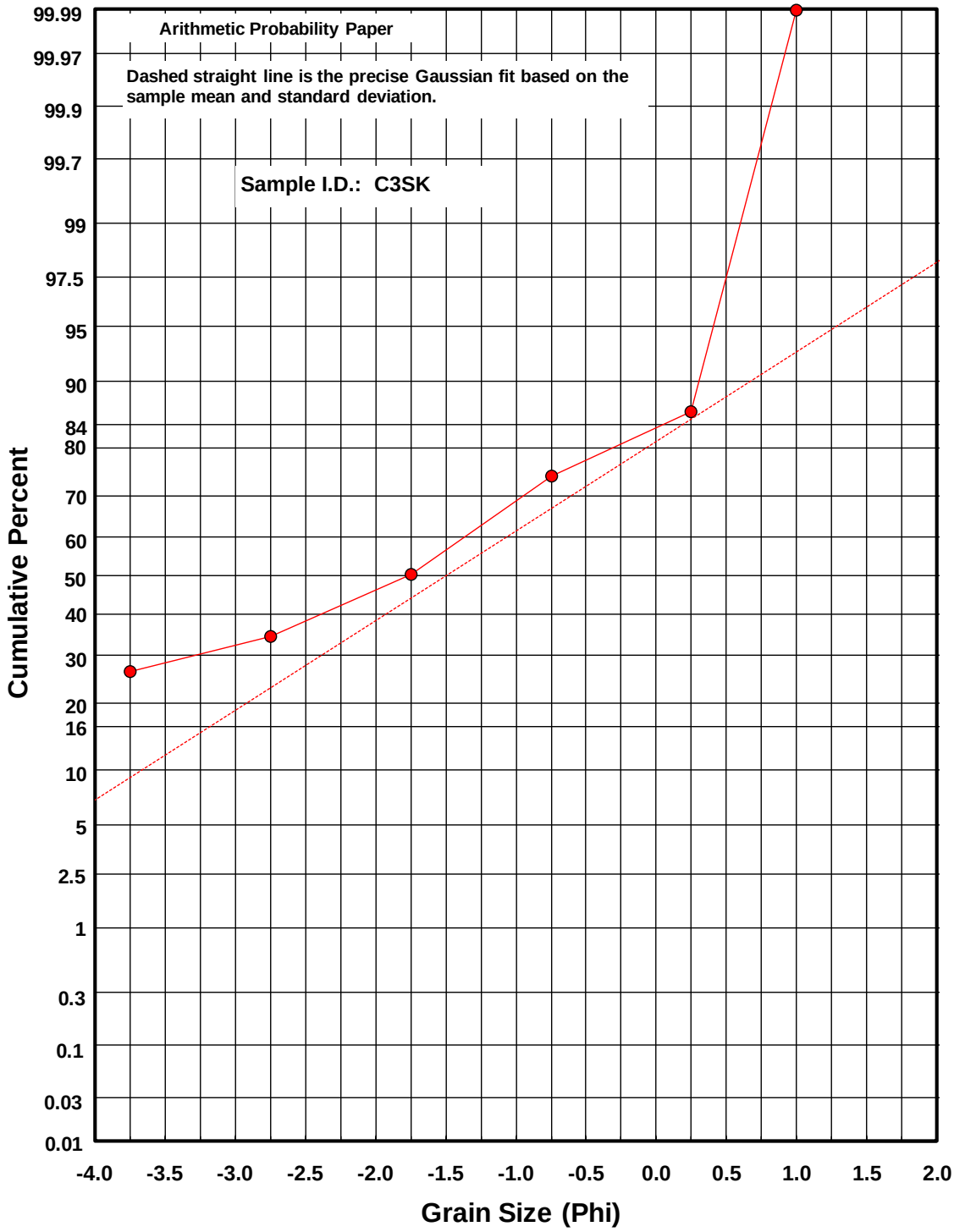
Arithmetic Probability Paper
Dashed straight line is the precise Gaussian fit based on the sample mean and standard deviation.
Sample I.D.: C3SK
Cumulative Percent
99.99
99.97
99.9
99.7
99
97.5
95
90
84
80
70
60
50
40
30
20
16
10
5
2.5
1
0.3
0.1
0.03
0.01
-4.0
-3.5
-3.0
-2.5
-2.0
-1.5
-1.0
-0.5
0.0
0.5
1.0
1.5
2.0
Grain Size (Phi)

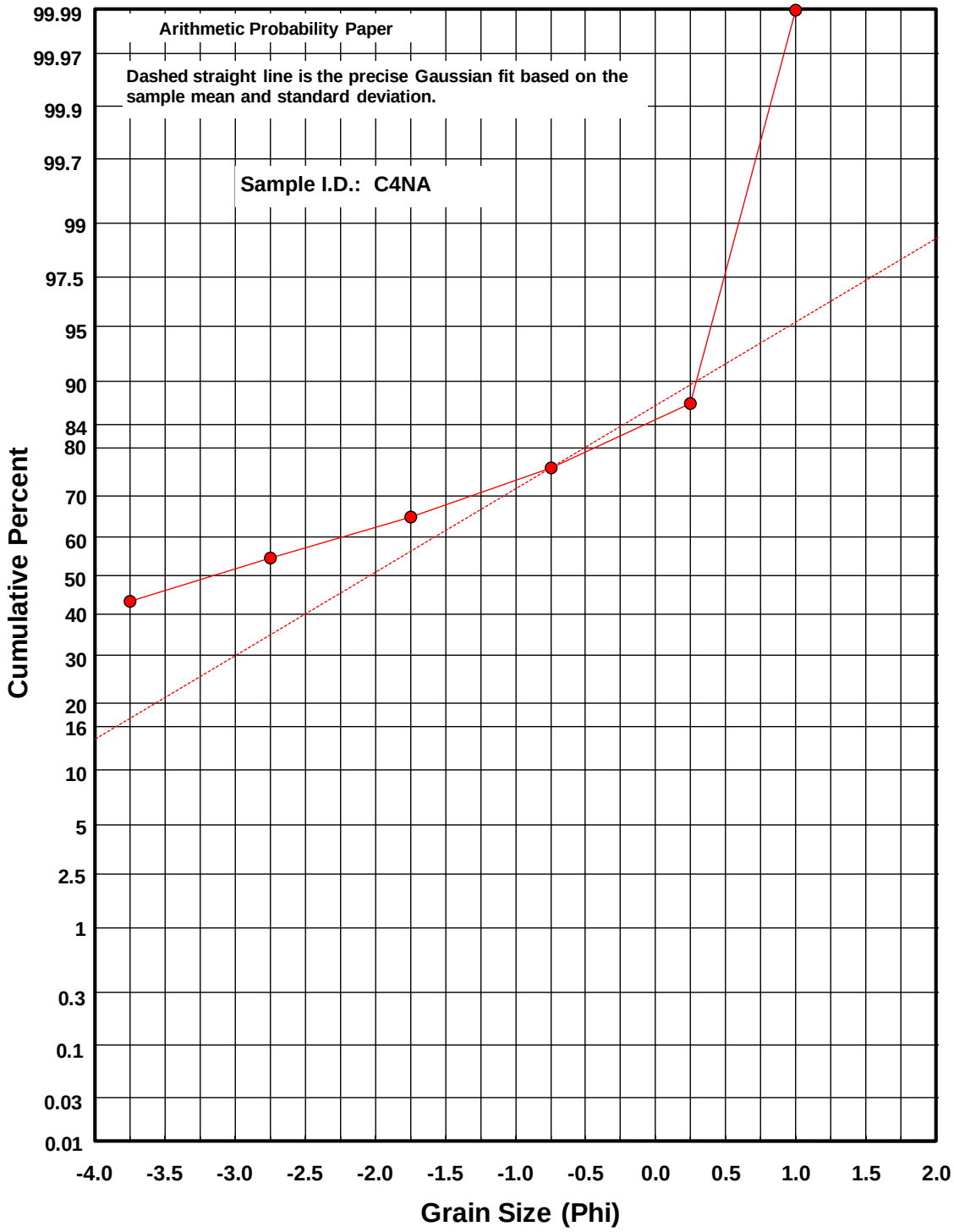
Arithmetic Probability Paper
Dashed straight line is the precise Gaussian fit based on the sample mean and standard deviation.
Sample I.D.: C4NA
Cumulative Percent
99.99
99.97
99.9
99.7
99
97.5
95
90
84
80
70
60
50
40
30
20
16
10
5
2.5
1
0.3
0.1
0.03
0.01
-4.0
-3.5
-3.0
-2.5
-2.0
-1.5
-1.0
-0.5
0.0
0.5
1.0
1.5
2.0
Grain Size (Phi)

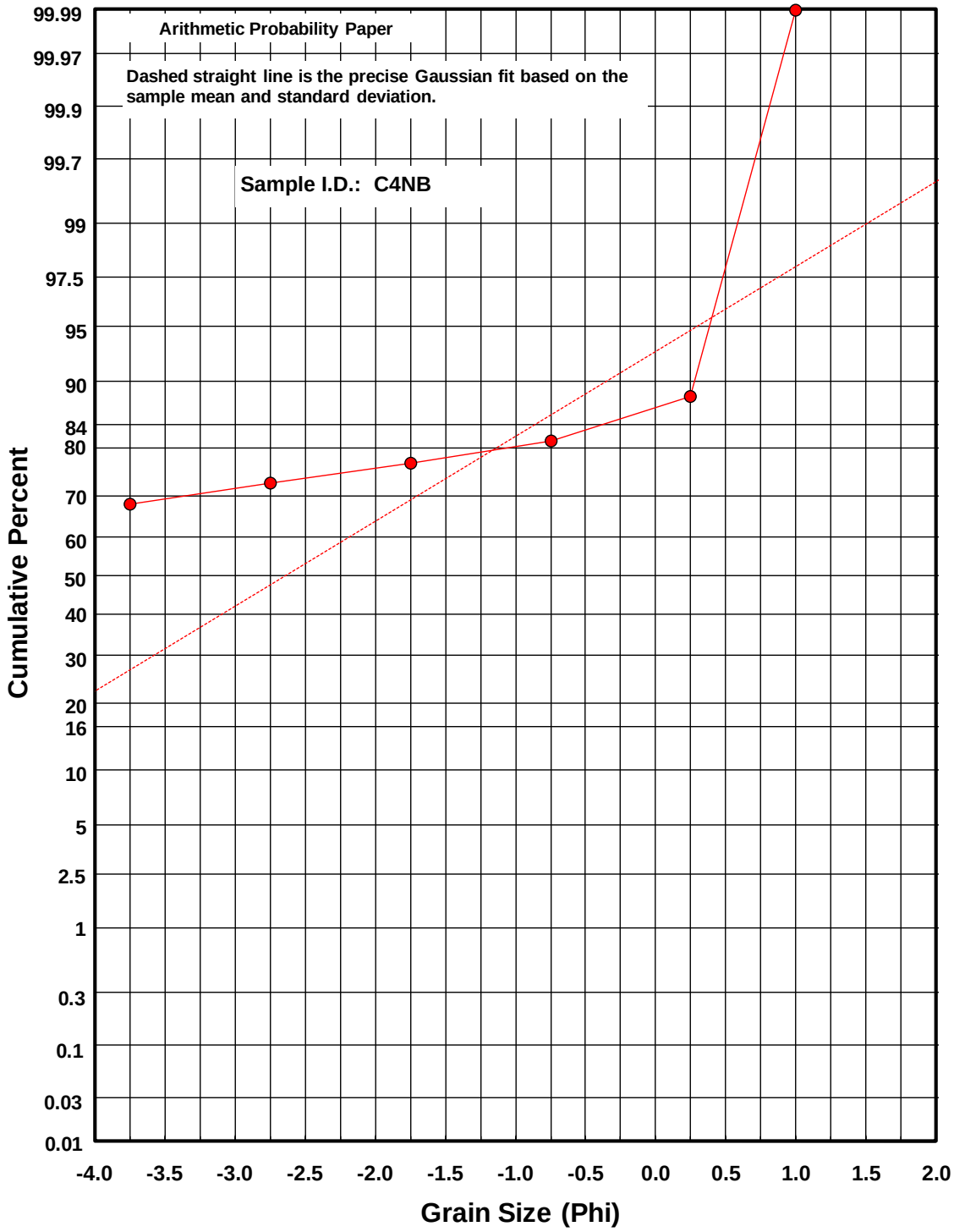
Arithmetic Probability Paper
Dashed straight line is the precise Gaussian fit based on the sample mean and standard deviation.
Sample I.D.: C4NB
Cumulative Percent
99.99
99.97
99.9
99.7
99
97.5
95
90
84
80
70
60
50
40
30
20
16
10
5
2.5
1
0.3
0.1
0.03
0.01
-4.0
-3.5
-3.0
-2.5
-2.0
-1.5
-1.0
-0.5
0.0
0.5
1.0
1.5
2.0
Grain Size (Phi)

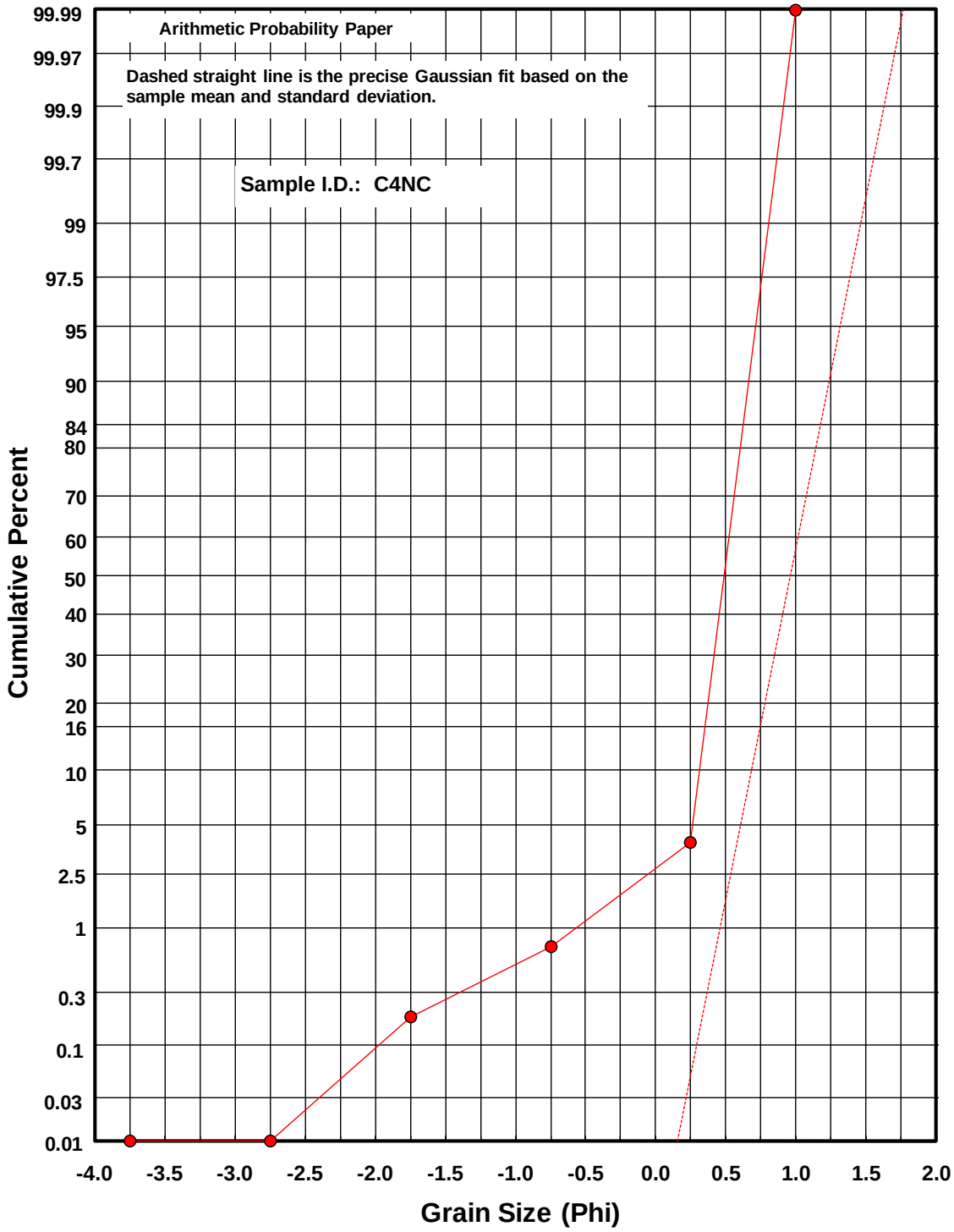
Arithmetic Probability Paper
Dashed straight line is the precise Gaussian fit based on the sample mean and standard deviation.
Sample I.D.: C4NC
Cumulative Percent
99.99
99.97
99.9
99.7
99
97.5
95
90
84
80
70
60
50
40
30
20
16
10
5
2.5
1
0.3
0.1
0.03
0.01
-4.0
-3.5
-3.0
-2.5
-2.0
-1.5
-1.0
-0.5
0.0
0.5
1.0
1.5
2.0
Grain Size (Phi)

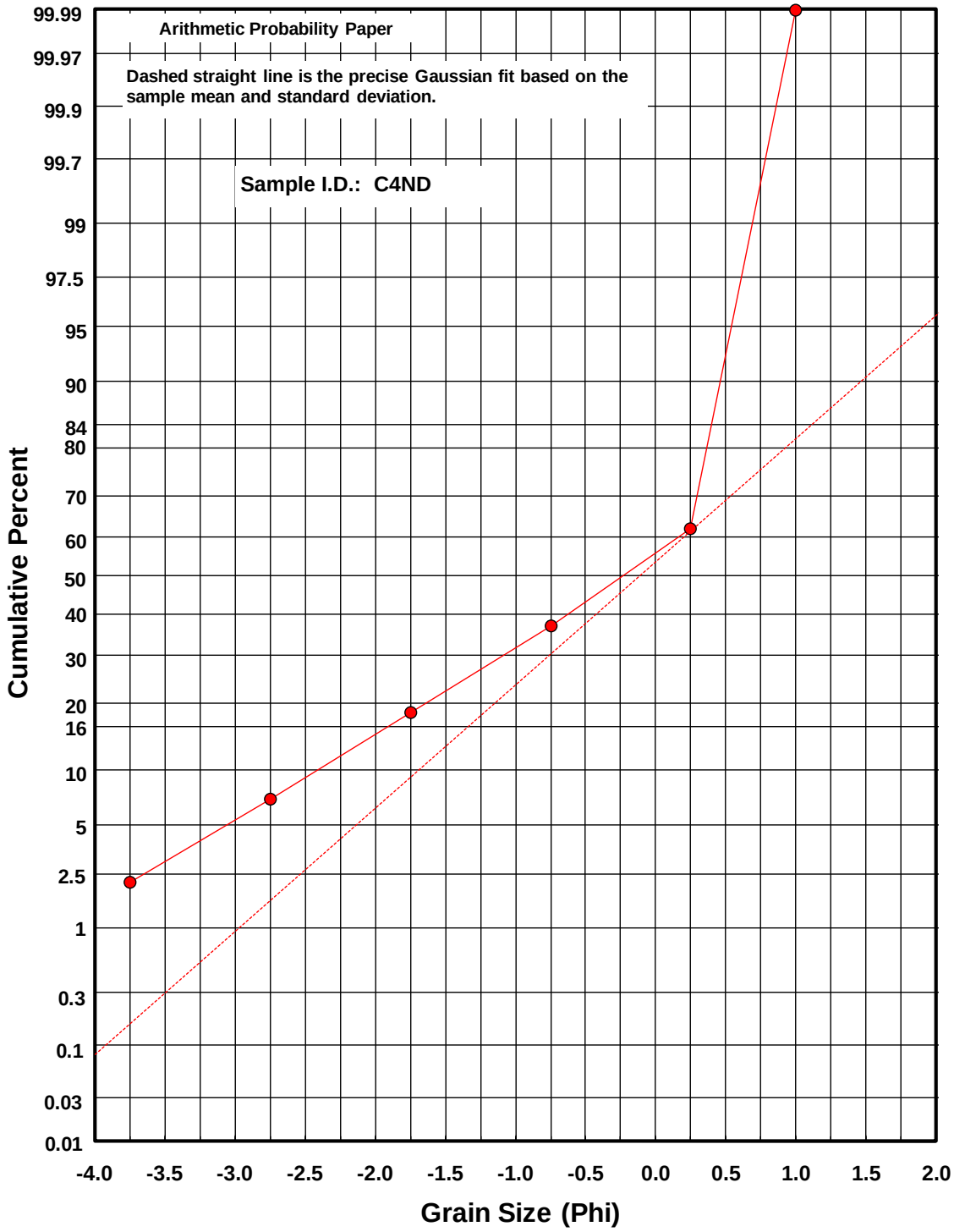
Arithmetic Probability Paper
Dashed straight line is the precise Gaussian fit based on the sample mean and standard deviation.
Sample I.D.: C4ND
Cumulative Percent
99.99
99.97
99.9
99.7
99
97.5
95
90
84
80
70
60
50
40
30
20
16
10
5
2.5
1
0.3
0.1
0.03
0.01
-4.0
-3.5
-3.0
-2.5
-2.0
-1.5
-1.0
-0.5
0.0
0.5
1.0
1.5
2.0
Grain Size (Phi)

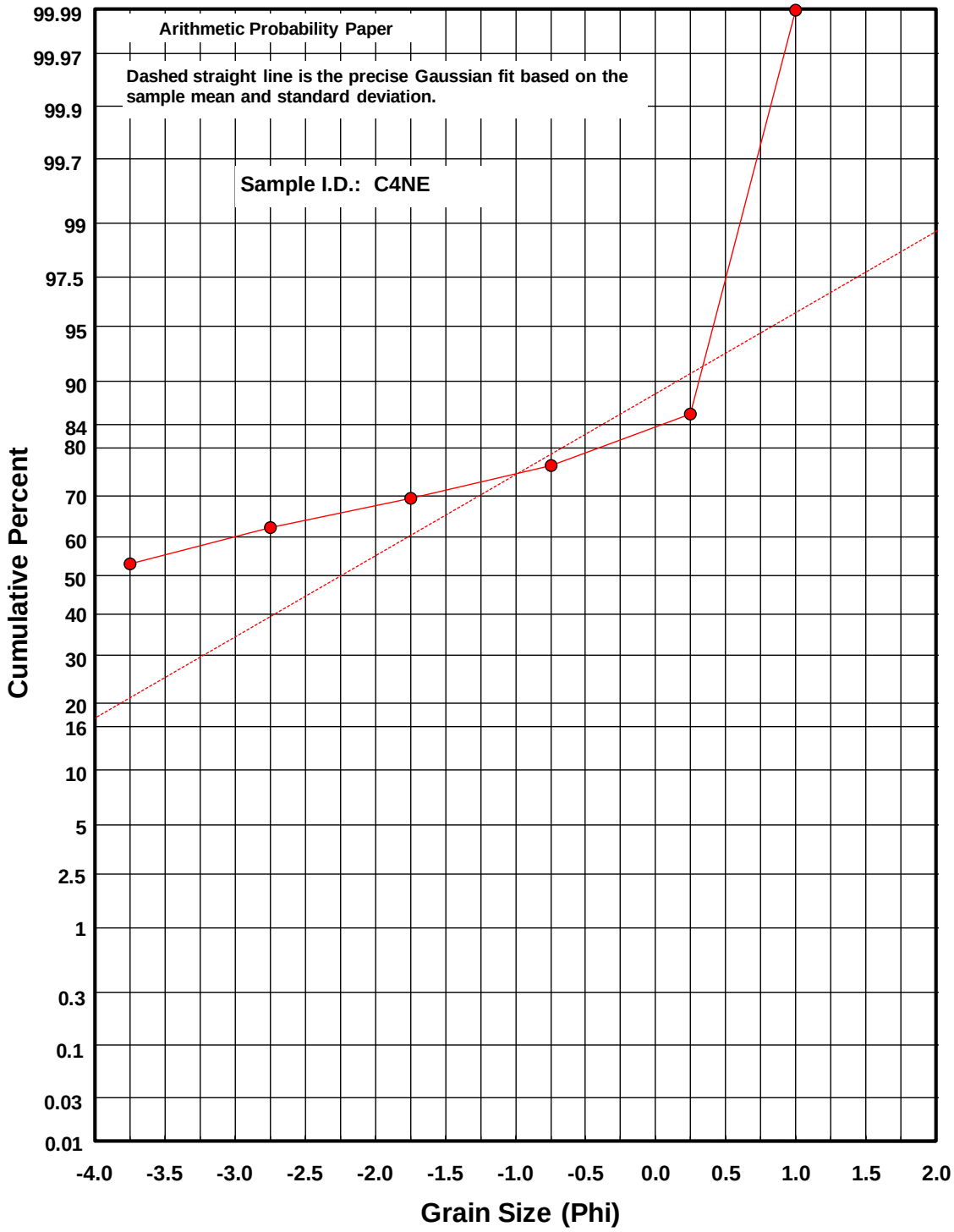
Arithmetic Probability Paper
Dashed straight line is the precise Gaussian fit based on the sample mean and standard deviation.
Sample I.D.: C4NE
Cumulative Percent
99.99
99.97
99.9
99.7
99
97.5
95
90
84
80
70
60
50
40
30
20
16
10
5
2.5
1
0.3
0.1
0.03
0.01
-4.0
-3.5
-3.0
-2.5
-2.0
-1.5
-1.0
-0.5
0.0
0.5
1.0
1.5
2.0
Grain Size (Phi)

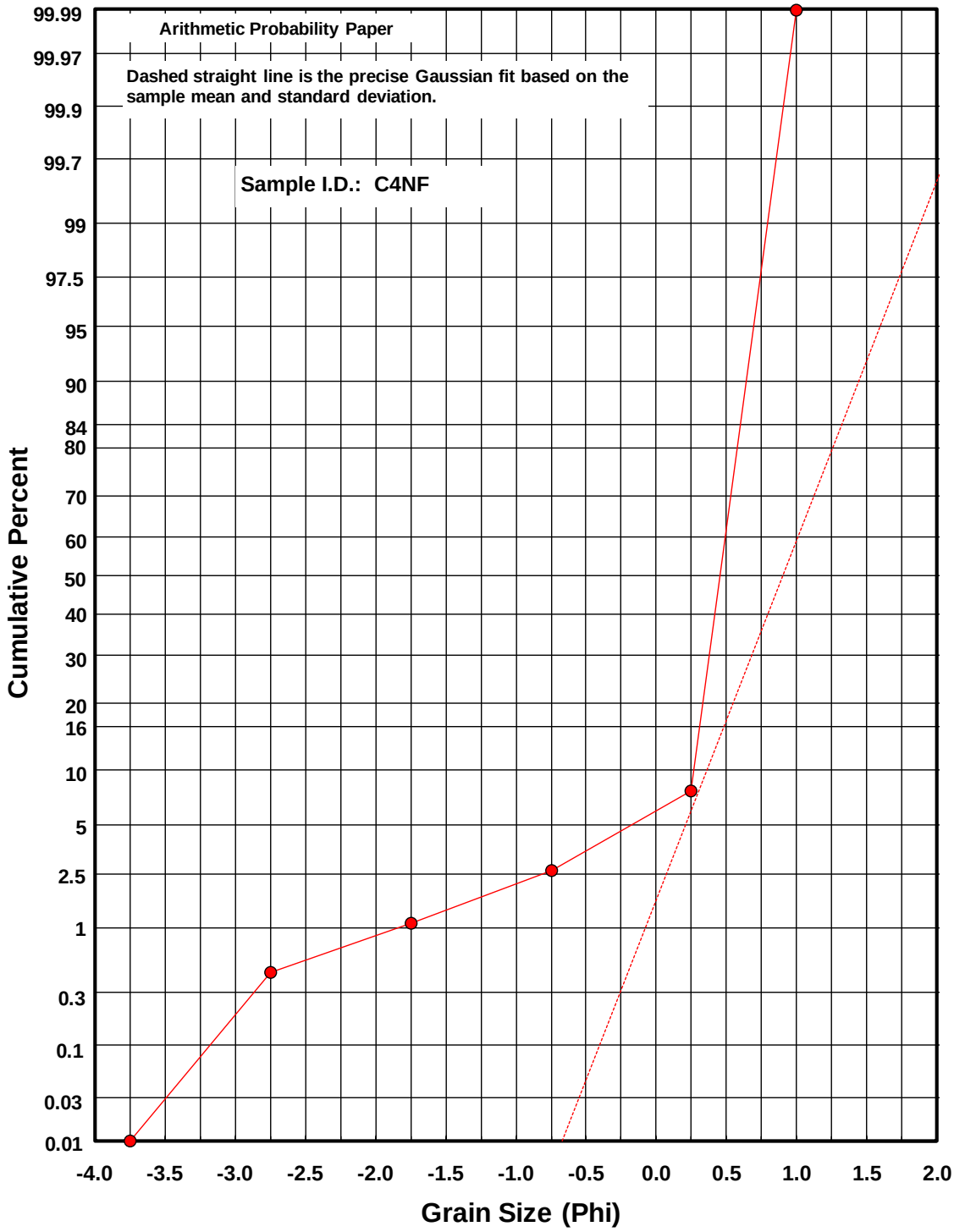
Arithmetic Probability Paper
Dashed straight line is the precise Gaussian fit based on the sample mean and standard deviation.
Sample I.D.: C4NF
Cumulative Percent
99.99
99.97
99.9
99.7
99
97.5
95
90
84
80
70
60
50
40
30
20
16
10
5
2.5
1
0.3
0.1
0.03
0.01
-4.0
-3.5
-3.0
-2.5
-2.0
-1.5
-1.0
-0.5
0.0
0.5
1.0
1.5
2.0
Grain Size (Phi)

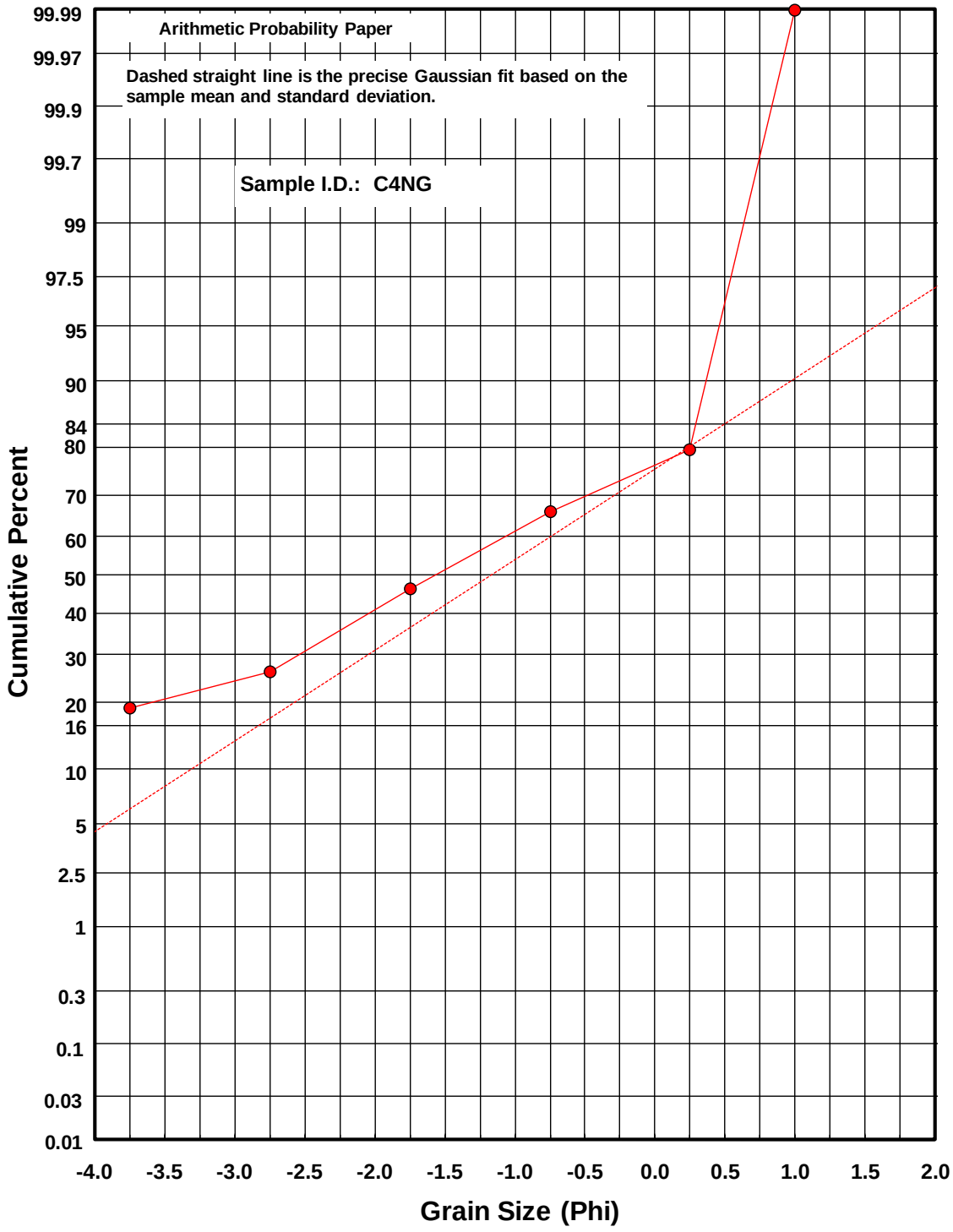
Arithmetic Probability Paper
Dashed straight line is the precise Gaussian fit based on the sample mean and standard deviation.
Sample I.D.: C4NG
Cumulative Percent
99.99
99.97
99.9
99.7
99
97.5
95
90
84
80
70
60
50
40
30
20
16
10
5
2.5
1
0.3
0.1
0.03
0.01
-4.0
-3.5
-3.0
-2.5
-2.0
-1.5
-1.0
-0.5
0.0
0.5
1.0
1.5
2.0
Grain Size (Phi)

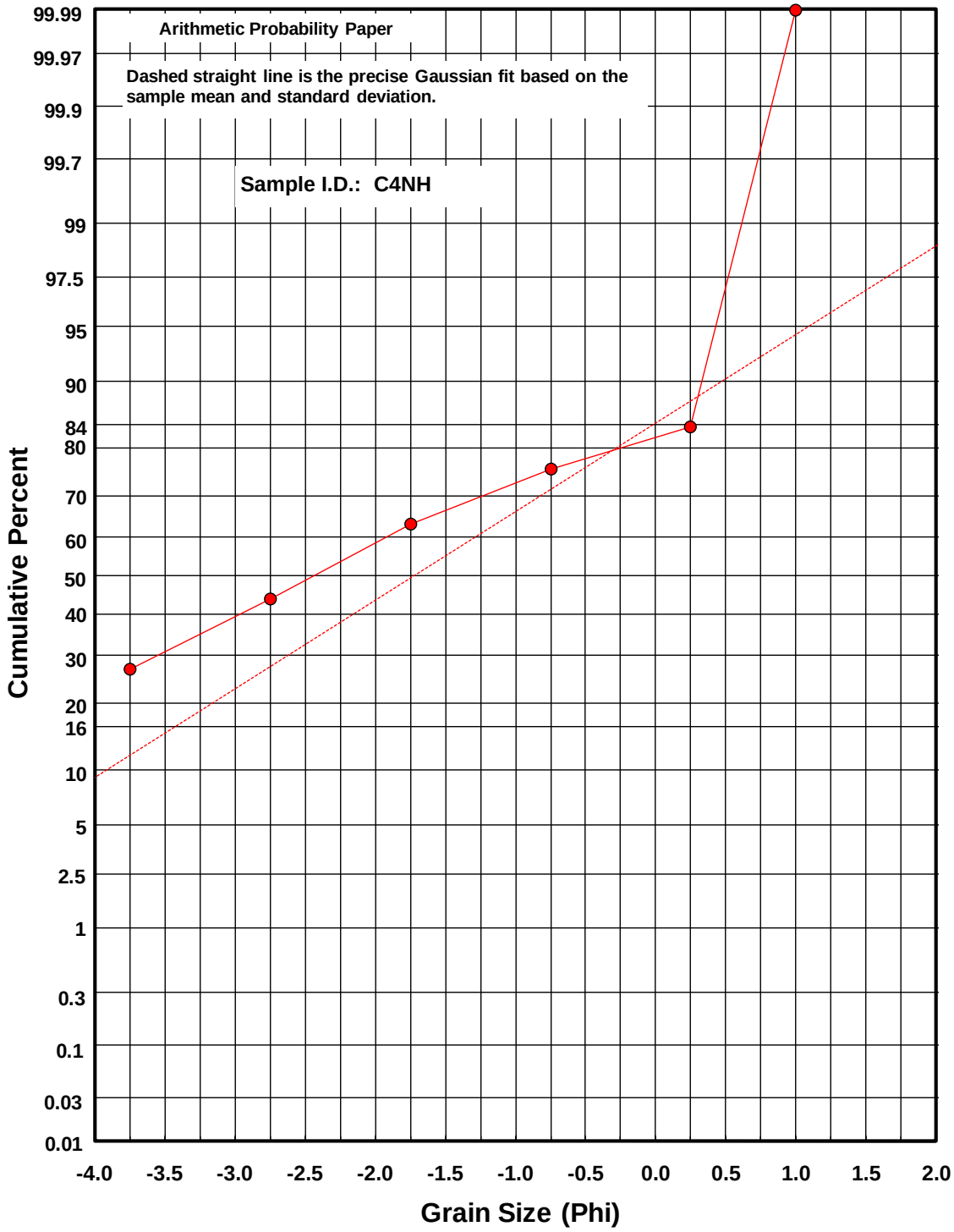
Arithmetic Probability Paper
Dashed straight line is the precise Gaussian fit based on the sample mean and standard deviation.
Sample I.D.: C4NH
Cumulative Percent
99.99
99.97
99.9
99.7
99
97.5
95
90
84
80
70
60
50
40
30
20
16
10
5
2.5
1
0.3
0.1
0.03
0.01
-4.0
-3.5
-3.0
-2.5
-2.0
-1.5
-1.0
-0.5
0.0
0.5
1.0
1.5
2.0
Grain Size (Phi)

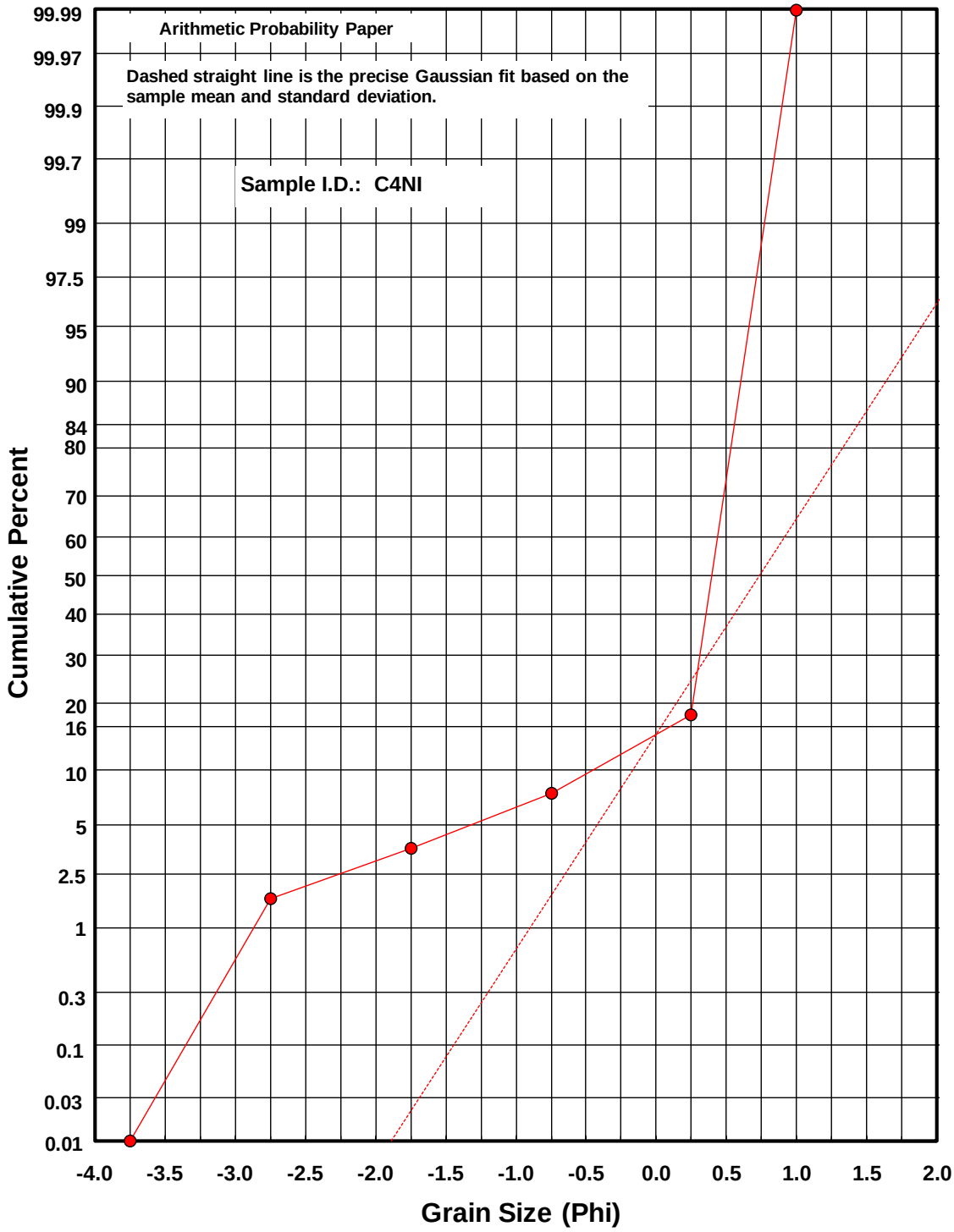
Arithmetic Probability Paper
Dashed straight line is the precise Gaussian fit based on the sample mean and standard deviation.
Sample I.D.: C4NI
Cumulative Percent
99.99
99.97
99.9
99.7
99
97.5
95
90
84
80
70
60
50
40
30
20
16
10
5
2.5
1
0.3
0.1
0.03
0.01
-4.0
-3.5
-3.0
-2.5
-2.0
-1.5
-1.0
-0.5
0.0
0.5
1.0
1.5
2.0
Grain Size (Phi)

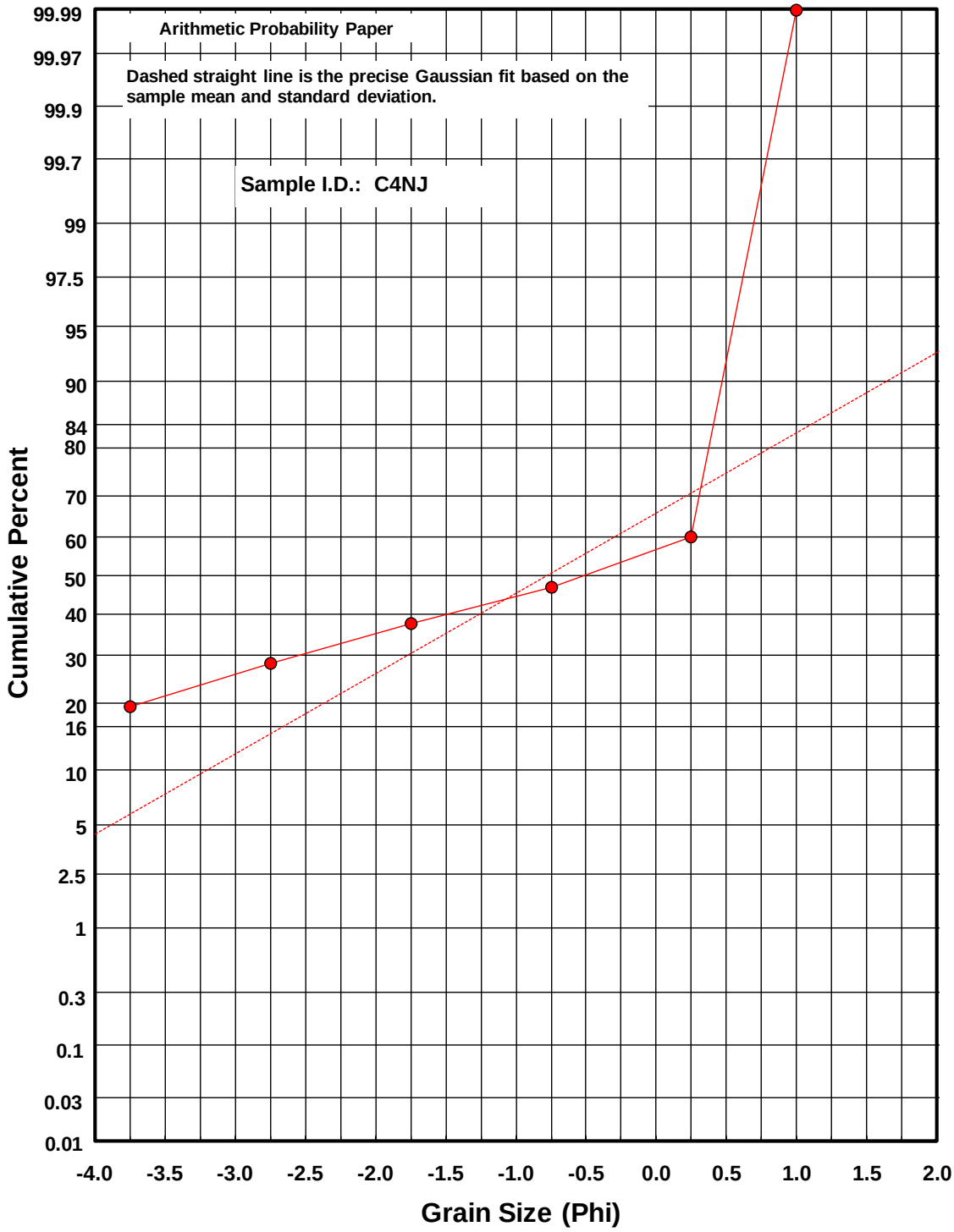
Arithmetic Probability Paper
Dashed straight line is the precise Gaussian fit based on the sample mean and standard deviation.
Sample I.D.: C4NJ
Cumulative Percent
99.99
99.97
99.9
99.7
99
97.5
95
90
84
80
70
60
50
40
30
20
16
10
5
2.5
1
0.3
0.1
0.03
0.01
-4.0
-3.5
-3.0
-2.5
-2.0
-1.5
-1.0
-0.5
0.0
0.5
1.0
1.5
2.0
Grain Size (Phi)

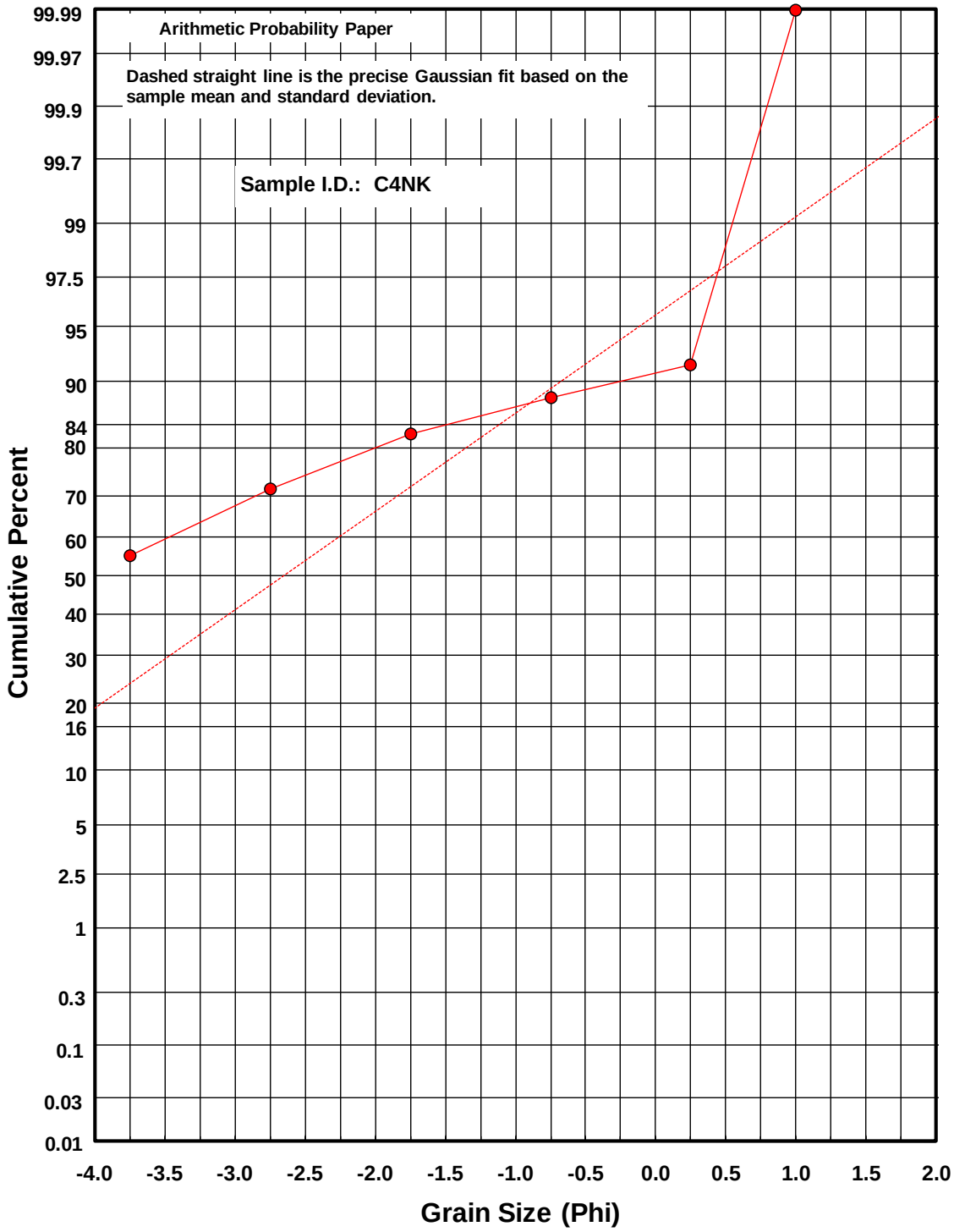
Arithmetic Probability Paper
Dashed straight line is the precise Gaussian fit based on the sample mean and standard deviation.
Sample I.D.: C4NK
Cumulative Percent
99.99
99.97
99.9
99.7
99
97.5
95
90
84
80
70
60
50
40
30
20
16
10
5
2.5
1
0.3
0.1
0.03
0.01
-4.0
-3.5
-3.0
-2.5
-2.0
-1.5
-1.0
-0.5
0.0
0.5
1.0
1.5
2.0
Grain Size (Phi)

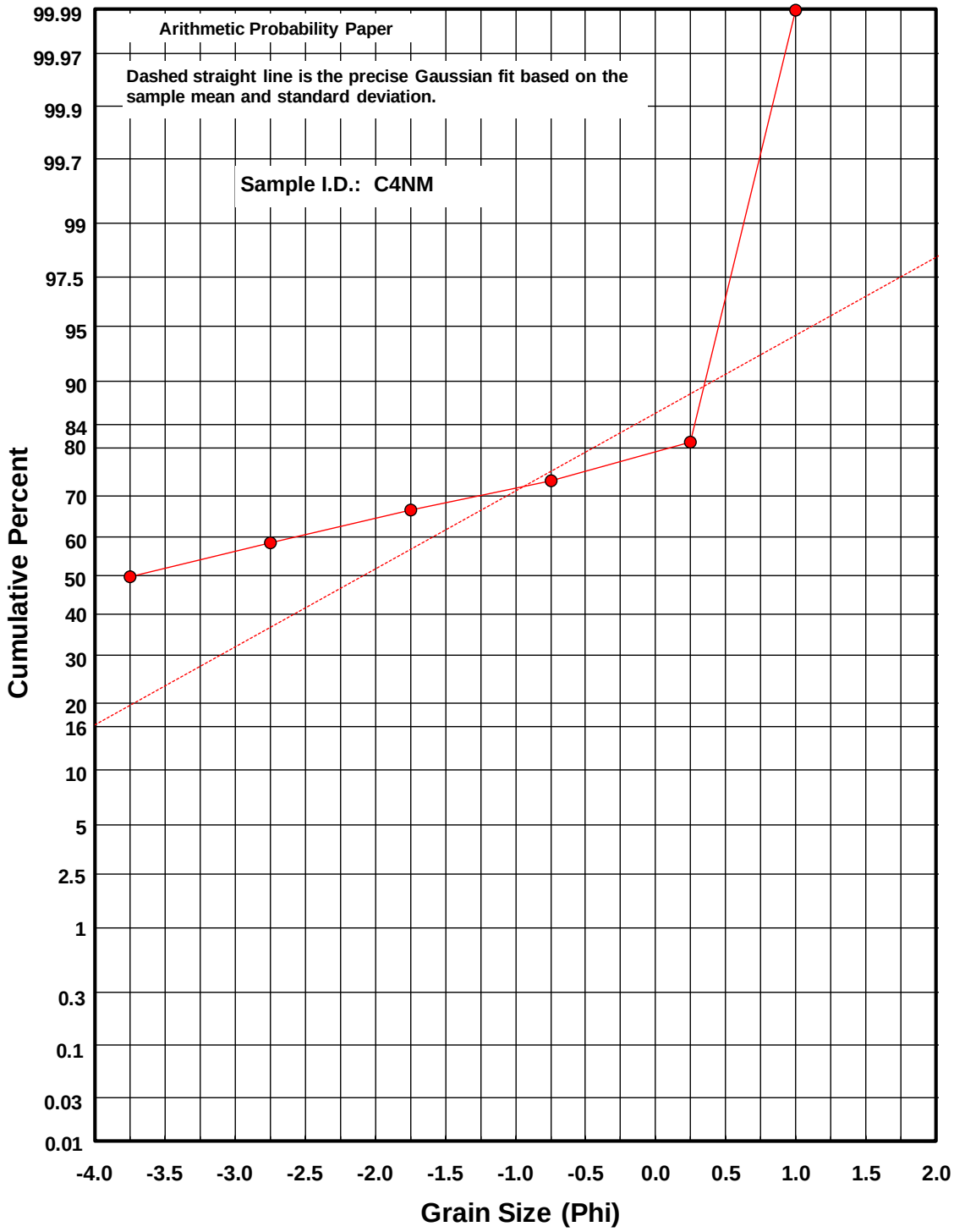
Arithmetic Probability Paper
Dashed straight line is the precise Gaussian fit based on the sample mean and standard deviation.
Sample I.D.: C4NM
Cumulative Percent
99.99
99.97
99.9
99.7
99
97.5
95
90
84
80
70
60
50
40
30
20
16
10
5
2.5
1
0.3
0.1
0.03
0.01
-4.0
-3.5
-3.0
-2.5
-2.0
-1.5
-1.0
-0.5
0.0
0.5
1.0
1.5
2.0
Grain Size (Phi)

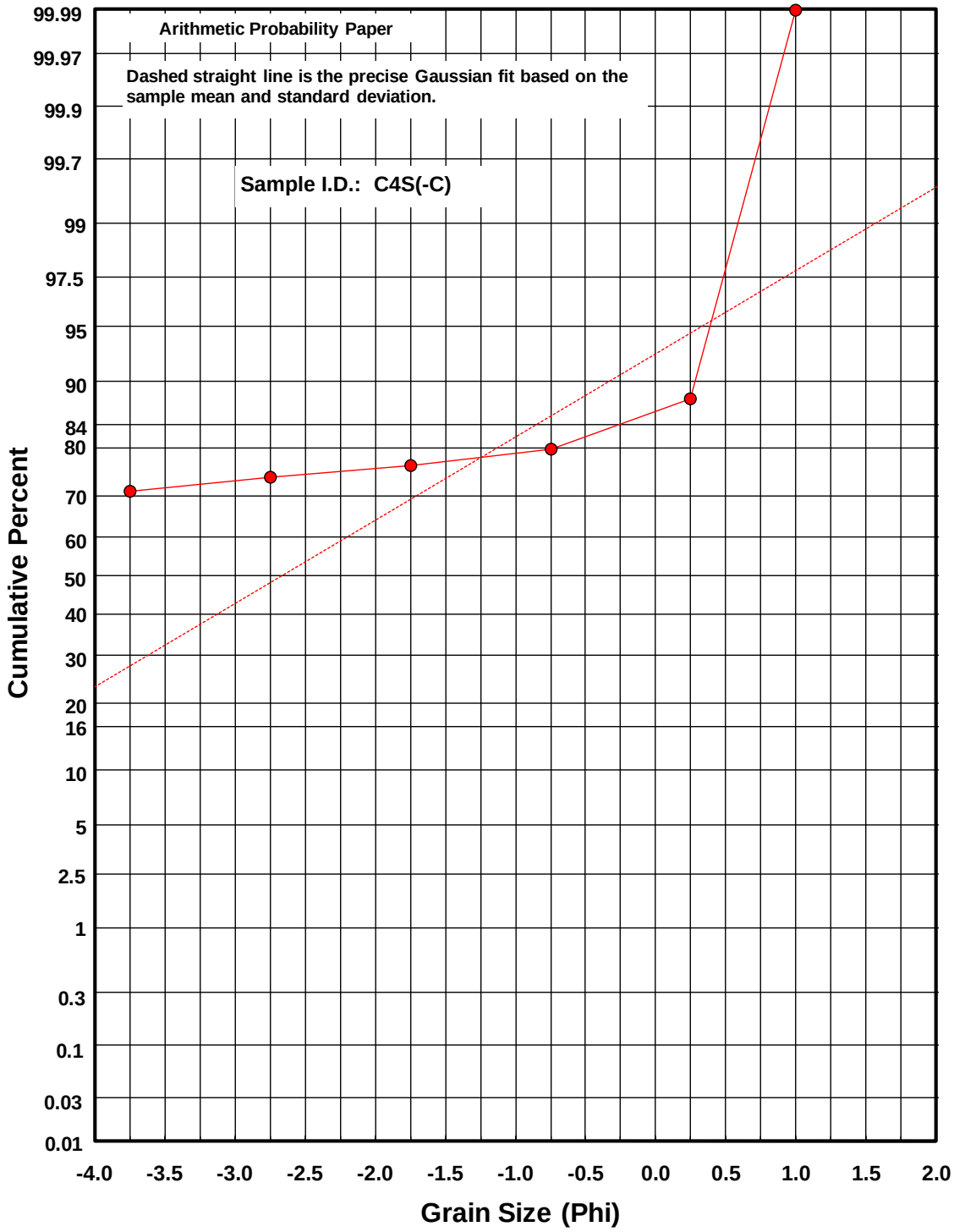
Arithmetic Probability Paper
Dashed straight line is the precise Gaussian fit based on the sample mean and standard deviation.
Sample I.D.: C4S(-C)
Cumulative Percent
99.99
99.97
99.9
99.7
99
97.5
95
90
84
80
70
60
50
40
30
20
16
10
5
2.5
1
0.3
0.1
0.03
0.01
-4.0
-3.5
-3.0
-2.5
-2.0
-1.5
-1.0
-0.5
0.0
0.5
1.0
1.5
2.0
Grain Size (Phi)

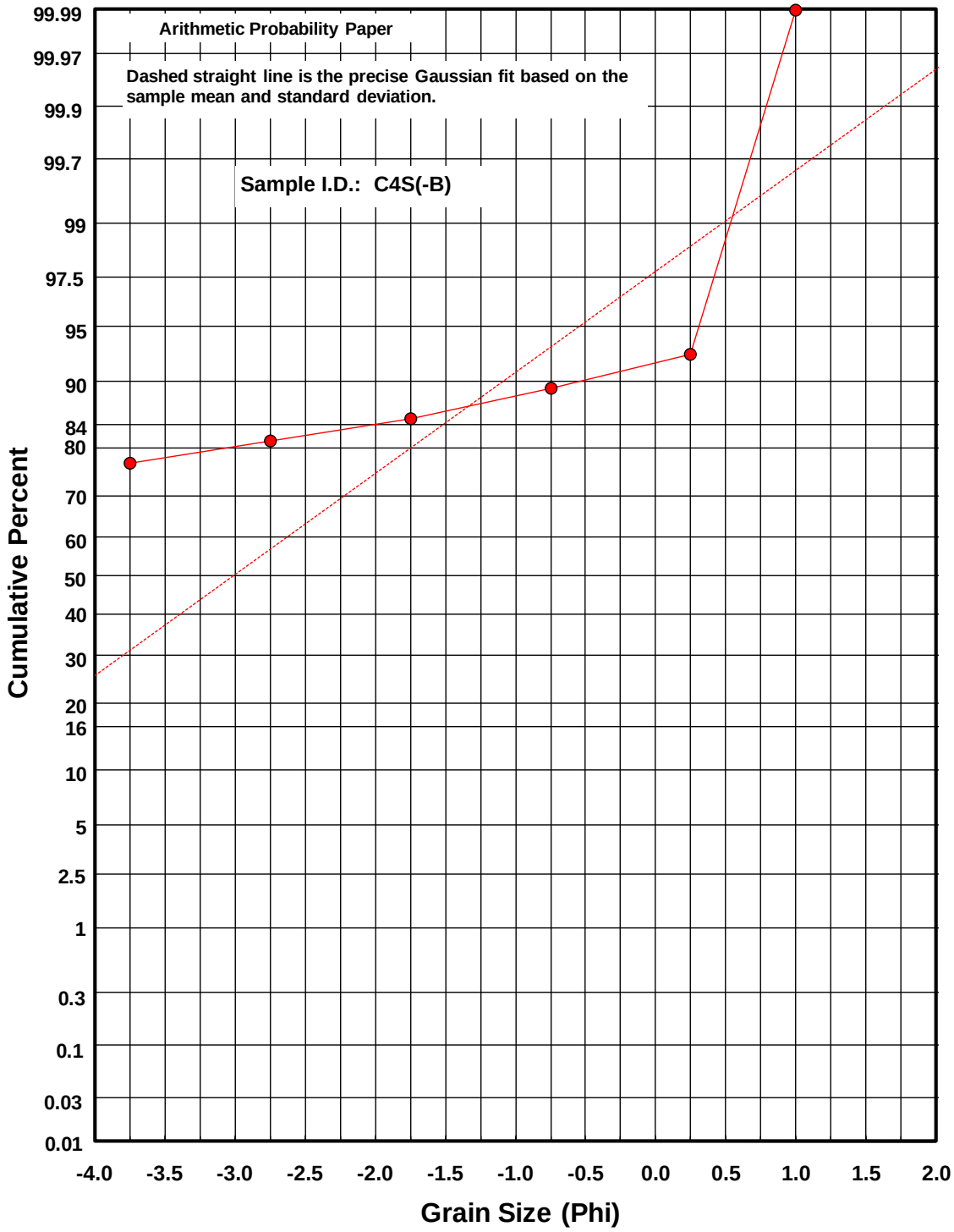
Arithmetic Probability Paper
Dashed straight line is the precise Gaussian fit based on the sample mean and standard deviation.
Sample I.D.: C4S(-B)
Cumulative Percent
99.99
99.97
99.9
99.7
99
97.5
95
90
84
80
70
60
50
40
30
20
16
10
5
2.5
1
0.3
0.1
0.03
0.01
-4.0
-3.5
-3.0
-2.5
-2.0
-1.5
-1.0
-0.5
0.0
0.5
1.0
1.5
2.0
Grain Size (Phi)

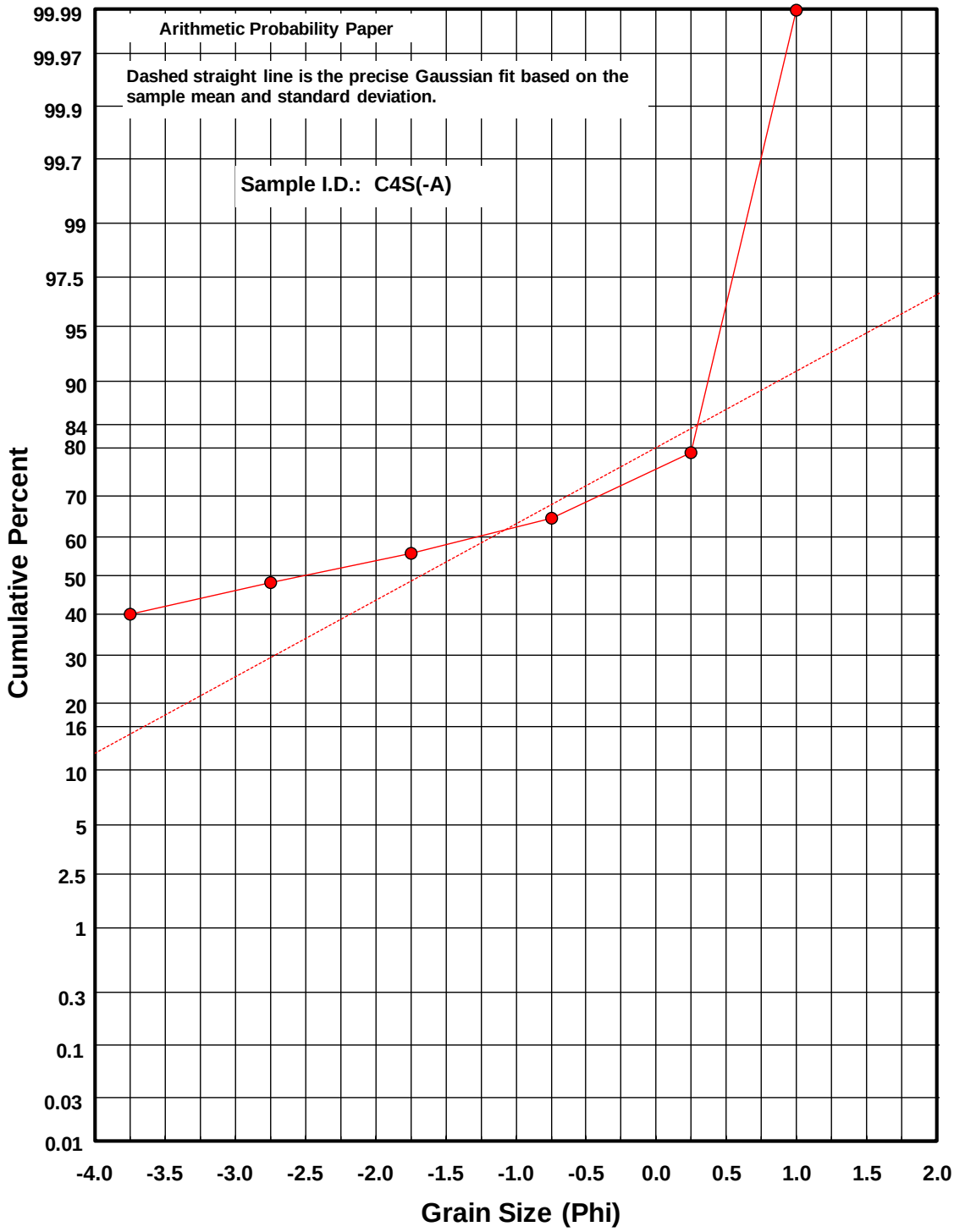
Arithmetic Probability Paper
Dashed straight line is the precise Gaussian fit based on the sample mean and standard deviation.
Sample I.D.: C4S(-A)
Cumulative Percent
99.99
99.97
99.9
99.7
99
97.5
95
90
84
80
70
60
50
40
30
20
16
10
5
2.5
1
0.3
0.1
0.03
0.01
-4.0
-3.5
-3.0
-2.5
-2.0
-1.5
-1.0
-0.5
0.0
0.5
1.0
1.5
2.0
Grain Size (Phi)

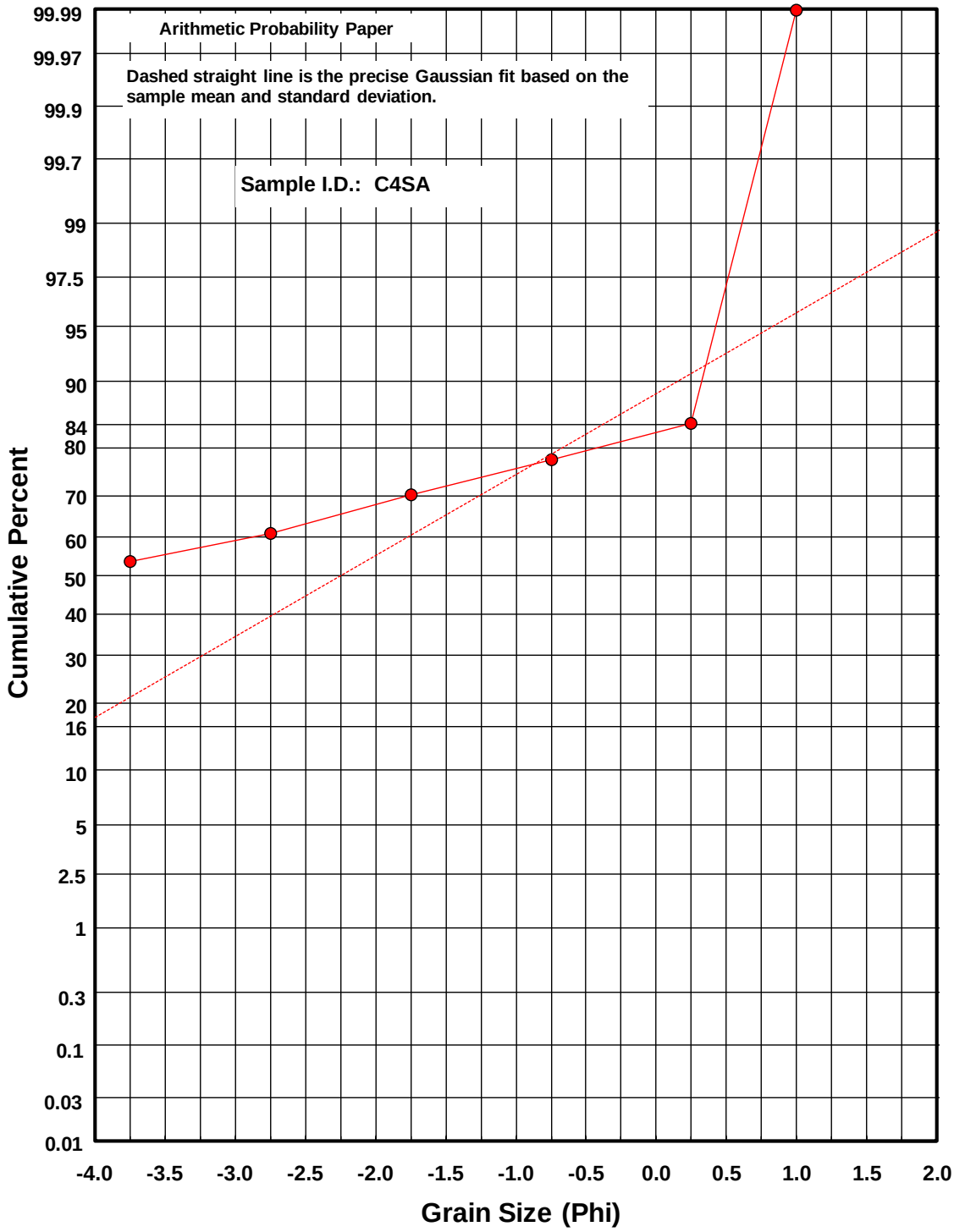
Arithmetic Probability Paper
Dashed straight line is the precise Gaussian fit based on the sample mean and standard deviation.
Sample I.D.: C4SA
Cumulative Percent
99.99
99.97
99.9
99.7
99
97.5
95
90
84
80
70
60
50
40
30
20
16
10
5
2.5
1
0.3
0.1
0.03
0.01
-4.0
-3.5
-3.0
-2.5
-2.0
-1.5
-1.0
-0.5
0.0
0.5
1.0
1.5
2.0
Grain Size (Phi)

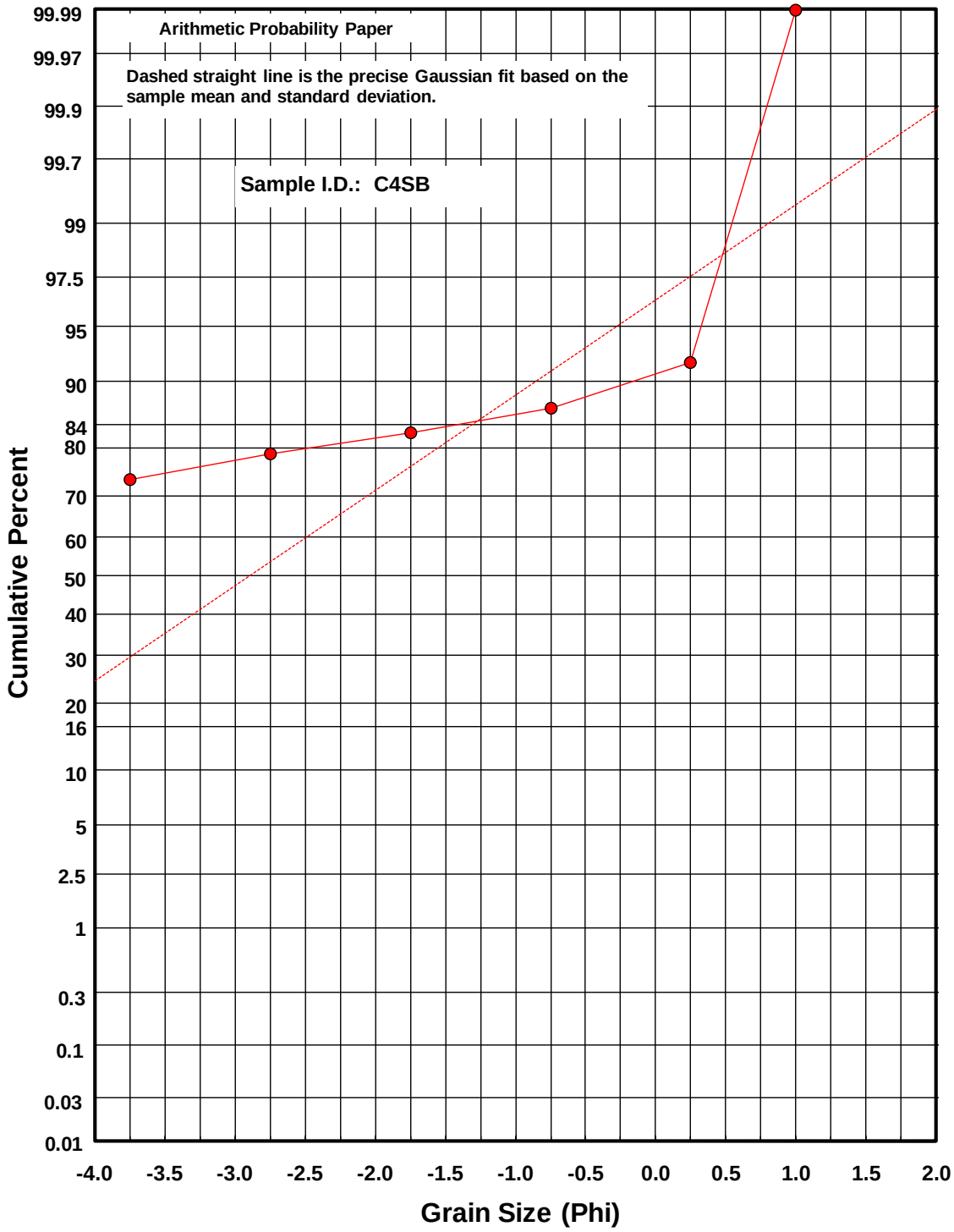
Arithmetic Probability Paper
Dashed straight line is the precise Gaussian fit based on the sample mean and standard deviation.
Sample I.D.: C4SB
Cumulative Percent
99.99
99.97
99.9
99.7
99
97.5
95
90
84
80
70
60
50
40
30
20
16
10
5
2.5
1
0.3
0.1
0.03
0.01
-4.0
-3.5
-3.0
-2.5
-2.0
-1.5
-1.0
-0.5
0.0
0.5
1.0
1.5
2.0
Grain Size (Phi)

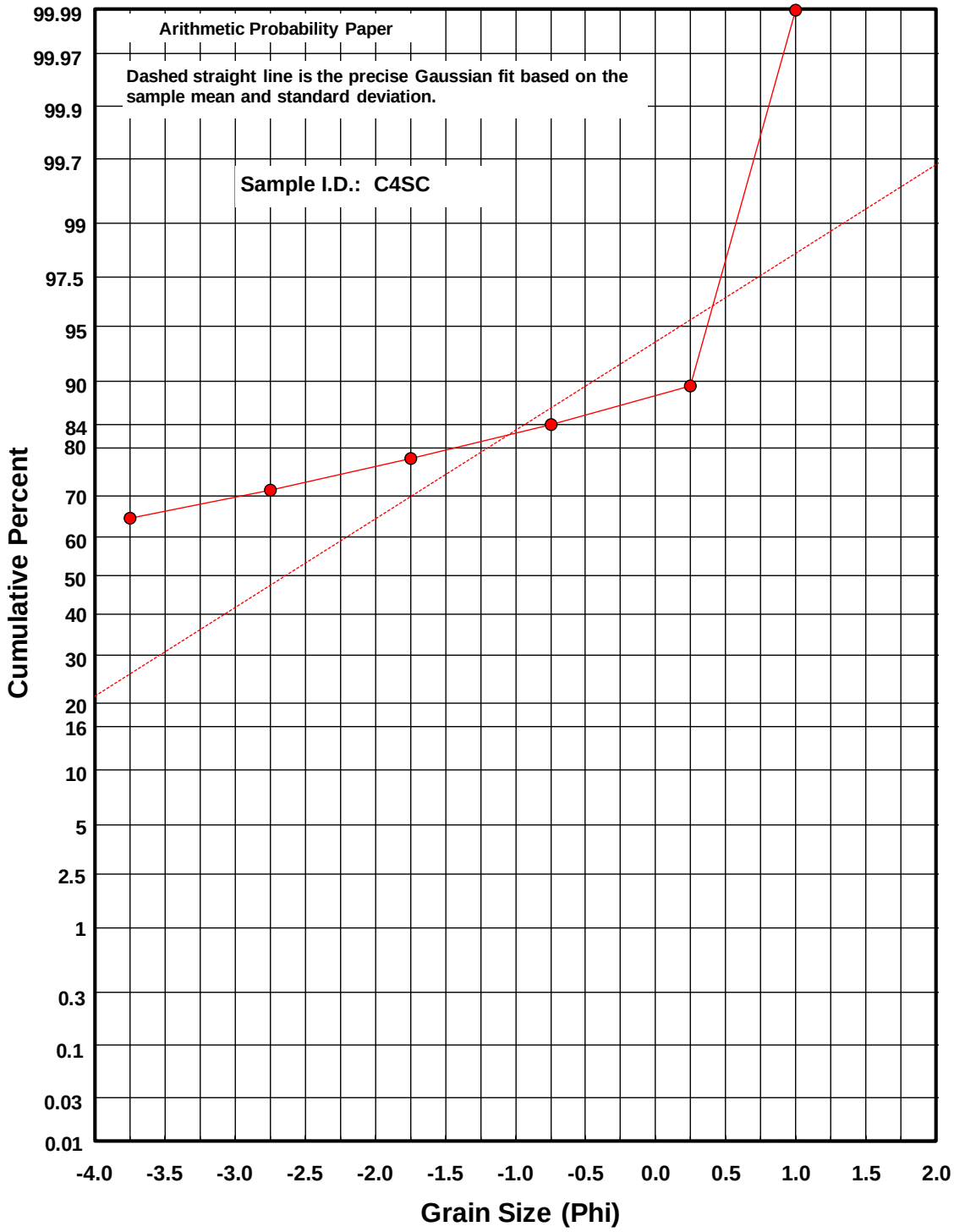
Arithmetic Probability Paper
Dashed straight line is the precise Gaussian fit based on the sample mean and standard deviation.
Sample I.D.: C4SC
Cumulative Percent
99.99
99.97
99.9
99.7
99
97.5
95
90
84
80
70
60
50
40
30
20
16
10
5
2.5
1
0.3
0.1
0.03
0.01
-4.0
-3.5
-3.0
-2.5
-2.0
-1.5
-1.0
-0.5
0.0
0.5
1.0
1.5
2.0
Grain Size (Phi)

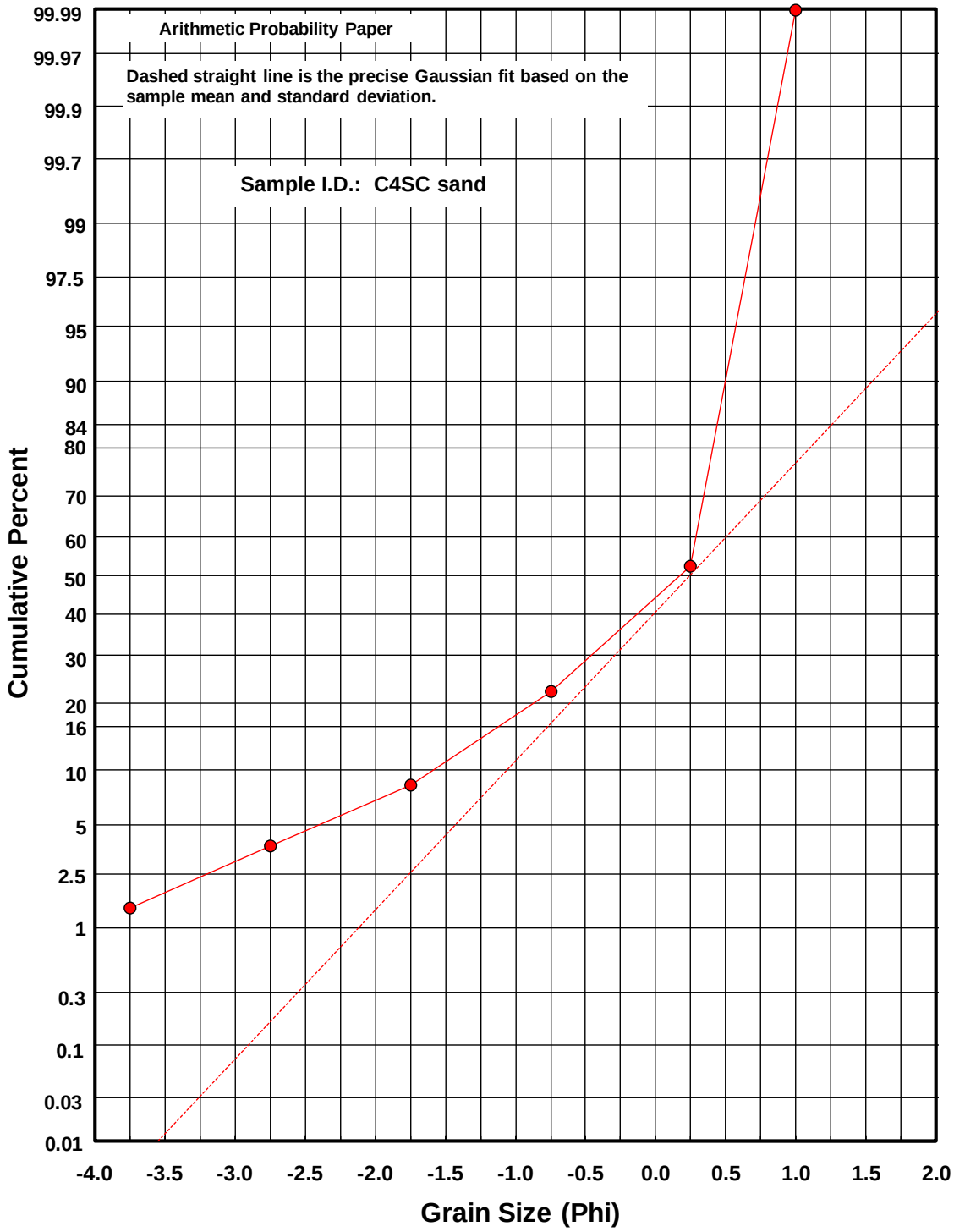
Arithmetic Probability Paper
Dashed straight line is the precise Gaussian fit based on the sample mean and standard deviation.
Sample I.D.: C4SC sand
Cumulative Percent
99.99
99.97
99.9
99.7
99
97.5
95
90
84
80
70
60
50
40
30
20
16
10
5
2.5
1
0.3
0.1
0.03
0.01
-4.0
-3.5
-3.0
-2.5
-2.0
-1.5
-1.0
-0.5
0.0
0.5
1.0
1.5
2.0
Grain Size (Phi)

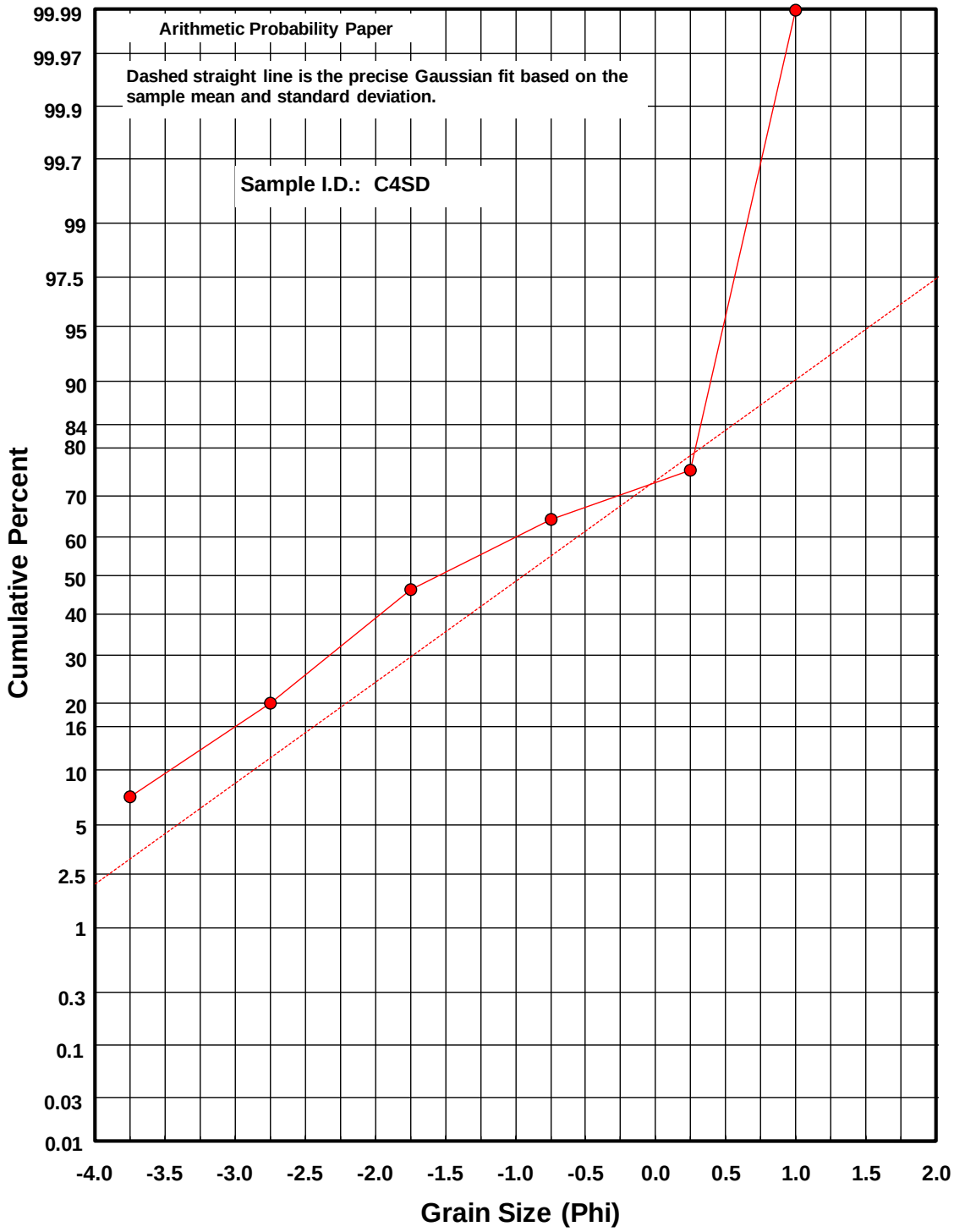
Arithmetic Probability Paper
Dashed straight line is the precise Gaussian fit based on the sample mean and standard deviation.
Sample I.D.: C4SD
Cumulative Percent
99.99
99.97
99.9
99.7
99
97.5
95
90
84
80
70
60
50
40
30
20
16
10
5
2.5
1
0.3
0.1
0.03
0.01
-4.0
-3.5
-3.0
-2.5
-2.0
-1.5
-1.0
-0.5
0.0
0.5
1.0
1.5
2.0
Grain Size (Phi)

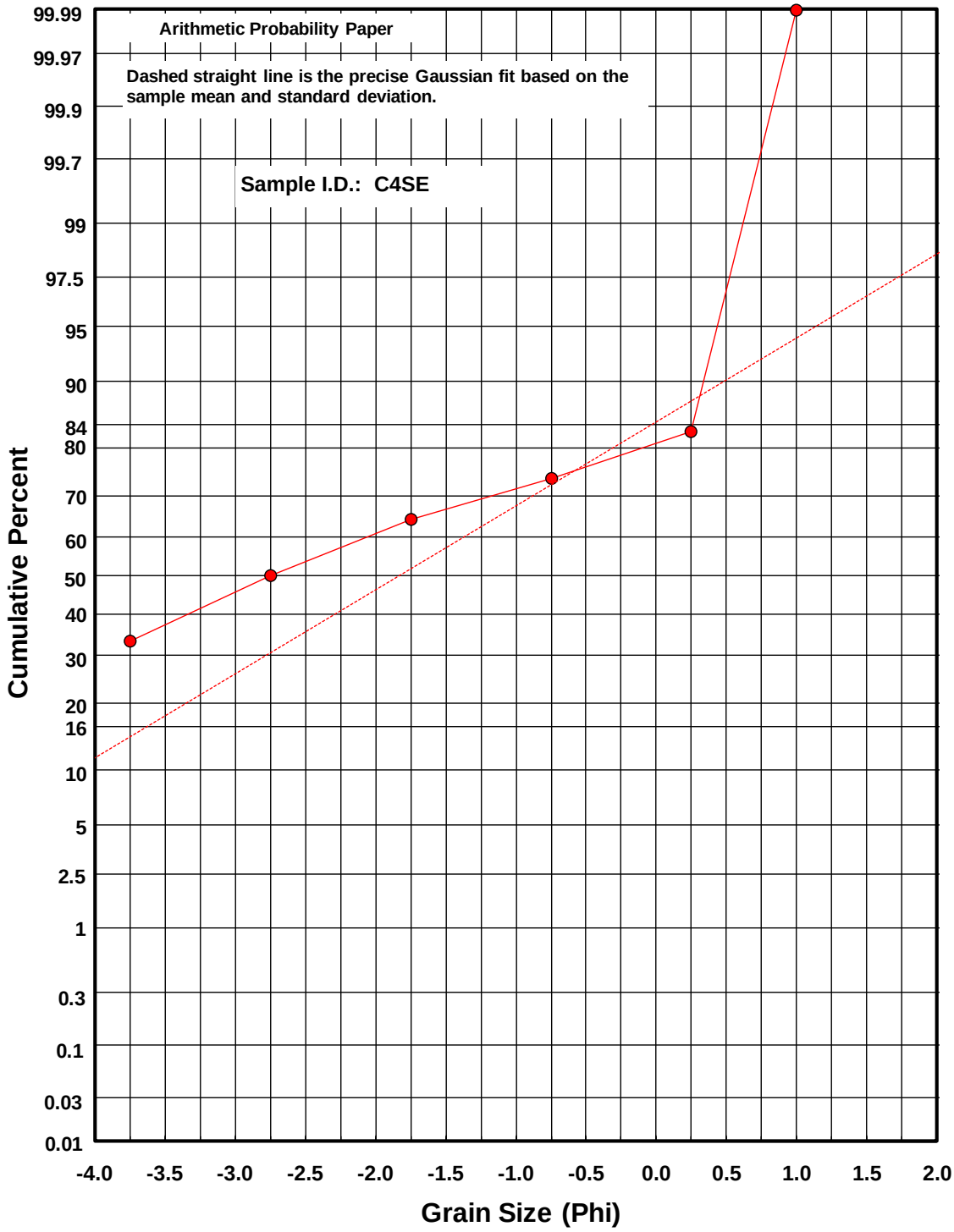
Arithmetic Probability Paper
Dashed straight line is the precise Gaussian fit based on the sample mean and standard deviation.
Sample I.D.: C4SE
Cumulative Percent
99.99
99.97
99.9
99.7
99
97.5
95
90
84
80
70
60
50
40
30
20
16
10
5
2.5
1
0.3
0.1
0.03
0.01
-4.0
-3.5
-3.0
-2.5
-2.0
-1.5
-1.0
-0.5
0.0
0.5
1.0
1.5
2.0
Grain Size (Phi)

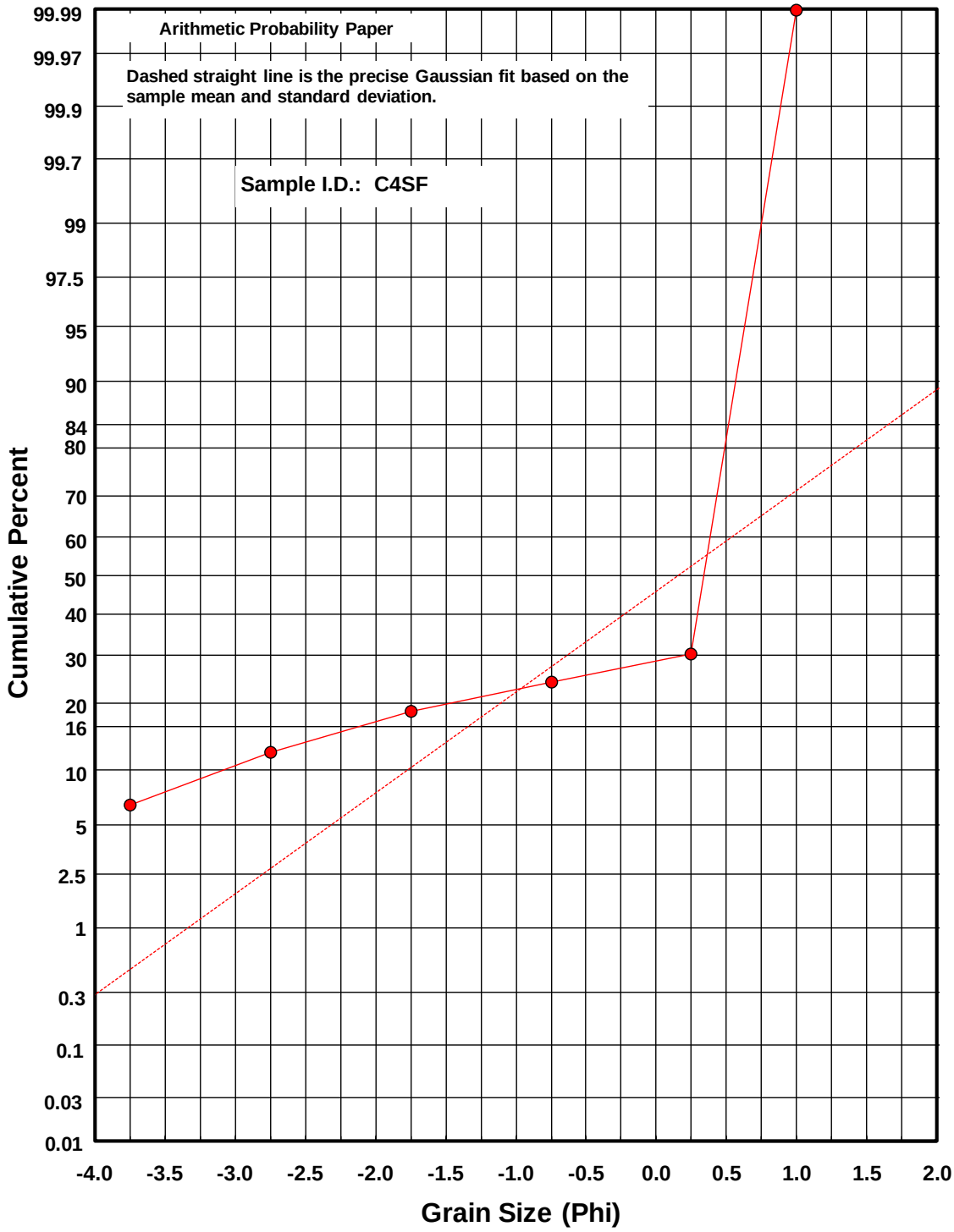
Arithmetic Probability Paper
Dashed straight line is the precise Gaussian fit based on the sample mean and standard deviation.
Sample I.D.: C4SF
Cumulative Percent
99.99
99.97
99.9
99.7
99
97.5
95
90
84
80
70
60
50
40
30
20
16
10
5
2.5
1
0.3
0.1
0.03
0.01
-4.0
-3.5
-3.0
-2.5
-2.0
-1.5
-1.0
-0.5
0.0
0.5
1.0
1.5
2.0
Grain Size (Phi)

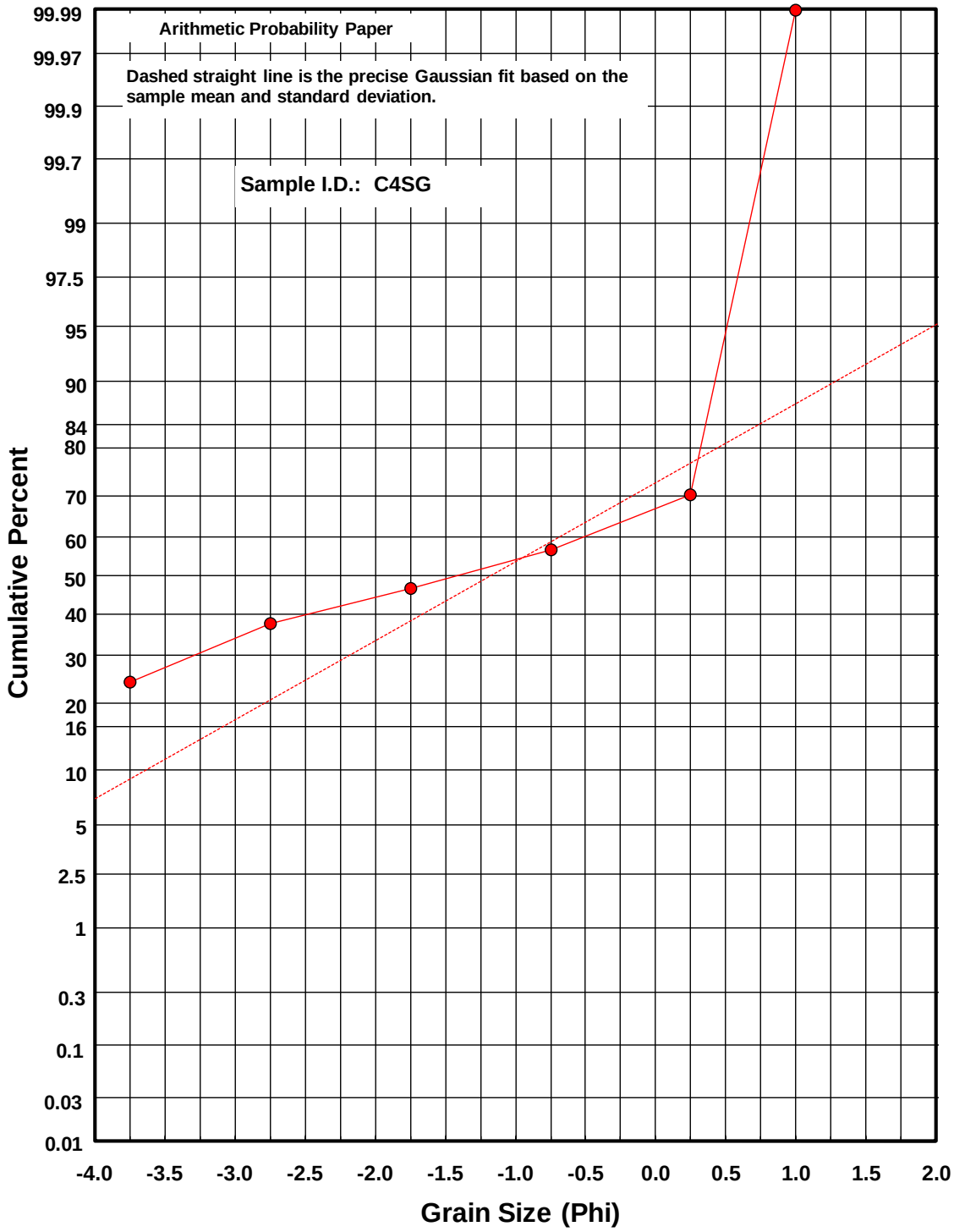
Arithmetic Probability Paper
Dashed straight line is the precise Gaussian fit based on the sample mean and standard deviation.
Sample I.D.: C4SG
Cumulative Percent
99.99
99.97
99.9
99.7
99
97.5
95
90
84
80
70
60
50
40
30
20
16
10
5
2.5
1
0.3
0.1
0.03
0.01
-4.0
-3.5
-3.0
-2.5
-2.0
-1.5
-1.0
-0.5
0.0
0.5
1.0
1.5
2.0
Grain Size (Phi)

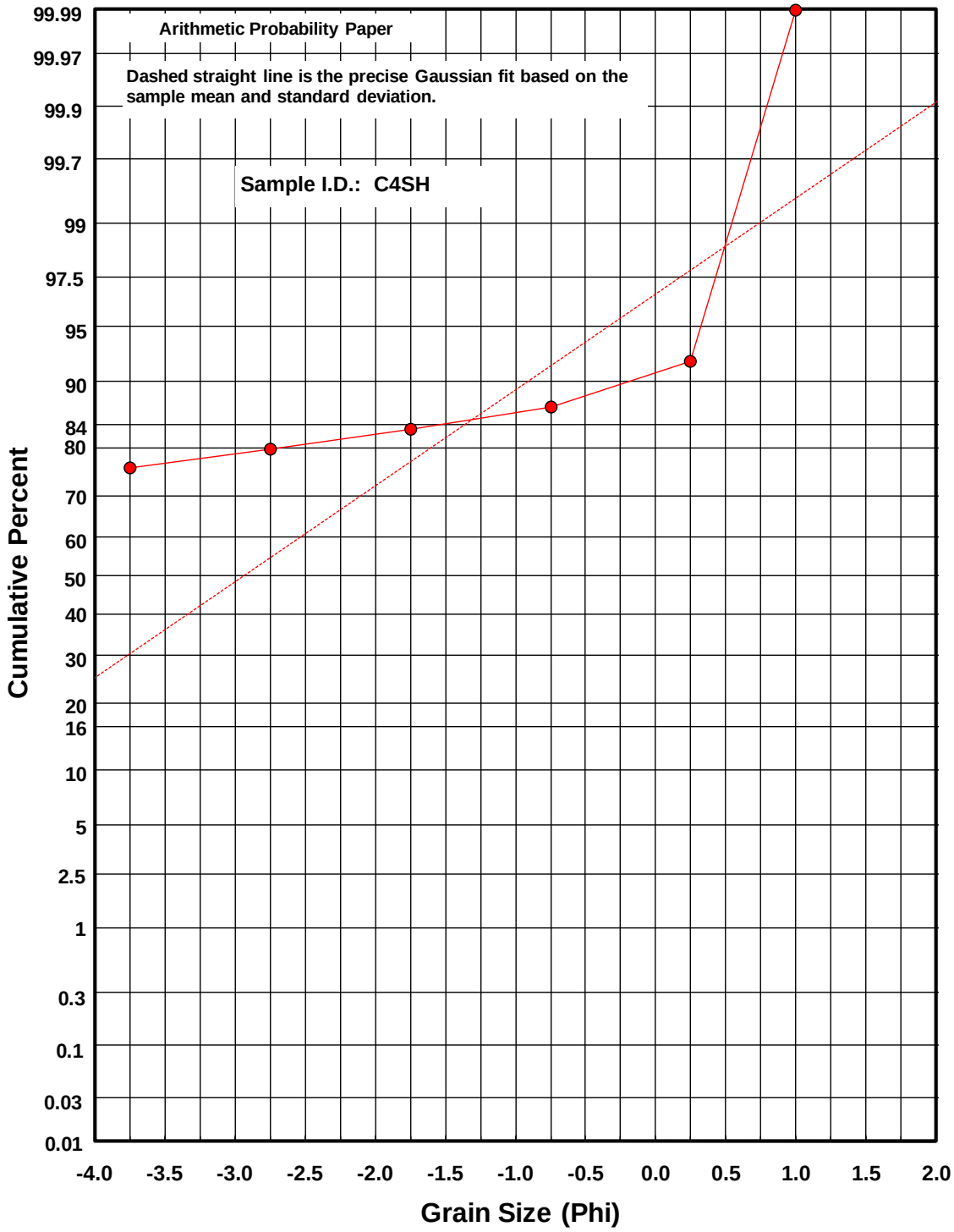
Arithmetic Probability Paper
Dashed straight line is the precise Gaussian fit based on the sample mean and standard deviation.
Sample I.D.: C4SH
Cumulative Percent
99.99
99.97
99.9
99.7
99
97.5
95
90
84
80
70
60
50
40
30
20
16
10
5
2.5
1
0.3
0.1
0.03
0.01
-4.0
-3.5
-3.0
-2.5
-2.0
-1.5
-1.0
-0.5
0.0
0.5
1.0
1.5
2.0
Grain Size (Phi)

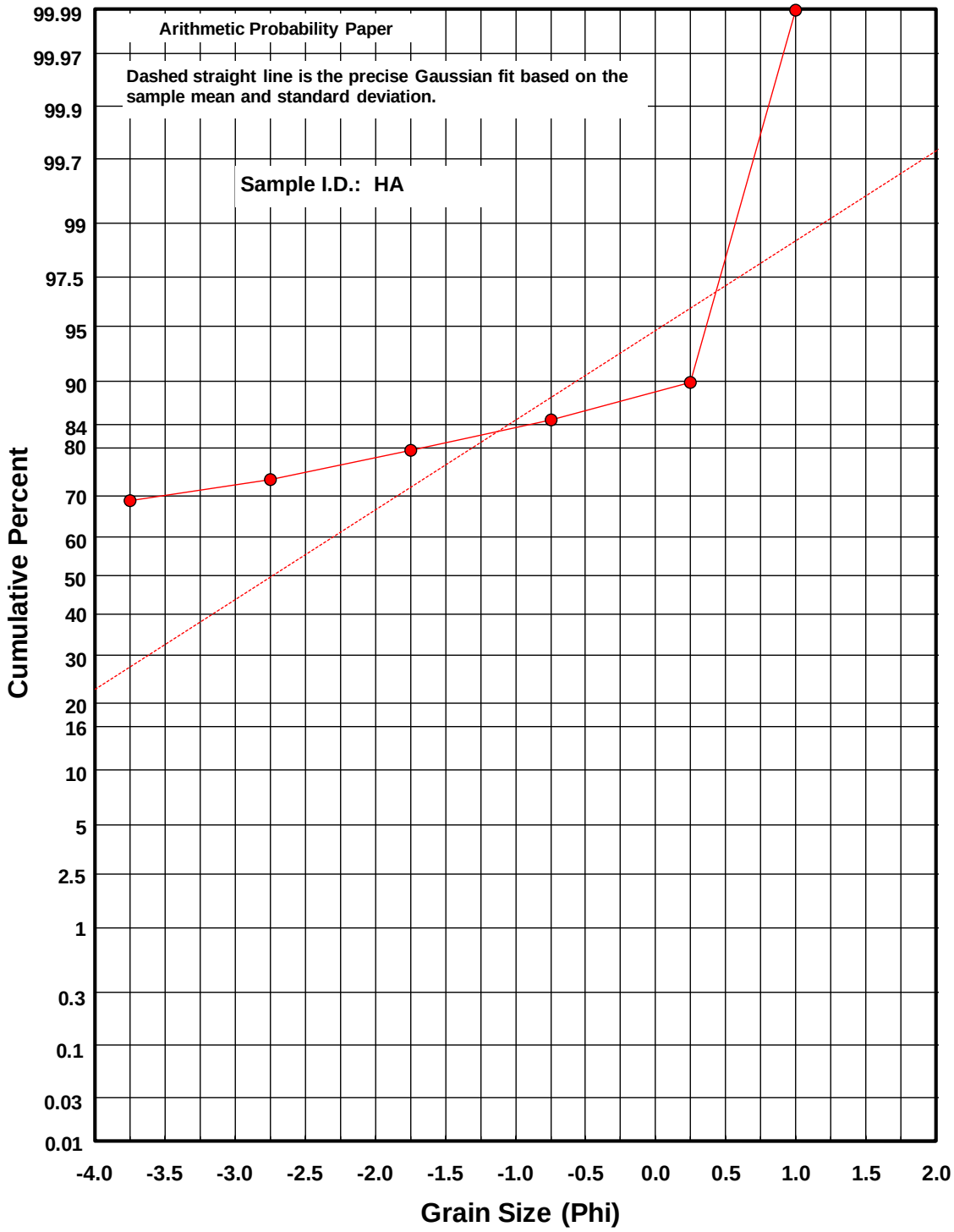
Arithmetic Probability Paper
Dashed straight line is the precise Gaussian fit based on the sample mean and standard deviation.
Sample I.D.: HA
Cumulative Percent
99.99
99.97
99.9
99.7
99
97.5
95
90
84
80
70
60
50
40
30
20
16
10
5
2.5
1
0.3
0.1
0.03
0.01
-4.0
-3.5
-3.0
-2.5
-2.0
-1.5
-1.0
-0.5
0.0
0.5
1.0
1.5
2.0
Grain Size (Phi)

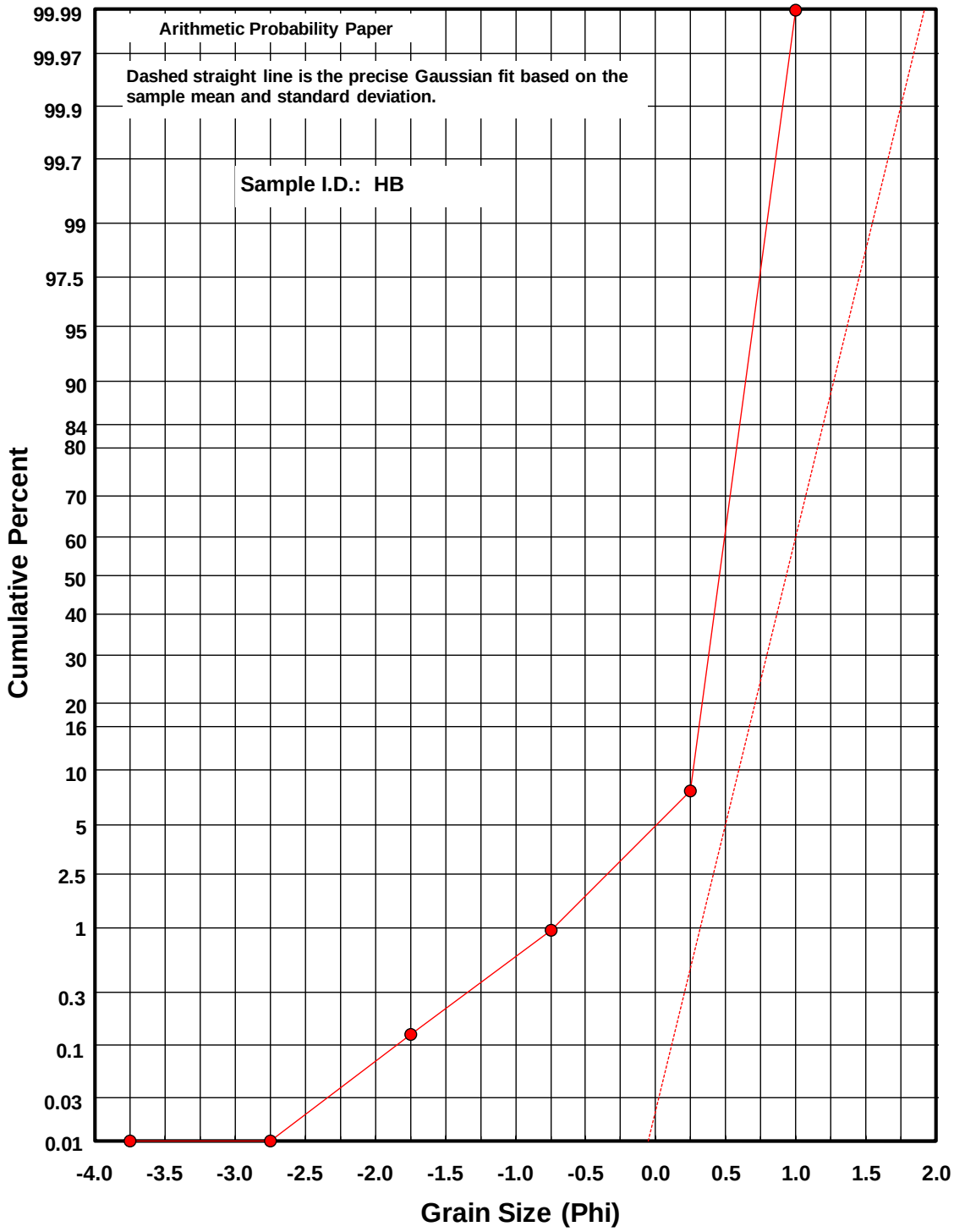
Arithmetic Probability Paper
Dashed straight line is the precise Gaussian fit based on the sample mean and standard deviation.
Sample I.D.: HB
Cumulative Percent
99.99
99.97
99.9
99.7
99
97.5
95
90
84
80
70
60
50
40
30
20
16
10
5
2.5
1
0.3
0.1
0.03
0.01
-4.0
-3.5
-3.0
-2.5
-2.0
-1.5
-1.0
-0.5
0.0
0.5
1.0
1.5
2.0
Grain Size (Phi)

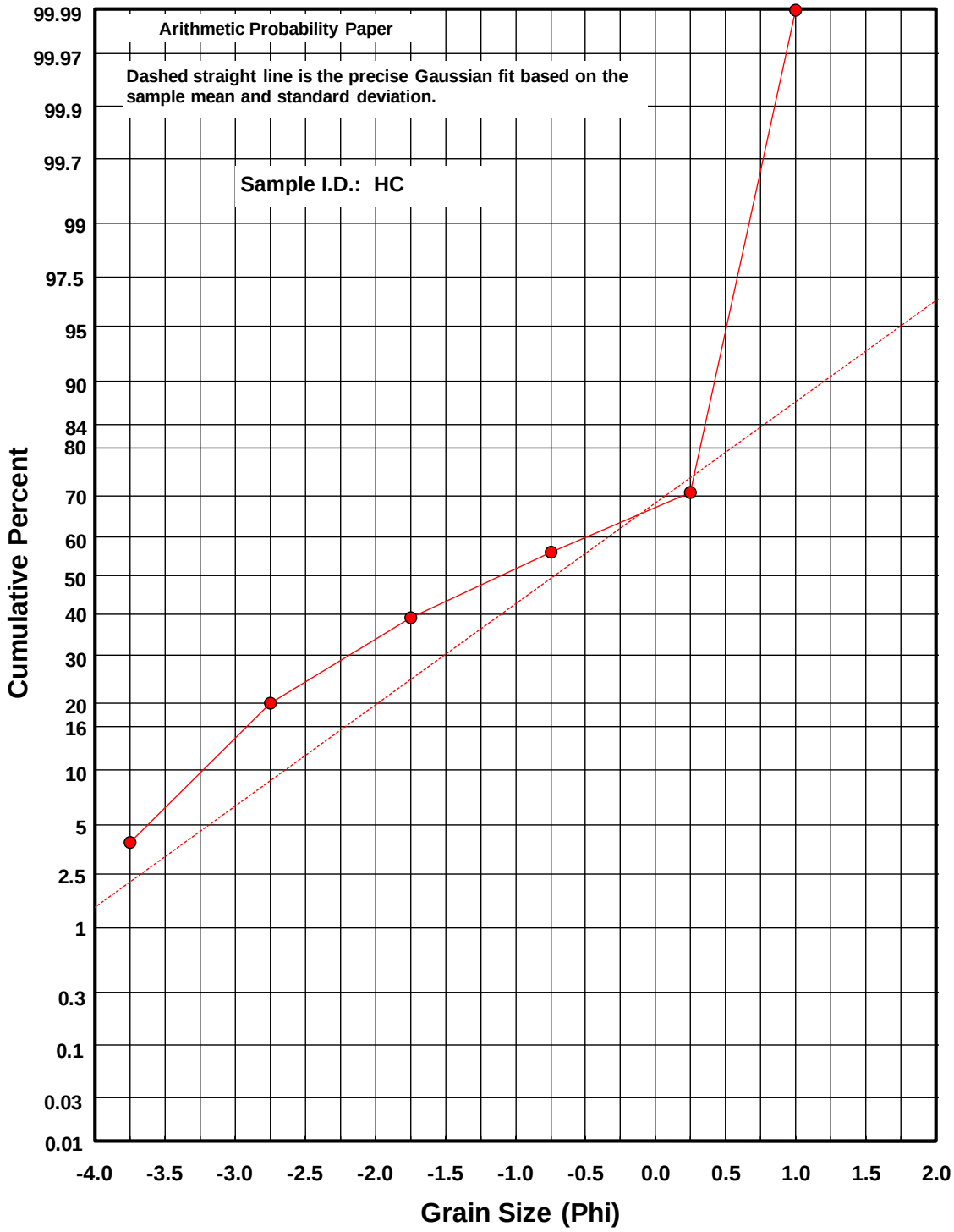
Arithmetic Probability Paper
Dashed straight line is the precise Gaussian fit based on the sample mean and standard deviation.
Sample I.D.: HC
Cumulative Percent
99.99
99.97
99.9
99.7
99
97.5
95
90
84
80
70
60
50
40
30
20
16
10
5
2.5
1
0.3
0.1
0.03
0.01
-4.0
-3.5
-3.0
-2.5
-2.0
-1.5
-1.0
-0.5
0.0
0.5
1.0
1.5
2.0
Grain Size (Phi)

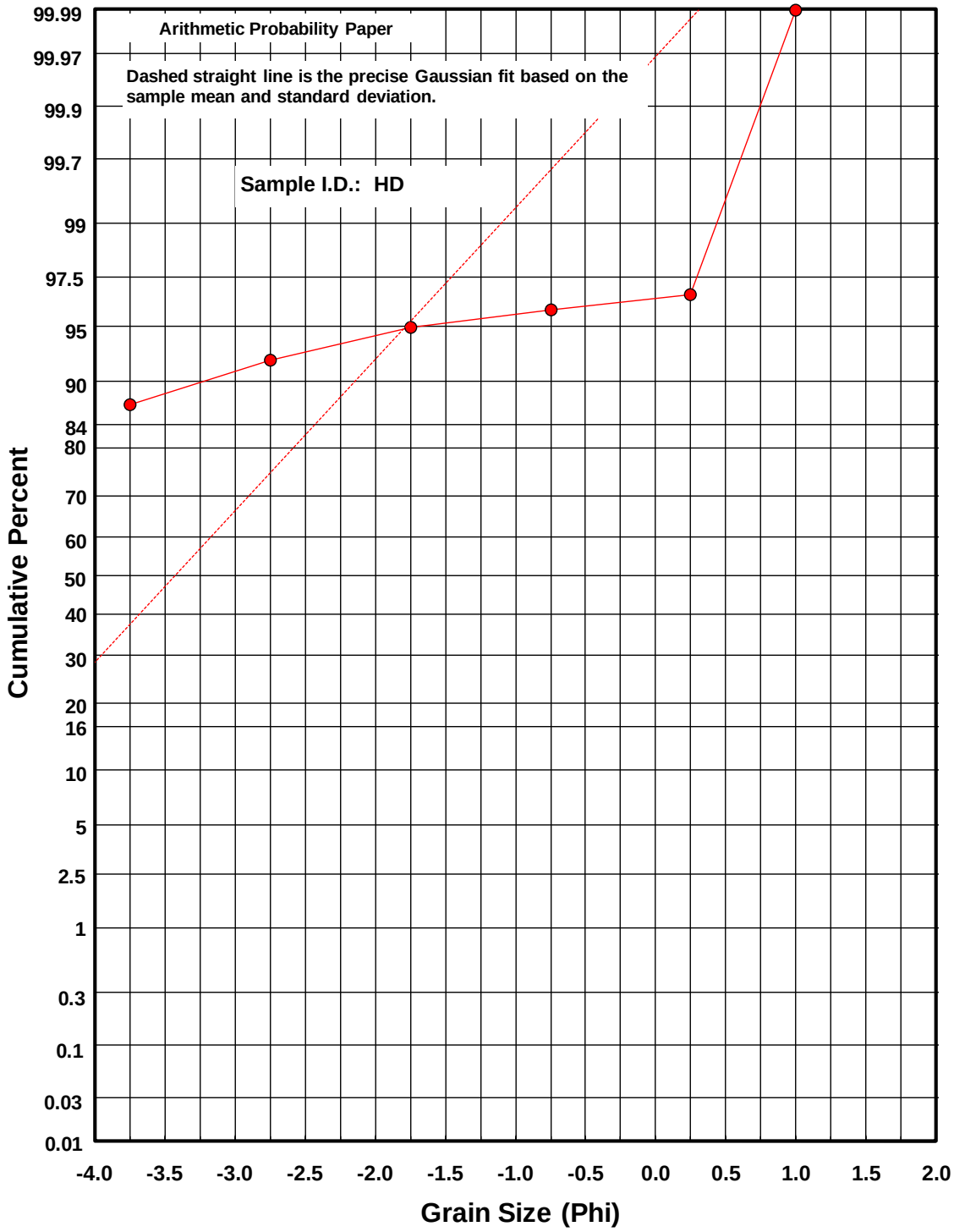
Arithmetic Probability Paper
Dashed straight line is the precise Gaussian fit based on the sample mean and standard deviation.
Sample I.D.: HD
Cumulative Percent
99.99
99.97
99.9
99.7
99
97.5
95
90
84
80
70
60
50
40
30
20
16
10
5
2.5
1
0.3
0.1
0.03
0.01
-4.0
-3.5
-3.0
-2.5
-2.0
-1.5
-1.0
-0.5
0.0
0.5
1.0
1.5
2.0
Grain Size (Phi)

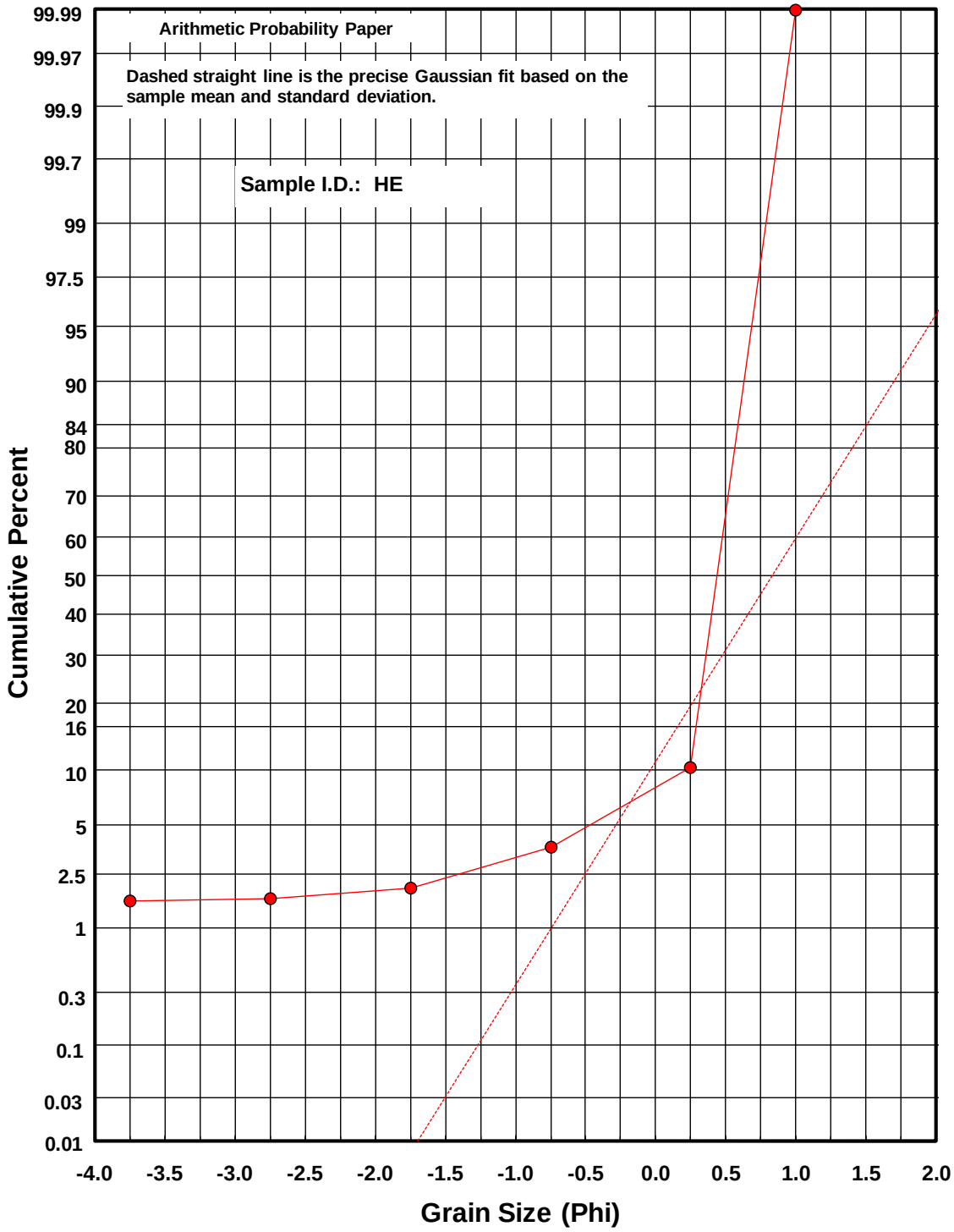
Arithmetic Probability Paper
Dashed straight line is the precise Gaussian fit based on the sample mean and standard deviation.
Sample I.D.: HE
Cumulative Percent
99.99
99.97
99.9
99.7
99
97.5
95
90
84
80
70
60
50
40
30
20
16
10
5
2.5
1
0.3
0.1
0.03
0.01
-4.0
-3.5
-3.0
-2.5
-2.0
-1.5
-1.0
-0.5
0.0
0.5
1.0
1.5
2.0
Grain Size (Phi)

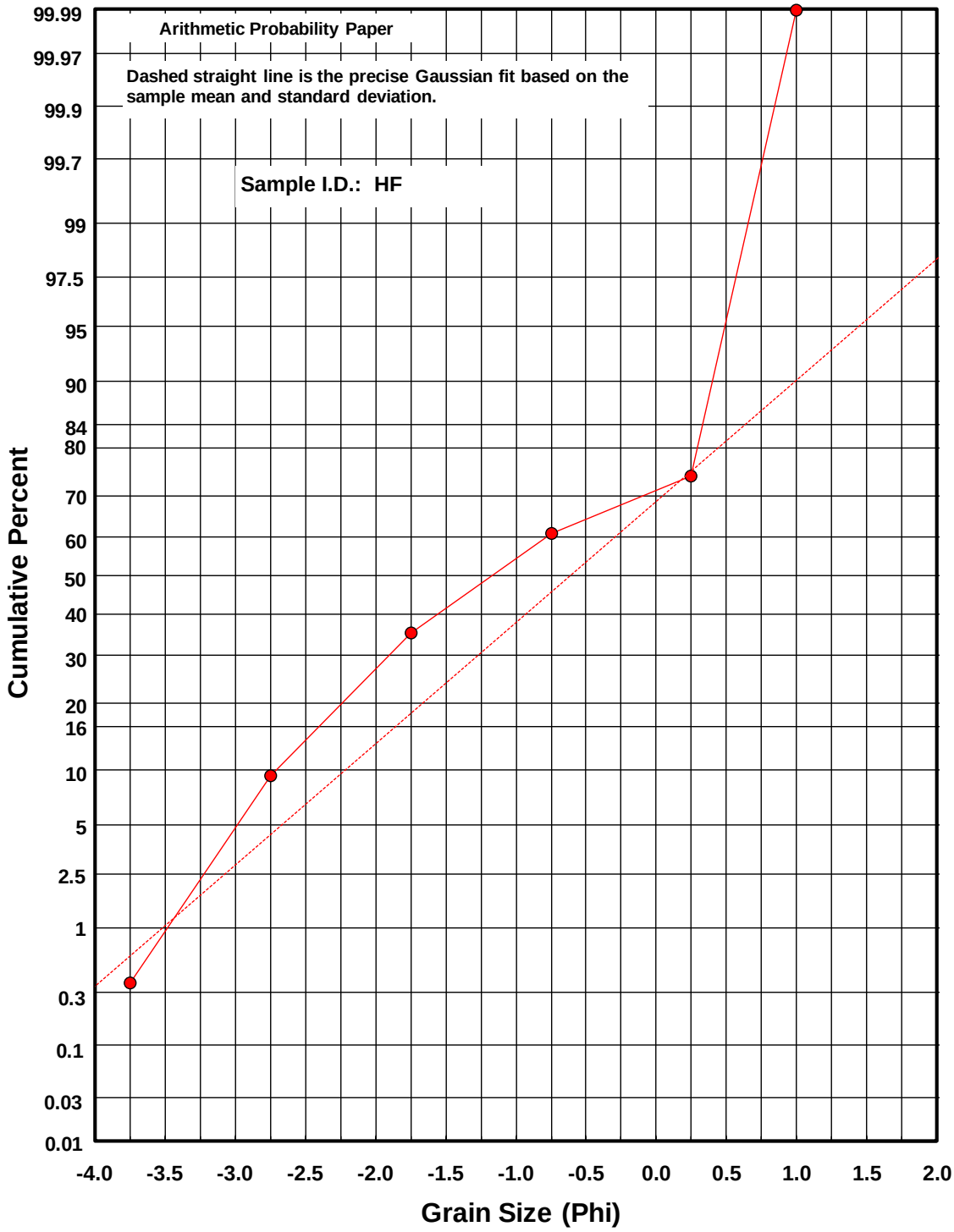
Arithmetic Probability Paper
Dashed straight line is the precise Gaussian fit based on the sample mean and standard deviation.
Sample I.D.: HF
Cumulative Percent
99.99
99.97
99.9
99.7
99
97.5
95
90
84
80
70
60
50
40
30
20
16
10
5
2.5
1
0.3
0.1
0.03
0.01
-4.0
-3.5
-3.0
-2.5
-2.0
-1.5
-1.0
-0.5
0.0
0.5
1.0
1.5
2.0
Grain Size (Phi)

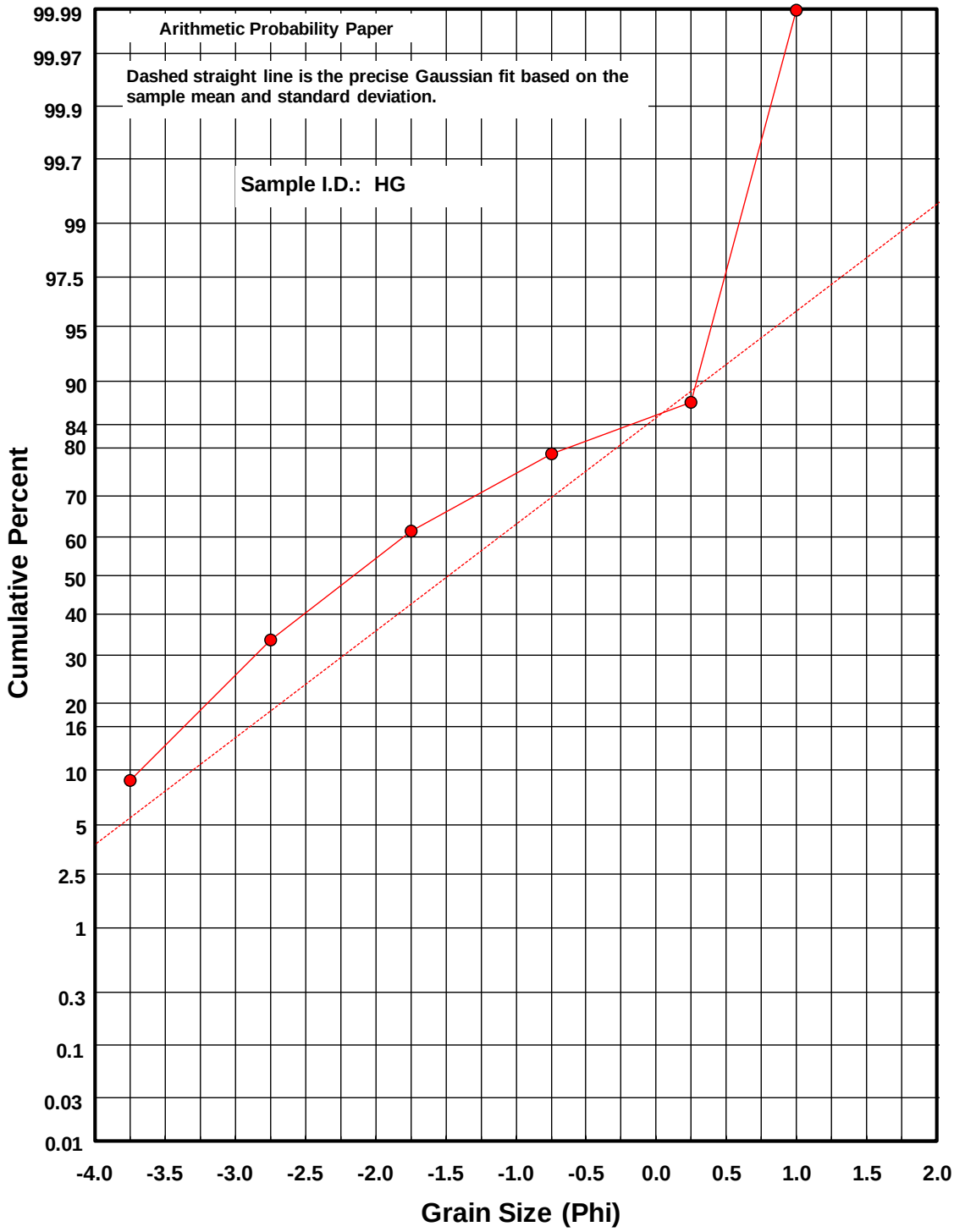
Arithmetic Probability Paper
Dashed straight line is the precise Gaussian fit based on the sample mean and standard deviation.
Sample I.D.: HG
Cumulative Percent
99.99
99.97
99.9
99.7
99
97.5
95
90
84
80
70
60
50
40
30
20
16
10
5
2.5
1
0.3
0.1
0.03
0.01
-4.0
-3.5
-3.0
-2.5
-2.0
-1.5
-1.0
-0.5
0.0
0.5
1.0
1.5
2.0
Grain Size (Phi)

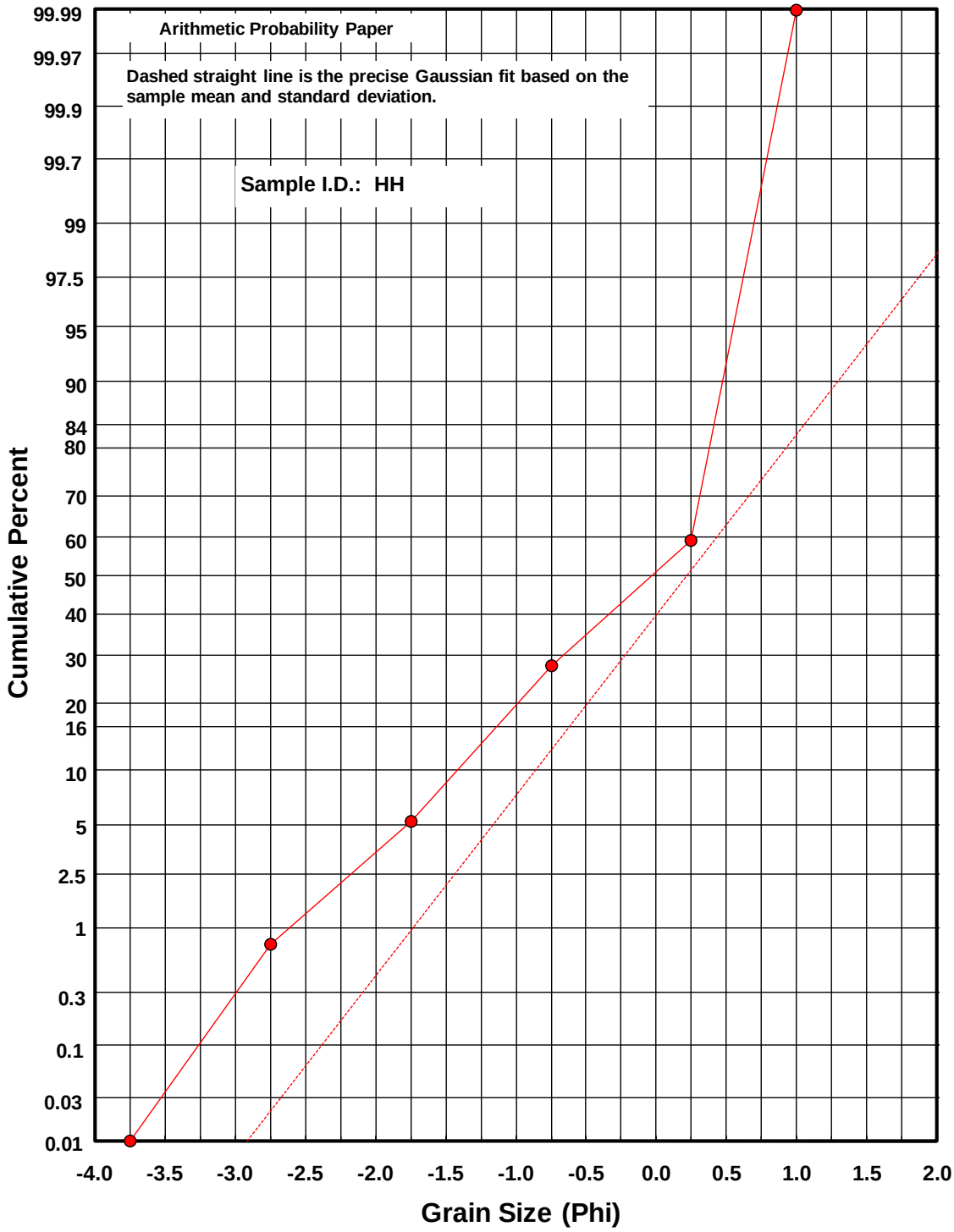
Arithmetic Probability Paper
Dashed straight line is the precise Gaussian fit based on the sample mean and standard deviation.
Sample I.D.: HH
Cumulative Percent
99.99
99.97
99.9
99.7
99
97.5
95
90
84
80
70
60
50
40
30
20
16
10
5
2.5
1
0.3
0.1
0.03
0.01
-4.0
-3.5
-3.0
-2.5
-2.0
-1.5
-1.0
-0.5
0.0
0.5
1.0
1.5
2.0
Grain Size (Phi)

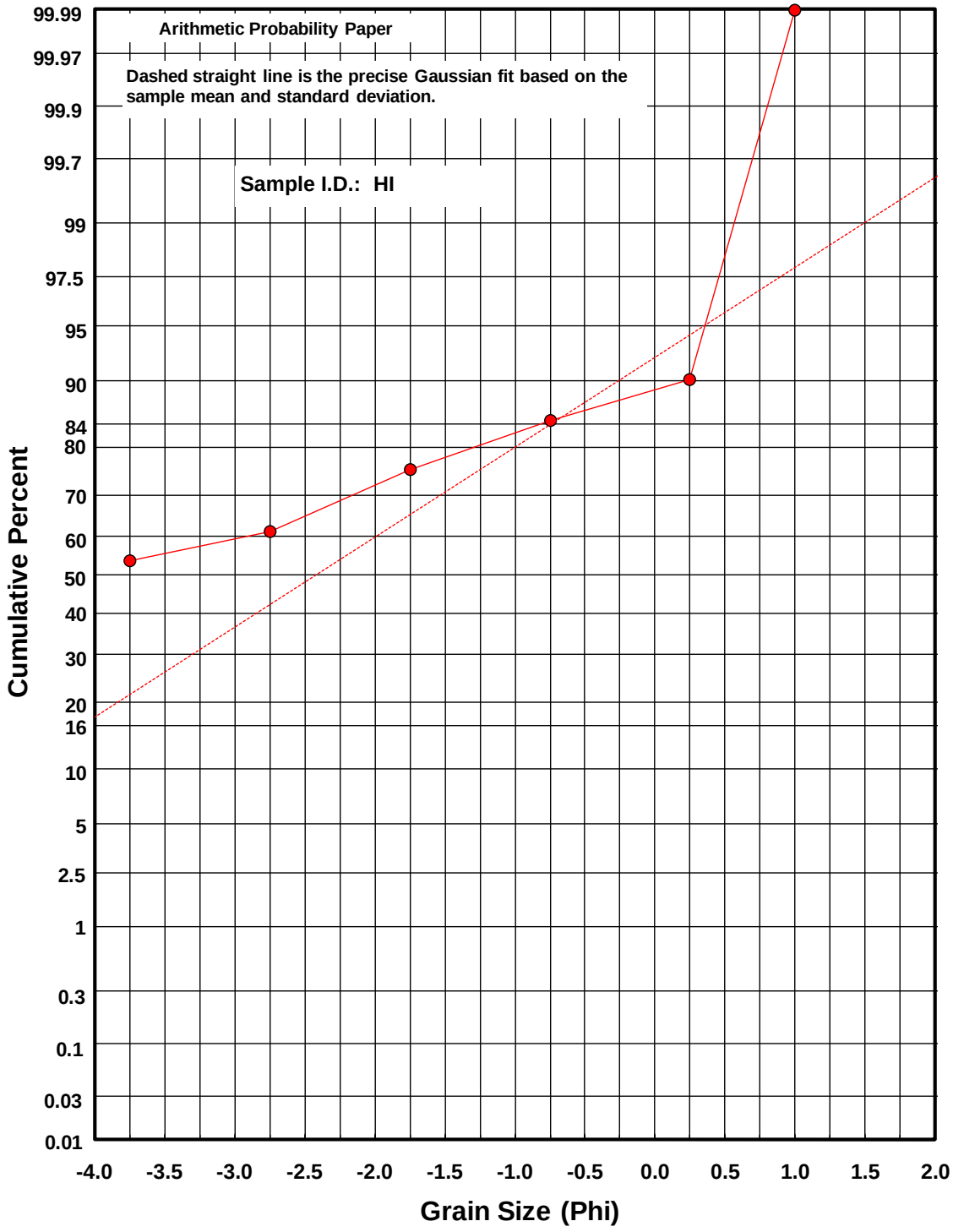
Arithmetic Probability Paper
Dashed straight line is the precise Gaussian fit based on the sample mean and standard deviation.
Sample I.D.: HI
Cumulative Percent
99.99
99.97
99.9
99.7
99
97.5
95
90
84
80
70
60
50
40
30
20
16
10
5
2.5
1
0.3
0.1
0.03
0.01
-4.0
-3.5
-3.0
-2.5
-2.0
-1.5
-1.0
-0.5
0.0
0.5
1.0
1.5
2.0
Grain Size (Phi)

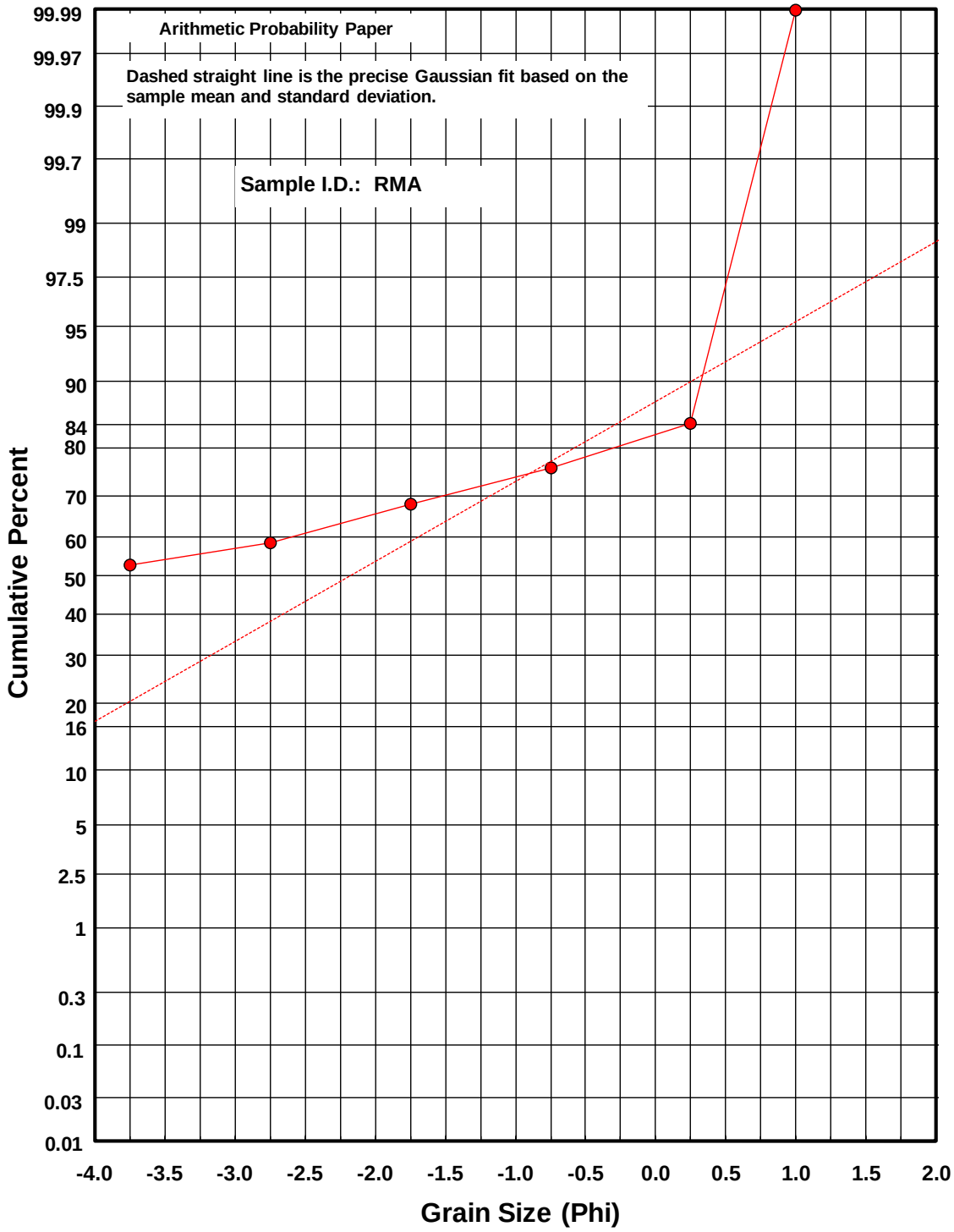
Arithmetic Probability Paper
Dashed straight line is the precise Gaussian fit based on the sample mean and standard deviation.
Sample I.D.: RMA
Cumulative Percent
99.99
99.97
99.9
99.7
99
97.5
95
90
84
80
70
60
50
40
30
20
16
10
5
2.5
1
0.3
0.1
0.03
0.01
-4.0
-3.5
-3.0
-2.5
-2.0
-1.5
-1.0
-0.5
0.0
0.5
1.0
1.5
2.0
Grain Size (Phi)

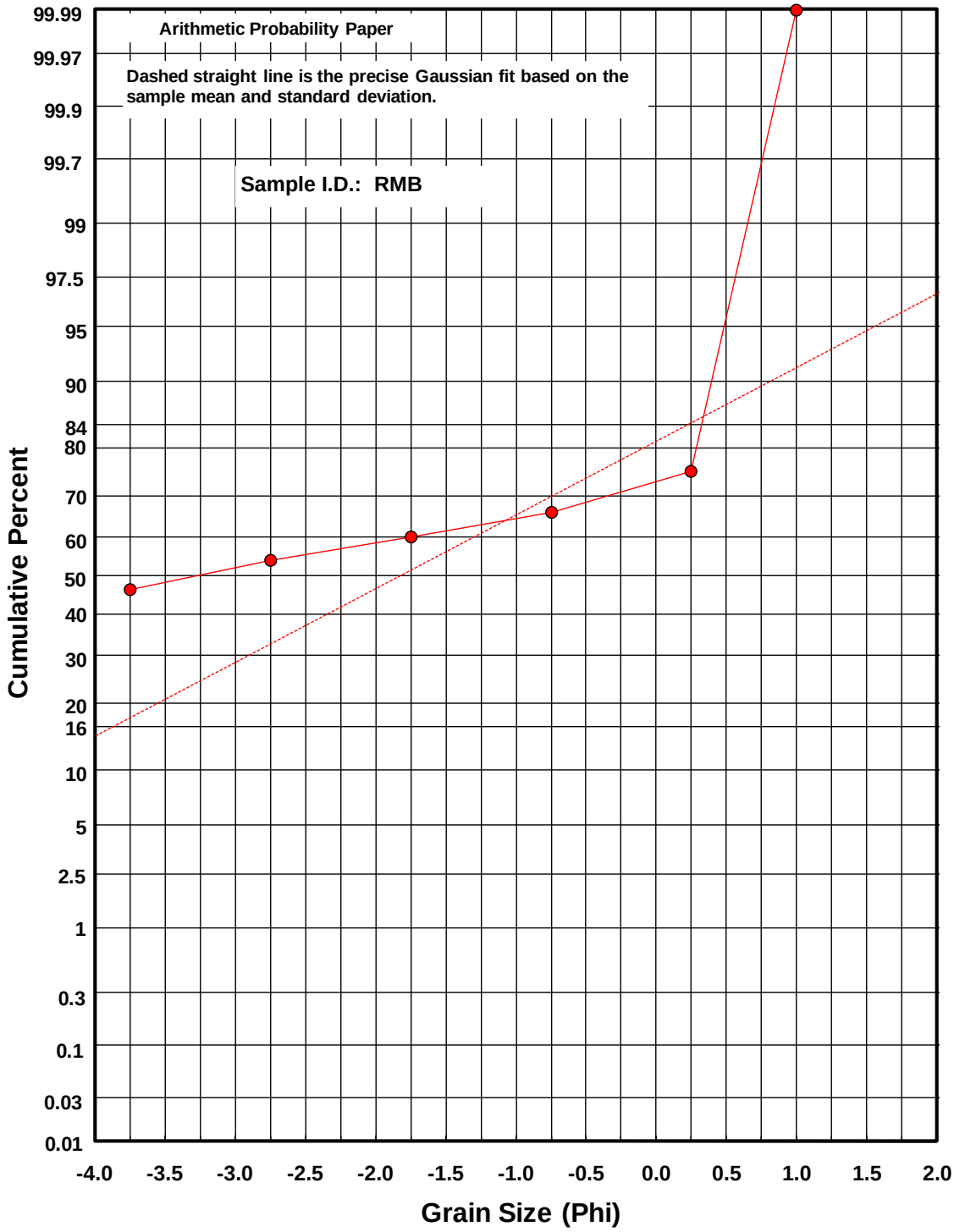
Arithmetic Probability Paper
Dashed straight line is the precise Gaussian fit based on the sample mean and standard deviation.
Sample I.D.: RMB
Cumulative Percent
99.99
99.97
99.9
99.7
99
97.5
95
90
84
80
70
60
50
40
30
20
16
10
5
2.5
1
0.3
0.1
0.03
0.01
-4.0
-3.5
-3.0
-2.5
-2.0
-1.5
-1.0
-0.5
0.0
0.5
1.0
1.5
2.0
Grain Size (Phi)

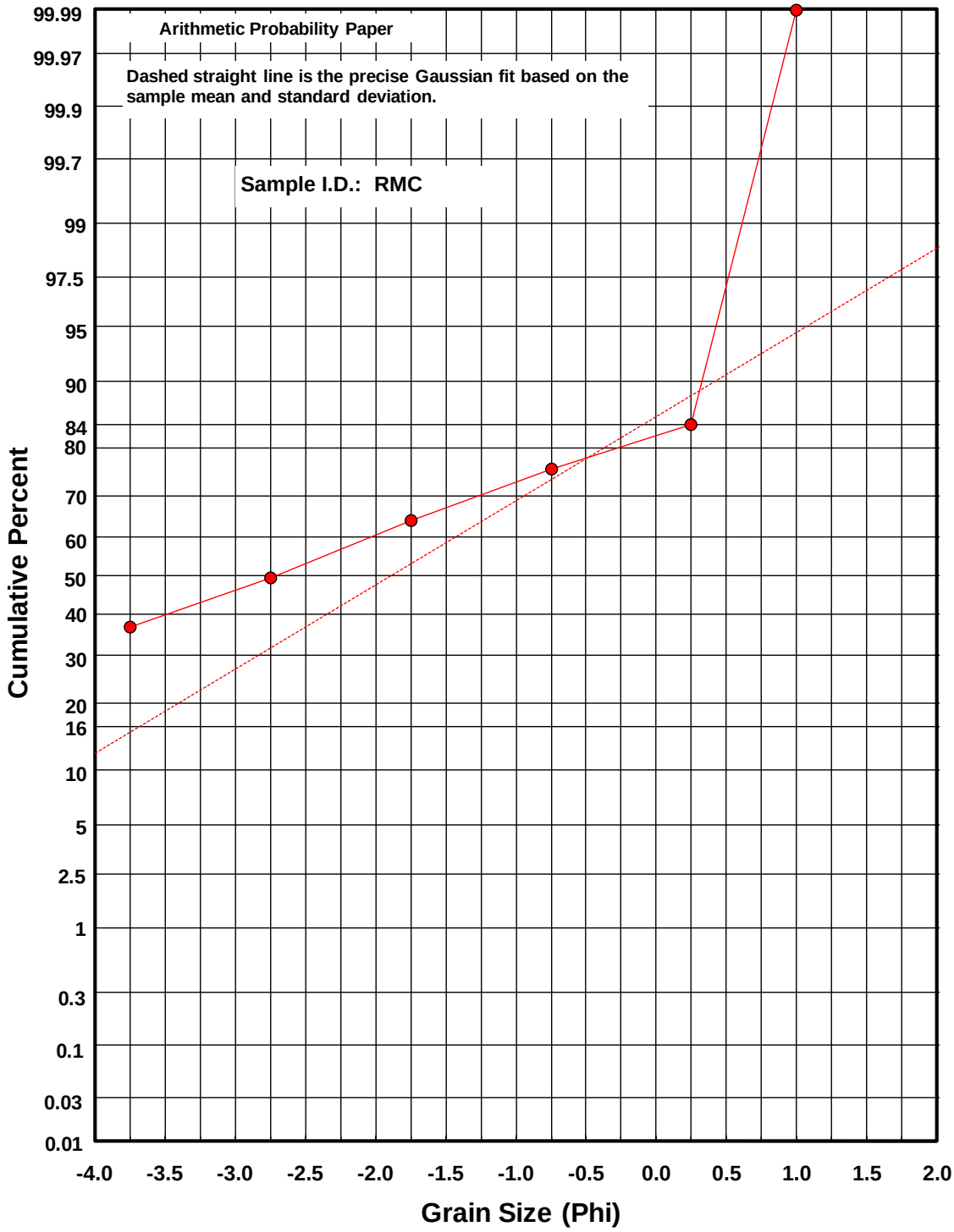
Arithmetic Probability Paper
Dashed straight line is the precise Gaussian fit based on the sample mean and standard deviation.
Sample I.D.: RMC
Cumulative Percent
99.99
99.97
99.9
99.7
99
97.5
95
90
84
80
70
60
50
40
30
20
16
10
5
2.5
1
0.3
0.1
0.03
0.01
-4.0
-3.5
-3.0
-2.5
-2.0
-1.5
-1.0
-0.5
0.0
0.5
1.0
1.5
2.0
Grain Size (Phi)

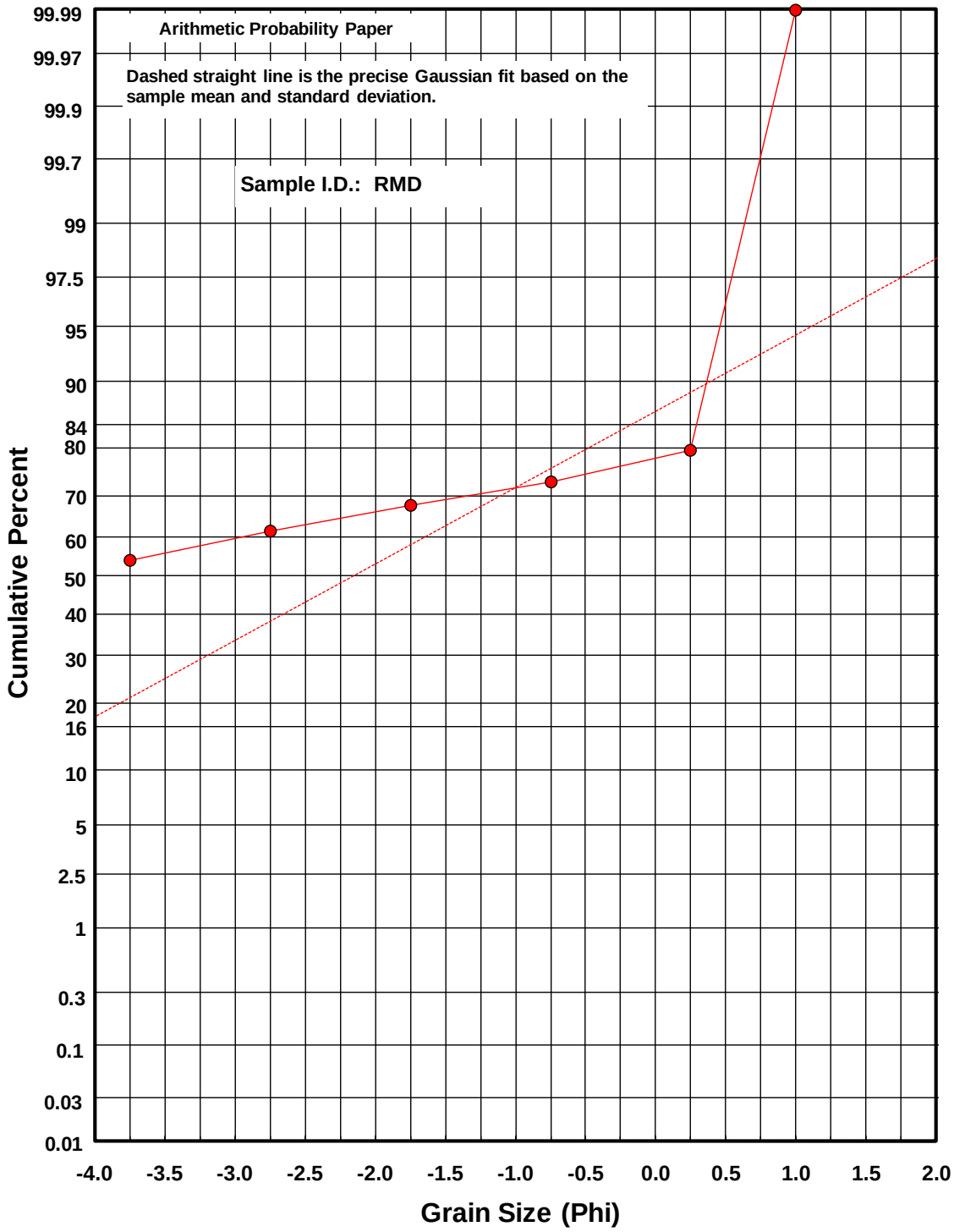
Arithmetic Probability Paper
Dashed straight line is the precise Gaussian fit based on the sample mean and standard deviation.
Sample I.D.: RMD
Cumulative Percent
99.99
99.97
99.9
99.7
99
97.5
95
90
84
80
70
60
50
40
30
20
16
10
5
2.5
1
0.3
0.1
0.03
0.01
-4.0
-3.5
-3.0
-2.5
-2.0
-1.5
-1.0
-0.5
0.0
0.5
1.0
1.5
2.0
Grain Size (Phi)

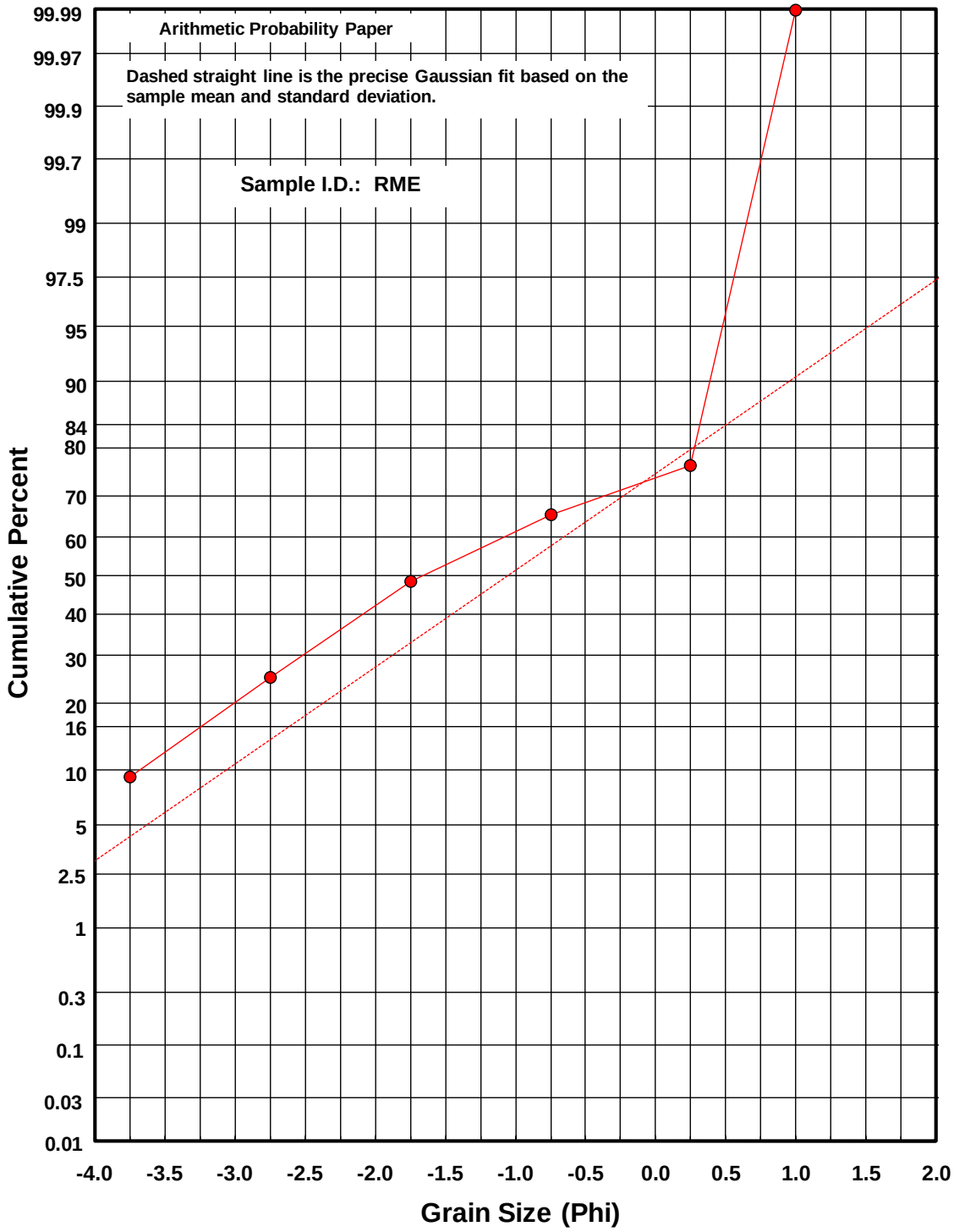
Arithmetic Probability Paper
Dashed straight line is the precise Gaussian fit based on the sample mean and standard deviation.
Sample I.D.: RME
Cumulative Percent
99.99
99.97
99.9
99.7
99
97.5
95
90
84
80
70
60
50
40
30
20
16
10
5
2.5
1
0.3
0.1
0.03
0.01
-4.0
-3.5
-3.0
-2.5
-2.0
-1.5
-1.0
-0.5
0.0
0.5
1.0
1.5
2.0
Grain Size (Phi)

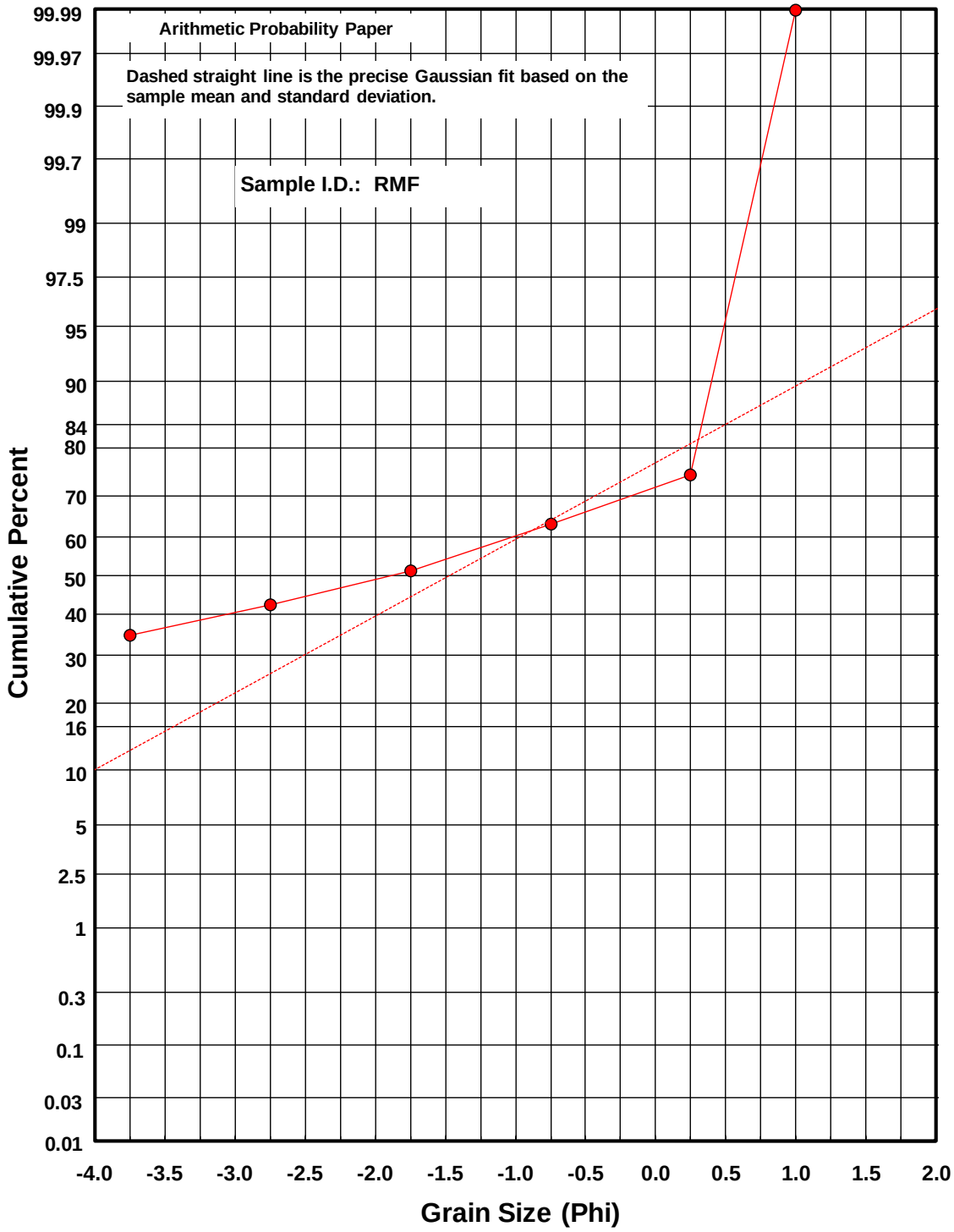
Arithmetic Probability Paper
Dashed straight line is the precise Gaussian fit based on the sample mean and standard deviation.
Sample I.D.: RMF
Cumulative Percent
99.99
99.97
99.9
99.7
99
97.5
95
90
84
80
70
60
50
40
30
20
16
10
5
2.5
1
0.3
0.1
0.03
0.01
-4.0
-3.5
-3.0
-2.5
-2.0
-1.5
-1.0
-0.5
0.0
0.5
1.0
1.5
2.0
Grain Size (Phi)

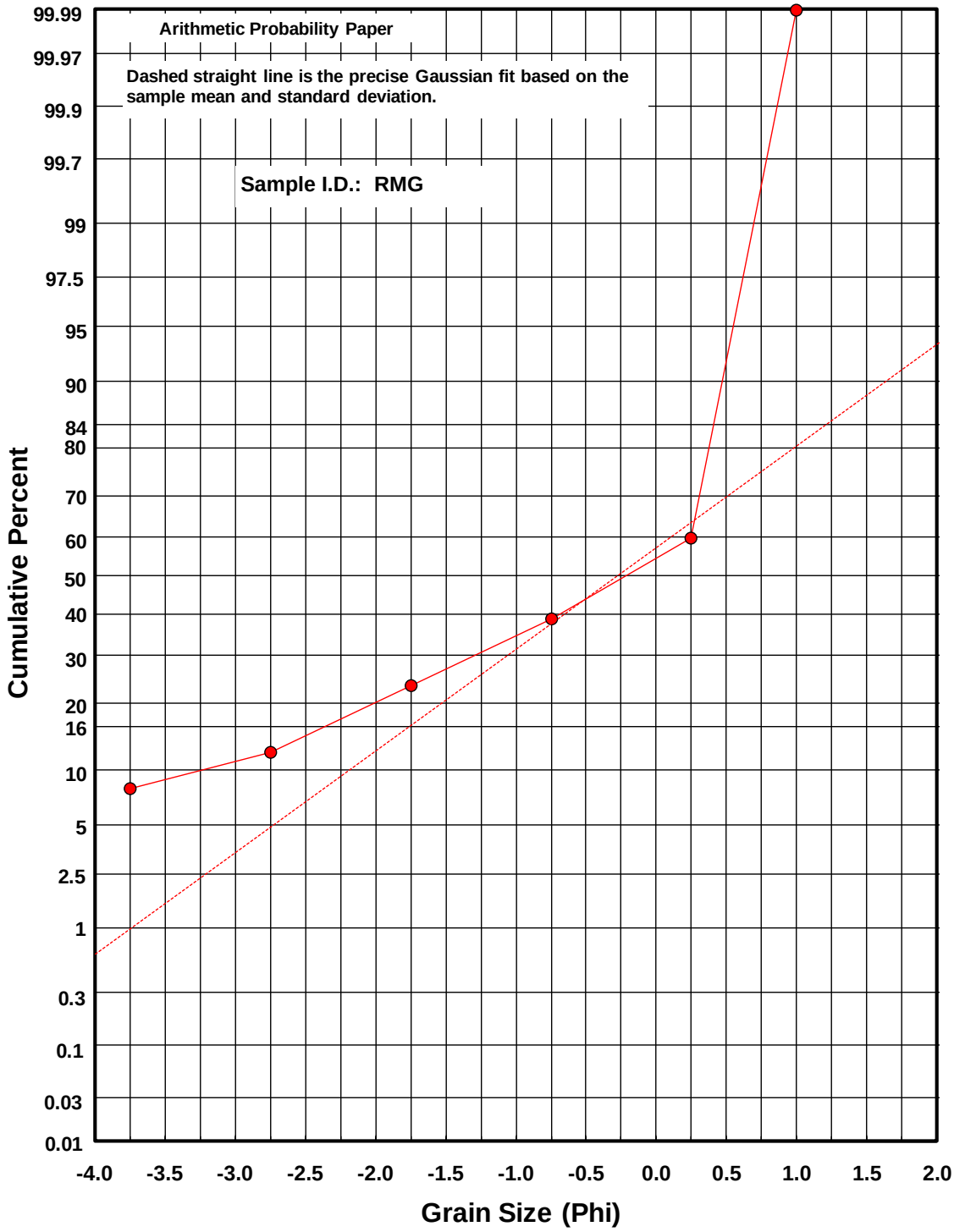
Arithmetic Probability Paper
Dashed straight line is the precise Gaussian fit based on the sample mean and standard deviation.
Sample I.D.: RMG
Cumulative Percent
99.99
99.97
99.9
99.7
99
97.5
95
90
84
80
70
60
50
40
30
20
16
10
5
2.5
1
0.3
0.1
0.03
0.01
-4.0
-3.5
-3.0
-2.5
-2.0
-1.5
-1.0
-0.5
0.0
0.5
1.0
1.5
2.0
Grain Size (Phi)

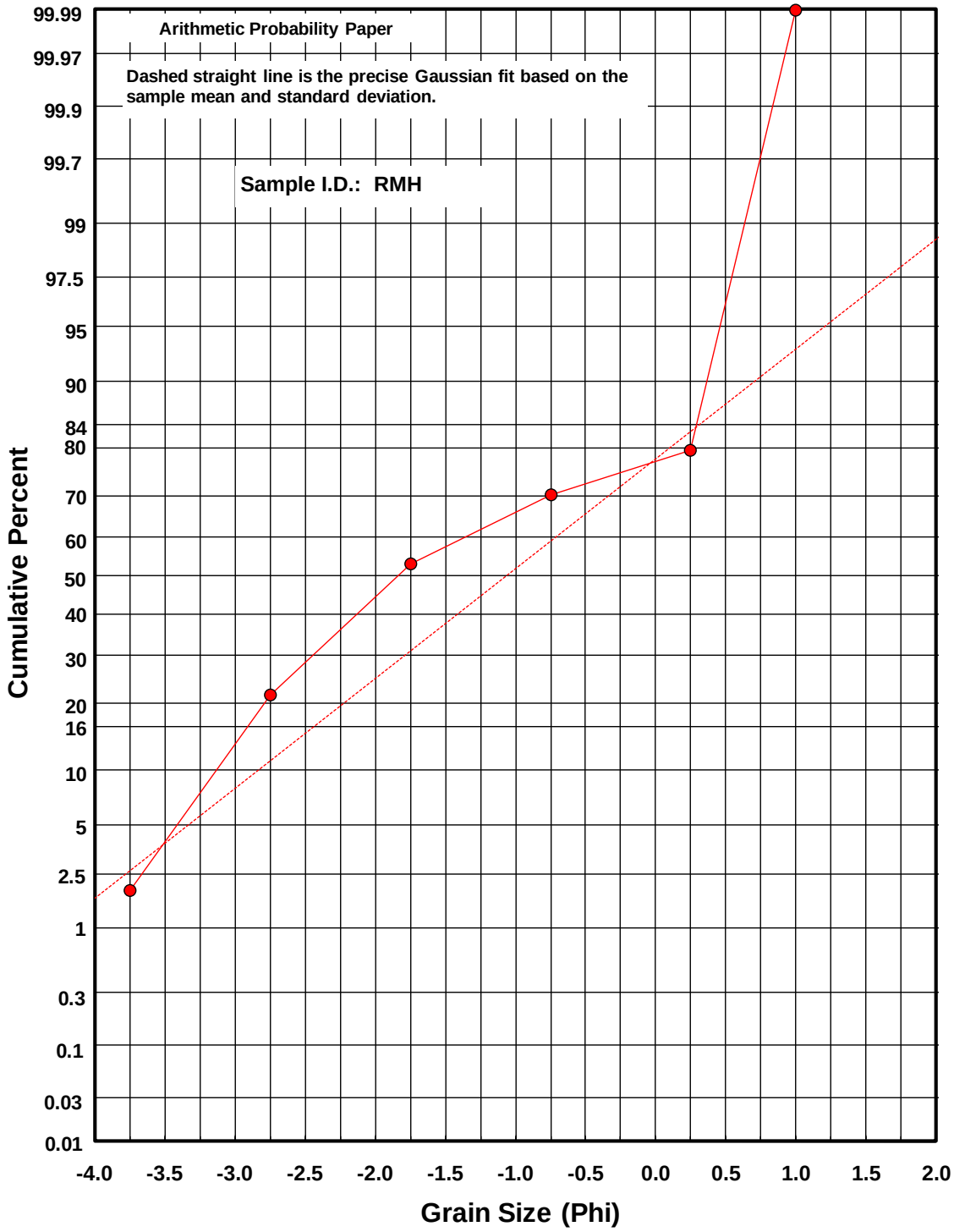
Arithmetic Probability Paper
Dashed straight line is the precise Gaussian fit based on the sample mean and standard deviation.
Sample I.D.: RMH
Cumulative Percent
99.99
99.97
99.9
99.7
99
97.5
95
90
84
80
70
60
50
40
30
20
16
10
5
2.5
1
0.3
0.1
0.03
0.01
-4.0
-3.5
-3.0
-2.5
-2.0
-1.5
-1.0
-0.5
0.0
0.5
1.0
1.5
2.0
Grain Size (Phi)

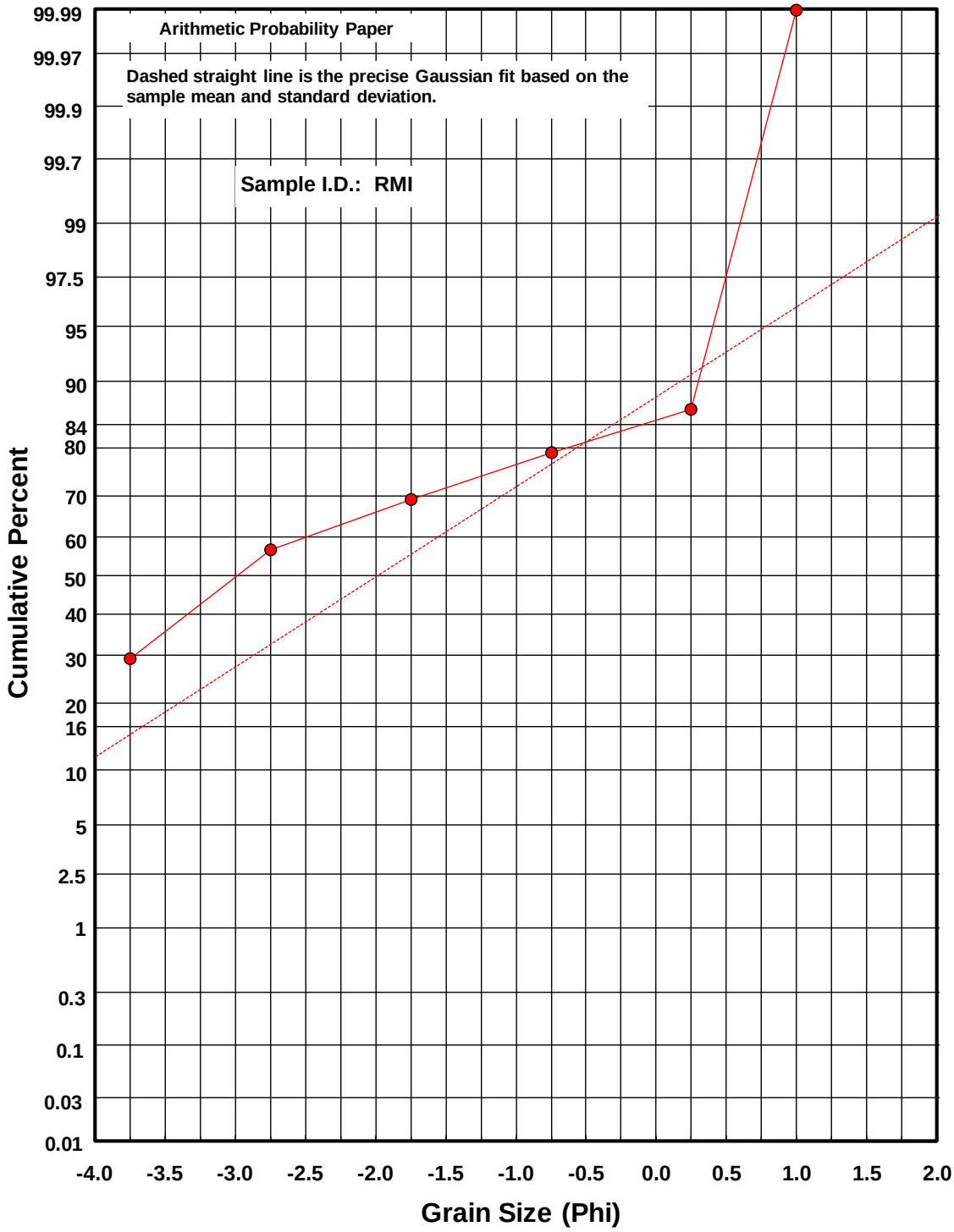
Arithmetic Probability Paper
Dashed straight line is the precise Gaussian fit based on the sample mean and standard deviation.
Sample I.D.: RMI
Cumulative Percent
99.99
99.97
99.9
99.7
99
97.5
95
90
84
80
70
60
50
40
30
20
16
10
5
2.5
1
0.3
0.1
0.03
0.01
-4.0
-3.5
-3.0
-2.5
-2.0
-1.5
-1.0
-0.5
0.0
0.5
1.0
1.5
2.0
Grain Size (Phi)

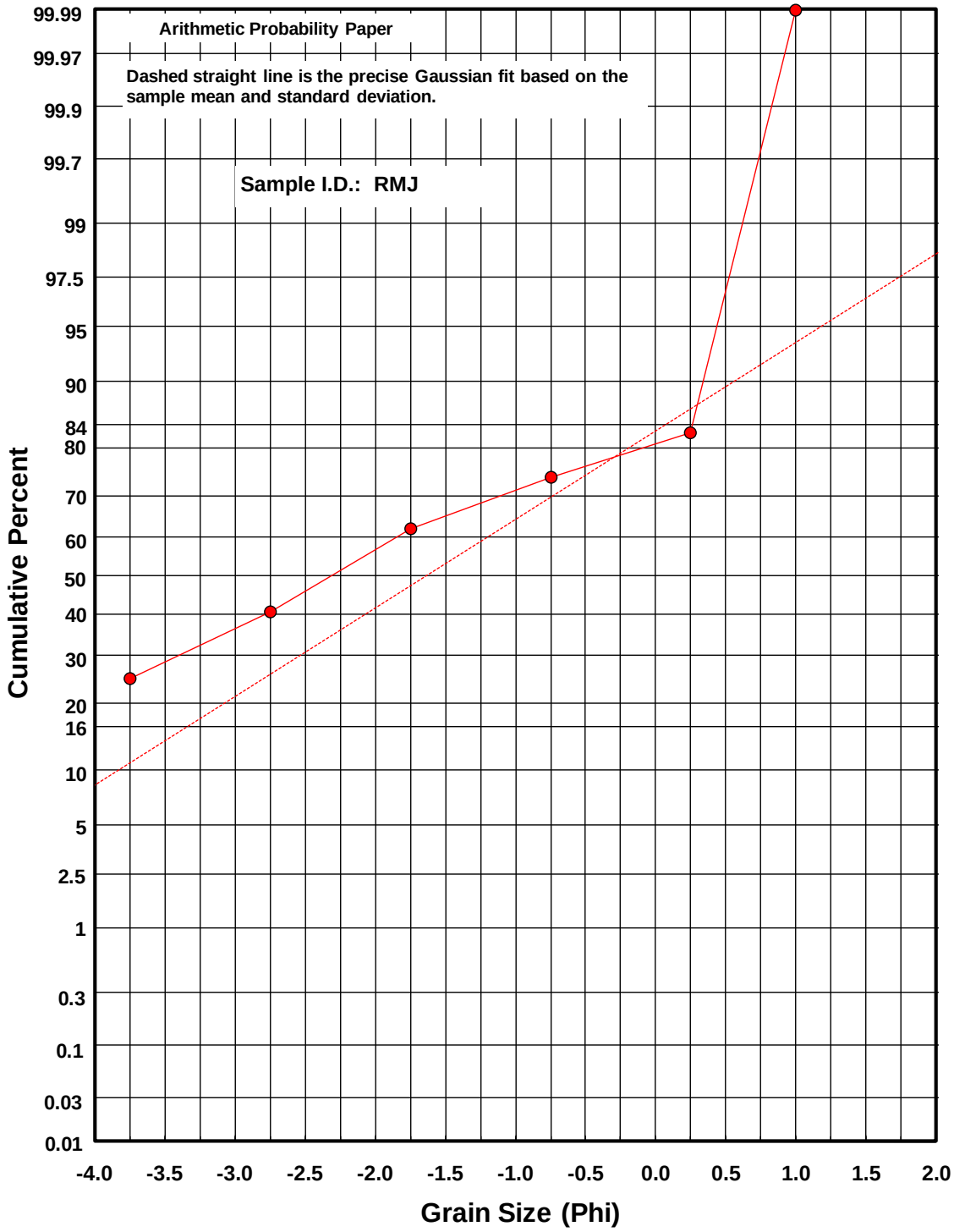
Arithmetic Probability Paper
Dashed straight line is the precise Gaussian fit based on the sample mean and standard deviation.
Sample I.D.: RMJ
Cumulative Percent
99.99
99.97
99.9
99.7
99
97.5
95
90
84
80
70
60
50
40
30
20
16
10
5
2.5
1
0.3
0.1
0.03
0.01
-4.0
-3.5
-3.0
-2.5
-2.0
-1.5
-1.0
-0.5
0.0
0.5
1.0
1.5
2.0
Grain Size (Phi)

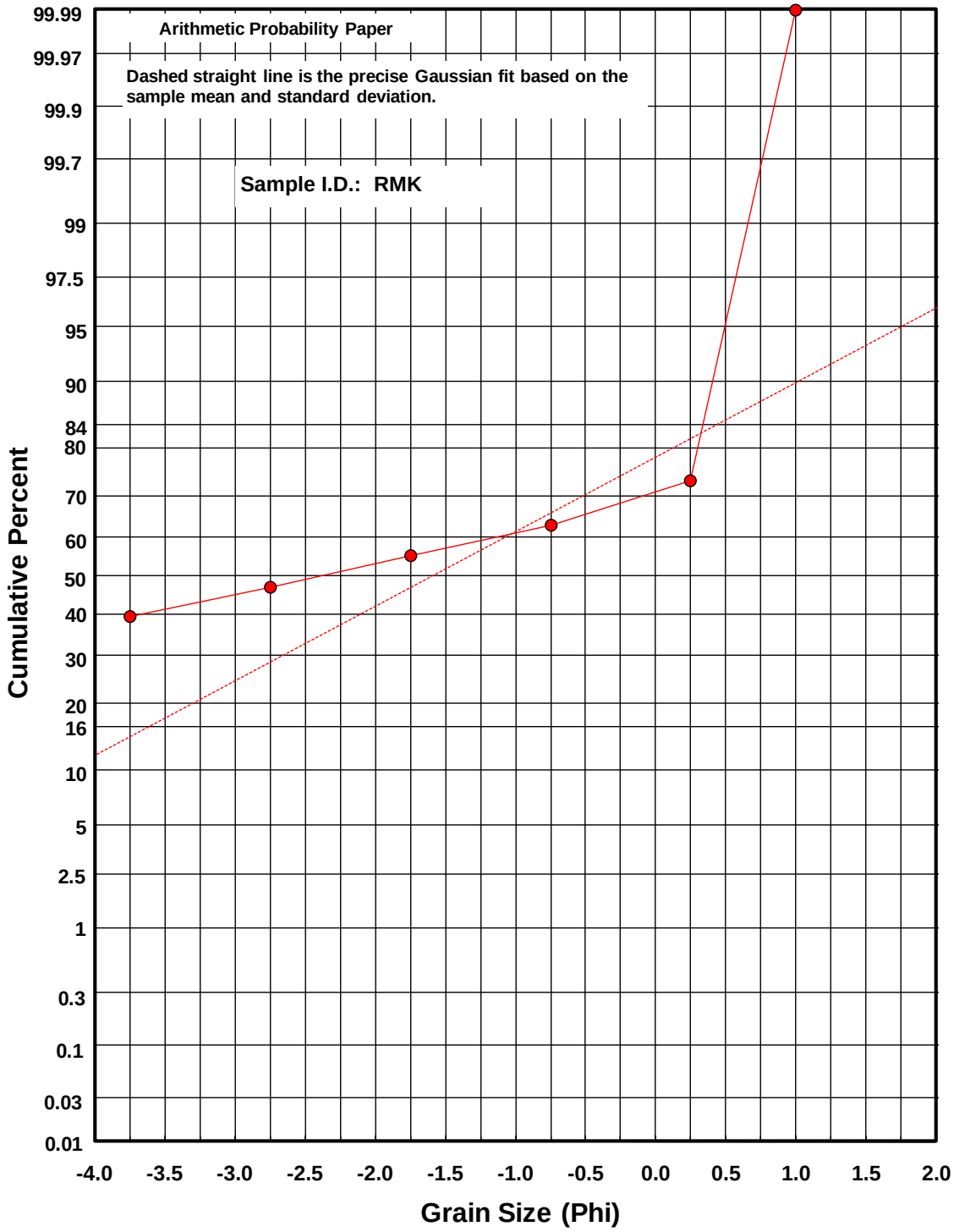
Arithmetic Probability Paper
Dashed straight line is the precise Gaussian fit based on the sample mean and standard deviation.
Sample I.D.: RMK
Cumulative Percent
99.99
99.97
99.9
99.7
99
97.5
95
90
84
80
70
60
50
40
30
20
16
10
5
2.5
1
0.3
0.1
0.03
0.01
-4.0
-3.5
-3.0
-2.5
-2.0
-1.5
-1.0
-0.5
0.0
0.5
1.0
1.5
2.0
Grain Size (Phi)

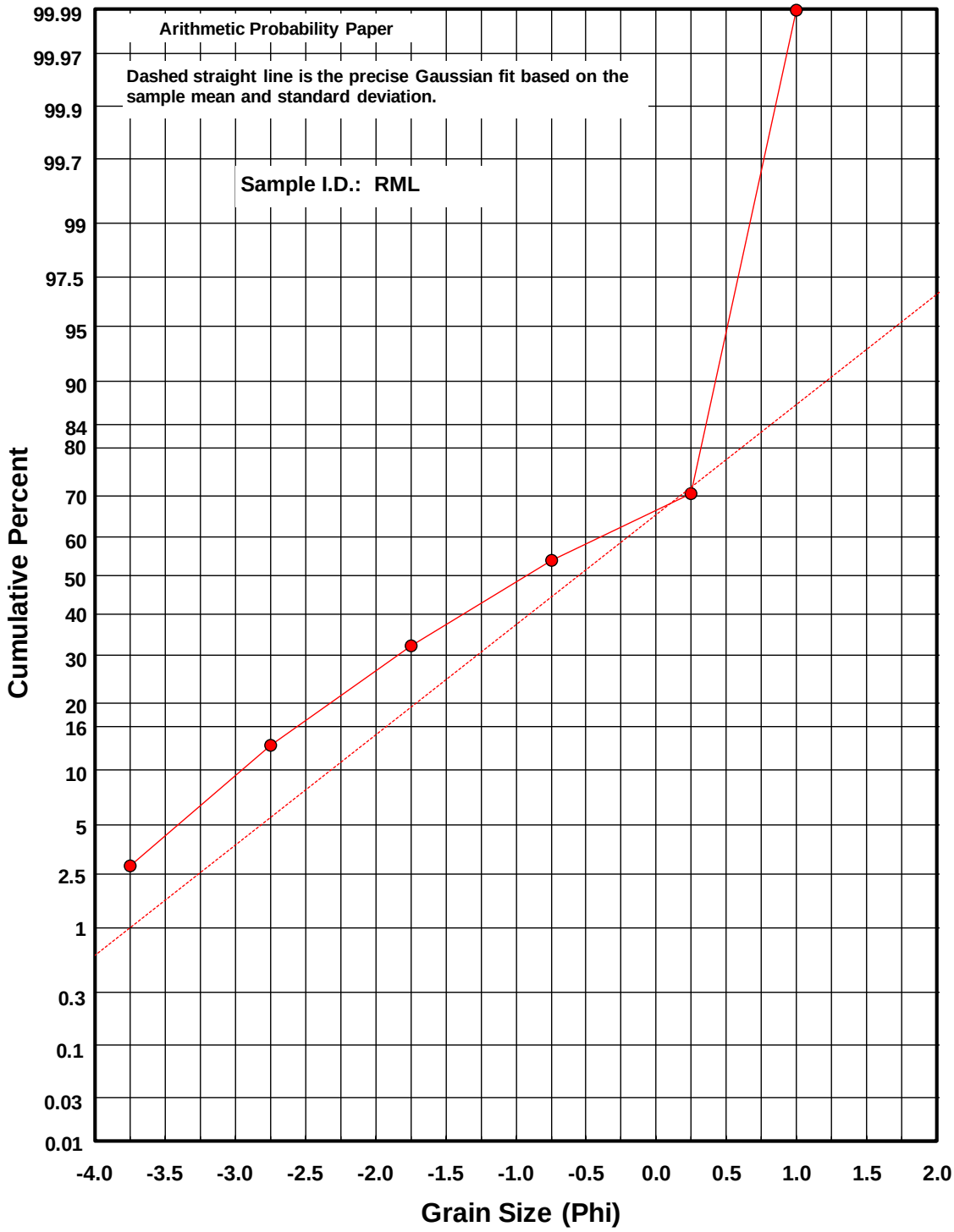
Arithmetic Probability Paper
Dashed straight line is the precise Gaussian fit based on the sample mean and standard deviation.
Sample I.D.: RML
Cumulative Percent
99.99
99.97
99.9
99.7
99
97.5
95
90
84
80
70
60
50
40
30
20
16
10
5
2.5
1
0.3
0.1
0.03
0.01
-4.0
-3.5
-3.0
-2.5
-2.0
-1.5
-1.0
-0.5
0.0
0.5
1.0
1.5
2.0
Grain Size (Phi)

VITA

Name: Timothy James Brunk

Address: Texas A&M University
Department of Geology and Geophysics, MS-3115
College Station, TX 77843-3115

Email Address: timone321@neo.tamu.edu

Education: B.A., Geology, Texas A&M University, 2008
M.S., Geology, Texas A&M University, 2010